Measuring the RFI Environment of the South African SKA Site

A thesis submitted in fulfilment of the
requirements for the degree of

MASTER OF SCIENCE

of

RHODES UNIVERSITY

by

PAUL JOHN MANNERS

February 2007

Abstract

The Square Kilometre Array (SKA) Project is an international effort to build the world's largest radio telescope. It will be 100 times more sensitive than any other radio telescope currently in existence and will consist of thousands of dishes placed at baselines up to 3000 km. In addition to its increased sensitivity it will operate over a very wide frequency range (current specification is 100 MHz - 22 GHz) and will use frequency bands not primarily allocated to radio astronomy. Because of this the telescope needs to be located at a site with low levels of radio frequency interference (RFI). This implies a site that is remote and away from human activity.

In bidding to host the SKA, South Africa was required to conduct an RFI survey at its proposed site for a period of 12 months. Apart from this core site, where more than half the SKA dishes may potentially be deployed, the measurement of remote sites in Southern Africa was also required. To conduct measurements at these sites, three mobile measurement systems were designed and built by the South African SKA Project. The design considerations, implementation and RFI measurements recorded during this campaign will be the focus for this dissertation.

Acknowledgements

I would like to offer my sincere thanks to a number of people who were involved and assisted during the RFI measurement campaign. The fact that South Africa has been shortlisted to host the SKA, subsequent to its bid submission, is a testament to the hard work and effort that was invested by the South African SKA Project team.

Firstly I would like to thank the RFI project manager, Gerhard Petrick. For his perseverance, patience, leadership and support throughout the RFI measurement campaign. I have benefited enormously from his experience and am very grateful to have had the opportunity of working with him.

Due to the nature of the project, expertise and support from many people was required. Without this support it would not have been possible to iterate the cycles of building, testing, re-building and re-testing the equipment as many times as we did. Most resources, expertise and support were provided by the staff at the Hartebeesthoek Radio Astronomy Observatory and for all their time and effort, I am very grateful. For the many technical discussions, encouragement and insight, I am indebted to Paul Prozesky, Mike Gaylard, Jonathan Quick and George Nicolson. Special mention is also made of Keith Jones and Japie Greeff, who without fail devoted enormous amounts of their own time, patience and coffee.

A number of months were spent in the Karoo conducting field measurements. During this time the RFI team lived on Losberg farm. Jan and Ronelle Louw, and their family provided us with accommodation and constantly made one feel at home. Their kindness and willingness to lend a hand in any situation is sincerely appreciated.

I am also grateful of the folks (Mum and Dad), who have continually provided encouragement, advice and shown a keen interest in my endeavours.

Finally to Prof. Justin Jonas for allowing me the opportunity to work on this project and for his ongoing support, advice and most especially patience throughout - I am very grateful. I have learned a great deal from his experience and those around me with whom I have come into contact with through this project. I am also appreciative of his financial support, initially through HartRAO and subsequently the SKA Project.

I would also like thank the people who proof-read this document: Adrian Tiplady and Nicole Nuppenau.

Every day in the Karoo is an adventure – the Author, April 2005

Contents

List of Figures

List of Tables

Chapter 1

RFI and the SKA Project

1.1 SKA Project

The Square Kilometre Array (SKA) Project is an international enterprise to build the world's largest radio telescope. The telescope will consist of thousands of interconnected dishes with baselines of up to 3000 km and will be 100 times more sensitive than any other telescope currently in existence (International SKA Project Office, 2006). The sensitivity of the instrument will be achieved by the aggregated surface area of the dishes, which in total will be a million square metres i.e. one square kilometre.

The proposal by the radio astronomy community to build the SKA will make way for a new generation of instruments, which will allow astronomers to answer fundamental questions about the origins and evolution of the Universe (International SKA Project Office, 2004).

With more than 50 institutions from around the world involved in the development of the SKA, a suitable site that maximises the scientific output and minimises risks, including costs, needs to be selected. The radio frequency interference (RFI) environment at the site is one of the main factors that influences the science potential of the SKA, and the evolution of the radio spectrum usage is one of the main risks to the project.

The countries bidding to host the telescope were Argentina, China, Australia and South Africa. However, following a recent short-listing of the bid submissions, only Australia and South Africa are presently being considered.

This thesis will detail the RFI measurement campaign that was undertaken by the South African SKA Project in preparation for its bid to host the SKA. The requirement for the characterisation of the radio frequency environment was fulfilled using three custom built measurement systems. The design details of these systems, the measurement protocol and the processing of the data will be the focus of this dissertation.

1.2 RFI in Radio Astronomy

A document entitled 'Request for Proposals for siting the SKA' (International SKA Project Office, 2004) was published by the International SKA Steering Committee (ISSC) to provide technical guidelines regarding the evaluation criteria for proposed sites.

A principle criteria for the site evaluation is that of a low-level RFI environment. Details of these RFI requirements and a protocol for its evaluation are contained in a supplementary document: SKA Memo 37 (Ambrosini et al., 2003), 'RFI Measurement Protocol for Candidate SKA Sites'. This document, from here on referred to as SKA Memo 37, is based on the International Telecommunication Union's (ITU) Recommendation RA.796-2 (International Telecommunication Union, 2003) specification that outlines the levels of RFI deemed harmful to radio astronomy.

The global allocation of radio frequency spectrum is coordinated internationally by the ITU. In South Africa, the national body that is responsible for local spectrum management, allocation and protection is the Independent Communications Authority of South Africa (ICASA).

One of the characteristics of the SKA that differs from previous generation radio telescopes is that it will operate in frequency bands far outside those allocated to primary radio astronomy usage by the ITU. These bands are discussed in the CRAF Handbook for Radio Astronomy (CRAF, 1997) and are included in Table 1.2. As a result of the instrument's broadband spectrum coverage and its increased sensitivity, it is important to find a location that is away from human activity. This site should have minimal man-made RFI, implying a site that is remote. It should also ensure that encroaching human activities do not affect its operation in the future.

While current specifications for the operating frequency of the SKA already cover a wide frequency range (100 MHz - 22 GHz), in future these specifications could extend even further: 60 MHz to 35 GHz. As a result, and due to the emergence of other radio astronomy projects such as C-BASS (Oxford University Physics, 2006) and the Karoo Array Telescope (KAT) (South African SKA Project, 2006a), which have similar requirements to the SKA, it has been suggested that bidding countries establish a radio quiet zone (RQZ). Such reserves will provide long-term protection for the instruments. In South Africa the legislation required to declare an RQZ in the Northern Cape is currently being promulgated. This legislation will be called the Astronomy Geographic Advantage (AGA) Bill and will give the minister

of Science and Technology the requisite powers to improve and preserve the radio frequency environment within the RQZ.

1.3 Design Considerations

Included in SKA Memo 37 are specifications for two complementary schedules of RFI measurements, named Mode 1 and Mode 2. The reason for two modes is to accommodate the characterisation of the core and the remote sites where the telescope dishes could potentially be situated. Summaries for the Mode 1 and Mode 2 specifications, as defined in Memo 37, are given in Tables 1.1 and 1.2 respectively.

Frequency Band GHz	RBW kHz	ΔT_{RBW} ms	Time s
0.070-0.150	3	10	1334
0.150-0.300	3	10	500
0.300-0.800	30	10	167
0.800-0.960	30	10	1000
0.960-1.400	1000	0.002	900
1.400-3.000	30	10	534
3.000-22.000	1000	10	190
Total			1.3 hrs

Table 1.1: SKA Memo 37 specification for Mode 1 RFI measurements, given a particular antenna azimuth pointing and polarisation. For each band a separate resolution bandwidth (RBW), dwell time (ΔT_{RBW}) and associated measurement time are defined. Such measurements need to be repeated to cover 360° in azimuth and both polarisation orientations.

Different sensitivity requirements for Mode 1 and 2 measurements were achieved through choice of dwell time (ΔT_{RBW}) and resolution bandwidth (RBW) for each frequency band. Bands with narrower RBW have a lower noise floor, and longer dwell times lead to better sensitivity in the measurements. This is clarified by the standard equation (International Telecommunication Union, 2003):

$$\frac{\Delta T}{T} = \frac{1}{\sqrt{\text{RBW} \times \tau}} \tag{1.1}$$

which expresses sensitivity as a signal-to-noise ratio ($\Delta T/T$), written in terms of RBW and measurement integration time (τ).

The purpose of the Mode 1 measurements was to identify strong RFI signals that could threaten the linearity of the SKA receivers. These measurements were performed in a relatively short space of time. While providing only coarse resolution, they gave a reasonable indication of the RFI environment. The Mode 1 measurements were also intended to measure

Frequency Band MHz	RBW kHz	ΔT_{RBW} msec	Time s	Radio Astronomy Usage
150-153	1	100	300	Continuum
153-322	3	10	564	
322-329	3	1000	2334	Deuterium (DI)
329-406	30	10	26	
406-410	30	10000	1334	Continuum
410-608	30	10	66	
608-614	30	10000	2000	Continuum
614-1000	30	10	129	
1000-1370	30	300	3700	Continuum
1370-1427	30	1000	1900	Hydrogen (HI), SETI
1427-1606	30	100	597	SETI
1606-1723	30	1000	3900	Hydroxyl (OH), SETI
1723-2655	30	10	311	
2655-2700	100	1000	450	Continuum
2700-3300	100	10	60	
3300-3400	100	1000	1000	Methyladyne (CH)
3400-4800	100	10	140	
4800-5000	100	1000	2000	Formaldehyde (H_2CO)
5000-6600	300	10	54	
6600-6700	300	1000	334	Methanol (CH_3OH)
6700-8600	300	10	64	
8600-8700	300	1000	334	Helium ($^3He^+$)
8700-12100	300	10	114	
12100-12200	300	1000	334	Methanol (CH_3OH)
12200-14400	300	10	127	
14400-14500	300	1000	334	Formaldehyde (H_2CO)
14500-18300	300	10	127	
18300-18400	300	1000	334	Cyclopropenylidene (C_3H_2)
18400-22000	300	10	120	
Total			6.4 hrs	

Table 1.2: SKA Memo 37 Specification for Mode 2 frequency bands for a single antenna pointing and polarisation. The narrow frequency bands are those that are of observation importance to radio astronomy (CRAF, 1997). Note that these bands have a narrower resolution bandwidth (RBW) and are integrated to lower sensitivity levels as determined by their longer dwell time (ΔT_{RBW}) and measurement time.

the high power L-Band interference from radar systems and other transient avionic signals. This was done by repeating many fast scans across the L-Band with a wide 1 MHz RBW.

The purpose of the Mode 2 measurements was to measure the weaker signals, which could compromise the fidelity of radio astronomy observations. These measurements concentrated on the frequency bands most relevant to radio astronomy, and were integrated to deeper sensitivity levels. To increase the sensitivity, bands generally had a narrower RBW. It was required that the measurements were conducted at the core site over a period of 12 months. Considering that approximately 75% of the collecting area of the SKA will be located at the core site, it was important that seasonal variances be monitored over a full year. The long monitoring period also increased the probability of observing transient anomalies such as tropospheric ducting and meteor scattering.

Using SKA Memo 37 as a guideline, RFI measuring equipment and protocols were designed to adhere to the Mode 1 and 2 specifications. The design of the system took into account issues relating to the SKA Site Spectrum Monitoring (SSSM) system (Millenaar, 2005). This system (SSSM) was developed by a third party, and was used to perform independent measurements at the core sites for each site proponent.

For the Mode 1 measurements, it was required that the receiver system have a system temperature (T_{SYS}) of 30000 K or less. The more sensitive Mode 2 measurements required that the system temperature was no greater than 300 K.

The operating frequency range was from 0.07 - 26.5 GHz, and included measurements for both polarisations, taken in all azimuth directions. Three systems were built – primarily to facilitate simultaneous measurements at the core and remote sites, but also to provide redundancy in case the core site system failed. Flexibility was therefore required to allow both modes of measurements to be performed independently of the specific system or site.

Apart from equipment specifications, further practical requirements were imposed on the design of the measurement systems. The sites were selected for being isolated from human activity, requiring that the systems to be mobile. In addition, systems often had to travel to regions with little road infrastructure and operate in harsh environmental conditions.

To avoid interference generated by human activity, it was also important that the systems could be left to run reliably and unassisted. Once the measurements had been initiated, the only manual intervention required was to refuel the diesel generator that provided power for the measurement equipment.

Finally, to ensure correct operation and monitor the health of the systems, it was required

that system checks were done before a new measurement schedule was initiated. These checks and the running of the systems in the field, were successfully operated by teams who had limited training with the system before they were sent into the field.

1.4 Structure of Thesis

The structure of this dissertation, is outlined below:

Chapter 2 deals with the design of the radio frequency sub-system of the RFI measurement systems. It also details the laboratory tests that were performed on the systems, to ensure that they met the specification requirements.

Chapter 3 details the control and data acquisition sub-system for the RFI measurement systems. A description of the hardware and software used to control the RF sub-system and the interaction between them is given.

Chapter 4 describes the exercises that were performed to identify and eradicate locally generated sources of RFI. This RFI was radiated by the RFI measurement system itself as well as other objects and equipment in the local environment.

Chapter 5 details the operation of the RFI measurement systems in the field. Procedures undertaken during the measurement campaign to ensure the continued stability of the systems, and the measurement parameters for the Mode 1 and Mode 2 measurements, are discussed.

Chapter 6 deals with the processing and analysis of the RFI measurement data. The calibration and processing procedures, as well as the tools developed to facilitate these functions, are described.

Chapter 7 summarises the RFI measurement results obtained from the Mode 1 and Mode 2 measurements conducted at the Karoo 3 core site[1]. Results showing the spectrum occupancy for this site are also shown. A comparison of the Mode 2 measurements performed during the ASTRON/SSSM site visit as well as measurements at selected remote sites are provided.

[1]It is pointed out that the actual RFI measurements were conducted at the site "RFI-K3", which is about 5 km from the "Karoo 3 core site". However, for the remainder of this dissertation, no distinction shall be made between the two; and preference shall be given to using the terminology "Karoo 3 core site".

Chapter 8 provides concluding comments of the results and outlines possible work for the future.

Appendices A - E Appendices relating to the main chapters (Chapters 2-6).

Appendix F is found on the accompanying CD, and contains electronic versions of source code and other related electronic media.

1.5 Scope of Work

While the structure of this dissertation is outlined in Section 1.4, this linear structure does not necessarily match the sequence of events in which the work for this project was done. To clarify these events and their chronological order an overview of the project time-line is shown in Figure 1.1.

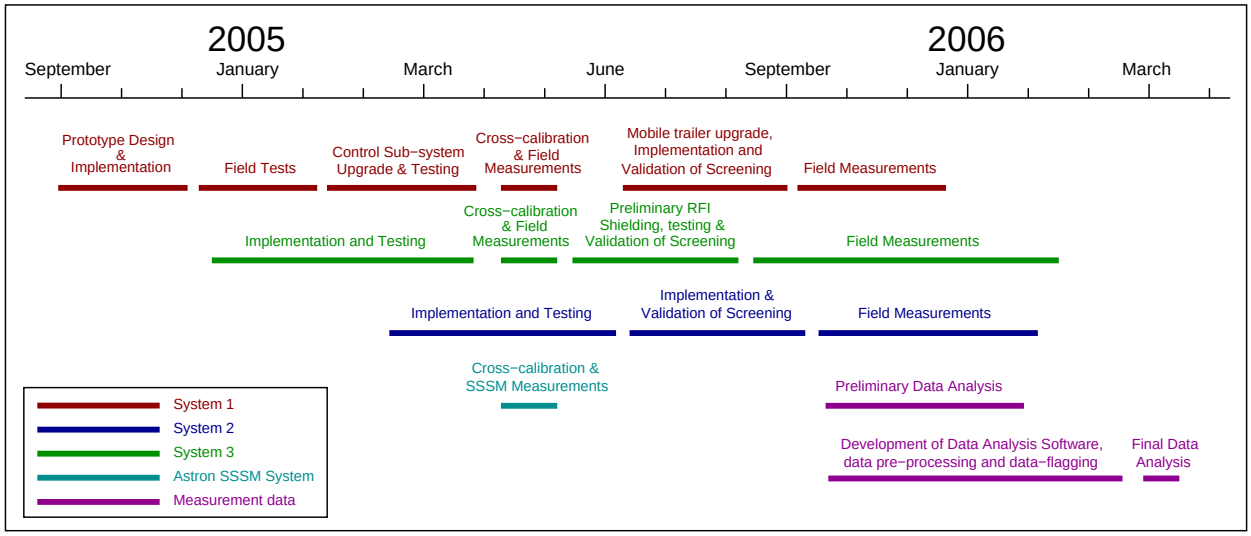

Figure 1.1: Time-line of the South African SKA RFI measurement campaign.

Due to the nature and extent of the RFI measurement campaign, credit is due to a number of people whose input and expertise facilitated the successful implementation and operation of the RFI measurement systems. The level of involvement from these people was determined by the SKA RFI Project Manager, Mr Gerhard Petrick, and was necessary in order to meet strict time constraints. Clarification of the involvement and the people responsible for the various aspects of the project is detailed below:

RF Circuitry was designed by Dr George Nicholson in consultation with Prof. Justin Jonas. The image rejection high pass filters were designed by Prof. Jonas and con-

structed in the mechanical workshop at the Hartebeesthoek Radio Astronomy Observatory (HartRAO). The RF Mast-Head Box was also constructed at HartRAO and the RF components were assembled by Mr Japie Greeff (HartRAO technician). The testing, analysis and software developed for measuring the RF assemblies was developed by the author with valuable input from Mr Gerhard Petrick and Mr Keith Jones (HartRAO engineer).

RF Control Logic and Electronics was designed by the author, who also built and tested the prototype control system with recommendations given by Mr Keith Jones. All printed circuit board (PCB) layouts were designed by Mr Keith Jones and assembled by Mr Japie Greeff. The author was responsible for testing the PCBs and designing the RF switching logic. The final production systems used a complex programmable logic device (CPLD) for the RF switching logic and this was implemented by Mr Paul Prozesky (HartRAO engineer). The author was responsible for developing the code for the microcontrollers used (Atmel AT90S8535 and ATmega8535) and Mr Paul Prozesky assisted in tracking down bugs associated with the code upgrade for the production system microcontroller (ATmega8535).

LabVIEW software that incorporated the frequency sweeper application (for laboratory tests), field measurement integrity check application and the main RFI measurement scheduler application, was developed by the author. The software for interfacing with the spectrum analyser for the RFI measurement scheduler application had been developed previously by Prof. Justin Jonas and was integrated into the main program. The code providing automation and interfacing with the microcontroller was developed by the author.

RFI measurements with the systems were conducted by the author up until August 2005. At this point, final automation and RFI shielding had been completed and the production systems were handed over to ICASA representatives. The cross-calibration exercise was performed by Mr Gerhard Petrick, Mr Japie Greeff, members of the ASTRON/SSSM team and the author. Representatives from ICASA were also present and assisted during this procedure.

Investigations of locally generated RFI and screening were performed at the Karoo 3 core site by ICASA representatives (Mr Dave Drew and Mr Danie Lombard), Mr

Gerhard Petrick and the author. Investigations of the self-generated RFI (of the system) were performed by Mr Keith Jones, Mr Gerhard Petrick and the author. The implementation of screening was performed by the abovementioned people with assistance from Mr Frans Durandt, Mr Pieter Stronkhorst, Mr Andre Van der Merwe, Mr Attie Van Wyk and Mr Jacques Grobler in the mechanical workshop at HartRAO. Numerous other mechanical issues were also attended to by the mechanical workshop team.

Data processing software was designed and developed by the author in consultation with Prof. Justin Jonas. An initial C program, developed by Prof. Jonas for RFI measurements conducted prior to the RFI campaign, was used in the preliminary data analysis stage. However new processing software used for the data management, data-flagging and production of output products (i.e. spectrum plots) for the SA SKA RFI Bid document (South African SKA Project, 2006b) were developed by the author. The data-flagging of the RFI measurement data was performed by Mr Gerhard Petrick and Prof. Justin Jonas.

Electronic media such as photographs and video clips were produced and collected from many sources during the course of the project. These sources included Mr Gerhard Petrick, Mr Keith Jones, Mr Rob Millenaar (ASTRON/SSSM team), the author and the ICASA representatives.

Chapter 2

Radio Frequency Sub-System

This chapter details the RF component of the RFI measurement system. It describes the design strategy, the components used, as well as procedures followed to calibrate it in the laboratory.

2.1 RF Requirements and Design

SKA Memo 37 specifies that the RF sub-system must operate from 70 MHz to 22 GHz. As discussed in Chapter 1, Mode 1 measurements required a T_{sys} of 30000 K and the Mode 2 measurements, 300 K.

The final design of the RF sub-system was duplicated for three measurement sets. Two of these sets were used for Mode 1 measurements and the third, Mode 2 measurements. The systems were identical apart from a post-amplifier and two low pass filters in System 2, that were necessary for the more sensitive Mode 2 measurements. Despite the differing system gain, it was feasible to conduct either mode of measurements on any of the three systems. If a Mode 1 system was used for Mode 2 measurements, the T_{sys} requirement was not met. This flexibility however, afforded a degree of redundancy in case System 2 were to fail. The main emphasis of the measurement campaign was for Mode 2 measurements at the core site over a period of 12 months, as required by the SKA RFP (International SKA Project Office, 2004).

System temperatures measured for each system were acceptable, according to their respective Mode 1 and 2 requirements. For Systems 1 and 3, used for the Mode 1 measurements, T_{sys} was measured to be below 20000 K. For System 2, used for Mode 2 measurements, T_{sys} was measured below 300 K across most of the operating frequency band. The details of these measurements are discussed in a separate section (Section 2.3.3) later in this

chapter.

In order to span the large operating frequency range, two Rohde & Schwarz antennas were used for each RFI measurement system. Figure 2.1 shows the System 2 antenna gains as a function of frequency. Similar plots for the other two systems are included in Appendix A.1. As the design and choice of RF components permitted measurements above 22 GHz, measurements at all sites were performed up to 26.5 GHz. It was necessary to measure down to 70 MHz despite the minimum SKA frequency specification of 100 MHz. This was done in order to identify the harmonics of signals that could potentially cause saturation of the SKA receivers.

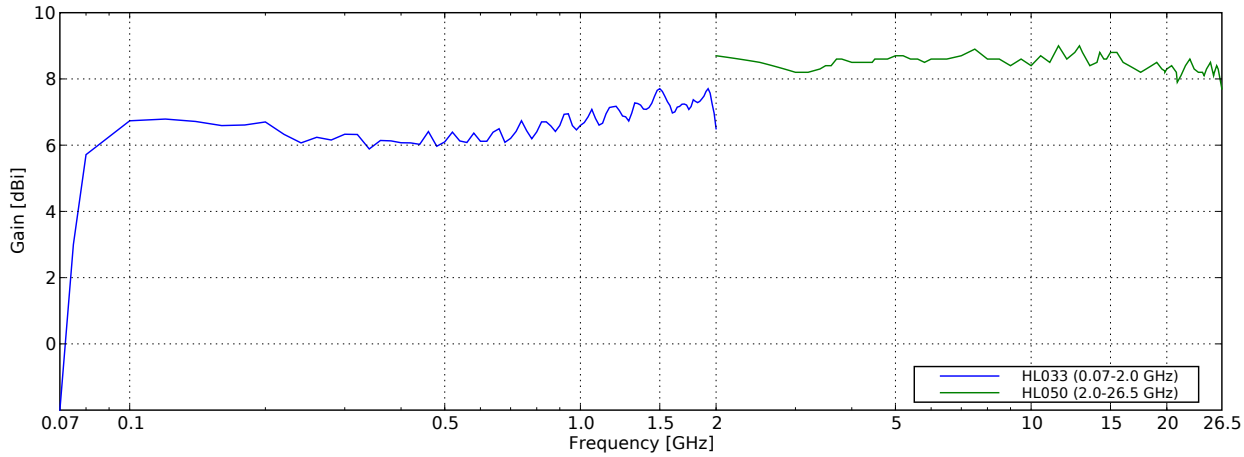

Figure 2.1: Antenna gains for RFI measurement System 2. For the Rohde & Schwarz HL033 antenna gain data was supplied by the manufacturer. No gain data was supplied with the Rohde & Schwarz HL050 antenna and so values were captured from the manufacturer's data sheets (Rohde & Schwarz, 2006a).

No single RF component was able to cover the full operating frequency range (70 MHz - 26.5 GHz). As a result, multiple components and various signal paths were needed. To reduce the frequencies on the down link, an upper side band (USB) heterodyne system was used for bands above 12.5 GHz. To cover this frequency range, two signal paths with local oscillators at 12 GHz and 18 GHz were used. These paths were Path C and Path D, and are indicated in Figure 2.2 along with the signal paths used for frequencies below 12.5 GHz.

Three Miteq low noise amplifiers (LNAs) with overlapping passbands were employed. The LNAs were needed to achieve the low T_{sys} required for the measurements, and had noise figures between 1.3 dB and 2.0 dB.

The operating frequency ranges for the LNAs, antennas and other components meant that RF co-axial switches were needed for the selection of different signal paths. Four co-

axial switches were used for this purpose and details of the RF signal paths are shown in Table 2.1. To ensure that there was low signal loss between the RF components, semi-rigid co-axial cables (Huber & Suhner EZ141) were constructed and installed in the RF assembly.

Signal Path	Frequency Band	LNA	LO	Antenna
A	0.07-2.0 GHz	1	-	HL033
A*	2.0-6.0 GHz	1	-	HL050
B	6.0-12.5 GHz	2	-	HL050
C	12.5-18.5 GHz	2	12 GHz	HL050
D	18.5-26.5 GHz	3	18 GHz	HL050

Table 2.1: The RF signal paths showing details of the LNA, LO and antenna selected for each path in the RFI measurement system.

The block diagram in Figure 2.2 shows the layout of the RF components used in the RF sub-system. The LNAs, switches, noise diode, LOs and mixers were placed in the Mast-Head Box. This was close to the antennas and reduced cable losses prior to amplification. To avoid aliasing in the heterodyne system, two image rejection high pass filters were used. The dimensions of standard waveguides did not provide suitable cut-off frequencies for this purpose and so custom waveguide sections were fabricated. These rectangular waveguides were designed to operate in the TE_{10} mode with the guide width a set to $\lambda_c/2$ and the desired cut-off wavelength λ_c (Wangsness, 1979). The mechanical designs in Appendix A.2 show that the filters had tapered transitions joining the standard and non-standard waveguide sections. This was to ensure correct matching over the transition region. A photograph of the 11.5 and 17.5 GHz image rejection filters used in System 1 is also provided in Appendix A.2.

For the LOs to be frequency stable, a 10 MHz reference signal was required. This signal was provided by the spectrum analyser and was split in the RF Mast-Head Box using a power splitter. As only half the original power was transmitted in each of the cables after the split, an amplifier, as depicted in the block diagram, was inserted before the power splitter. It was found that the reference signal cable would become a source of self-generated interference and this is discussed in Chapter 4 along with other sources of locally generated interference.

An Agilent 346C noise diode was included in the RF signal path for calibration of the flux scale. The RF switches allowed either the antenna or the noise diode to be selected as input to the various signal paths. It was intended that the noise diode would be used for calibration of system gain (as required by SKA Memo 37), but instead it was only used for system temperature calibration and system health checks during operation in the field.

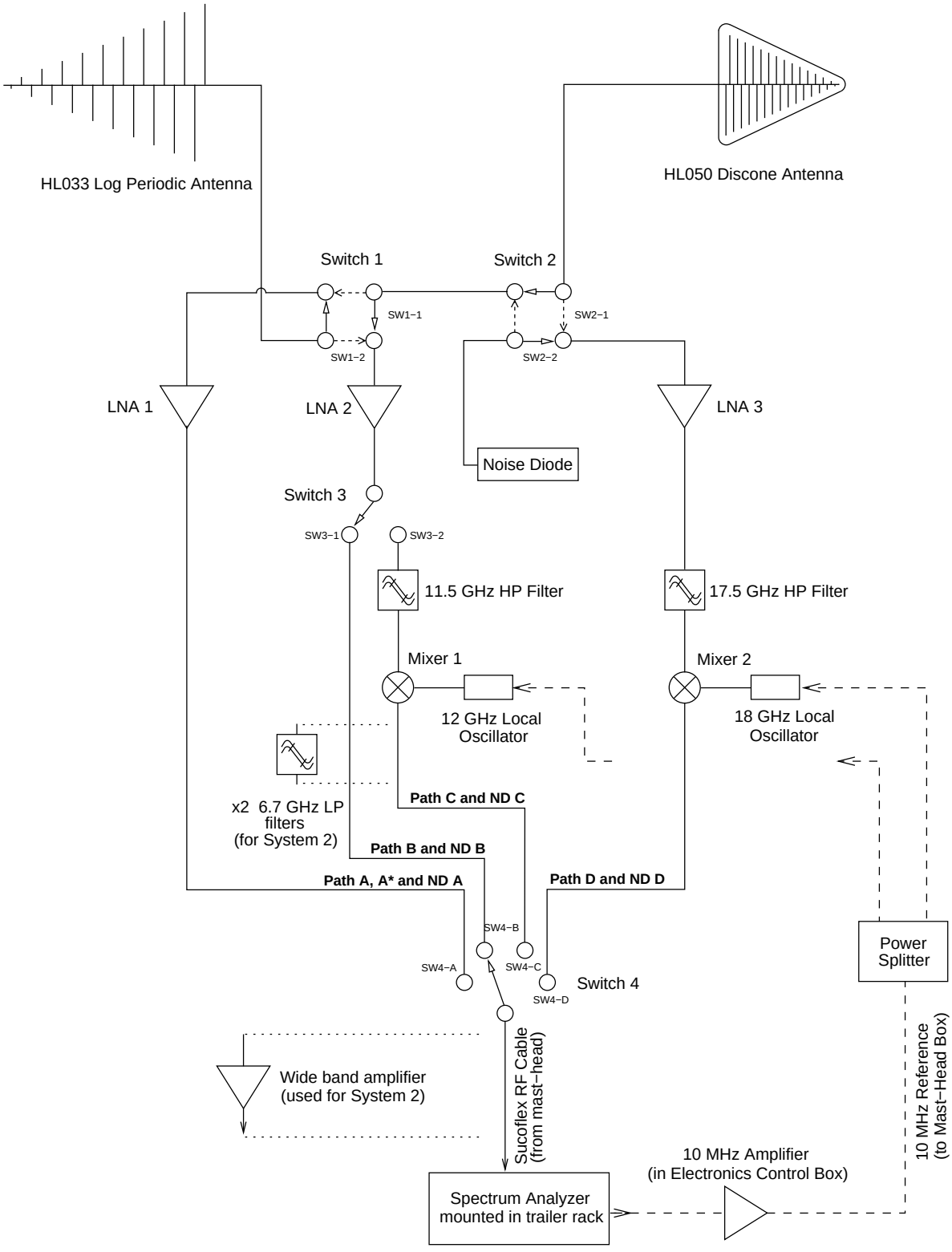

Figure 2.2: Block diagram of RF path layout for the RF sub-system. For System 2 a low noise wide band amplifier was inserted after Switch 4. As indicated this system also had two in-line filters in Path C which filtered out the 12 GHz LO signal present in the mixer output and avoided saturation in this amplifier.

The paths allowing the selection of the noise diode increased the total number of selectable RF signal path permutations. These paths, as well as a *default* path in which neither the amplifiers nor the antennas were selected, are shown in Table 2.2.

Signal Path	Frequency Band	LNA	LO	Signal Input
ND A	0.07-6.0 GHz	1	-	noise diode
ND B	6.0-12.5 GHz	2	-	noise diode
ND C	12.5-18.5 GHz	2	12 GHz	noise diode
ND D	18.5-26.5 GHz	3	18 GHz	noise diode
default	none	-	-	none

Table 2.2: The RF signal paths allowing the noise diode to be selected as an input signal to the RFI measurement system. The *default* path was the 'off state' and did not have any components connected or turned on. Path ND A was the noise diode calibration path used for Paths A and A*, and relates to the frequency bands 0.07 - 6.0 GHz shown in Table 2.1.

A summary of the gain budget for Systems 1 and 3 is shown in Table 2.3. To give a first-order estimate of the total gain of the system, nominal values for the antennas, LNAs and insertion losses for the mixers have been used. A similar summary for System 2 is provided in Table 2.4, with a further 14 dB of gain indicated for the wide band post-amplifier used in this system. As the co-axial cable losses have not been accounted for, these calculations are optimistic when compared to the measured gains, especially for the higher frequency bands. A system gain and noise budget, covered in the following section, took into account these losses and indicated a closer correspondence to the measured values. Thorough system gain tests were performed in the laboratory on all measurement systems, discussed in Section 2.3.2.

Signal Path	Frequency Range GHz	Antenna	G_{ant} dB	LNA	G_{LNA} dB	G_{mix} dB	G_{WBA} dB	G_{sys} dB
A	0.07 - 2.0	HL033	6.5	1	36	0	0	42.5
A*	2.0 - 6.0	HL050	8.5	1	36	0	0	44.5
B	6.0 - 12.5	HL050	8.5	2	34	0	0	42.5
C	12.5 - 18.5	HL050	8.5	2	34	-10	0	32.5
D	18.5 - 26.5	HL050	8.5	3	32	-10	0	30.5

Table 2.3: The estimated system gain based on nominal gains of the antennas, LNAs and mixers in Systems 1 and 3. G_{WBA} is the gain of the wide band amplifier, used only in System 2.

RF signals detected by the measurement systems were measured by an Agilent spectrum analyser assigned to each system. An HP8535E analyser was used for System 3 and two HP8563EC analysers performed the measurements for Systems 1 and 3. Although the op-

Signal Path	Frequency Range GHz	Antenna	G_{ant} dB	LNA	G_{LNA} dB	G_{mix} dB	G_{WBA} dB	G_{sys} dB
A	0.07 - 2.0	HL033	6.5	1	36	0	14.0	56.5
A*	2.0 - 6.0	HL050	8.5	1	36	0	14.0	58.5
B	6.0 - 12.5	HL050	8.5	2	34	0	14.0	56.5
C	12.5 - 18.5	HL050	8.5	2	34	-10	14.0	46.5
D	18.5 - 26.5	HL050	8.5	3	32	-10	14.0	44.5

Table 2.4: The estimated system gain based on nominal gains of the antennas, LNAs and mixers in System 2. G_{WBA} is the gain of the wide band post-amplifier which was only employed in System 2.

erating frequency range of the instruments is 100 kHz to 26.5 GHz, the highest frequency measured was only 12.5 GHz. This was due to the heterodyne design of the RF sub-system, which was necessary to reduce cable losses in the upper frequency bands. A low loss Huber & Suhner Sucoflex 104 cable connected the RF front-end (in the Mast-Head Box) to the spectrum analyser housed in a rack in the trailer cabin. The set-up of the trailer and one of the measurement systems is shown in Figure 2.3 along with a photograph of the RF components inside the Mast-Head Box. Further photographs of the RF assembly are shown in Appendix A.3.

2.2 System Gain and Noise Budget

While building the first system, it was necessary to confirm that it was functioning correctly. To do this, a theoretical gain and system noise budget was computed. A noise figure value was assigned to the components in each signal path (i.e. A, A*, B, C, D) and these were used to determine the effective T_{sys}.

The semi-rigid cables connecting the RF components were removed from the system and their individual losses measured. A value for each cable was selected indicating the maximum loss over the cable's operating frequency. For the other components (LNAs and mixers), a nominal value specified in the manufacturer's data sheet was used. Table 2.5 lists the values used for the components in System 1. The system gain budget that summarises these values is shown in Table 2.6.

The effective noise temperature (T_n) for each component in Table 2.5 was calculated. Using these values and Friis' formula:

$$T_{\text{sys}} = T_1 + \frac{T_2}{G_1} + \frac{T_3}{G_1 G_2} + \dots \tag{2.1}$$

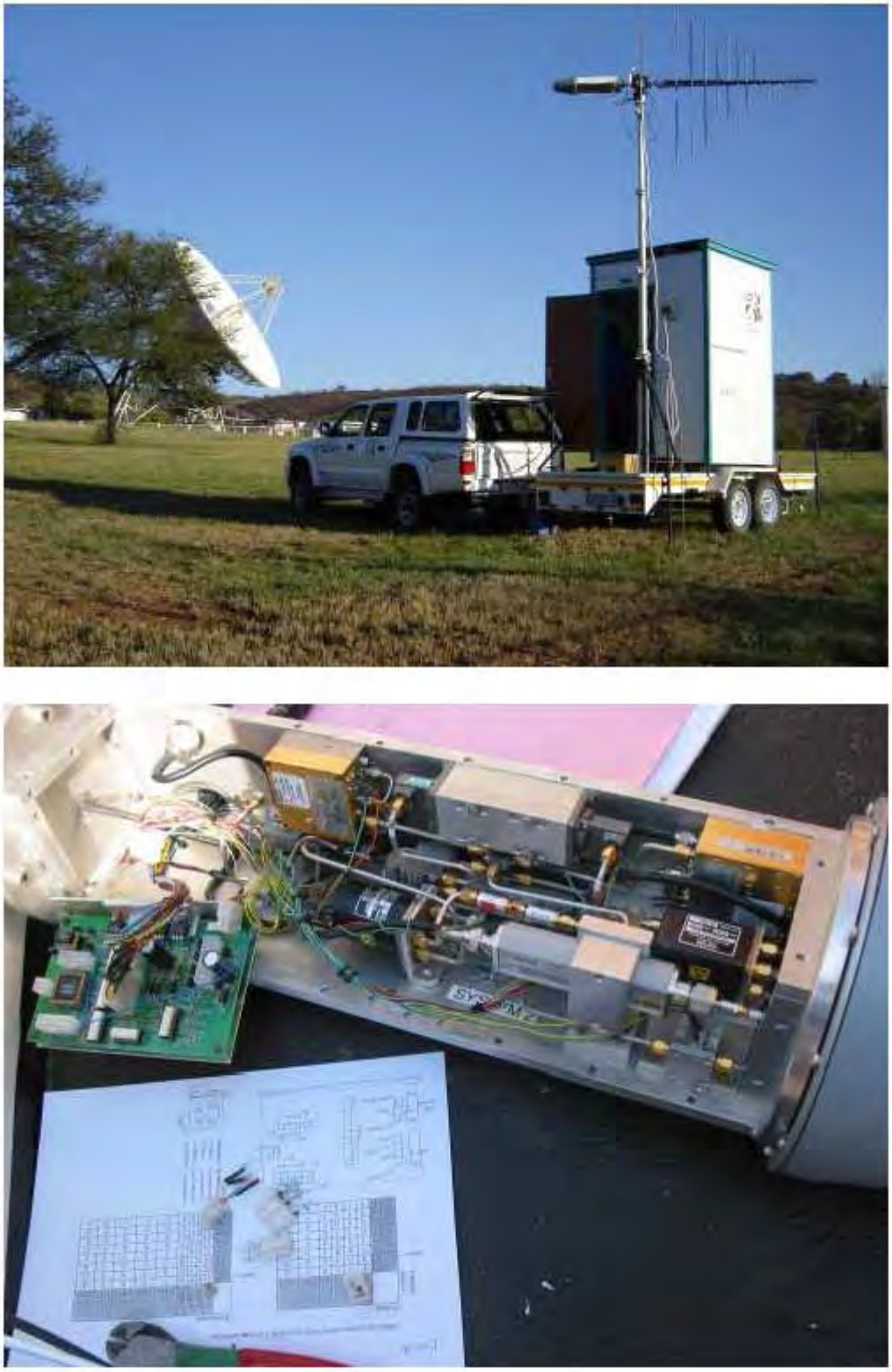

Figure 2.3: Top: The RFI measurement System 3 set up for 'soak' tests at the Hartebeesthoek Radio Astronomy Observatory. Control and RF signal cables connect the Mast-Head Box on the top of the pneumatic mast to equipment such as the control electronics, Control PC and spectrum analyser housed in the trailer cabin. Bottom: An inside view of the RF Mast-Head Box during testing. A printed circuit board (RF Logic PCB) provides power and control logic for the RF components.

Component	Path A	Path A*	Path B	Path C	Path D
Cable	-0.01	-0.05	-0.25	-0.4	-0.75
Switch 2	-	-0.2	-0.4	-0.5	-0.7
Cable	-	-0.05	-0.4	-0.4	-1.5
Switch 1	-0.2	-0.2	-0.4	-0.5	-
Cable	-0.2	-0.2	-1.2	-0.6	-
LNA	36	36	34	34	32
Cable	-0.3	-0.3	-0.5	-0.65	-1.75
Switch 3	-	-	-0.4	-0.5	-
Cable	-	-	-	-0.8	-
HP Filter	-	-	-1	-0.5	-1
Cable	-	-	-	-1	-6
Mixer	-	-	-	-10	-8
Cable	-	-	-	-2	-0.2
Switch 4	-0.2	-0.3	-0.4	-0.3	-0.3
Cable	-0.1	-0.4	-0.6	-0.4	-0.45
Sucoflex	-3	-6	-9	-6	-7

Table 2.5: The nominal gains and losses (in dB) for the components applicable to each signal path in Systems 1 and 3. Components are listed according to their layout as shown in Figure 2.2 i.e. from top to bottom. The first co-axial cable in the list was connected to one of the antennas and the Sucoflex cable connected to the spectrum analyser.

in Equation 2.1, the effective T_{sys} was determined. This calculation also took into account the noise contribution of the spectrum analyser, calculated from the displayed average noise level (DANL) specified in the manufacturer's operating manual (Agilent Technologies, 2004a).

The system gain and noise budgets were calculated for System 2. A similar performance summary is shown in Table 2.7. Comparing T_{sys} to that of System 1 (Table 2.6), a significant improvement can be seen. This is due to the wide band post-amplifier employed, which facilitated a lower T_{sys} for the higher frequency bands. While the gain budget for this system shows a marked performance improvement over System 1, these values vary significantly in comparison to the estimated system gain shown in Table 2.4. This is attributed to the fact that co-axial cable measurements were only conducted for System 1 and were used for the System 2 budget calculations.

Path		A	A*	B	C	D
Gain [dB]	with antenna	38.50	36.30	27.45	17.45	12.35
	without antenna	32.00	28.30	19.45	9.45	4.35
T_{sys} [K]		190.12	283.00	1323.87	8534.93	27362.29

Table 2.6: Summary gain and noise budget for Systems 1 and 3.

In the following sections of this chapter (Sections 2.3.2 and 2.3.3), laboratory measure-

Path		A	A*	B	C	D
Gain [dB]	with antenna	52.40	50.40	40.85	31.05	25.90
	without antenna	45.90	41.90	32.85	23.05	17.90
T_{sys} [K]		146.20	180.27	536.49	651.55	1855.76

Table 2.7: Summary gain and noise budget for System 2.

ments that were performed to determine the system gain and T_{sys} directly are discussed. A comparison with the theoretical calculations done for the system gain and noise budget show some variances, especially at higher frequencies. For the system gain, the measured values are much higher than those calculated for the gain budget. Similarly, the measured T_{sys} is higher than that of the noise budget calculations. This is explained by the choice of cable loss, that was overestimated for most of the cables' operating range in the budget calculations. Confirmation of this is shown in Figure 2.4 where specific component values at selected frequencies were used. As the measurement of the cables was done independently of the RF measurement system, it is also noted that some variances due to component mismatch and hence associated voltage standing wave ratio (VSWR) ripples were not taken into account.

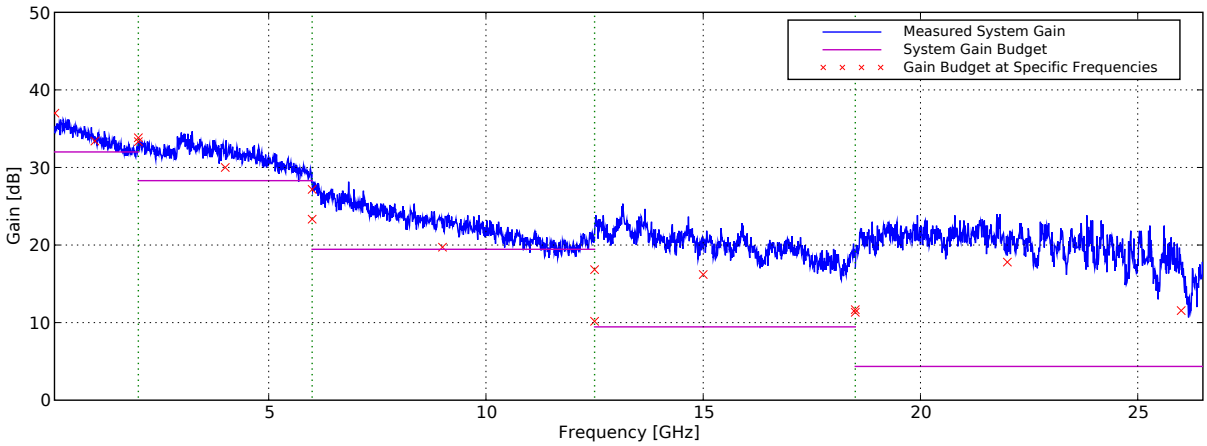

Figure 2.4: Comparison of the gain budget and measured system gain for System 1. Note that the gain budget determined using the component losses at specific frequencies yields results that are closer to those of the measured system gain. The vertical green lines indicate the frequency breaks for different signal paths.

2.3 Laboratory Tests

Laboratory tests were performed on the RF co-axial cables, the image rejection filters, and the complete RF receiver system to measure their frequency responses.

The measurements of the co-axial cables were done for the initial performance tests as described in the system gain and noise budget calculations. The image rejection filters were measured to verify the filter pass bands and cut-off frequencies. Tests on the complete RF receiver system were also performed and these were used for calibration purposes and the determination of matched load spectra.

As a network analyser was not available at the time, the measurements were performed using a test-bench consisting of a frequency synthesiser, power meter and spectrum analyser. These instruments were connected to a HPIB bus, which was controlled by a PC running applications developed in LabVIEW. Initial measurements were done manually. However, to reduce human error and speed up the process, the procedures were automated as much as possible using LabVIEW applications.

Figure 2.5 shows the general layout of the instruments used to conduct the laboratory tests. In most cases data from the measurements were saved to file and used for later off-line analysis.

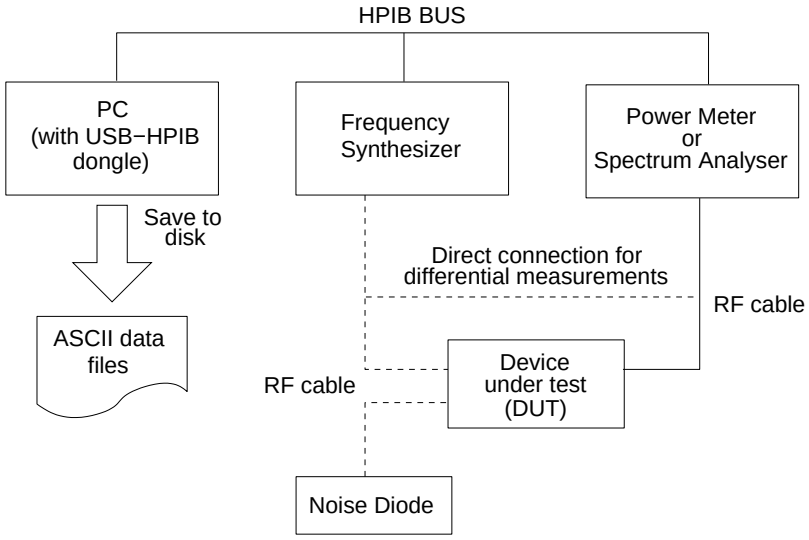

Figure 2.5: Test-bench layout for the laboratory tests. The devices under test were either the RF co-axial cables, image rejection filters or the complete RF system.

2.3.1 Filter Pass Band

To determine the performance of the image rejection filters, differential measurements were made using an HP8360L synthesiser, HP411 power meter and LabVIEW frequency sweeper application. The synthesiser and power meter were configured through software to track each other, and measurements were done in incremental frequency steps across a user-specified bandwidth. The adjustment of other user parameters included the start frequency, stop

frequency, frequency step size and synthesiser power level. The front panel (user interface) and block diagram (source code) for this application are shown in Appendix A.4.

The devices under test were the 11.5 and 17.5 GHz high pass image rejection filters. As shown in Figure 2.5, these devices were connected to the frequency synthesiser and power meter via low-loss RF co-axial cables. A known signal level was then injected at the input of the filter and this was measured by the power meter and recorded to disk on the PC.

For differential calculations to be performed, a second frequency sweep was performed with the filter replaced by a precision adapter. This ensured that anomalies in the test cables, adapters and instruments were removed from the measurement data. The differential calculations for the System 2 filters are shown in Figure 2.6. These plots indicate flat pass bands and cut-off frequencies close to their design specifications.

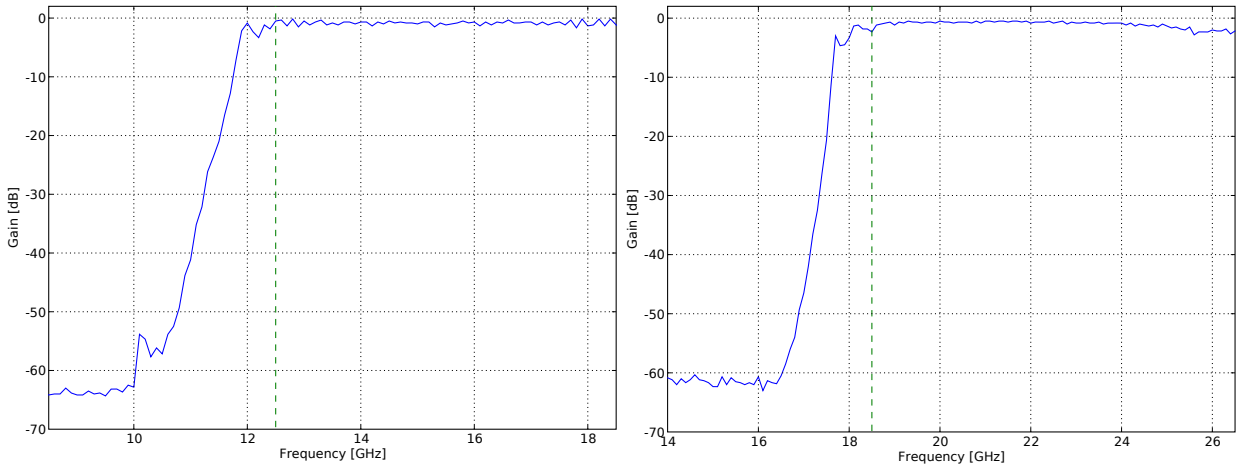

Figure 2.6: Left: Frequency sweep plot of 11.5 GHz image rejection filter for System 2. Right: Frequency sweep plot of 17.5 GHz image rejection filter for System 2. The dotted green line indicates the signal path transitions at 12.5 and 18.5 GHz.

The cut-off frequencies of the filters were chosen to exclude the lower sideband (LSB) images. The IF signals have a lower frequency limit of 500 MHz that avoids the region of passband ripple, and further improves the LSB image rejection.

The filters from all three systems performed according to specification and a comparison is shown in Appendix A.5.

2.3.2 System Gain

The frequency sweeper application developed for measuring the image rejection filters and the co-axial cables was extended to characterise the complete RF system. This procedure was termed the “direct gain method”; it was used for the calibration of the system and hence

the flux scale for the measurements. Additions made to the application included a facility to use two other synthesisers (Hewlett Packard HL8340B and Rohde & Schwarz SMR40) and a facility for signal tracking in the mixed-down signal paths. The power meter was replaced by the spectrum analyser designated to each system and care was taken to ensure that the input signal levels were acceptable for the very sensitive RF front-ends. To avoid damage to the RF front-ends, the input levels were set to -85 dBm.

Reasons for using multiple signal sources arose from the following logistical circumstances:

- A certified re-calibration of the original synthesiser (HP8360L) had not been performed recently. Besides this, the instrument was not suitable for these tests due to the minimum limit of -20 dBm on the output level. No suitable high-precision attenuators were available to reduce signal level;

- The access to rented synthesisers was limited, which meant it was not always possible to use the same instrument.

To conduct the tests, the antennas were disconnected and the output from the synthesiser was connected to the front-end of the system. Measurements were made in 10 MHz steps across the operating frequency (0.07-26.5 GHz) with the RF switching being done manually for each frequency path.

The frequency paths were measured independently and Figure 2.7 shows a plot of the combined results for System 2. Comparison with the system gain in Table 2.7 indicates that the measured gain was generally underestimated by the gain budget. This corresponds to observations made for System 1 (Section 2.2), and is attributed to the choice of component values used in the gain budget calculations for System 2.

The direct gain tests were performed in the laboratory prior to deployment of each system. To provide meaningful calibration data during the field measurements, it was intended that noise power measurements of the noise diode would be used to calculate the system gain. This regular infield calibration was a requirement of SKA Memo 37 but it was found to be unsuitable for this purpose.

Due to the way in which spectrum analysers measure noise power, there were discrepancies of about 4 dB (South African SKA Project, 2006b) between the direct gain method and the noise diode gain method. According to Agilent Application Note 150 (Agilent Technologies, 2004a), Agilent spectrum analysers indicate values lower than the actual value

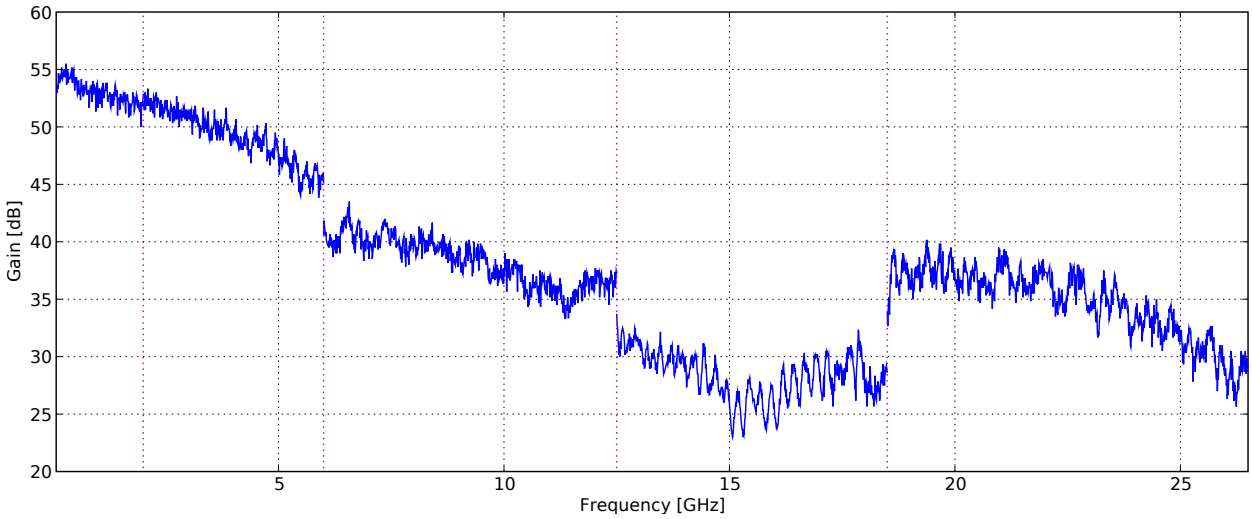

Figure 2.7: System gain measured by the direct gain method for System 2. The measured gain for the signal paths A, A*, B, C and D are shown where the path transitions are indicated by the vertical pink lines.

when measuring noise signals. This is due to the combined effects of the components used in the instrument, namely the IF filter, logarithmic amplifier, envelope detector and video filter. The components in the spectrum analyser IF and video chain were not characterised or defined anywhere in the Agilent instrument documentation. Hence it was not possible to predict their exact response to broadband stochastic signals and so the noise diode gain method was not used to calculate system gain.

2.3.3 System Temperature

Although the noise diode was not used for absolute gain tests, it was used for monitoring relative gain variations during the measurement campaign and also for performing measurements in the laboratory.

Noise diodes are commonly used in the calibration and performance characterisation of radio telescope receiver systems (Kraus, 1966). The principles are well understood and the procedure is termed the Y-factor method. The Y-factor $Y(f)$ defined in Equation 2.2 is the ratio of P_{on} to P_{off},

$$Y(f) = \frac{P_{on}[W]}{P_{off}[W]} \tag{2.2}$$

which are the frequency dependent power levels measured by the spectrum analyser when the noise diode is turned on and off. An effective system noise temperature was calculated

for the paths in each measurement system as:

$$T_{\text{sys}} = \left(\frac{\text{ENR}(f)}{Y(f) - 1} \right) T_0[K] \tag{2.3}$$

where $\text{ENR}(f)$ is the frequency dependent excess noise ratio (ENR) of the noise diode, defined (Agilent Technologies, 2004b) as:

$$\text{ENR}(f) = \frac{T_{on} - T_{off}}{T_0} \tag{2.4}$$

T_0, the physical temperature of the diode, is constant and is set to 290 K. The ENR data used in Equation 2.3 was provided by the manufacturer and are shown in Appendix A.6 for the noise diodes in each system.

For the laboratory tests, the RFI measurement system was set up as it would have been in the field. In terms of Figure 2.5, this meant that the spectrum analyser designated to each system was essentially the measurement device and the respective RF front-end, the device under test (DUT). The diagram indicates the noise diode as being separate of the DUT; however, physically it was located inside the RF Mast-Head Box and was connected as part of the RF assembly.

Using the application developed for conducting the RFI field measurements, a sequence of measurements was executed for each noise diode signal path in the system. During a measurement the RF switches were switched automatically, disconnecting the antennas and connecting the noise diode to the RF system input. In order to perform the Y-factor measurements two frequency sweeps were done for each path: one with the noise diode powered on and one with it powered off.

Table 2.8 shows the parameters used for the various signal paths measured for the noise diode calibration method. These values were used for the T_{sys} laboratory tests as well as the regular calibration measurements performed as part of the RFI measurement schedule.

The noise diode measurements and calculated T_{sys} for all noise diode signal paths in System 2, are shown in Figure 2.8. This plot indicates that the system surpassed the $T_{\text{sys}} < 300\,\text{K}$ specification for Mode 2 measurements with the exception of signal path ND C (12.5 - 18.5 GHz). Similar performance plots for the other two systems are shown in Appendix A.7; these systems performed well below the specifications for Mode 1 measurements across the whole operating frequency (70 MHz - 26.5 GHz). Because the measured noise temperature depends only on the ratio of spectrum analyser power measurements (the Y-factor), it is not affected by the systematic measurement error in absolute power for noise signals described in Section 2.3.2.

Signal Path	$f_{low} - f_{high}$ MHz	Δf_{sweep} MHz	ΔT_{sweep} sec	RBW MHz	VBW Hz
ND A	70 - 2000	482.5	4.1	1	300
ND A	2000 - 6000	500	4.2	1	300
ND B	6000 - 12500	650	5.5	1	300
ND C	12500 - 18500	600	5.0	1	300
ND D	18500 - 26500	800	6.7	1	300

Table 2.8: The noise diode frequency bands and parameters used for calibrating T_{sys} in the laboratory. To cover the frequency range ($f_{low} - f_{high}$) for each band, multiple scans were required with the spectrum analyser frequency span Δf_{sweep}. These scans were performed on the spectrum analyser with the associated sweep time (ΔT_{sweep}), resolution bandwidth (RBW) and video bandwidth (VBW) settings for each path.

The system gain G_{sys} for System 2 is shown in Figure 2.8 and was determined as:

$$G_{\text{sys}}[\text{dB}] = 10 \log \left(\frac{P_{on}\,[W] - P_{off}\,[W]}{\text{RBW}\,[\text{Hz}] \times k \times 300 \times 10^{\frac{\text{ENR(f)}\,[\text{dB}]}{10}}} \right) \tag{2.5}$$

where k is Boltzmann's constant. Comparison with the direct gain measurements in Figure 2.7 illustrates an offset associated with the ENR in noise power measurements by spectrum analysers. Notice that both gain plots show the same structure, such as VSWR ripples.

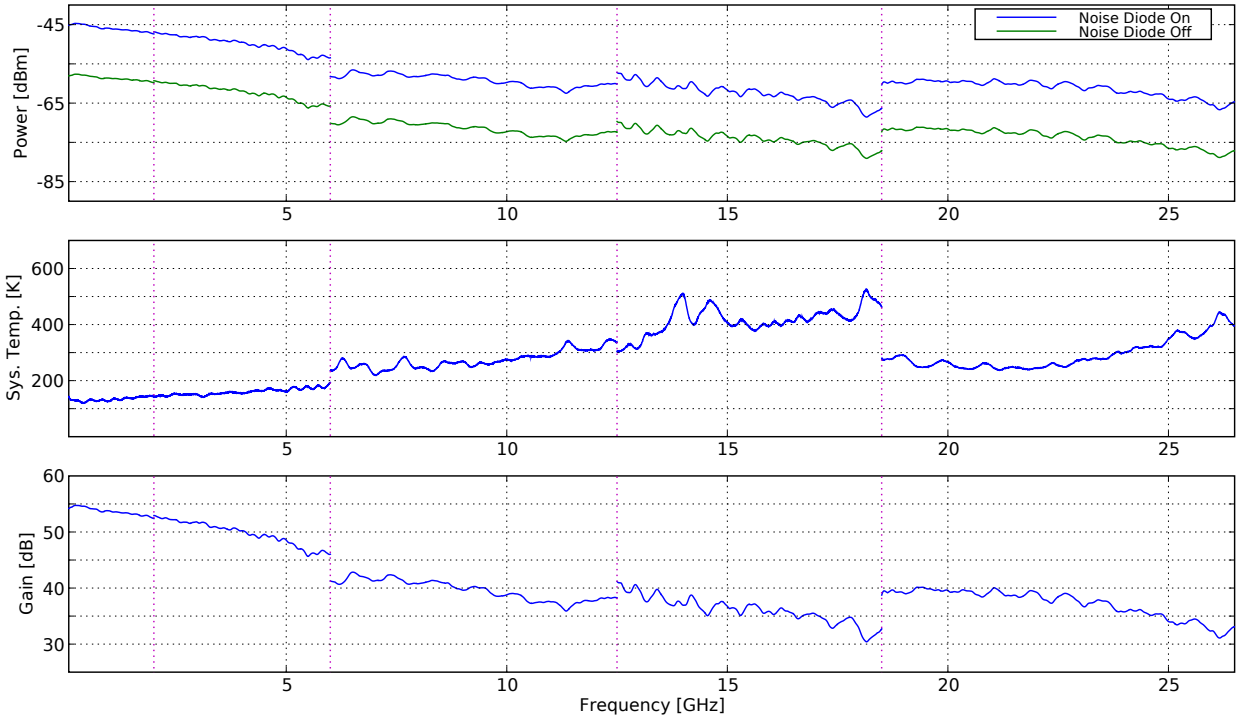

Figure 2.8: Laboratory tests performed for RFI measurement System 2. Linear filtering was done prior to the data processing to smooth out the inherent noise in the on and off noise diode data. Top: Noise Diode calibration measurements. Middle: System Temperature. Bottom: System Gain.

2.3.4 Matched Load Spectra

SKA Memo 37 required that provision was made for matched load spectra of the RFI measurement systems. This provided a check that no internal interference was being injected into the RF signal path after the antenna terminals. It also provided a means of investigating VSWR induced baseline ripples.

The calibration noise diode provided a convenient $50\,\Omega$ matched load to connect to the input terminals of the RF receiver system via the RF switches. Data for this procedure was derived from the measurements used to calculate $T_{\rm sys}$ (Section 2.3.3). In this case the data was used to calculate the output spectrum in units of equivalent incident signal flux using:

$$\begin{aligned} S(f)_{\rm load}\,[{\rm W.m^{-2}.Hz^{-1}}] &= \frac{8\pi}{G_{ant}(f)} \times \frac{P_{\rm load}(f) \times k \times T_0 \times {\rm ENR}(f)}{P_{\rm on}(f) - P_{\rm off}(f)} \\ &\quad \times \frac{f^2\,[{\rm Hz^2}]}{c^2\,[{\rm m^2.s^{-2}}]} \end{aligned} \tag{2.6}$$

where $P_{\rm load}$ is the detected power with the noise diode either in its on or off state. G_{ant} is the frequency dependent antenna gain.

The matched load spectra plot for System 2 is shown in Figure 2.9. It shows that the RF signal path between the input of the receiver system and the spectrum analyser was intact, and no extraneous signals from the surrounding electronics or RF components in the Mast-Head Box were being injected into the system signal paths. Systems 1 and 3 indicated similar results. The matched load spectra for these systems are located in Appendix A.8.

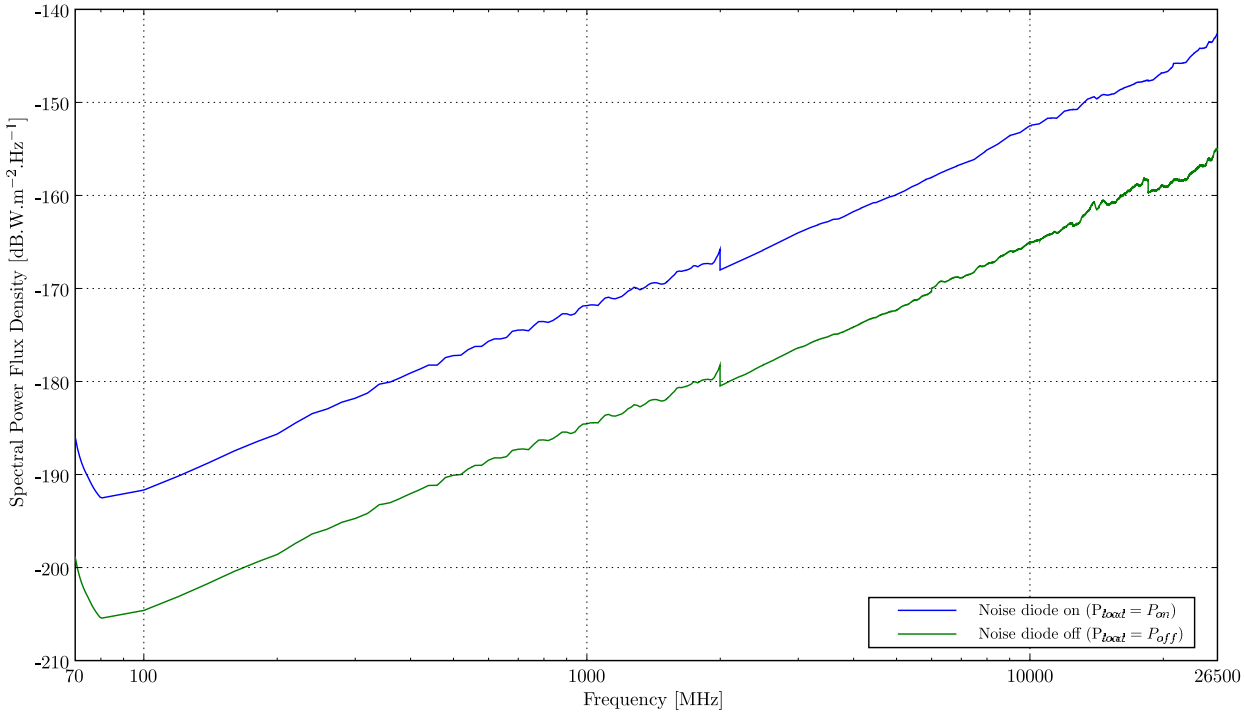

Figure 2.9: Matched load spectra for RFI System 2.

Chapter 3

Control and Data Acquisition Sub-System

This chapter details the control and data acquisition sub-system of the RFI measurement system. It explains the physical layout, the hardware and the software used. The improvement to the performance of the control software when moving from the prototype system to the final design is outlined in Section 3.4.

3.1 Background

The control sub-system was developed in two stages. The first stage involved the building of a prototype system. This was refined to a final design that was implemented on all three measurement systems.

During the process, upgrades were made to the physical layout, the hardware and the software. Significant upgrades were made to the trailer, the motor system for controlling antenna positioning and the control electronics. Relevant changes to the microcontroller and the measurement schedule software were made to accommodate these upgrades. This will be dealt with in Section 3.2.5 on the prototype system after the final design has been discussed.

An effort was made to screen the electro-magnetic interference (EMI) from all electronic devices, and the LCD monitor, keyboard and mouse were removed from the Control PC. To operate the Control PC, a laptop running VNC was used to connect remotely over an Ethernet LAN. The VNC application allowed the Control PC desktop to be shared and controlled from a laptop as if were its own desktop. Details of the efforts to screen the control system from EMI are discussed in Chapter 4. A set of photographs in Appendix B.1 show the prototype and production systems.

3.2 Hardware

3.2.1 Layout Overview

The block diagram in Figure 3.1 shows the layout for the control sub-system on the RFI measurement trailer.

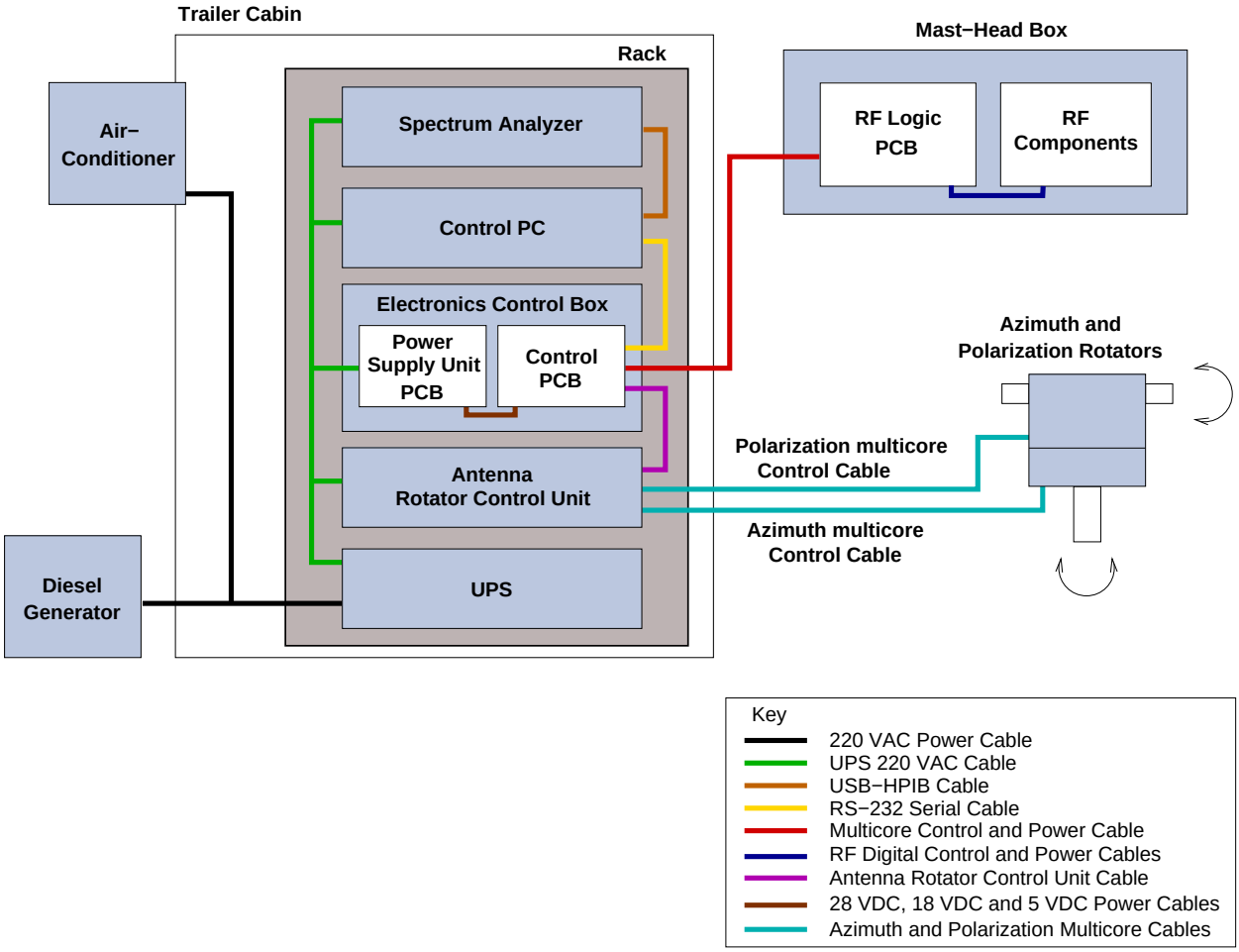

Figure 3.1: Block diagram of the layout of the control and data acquisition sub-system for the RFI measurement trailer. The RF co-axial cables have been omitted and only the control cables are indicated. Details of the RF cables are outlined in Table 3.1 which lists all cables used in the RFI Measurement System.

A diesel generator mounted on the trailer provided power to an air-conditioner and an uninterruptable power supply (UPS) in the trailer cabin. The UPS was used to provide a reliable power source for the spectrum analyser, Control PC, Electronics Control Box and Antenna Rotator Control Unit. The air-conditioner provided a stable environment for the instruments in the cabin.

The control and data acquisition software ran on a rack-mounted PC in the cabin. A microcontroller on the Control printed circuit board (PCB) handled the low-level tasks

associated with the Antenna Rotator Control Unit and the RF Logic PCB in the Mast-Head Box. The Control PC communicated with the microcontroller in the Electronics Control Box via an RS-232 link.

Communication between the spectrum analyser and the Control PC was done via a USB-HPIB dongle, which allowed commands to be sent to the spectrum analyser and data to be read back to the PC.

The cables indicated in Figure 3.1 connected, controlled or supplied power to each of the components in the RFI measurement system. Details of these cables, and the RF signal cables that are not included in the figure, are listed in Table 3.1.

Cable	Details
220 VAC Power Cable	Standard copper mains cable used to wire the trailer cabin plug sockets. EMI line filters used on the UPS input and output lines.
UPS 220 VAC Cable	Standard power cable with EMI line filters on the Faraday cages for the UPS (output), spectrum analyser, Electronics Control Box and Control PC chassis.
USB-HPIB	A commercial USB-HPIB dongle connected the Control PC USB port to the spectrum analyser HPIB port.
RS-232 Serial Cable	Screened serial cable with metallic connectors for shielding on the Electronics Control Box and Control PC interfaces.
Multi-core Control and Power Cable	10 m, screened 19 core cable carrying power and digital signal lines from the Control PCB in the Electronics Control Box to RF Logic PCB in the Mast-Head Box. Cannon connectors used for shielding on both interfaces.
RF Digital Control and Power Cables	Internal wiring in the Mast-Head Box with Molex connectors on all interfaces on the RF Logic PCB.
Antenna Rotator Control Unit Cable	Screened cable with manufacturer supplied connector on Antenna Rotator Control Unit.
28 VDC, 18 VDC and 5 VDC Power Cables	Internal wiring in the Electronics Control Box for supplying power to the Control PCB and 10 MHz reference amplifier.
Azimuth and Polarisation Multi-core Cables	Two screened 7 core cables with manufacturer supplied connectors to the Azimuth and Polarisation Rotators.
Sucoflex RF Signal Cable	A Sucoflex 104 RF cable with N-type connectors connecting the RF output on Mast-Head Box to the spectrum analyser.
10 MHz Reference Cables	A RG-223 cable connected the 10 MHz spectrum analyser output to the 10 MHz amplifier in the Electronics Control Box. A 10 m RG-223 cable connected the Electronics Control Box to the power splitter in the Mast-Head Box.

Table 3.1: List of the cables used to connect the Mast-Head Box, Antenna Azimuth and Polarisation Rotators, and the rack-mounted instruments in the trailer cabin.

3.2.2 The Control PCB

The rack-mounted Electronics Control Box housed the power supplies for the Control PCB and provided power to the RF components in the Mast-Head Box via the RF Logic PCB. In the three production systems, the microcontroller used for the system control was an Atmel ATmega8535. The RF switching, antenna polarisation and azimuth rotator control were handled by the microcontroller on the Control PCB. These functions are dealt with in Sections 3.2.3 and 3.2.4 later in this chapter.

All control functions handled by the microcontroller were initiated by ASCII commands sent from the Control PC via an RS-232 interface. The incoming serial line was converted to a multi-drop RS-485 bus and then into TTL for the microcontroller. The multi-drop communication allowed commands sent to the microcontroller to be echoed back to the PC regardless of whether the microcontroller was operational or not. This formed a suitable check that the Electronics Control Box was powered on and that there was continuity in the communication lines. The schematics for the Control PCB and Power Supply Unit PCB are shown in Appendix B.3 and B.2 respectively along with photographs and PCB layouts.

The diagram in Figure 3.2 shows the relationship between each of the control system components. As illustrated, a temperature sensor was used by the microcontroller for monitoring the RF components inside the RF Mast-Head Box during operation. An Analog Devices TMP36 temperature sensor was installed in the Mast-Head Box and its output was connected to the microcontroller via lines in the Multi-core Control and Power Cable.

To reduce radiation of the switching and clocking signals from the microcontroller, a Faraday cage was built around the Control PCB and feed-through capacitors and ferrite chokes were used on all incoming and outgoing lines. The digital signal lines were also optically isolated to further reduce EMI. The photograph in Figure 3.3 shows the Power Supply Unit PCB and Control PCB installed in the Electronics Control Box along with ferrite chokes and Control PCB Faraday cage.

3.2.3 RF Switching and RF Logic

The switching of the RF components in the Mast-Head Box was controlled by the RFI Measurement Scheduler application running on the Control PC via the Control PCB. Six encoded switching lines from the Control PCB were connected to a Xilinx XC9572XL CPLD on the RF Logic PCB in the Mast-Head Box via the 10 metre Multi-core Control and Power

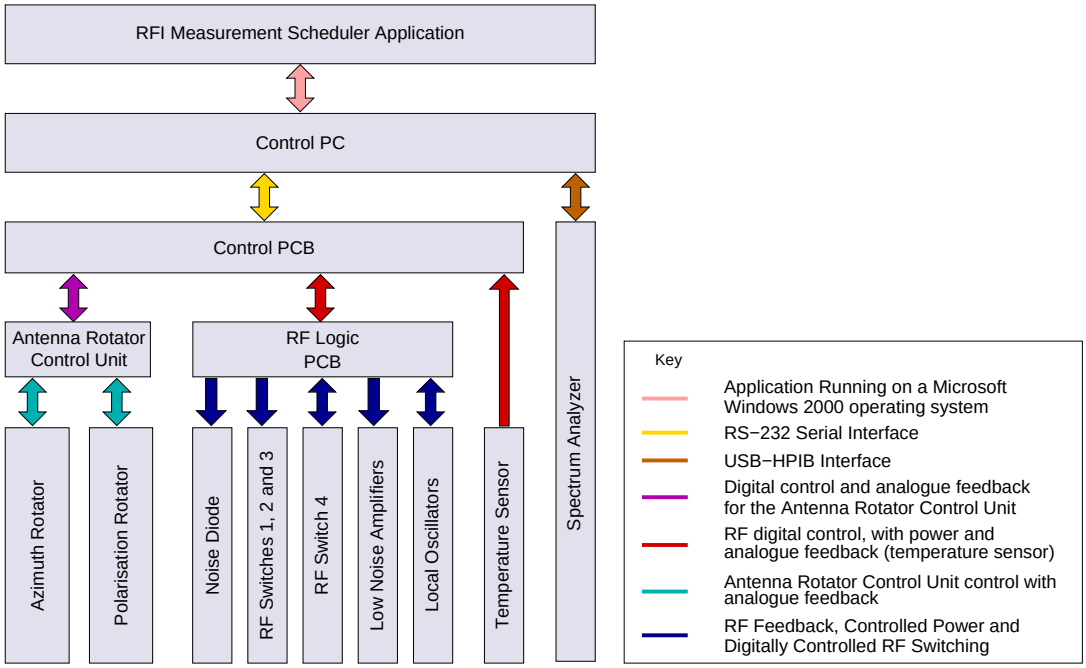

Figure 3.2: Logical layout of the components and interfaces for the Control and Data Acquisition Sub-System. While the temperature sensor received power from the regulated power supplies on the RF Logic PCB, the temperature feedback was connected to the Control PCB (microcontroller) via linear optocouplers, and no logic or control functions were performed by the RF Logic PCB.

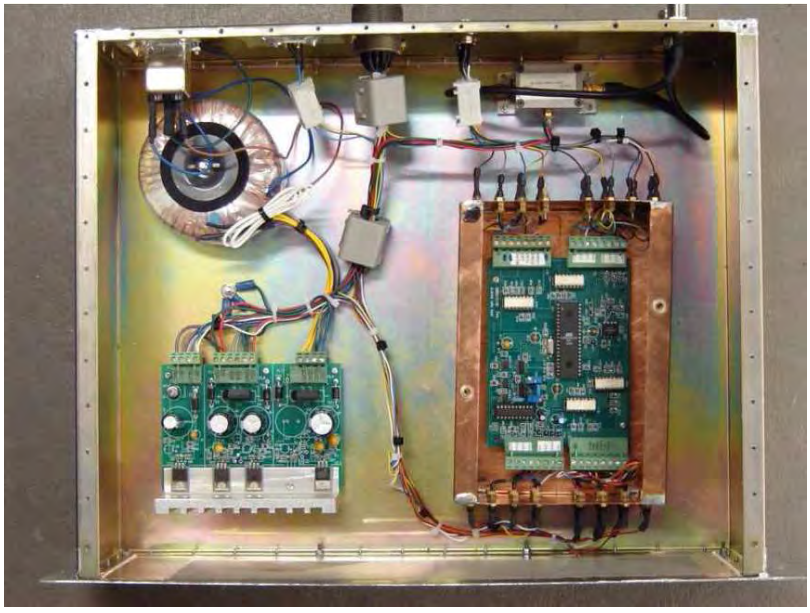

Figure 3.3: Electronics Control Box with the Power Supply Unit PCB (bottom left) and Control PCB (right). The lid for the Faraday cage surrounding the Control PCB with the microcontroller has been removed for the photograph and the feed-through capacitors can be seen at the top and bottom of this copper box. Ferrite chokes are attached to all cables passing through the back panel (top) of the Electronics Control Box and the amplifier for the 10 MHz reference signal is mounted between this panel and the Control PCB.

Cable. The CPLD decoded the switching lines and directed the switching of the RF coaxial switches and power supplies for the noise diode, LOs and LNAs. Raw DC power was provided by the Electronics Control Box while the RF Logic PCB regulated power supplies for the Mast-Head Box components.

Two different electronic mechanisms were required for the RF switches. The first type of switch required a latched signal, and the second a pulsed signal of duration > 50 ms. The commands sent to the microcontroller contained state information for each of the six switching lines. These lines were encoded separately for the latched and pulsed line groups and were decoded by the CPLD to provide the logic for the RF switches and power supplies for the RF components (e.g. noise diode, LOs and LNAs). Table 3.2 summarises the combinations of latched and pulsed switching line states for the RF component switching states.

RF Switching State	RF Path	Data Byte (in hexadecimal)	Pulsed Switching Lines (PULSE)	Latched Switching Lines (LATCH)	LNA	Local Oscillator	RF Switch 1 Position	RF Switch 2 Position	RF Switch 3 Position	RF Switch 4 Position
0	A	18	011	000	1	None	SW1-1	SW2-2	SW3-2	SW4-A
1	A*	00	000	000	1	None	SW1-2	SW2-2	SW3-1	SW4-A
2	ND A	20	100	000	1	None	SW1-2	SW2-1	SW3-1	SW4-A
3	B	11	010	001	2	None	SW1-1	SW2-2	SW3-1	SW4-B
4	ND B	31	110	001	2	None	SW1-1	SW2-1	SW3-1	SW4-B
5	C	1A	011	010	2	12 GHz	SW1-1	SW2-2	SW3-2	SW4-C
6	ND C	3A	111	010	2	12 GHz	SW1-1	SW2-1	SW3-2	SW4-C
7	D	23	100	011	3	18 GHz	SW1-2	SW2-1	SW3-1	SW4-D
8	ND D	03	000	011	3	18 GHz	SW1-2	SW2-2	SW3-1	SW4-D
9	default	0C	001	100	None	None	None	None	None	None

Table 3.2: Summary of the RF component switching states for each allowable RF signal path. RF Switch positions relate to those indicated in the RF layout block diagram (Figure 2.2 in Chapter 2). For each RF path the bit information indicating the state of the pulsed and latched switching lines was concatenated in binary format to form a Data Byte where the two most significant bits were unused and set to 0.

In terms of selecting a valid RF path neither the microcontroller nor the CPLD were made aware of incorrect combinations of latched and pulsed input lines. Instead, valid combinations were stored in the RFI Measurement Scheduler application, which permitted only the allowed switching states to be selected. The specific information stored took the form of a unique *Data Byte* (indicated in Table 3.2). This byte constituted part of the

command message sent to the microcontroller from the Control PC.

Unused states for each of the switching line groups were mapped to the *default* state by the CPLD where all switchable RF components were powered off and no switching was performed on the RF switches. The truth tables shown in Tables B.1 and B.2 of Appendix B.5 detail all states for the latched and pulsed switching signals.

Some of the RF components provided feedback information about their current state. The feedback lines indicating the frequency lock for the LOs and those indicating the mechanical position for Switch 4 were connected to the microcontroller via the CPLD. To reduce the number of pins used on the microcontroller and also the number of signal lines used in the Multi-core Control and Power Cable, the feedback lines from Switch 4 were encoded by the CPLD. As the information concerning the state of the other RF components was incomplete, no attempt was made to deal with switching malfunctions automatically. Instead, feedback information was used for testing purposes only. Table B.3 in Appendix B.5 details the encoded feedback lines from Switch 4. The CPLD logic used for the RF switching and feedback lines is shown in Figure B.15 of the same appendix. A photograph of the RF Logic PCB connected inside the Mast-Head Box is shown in Figure 3.4.

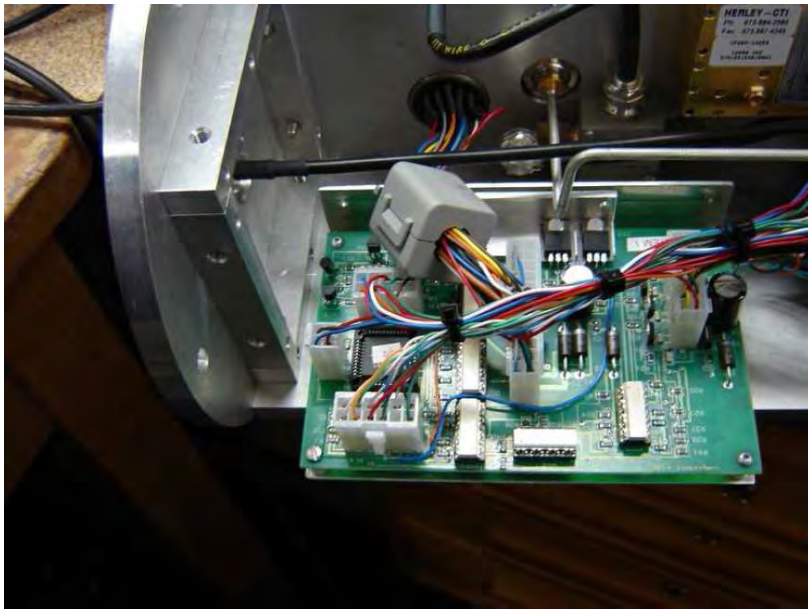

Figure 3.4: Photograph of RF Logic PCB connected inside Mast-Head Box. To reduce EMI a large ferrite choke is clamped to the power and signal lines (from the Multi-core Control and Power Cable) as they enter the Mast-Head Box via the panel mount connector on the back panel. These lines connect to the centre socket on the RF Logic PCB and the remaining connectors connect power and CPLD decoded control lines to the RF components.

3.2.4 Antenna Control

The RFI measurement protocol, SKA Memo 37, required that the antennas be pointed towards any azimuth, and that they could be configured for reception of either horizontal or vertical polarisation. To facilitate this, a commercial mast-head mounted antenna rotator and its associated control unit were used (Yaesu G-5500). The Antenna Rotator Control Unit provided an interface for manual and remote operation of the polarisation and azimuth rotators. Using the remote interface, two control lines and one feedback line were used by the microcontroller to track and position each of the rotators as shown in Figure 3.5.

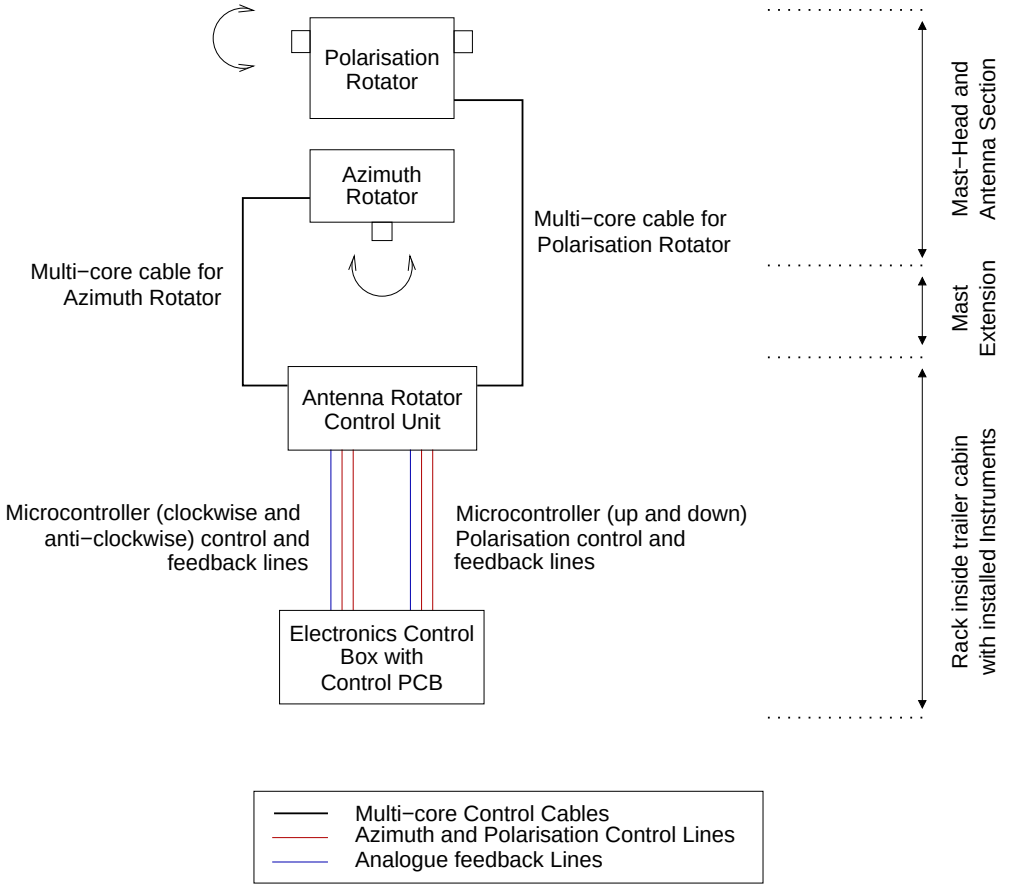

Figure 3.5: Diagram of the antenna control system showing the interfaces between the microcontroller on the Control PCB, the Antenna Rotator Control Unit and both the azimuth and polarisation rotators.

The feedback lines that were position-defined output voltages from the rotators were measured by the analog-to-digital converter (ADC) in the microcontroller. The azimuth and polarisation rotators allowed 450 degrees and 180 degrees of rotation respectively. As only 360 (azimuth) and 90 degrees (polarisation) were needed to position the antennas, an offset was added to move the operating regions away from the limits of the mechanical constraints. This also helped to avoid misalignment and non-linearity issues that were experienced on

the potentiometer feedback for positions close to the limits. Full flexibility for reconfiguring these positions was provided by position information sent to the microcontroller from the Control PC. This allowed the rotators to be positioned at any point.

3.2.5 Prototype System

The prototype system allowed verification of the system design before it was duplicated on the remaining two systems (Systems 2 and 3). After a design review of the prototype, various upgrades and modifications were made. This became System 1, which was one of the production systems used for remote site RFI measurements.

The microcontroller used in the prototype was an Atmel AT90S8535. Due to component availability problems, this was upgraded to an ATmega8535 in the three production systems. The prototype logic for decoding the switching signals in the Mast-Head Box was implemented using standard logic ICs. These proved to be difficult to debug and time consuming to assemble. A single chip solution, in the form of the Xilinx XC9572XL CPLD, was therefore opted for. The so-called Control PCB and RF Logic PCB had both been assembled on veroboard for the prototype but these were replaced with printed circuit boards in the production systems.

As no Antenna Rotator Control Unit or Azimuth Rotator were available at the time the prototype was assembled, a customised assembly for the azimuth rotation was developed. This assembly consisted of a DC motor connected to a gearbox and a Leine & Linde 672 serial angle encoder fixed at the base of the mast on the trailer. On command, the angle encoder provided position feedback to the microcontroller, in the form of ASCII messages (Leine & Linde, 2001). Due to the need for bi-direction communication between the Control PC and microcontroller as well as the angle encoder and the microcontroller, a multidrop RS-485 serial interface was used. In order to direct the position of the DC motor based on the angle encoder feedback, an H-bridge (LMD18200) was provided to interface the digital control lines from the microcontroller to the DC motor. A crude proportional control system with pulse width modulation was used to control the rotation of the mast.

For providing the antenna polarisation rotation, a refurbished polarisation rotator was used in conjuction with two relays and the rotator's potentiometer feedback. Two control lines from the microcontroller directed the polarisation rotator via the relays and the potentiometer output voltage was read by the ADC on the microcontroller.

While the prototype hardware used for antenna control was found to be reliable it was not

suited for duplication on the other two measurement systems due to component availability. Instead it was replaced by the Antenna Control Unit, Polarisation Rotator and Azimuth Rotator and only the RS-485 bus was retained. As mentioned, the configuration of the bus was found to be suitable for diagnostic purposes as it allowed commands sent by the Control PC to be echoed back, regardless of whether the microcontroller had received them or not. Using this test during field operations, two PCI serial cards with unreliable ground connections were identified and removed from the system.

The message protocol used by the angle encoder was already part of the microcontroller control code. It was found to be robust, and therefore was retained for use in the production systems. The details regarding the protocol and the control messages will be discussed in Section 3.3.2.

The last major change for the prototype system was to the trailer on which the telescopic mast was mounted and the rack containing the instruments such as the spectrum analyser, Control PC and Electronics Control Box. For the prototype, the rack was placed inside a container at the Karoo 3 core site. The control and RF cables were fed through a cable feed hole in the wall to a prototype trailer outside. The three production systems had the rack mounted inside the cabin trailer in which the instruments were permanently installed.

3.3 Software

This section describes the RFI Measurement Scheduler software running on the Control PC, the microcontroller control software and the interaction between them.

3.3.1 RFI Measurement Scheduler

The RFI measurement schedule software was developed in the National Instruments LabVIEW environment. A LabVIEW program is called a virtual instrument (VI) and its appearance and operation imitates physical instruments such as spectrum analysers and power meters (National Instruments, 2006). A virtual instrument consists of a user interface with visible control and indicator objects. The function of the controls is to mimic the dials, knobs, push buttons and other physical items that are found on an instrument's front panel. Examples of indicators would be items such as LEDs or graphs. Associated with the front panel is a block diagram, which is the code that interfaces the front panel objects with the instruments. The code resembles a flow chart with interconnections between virtual instru-

ments indicating the data-flow between them. At this abstract level, a LabVIEW application can be used to control and communicate with multiple instruments using a single interface. Figure 3.6 shows the front panel interface for the RFI Measurement Scheduler VI and a section of the associated block diagram is shown in Figure 3.7. The complete block diagram for the RFI Measurement Scheduler VI is detailed in Appendix B.6.

The RFI Measurement Scheduler VI controlled all aspects of the system hardware, either by commands sent via the RS-232 serial line to the microcontroller or via the USB-HPIB interface to the Agilent spectrum analyser.

The frequency spectrum (70 MHz - 26.5 GHz) was broken up into the frequency bands, as per SKA Memo 37. These bands are specified later in Tables 5.1 (Mode 1) and 5.3 (Mode 2) of Chapter 5.

Each frequency band represented a separate measurement for the RFI Measurement Scheduler VI. Measurements were defined in a schedule file that contained the associated measurement parameters for the set-up of the spectrum analyser, RF sub-system and antenna control sub-system. The schedule file was a "tab-delimited" ASCII text file where each row represented a measurement and the columns the associated parameters. The details of the fields used in the schedule file are shown in Table 3.3 and the Mode 1 and Mode 2 schedules are provided in Appendices F.1 and F.2 respectively.

Field No.	Field Name	Comments
1	Measurement Number	Integer representing the current row/measurement
2	Band Start Frequency	Float value in MHz
3	Band Stop Frequency	Float value in MHz
4	Frequency Span	Spectrum analyser span (sub-scan); float value in MHz
5	Unused	Reserved for debugging; Float value
6	Resolution Bandwidth	Spectrum analyser setting; integer value in kHz
7	Video Bandwidth	Spectrum analyser setting; integer value in Hz
8	Sub-scan Sweep Time	Spectrum analyser span sweep time [sec]; float value
9	Band Repeats	No. of repeats across the frequency band; integer value
10	Reference Level	Spectrum analyser reference level in dB; integer value
11	RF Switching State	Integer representing the RF Path (from Table 3.2)
12	Noise Diode State	Off state = '0', on state = '1'; integer value
13	Antenna Polarisation	Horizontal = '0', vertical = '1'; integer value
14	Unused	Reserved for future use and debugging; integer value
15	Azimuth Pointing	Current azimuth pointing; (1-3) or (1-5); integer value
16	No. of Azimuth Pointings	Total No. of azimuth pointings; (3 or 5); integer value

Table 3.3: Definition of the fields in the schedule file which were used as input to the RFI Measurement Scheduler VI.

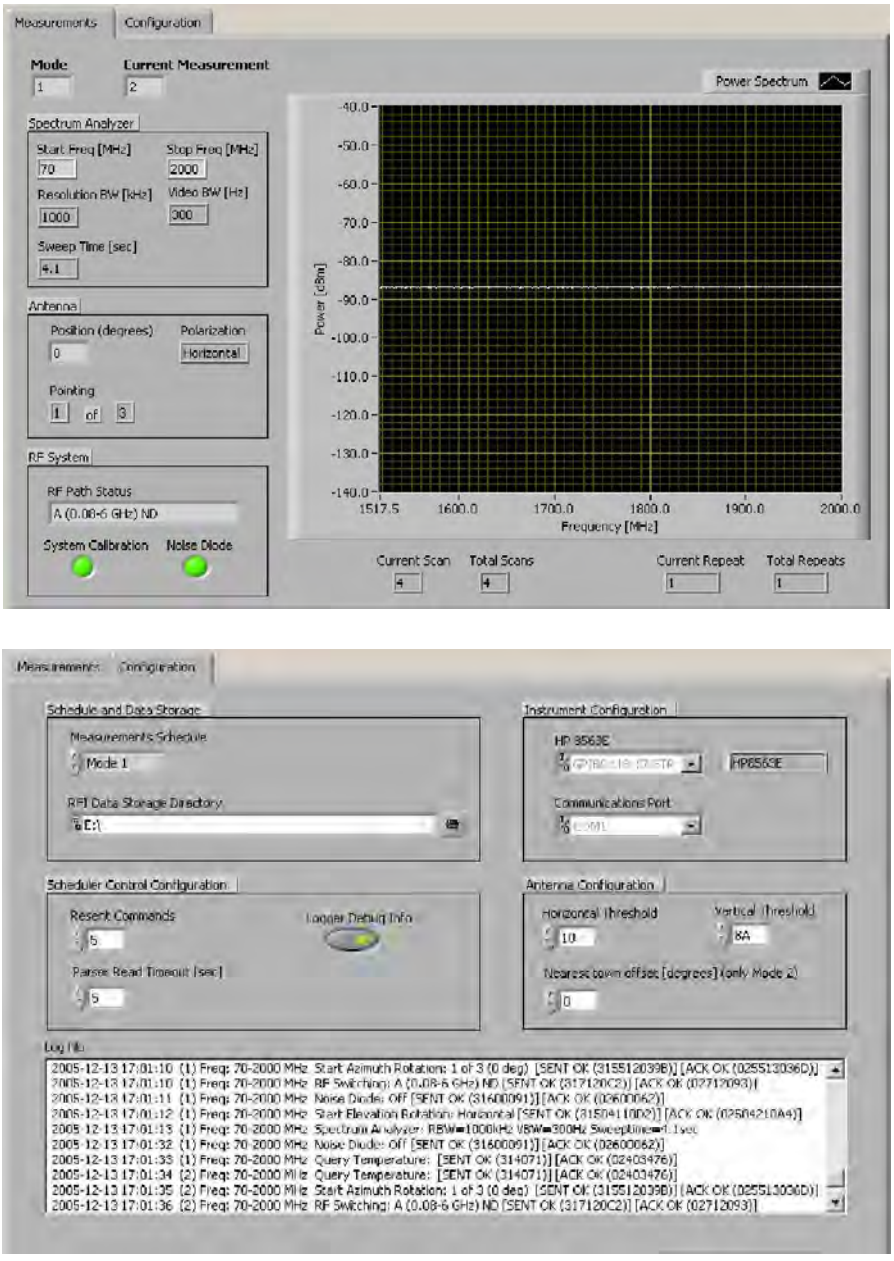

Figure 3.6: Top: The front panel of the RFI Measurement Scheduler Application showing the measurement of RFI data by the spectrum analyser. Bottom: Configuration panel used to adjust instrument and measurement settings. The Log File window at the bottom of this panel shows specific details regarding the communication and control of the microcontroller and spectrum analyser.

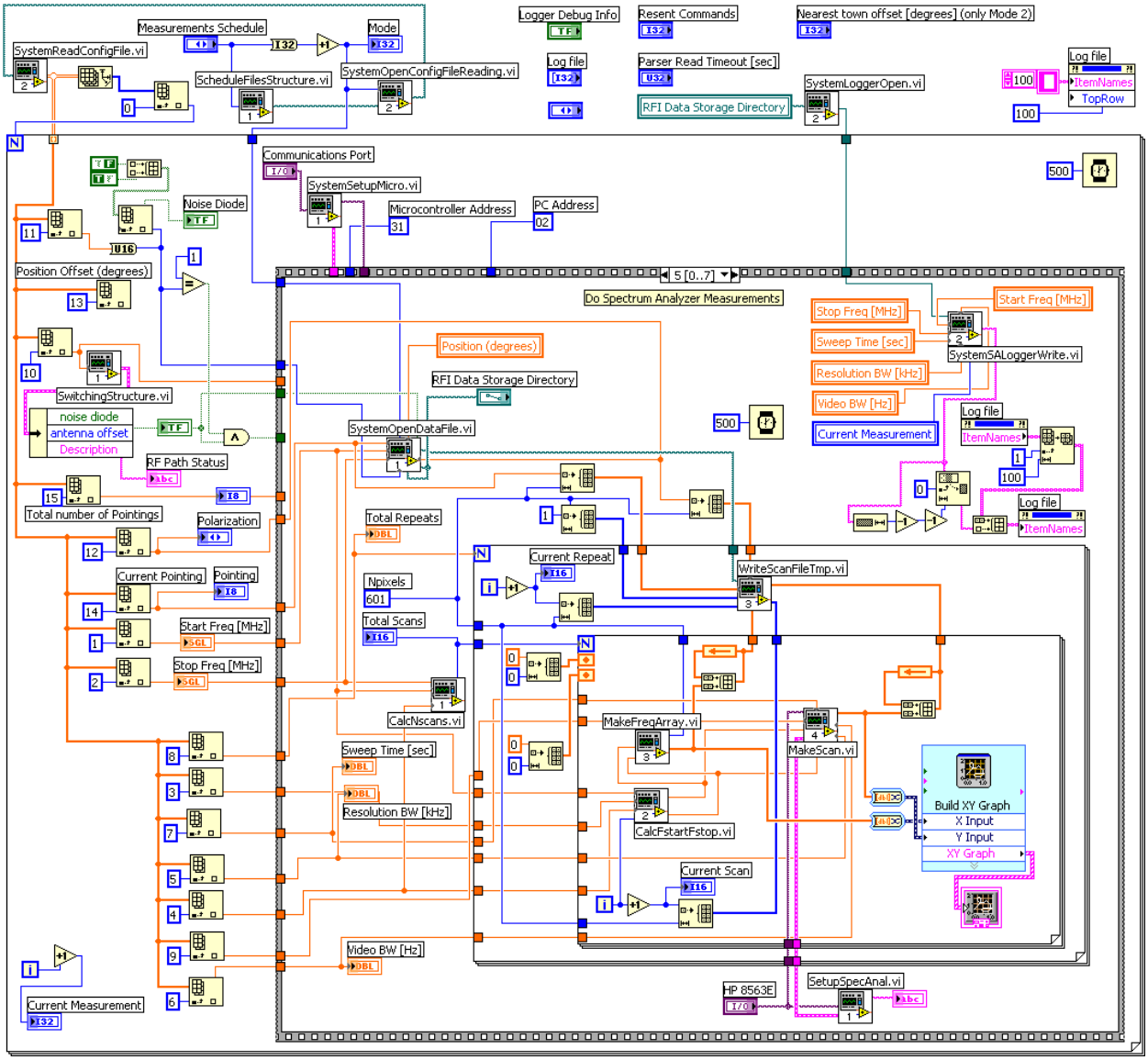

Figure 3.7: LabVIEW block diagram of the RFI Measurement Scheduler VI. Due to the way in which the LabVIEW block diagrams are displayed only the case for controlling the spectrum analyser and saving the data to disk is shown here. A complete block diagram along with the other cases for controlling the noise diode, RF switching, antenna azimuth, antenna polarisation and temperature measurements are shown in Appendix B.6.

For each measurement the application ran a set of sequential operations that were used to set up and control the hardware. The operations used the parameters specified in the schedule file. Figure 3.8 shows the sequence for each measurement.

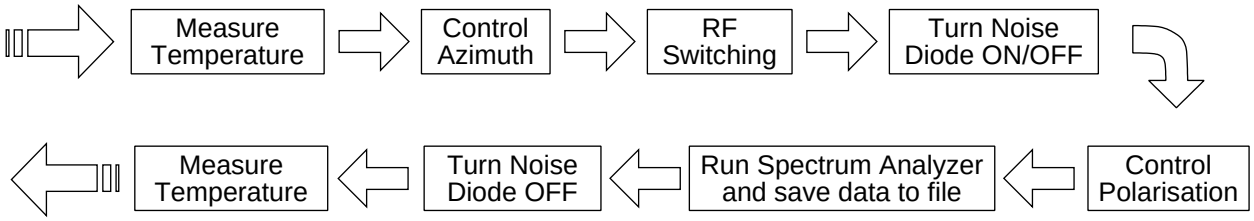

Figure 3.8: Sequence of operations performed for each measurement by the RFI Measurement Scheduler VI.

For control of the microcontroller, each command sent by the Control PC was acknowledged once the requested operation had been completed. This acknowledgement took the form of a reply message from the microcontroller and was parsed for errors by the scheduler application. In the case that an error occurred (i.e. malformed reply message) or there was no acknowledgement, the scheduler re-sent the command another 4 times with an incremental timeout between each successive attempt. Failing this, the scheduler continued with the next measurement operation in the sequence.

Using the Configuration tab on the front panel (Figure 3.6), an operator could select a predefined schedule of measurements: either Mode 1 or Mode 2. Once a directory for storing the data had been specified and the measurements initiated, the system would run unassisted for 27 hours (Mode 1) or 11 days (Mode 2). During operation, the interaction between the microcontroller and spectrum analyser was displayed in the log window and recorded to file for off-line analysis. The interface also allowed for the adjustment of the positions used to set up the polarisation rotator. Fine tuning adjustments to the antenna azimuth positions occurred less frequently and so this information was hidden from the operator.

The data received via the USB-HPIB interface from the spectrum analyser were in 10-bit binary format and represented dBm power values measured for each frequency sweep. The RFI Measurement Scheduler VI converted these binary values to ASCII using:

$$\mathrm{P}_a = (\mathrm{P}_b/6) + \text{Spectrum Analyser Reference Level} - 100 \tag{3.1}$$

where P_a is the dBm power value in ASCII and P_b the value in 10-bit binary format. The resolution of the data was $\frac{1}{6}$ dBm and the power values were recorded to a separate file for each measurement. The associated frequency values were calculated by the RFI Measurement Scheduler VI and these were stored along the power values in a "tab-delimited" text

file. The text file contained columns for frequency and power with one measurement point per row.

The schedule files for the Mode 1 and Mode 2 measurements contained RFI measurements and noise diode calibration measurements. The RFI measurements were done with the RF signal paths selected (A, A*, B, C, D) and for the noise diode measurements the noise diode paths (ND A, ND B, ND C, ND D) were used. The data format for both types of measurements was the same and the names of the noise diode measurement files indicated the noise diode state: ON or OFF. To identify the files, other parameters (e.g. measurement timestamp, azimuth pointing) were also embedded in the file name. These are discussed in the Data Processing chapter (Chapter 6).

3.3.2 Microcontroller

Control messages consisting of ASCII characters were sent from the Control PC's RS-232 serial port to the microcontroller. In addition, the microcontroller sent reply messages back to the Control PC. The messages were variable in length and consisted of an Address Byte, Control Byte and Checksum Byte. In some cases it was necessary for additional information to be communicated, thus a Data Byte and Sub-Control Byte were also used. The format of the messages sent and received by the Control PC are shown in Figure 3.9.

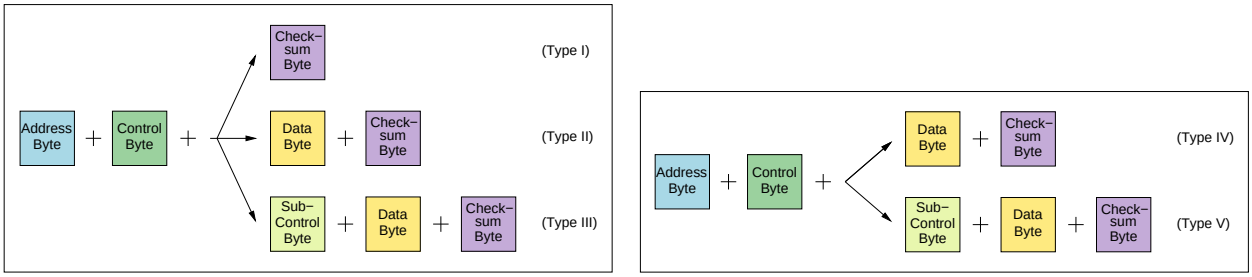

Figure 3.9: The format of the control messages used for communication between the Control PC and microcontroller. Left: The control messages sent from the Control PC to the microcontroller. The Address Byte is set to the configured address of the microcontroller. Right: Reply messages sent from the microcontroller to the Control PC. The Address Byte is set to the configured address of the Control PC.

The control routines of the microcontroller were all implemented using interrupts. Figure 3.10 shows an outline of the USART Receive Complete Interrupt, which was the main interrupt routine used for parsing the control messages and initiating hardware control. To distinguish between the different stages of control within the interrupt procedures, a state variable was used. These states are outlined by the state diagram in Figure 3.11 and a de-

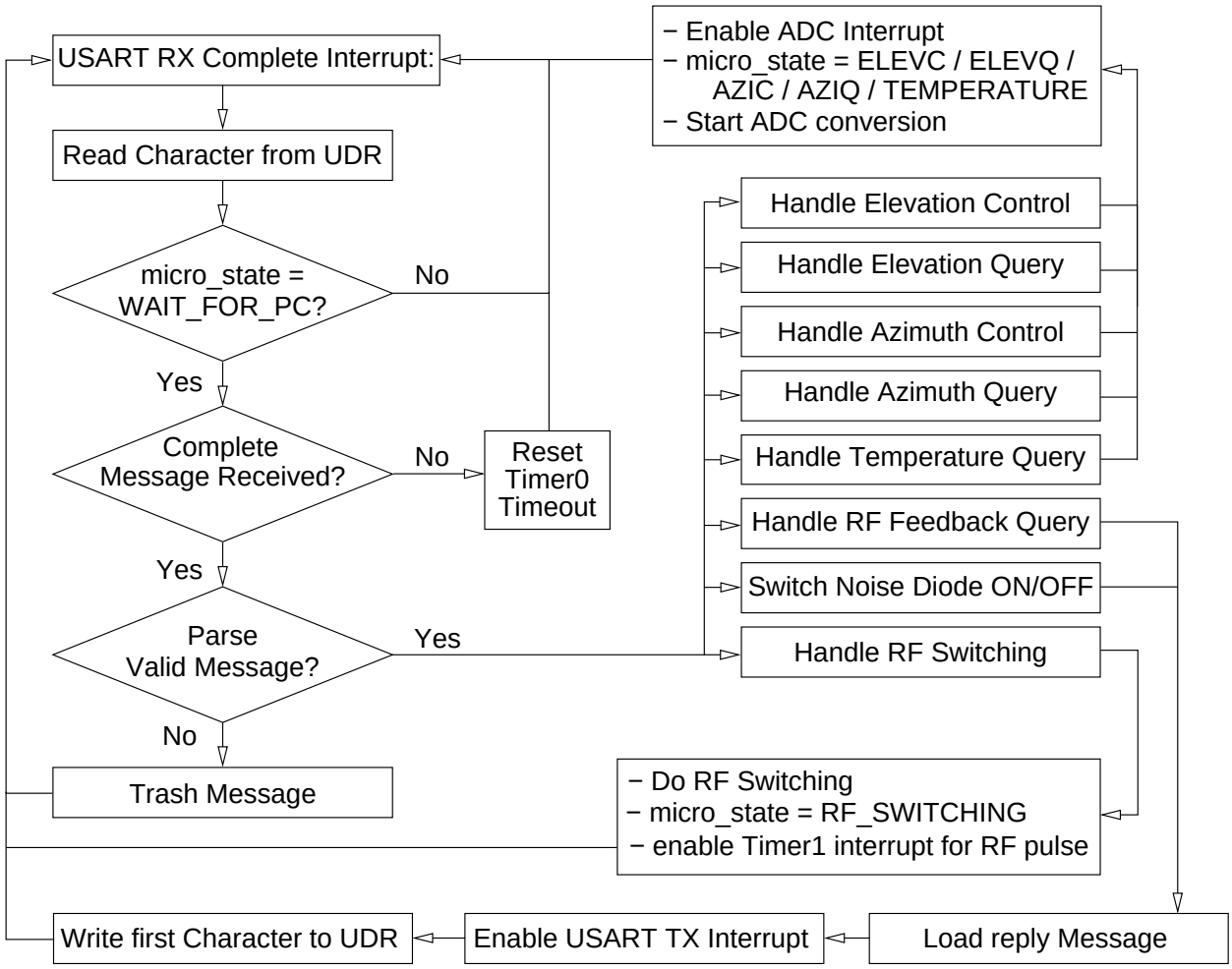

Figure 3.10: Overview of the USART Character Receive Complete Interrupt.

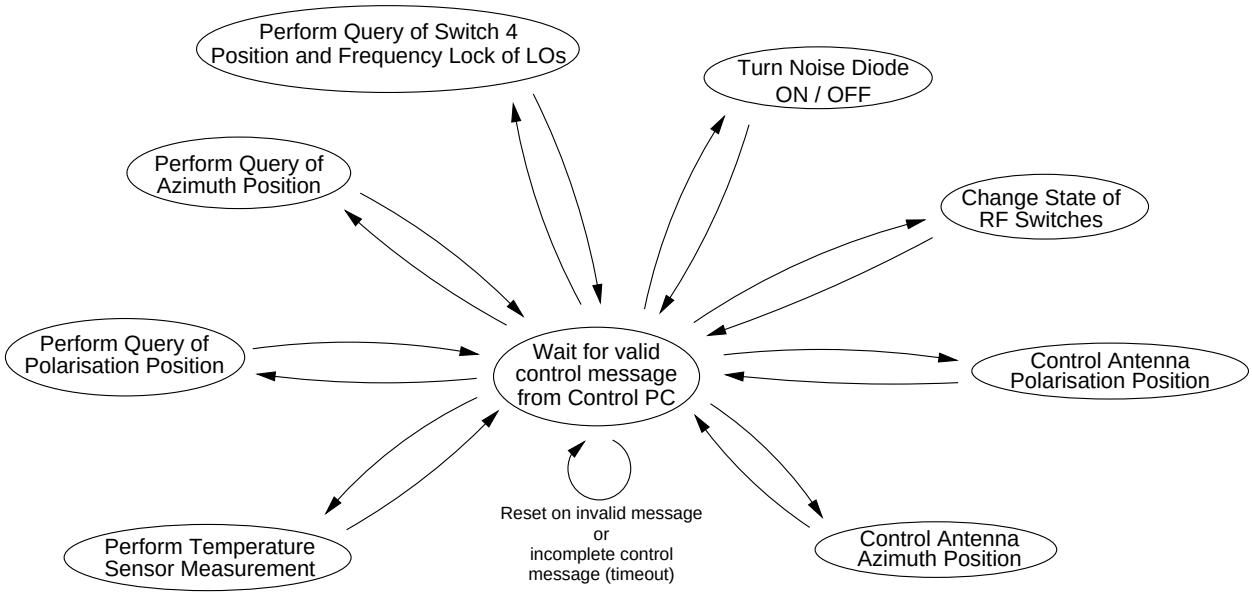

Figure 3.11: Microcontroller state diagram. The transitions to each of the different states occurs after a valid control message has been parsed by the microcontroller. The transition returning to the state where the microcontroller waits for the next control message occurs when the reply message has been sent to the Control PC.

tailed flow chart of the control can be found in Appendix B.7. The microcontroller assembly code on which these figures are based is shown in Appendix F.3.

The microcontroller only performed an operation when a correctly formed control message had been received and it was in the correct state. A timer was used to discard partially received messages after a timeout period set from the time after the last received byte. The Address Byte, Control Byte, and Checksum Byte were all parsed by the microcontroller and the message length was also used for validation. As indicated in Figure 3.11, incorrectly formed or invalid messages caused the state of the microcontroller to be reset, and any partially received message was discarded (after the timeout).

Only valid control messages were acknowledged by sending a reply message back to the Control PC. A list of these reply messages along with the control message originally sent is shown in Table 3.4.

With the exception of the Address and Checksum Bytes, the reply messages generally contained the same information as the control commands. The time the reply messages were sent depended on the nature of the control operation. Some actions required other operations to be executed, so the reply was initiated from the interrupt procedure used to perform the action. This was done for the RF switching, which needed to wait 50 ms for a timer interrupt in creating the pulse on some of the switching control lines. Other actions required a sequence of operations and interrupts before the control action had been completed and therefore took somewhat longer. The use of the ADC to position the azimuth and polarisation rotator was an example of this. Once the action had been completed the reply message was loaded, USART Transmit Complete Interrupt enabled and the first character of the message sent. The USART Transmit Complete Interrupt was used to send the remaining characters and reset the state variable of the microcontroller when it had finished.

As shown in Table 3.4, four query commands were built into the microcontroller command set: query temperature sensor, query state of RF switches, query polarisation rotator position and query azimuth rotator position. The polarisation rotator and azimuth rotator query commands were used to determine the ADC measured values of each of the rotators. These values were used for setting up the positions of the antenna rotators and the position data was stored in the RFI Measurement Scheduler VI. This was done manually for each RFI measurement system.

The query temperature sensor command used the ADC for temperature measurements and the Data Byte values in the reply messages were recorded to the log file by the RFI

Control Function	Type	Sent from or Reply to Control PC	Control Byte	Sub-Control Byte	Data Byte
Query Temperature Sensor	I	Sent	40	-	No Data Byte for Type I.
	IV	Reply	40	-	8 MSB from 10-bit A/D conversion (00-FF).
Change Noise Diode State	II	Sent	60	-	FF for noise diode ON, 00 for noise diode OFF.
	IV	Reply	60	-	Same as sent Data Byte.
Change State of RF Switches	II	Sent	71	- -	Data Byte specified for an RF Path in Table 3.2.
	IV	Reply	71	-	Same as sent Data Byte.
Query Polarisation Rotator Position	III	Sent	50	11	Arbitrary Data Byte.
	V	Reply	50	11	8 MSB from 10-bit A/D conversion (00-FF).
Change Position of Polarisation Rotator	III	Sent	50	41	00-FF (scaled relative to 180 degrees of rotator).
	V	Reply	50	42	Same as sent Data Byte.
Stop Rotation of Polarisation Rotator	III	Sent	50	42	Arbitrary Data Byte.
	V	Reply	50	42	Arbitrary Data Byte.
Query Azimuth Rotator Position	III	Sent	55	14	Arbitrary Data Byte.
	V	Reply	55	14	8 MSB from 10-bit A/D conversion (00-FF).
Change Position of Azimuth Rotator	III	Sent	55	12	00-FF (scaled relative to 450 degrees of rotator).
	V	Reply	55	13	Same as sent Data Byte.
Stop Rotation of Azimuth Rotator	III	Sent	55	13	Arbitrary Data Byte.
	V	Reply	55	13	Arbitrary Data Byte.
Query State of RF Switches	I	Sent	20	-	No Data Byte for Type I.
	IV	Reply	20	-	Encoded state of Switch 4 and LOs.

Table 3.4: Definition of the message protocol used for communication between the micro-controller and Control PC. Valid commands and responses are listed with the allowable byte values shown for the Control Byte, Sub-Control Byte and Data Byte. The format for each message is defined by its Message Type, which relates to the diagrams in Figure 3.9.

Measurement Scheduler VI.

It was decided that temperature sensing would only be used for monitoring and that no action would be taken to stop the measurement cycle if something went wrong. During measurements performed in April 2005, one of the oscillators in System 2 failed. At the time, this fault was believed to have been caused either by overheating or by moisture getting into the Mast-Head Box. With proper temperature monitoring in the production systems this fault was subsequently attributed to mechanical vibration caused during the transportation of equipment to site.

3.4 Scheduler Performance

In the process of moving from the prototype system to the final design, it was noted that certain aspects of the microcontroller and scheduler interaction needed to be fine-tuned. The theoretical calculation for the measurement time on the spectrum analyser was calculated as 0.36 and 4.30 days for the Mode 1 and Mode 2 schedules respectively. The actual measurement time was however worked out to be closer to 11 days for the Mode 2 measurements and 1.3 days for the Mode 1 measurements.

These overheads were partially due to the readout latency of the spectrum analyser as well as time to store the data to disk – which were unavoidable. For the prototype system, timeouts of between 5 seconds and 2 minutes were used between each of the control commands sent to the microcontroller. As the reply messages were not being used at this time, this was necessary to allow procedures such as the antenna rotation to finish. Using the maximum time for the command completion, the wasted time was significant, particularly for the Mode 2 schedule which had 832 measurements. In the final system, the scheduler application utilised the microcontroller reply messages as an indication of when the operations had been completed and this lowered the total measurement time.

Chapter 4

Locally Generated RFI

This chapter deals with the identification and eradication of locally generated sources of RFI. This RFI was radiated by the measurement system itself (self-generated) and by other objects and equipment in the local environment.

4.1 Background

The degree to which the locally generated RFI affected the prototype measurement system was much more severe than had been anticipated. At the outset it was known that the system was sensitive, however the strength and nature of the sources was underestimated. These assumptions were based on two premises:

(i) that the detection of self-generated interference would be negligible due to the fact that the antennas were physically separated from the rack-mounted electronics by more than 5 metres, with intervening metallic enclosures;

(ii) that the RFI measurement sites were typically remote and isolated from human activity and as such, the local environment (i.e. within 1 km) would have negligible levels of interference.

A problem that precluded the identification of interference early on was that the tests for the prototype system were conducted at HartRAO, an environment with substantial RFI in the region below about 1 GHz. This meant that it was difficult to distinguish between the locally generated interference in the environment and that of the system.

While the HartRAO facility is situated in a valley, which shields it from commercial broadcast signals, the local radio frequency environment was found to be unsuitable as a site for extremely sensitive self-generated RFI testing. Human activity and electronic devices

such as personal computers created broadband interference, which was made worse by the fact that these initial tests were done close to the office buildings. This local interference does not affect the operation of the HartRAO telescope as its lowest operating frequency is 1.6 GHz.

After the prototype system had been deployed to the field, it was possible to isolate individual sources of locally generated interference. Subsequent to the prototype field tests, an effort was made to more effectively screen all system hardware in the final system design. Preliminary investigations of the screening and self-generated RFI were done at the observatory, at locations away from offices where there was electronic equipment and human activity. At a later stage, thorough tests were conducted in an anechoic chamber facility run by the Institute of Satellite and Software Applications (ISSA) at Houwteq. This was done to validate the shielding efforts implemented. The self-generated RFI from the system was measured to have been significantly reduced.

During the investigation of local RFI sources, interference sources in the local environment around the Karoo 3 core site were also identified and removed or attenuated.

4.2 The Karoo 3 Core Site Local Environment

Mode 2 measurements were conducted at the Karoo 3 core site by the South African SKA Project. The 'Request for Proposals for Siting the SKA' (International SKA Project Office, 2004) required that these measurements be performed over a period of 12 months in order to characterise the radio frequency environment.

In addition to the measurements conducted by the South African SKA Project, a team from ASTRON (the Netherlands Foundation for Research in Astronomy) also performed measurements at the site. During the course of the year the ASTRON team visited each site proponent and undertook measurements of their own with the SKA Site Spectrum Monitoring (SSSM) system (Millenaar, 2005). Apart from the RFI measurements, a further purpose of this visit was to cross-calibrate the SSSM system with the measurement systems of site proponents.

To accommodate the year-long measurements and the visit by the ASTRON/SSSM team, a prefabricated container was installed at the Karoo 3 core site. This formed a base of operations for the measurements performed in the Karoo and the surrounding remote sites in the area. The container consisted of three rooms: one for each measurement team and

their equipment, and one for a communal area equipped with kitchen amenities. A three-phase diesel generator provided power to the container and each room was connected to a separate phase.

To ensure that representative measurements of the core site environment were performed, it was necessary that all locally generated interference was defeated. While it was known at the outset that there may be locally generated interference at the site, the full extent was only realised during the initial field tests with the prototype system in December 2004. Despite the interference at the site being far lower than at HartRAO, Figure 4.1 shows that what

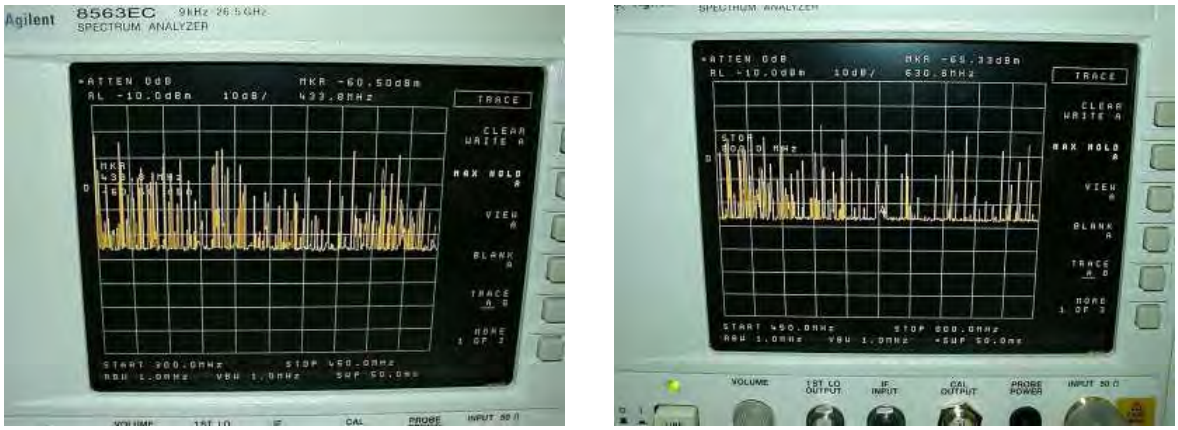

Figure 4.1: Screen-shots of the locally generated RFI measured by the prototype system at the core site in December 2004. Left: Interference shown on the spectrum analyser from 300 - 450 MHz. Right: Interference from 450 - 800 MHz.

was detected was still significant. As the prototype system was far enough removed from other human activity, it was possible to distinguish the system's self-generated interference from that of the environment, and isolate specific sources.

A systematic approach was adopted and the identification of RFI sources was performed using the RFI measurement system antennas, a handheld directional antenna (Rohde & Schwartz HE200), and near-field probes (Hewlett Packard 11940A and 11941A) as detectors. The system antennas were used for coarse direction finding, while the handheld antenna and near-field probes were used for pinpointing the RFI sources. An ICASA direction finding (DF) vehicle equipped with its own antennas and measurement equipment was also made available. It was used to assist in the identification of RFI sources. These sources are listed in Appendix C.1. The photograph in Figure 4.2 shows the front of the core site container taken during these exercises; with additional photographs shown in Appendix C.2.

Figure 4.2: Measurement container at the Karoo 3 Core site with the ICASA DF vehicle and the prototype measurement system.

4.2.1 Local Sources of RFI

Some of the locally-generated RFI originated from quite obscure sources, including "passive devices". Because of the frequency scanning operation of the spectrum analyser, repeating impulsive signals (such as static discharges) appeared as combs of CW signals on screen (see Figure 4.1) and in the recorded data.

One of the impulsive sources at the site was a portable gazebo that was used to provide protection for vehicles. The gazebo frame consisted of steel pipes strung together by a combination of metal chain and elastic cord that was threaded through the pipes. It was found that the contact of the links of the metal chain with the inside of the pipes and with each other caused interference, especially when the wind caused the frame to shake. Similar static discharges, caused by use of the nylon camping chairs, were also detected by the RFI measurement system. The gazebos were removed from site and the nylon chairs replaced with canvas equivalents. A photograph of the metal chain inside one of the gazebo poles is shown in Figure 4.3.

The motion detector spotlights on the container were shown to create interference when triggered at night. These were disconnected and the fluorescent lights on the inside and

around the outside of the container were kept on at all times. This was to avoid interference from arcing in the starter unit when they were switched on.

It was found that the mechanical design of the telescopic mast gave rise to intermittent interference during windy conditions. This was caused by a loose metal collar at the top of the mast, and the mast segments that were electrically isolated from one another by silicon pneumatic seals. An immediate solution to these problems was to remove the collar and ground each mast segment to the trailer using copper wire as shown in Figure 4.3. At a later stage an earth-mat consisting of buried radial conductors was laid around the site of the container and this was used as a grounding point for the RFI measurement system and the container. A video clip showing the effect of this mast-induced interference before the grounding was implemented can be found in Appendix F.4.

Figure 4.3: Left: The metal chain inside the gazebo poles which caused interference at the Karoo 3 core site. Right: Initial earthing of the mast segments using copper wire. Note the guide-rope collar which is still attached to the mast at this stage.

4.2.2 Self-generated RFI

Further interference coming from the rack-mounted equipment in one of the measurement rooms was also measured. An unused input pin on a CMOS logic chip in the Electronics Control Box was left floating, which lead to oscillation of the unused gate. This oscillation induced a current on the control lines connected to the Mast-Head Box, resulting in RFI radiation. Replacement by a chip from a different family was used as an interim solution and in the final system design a PCB layout that did not have this problem was developed for the control electronics.

During the visit by the ASTRON/SSSM team it was found that harmonics of the 10 MHz

frequency reference line from the spectrum analyser were detectable beyond 150 MHz. Using the near-field probes it was also shown that other sources of interference coming from the LCD monitor, Control PC, mouse, keyboard and spectrum analyser could also be detected. The attenuation and removal of these sources will be dealt with in the following section.

4.3 Identifying and Defeating Self-Generated RFI

On advice from a commercial company specialising in RFI mitigation (MESA Solutions (Pty) Ltd.), various solutions to the self-generated RFI were implemented in the three final production systems. As a precaution, all electronic devices were screened and enclosed in Faraday cages fabricated from aluminium or copper sheets and brass mesh.

4.3.1 Defeating Common Mode Currents

A common source of self-generated interference in the system was radiation coming from the control and power cables. These cables interconnected the various system components and it was shown (MESA Solutions (Pty) Ltd., 2005a) that the cause of the interference was due to common mode currents flowing along them.

According to Williams (Williams, 2001), various strategies can be used to defeat common mode currents. The general strategy is to identify the common mode current loops and provide alternative paths of lower impedance for these currents to return to their source. Typically this is achieved by improving the grounding between instruments and by adjusting the impedance of the cables along which they flow.

The final production systems had their electronic equipment permanently installed in the rack, inside the trailer cabin. A substantial copper busbar was installed to ensure components were properly grounded and to constrain stray currents that may have lead to radiation. The busbar was bonded to the Faraday cages and equipment chassis mounted in the rack. Power cables and interconnecting signal lines were strapped to the busbar to increase their impedance and reduce common mode currents flowing between equipment items. The busbar was connected to the diesel generator earth, the mast earthing cables and a copper earthing stake driven into the ground next to the trailer. Figure 4.4 shows the rack with the busbar installed and connected to the rack-mount instruments in the measurement trailer.

In-line mains filters were inserted for all power line connections, and panel mounted

Figure 4.4: Left: The trailer rack with the measurement system equipment installed and the cables strapped to the copper busbar. Right: A close-up view of the busbar attached to the Electronics Control Box and Control PC.

bulkhead connectors were soldered on to the back panels of the instruments. Ferrite chokes were used on the cables in the rack: in some cases inside and outside the equipment cages. Cables were also wrapped multiple times around the chokes, which improved their impedance characteristics and effectiveness in constraining common mode currents.

4.3.2 Screening of the UPS

Radiated interference was detected with the near field probes on the front panel of the UPS, where the power button and LCD display were mounted. This was defeated by placing a ferrite choke on the control line ribbon cable as shown in Figure 4.5. Extra ferrite chokes and an in-line mains filter were also placed inside the UPS chassis. The UPS was placed inside a Faraday cage fabricated from copper sheeting for the frame and brass mesh.

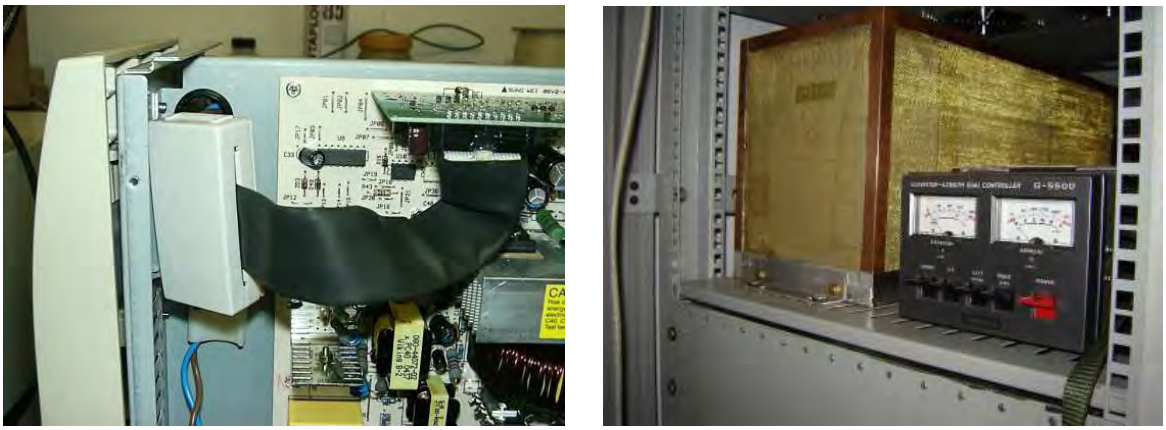

Figure 4.5: Left: UPS with ferrite on the ribbon cable going to the front panel. Right: The UPS mounted in the Faraday cage and installed in the trailer rack. The Antenna Rotator Control Unit (right) was installed next to the UPS in the rack.

Further modifications made to the UPS included the reconnection of the multiple grounding points to a single point inside the unit. The multiple grounding points had been a design flaw that had been shipped with the UPS units from the manufacturer.

4.3.3 Control PC Screening

Using the near field probes, many sources of RFI were found to be associated with the Control PC motherboard and cables. To reduce the level of interference coming out of the rear slots on the PC chassis, the motherboard and power supply were re-mounted so that they were located further away from the back panel of the rack-mount box. A new rear panel was constructed from brass mesh, and feed-through connectors for the USB, RS-232 and mains power were soldered to the middle of the panel. The monitor, keyboard and mouse were removed from the Control PC in order to eliminate their unwanted RFI emissions. Their functionality was replaced by an Ethernet LAN connector that was placed on the front of the Control PC. This connection was used to allow a removable laptop to remotely control the PC using the remote desktop application VNC. After a schedule of measurements had been initiated, the Ethernet cable was disconnected and a strip of aluminium foil was used to cover the Ethernet connector. The laptop was turned off and removed from the site.

A sheet of aluminium was attached to the front of the PC chassis to cover apertures that might radiate and small apertures with brass mesh coverings were used for physical access to the power and reset buttons. A separate in-line mains filter was placed inside the PC chassis. Ferrite chokes were used on the cables feeding to the outside of the PC enclosure, as shown in Figure 4.6. On the edges of the PC lid, a gasket made from the external conductor of an RG-223 co-axial cable was used to provide reliable electrical contact between the lid and the sides of the enclosure.

4.3.4 Electronics Control Box Screening

The seams on the Electronics Control Box were sealed with aluminium tape to prevent radiation from small gaps between joins. The microcontroller on the Control PCB used a crystal oscillator running at 8 MHz and the harmonics of this clock signal were detected up to 288 MHz, as detailed in the list of interference sources in Appendix C.1. To attenuate the radiation due to clocking signals associated with the microcontroller and crystal oscillator, a separate Faraday cage was build around the Control PCB using copper sheeting. Feed-through capacitors and ferrite beads were used on all lines into the Control PCB box. This

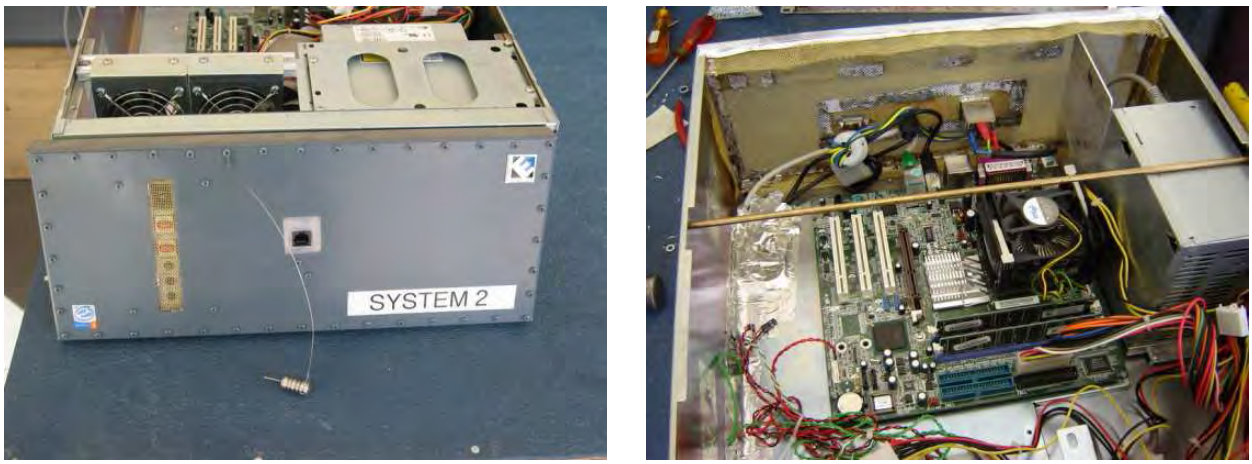

Figure 4.6: Left: Front panel of the Control PC for System 2 showing the Ethernet socket and the cut-outs for the power and reset buttons. Right: Internal screening, ferrite chokes and bulkhead connectors on the back panel of the Control PC.

is shown in Figure B.8 of Appendix B.3. Additional ferrite chokes were placed on the power and signal lines inside the Electronics Control Box.

4.3.5 Spectrum Analyser Screening

To implement a Faraday cage for the spectrum analyser, an aluminium frame supporting brass mesh screening was fabricated to allow for airflow and the viewing of the monitor display. All cables were re-routed to the back of the enclosure and bulkhead connectors were used to transfer signals and power through the rear panel. A low loss semi-rigid cable was used to connect the front panel input of the Agilent analyser to an N-type bulkhead connector at the back.

It was found that the 10 MHz reference signal from the spectrum analyser was not sinusoidal as expected. The square wave signal produced high-order odd harmonics that were radiated by the cable feeding the 10 MHz frequency reference to the Mast-Head Box. To remove the unwanted harmonics, three in-line low-pass filters were placed on the reference cable inside the screened box. Measurements taken of the reference signal with and without these filters are shown in Figure 4.7. Photographs of the spectrum analyser Faraday cage can be found in Appendix C.3.

4.4 Preliminary Validation of the Screening

In an attempt to validate some of the shielding exercises applied to the equipment, a series of preliminary tests were carried out at HartRAO. An empty building located away from

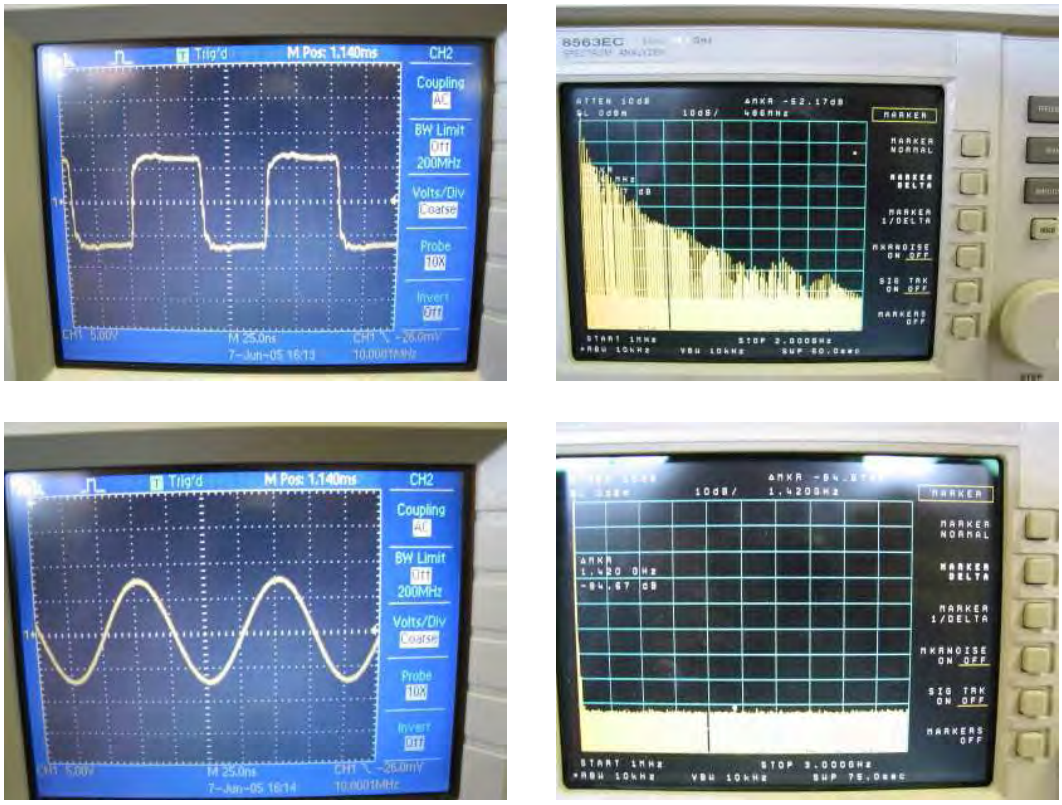

Figure 4.7: The top two images show the oscilloscope trace (left) and the spectrum analyser sweep (right) of the 10 MHz reference signal without the in-line filters. The frequency range for the spectrum analyser is 1 MHz-2 GHz. The bottom images show the same screen-shots but with the in-line filters installed and the spectrum analyser set to 1 MHz-3 GHz range.

human activity and with minimal interference from computers was chosen as a suitable site to conduct these tests.

The sub-system components of the measurement system were placed on a bench and a Rohde & Schwarz HL033 antenna connected to an Anritsu portable spectrum analyser (MS2721A) was set up approximately 3 metres from the devices being tested. The layout of the test set-up is shown in Figure 4.8 and a photograph taken during the procedure may be found in Appendix C.4.

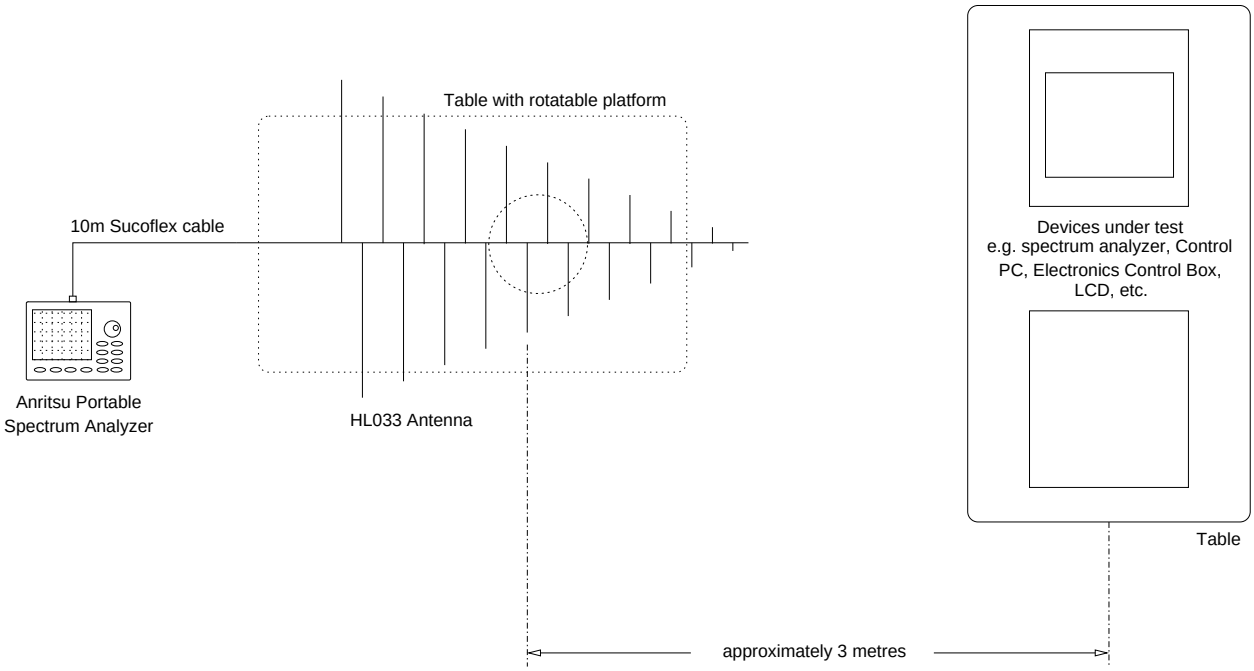

Figure 4.8: Physical layout of the test set-up used to determine the effectiveness of the screening of the RFI measurement system.

In order to identify sources of interference, the sub-systems were powered on and turned off in various permutations, and screen-shots were recorded by the Anritsu spectrum analyser. Due to interference from the environment, it was necessary to take residual background screen-shots with all of the equipment turned off. As an example, comparative screen-shots for the RFI produced by the flat screen LCD monitor are shown in Figure 4.9.

The investigation into the interference from the LCD monitor resulted in a decision to remove the monitor from the system. During similar investigations it was revealed that broadband interference was also generated by other peripheral devices, namely the keyboard and mouse. These too were removed from the RFI measurement system and the functions of these peripherals were performed by a laptop computer running the VNC application as previously mentioned.

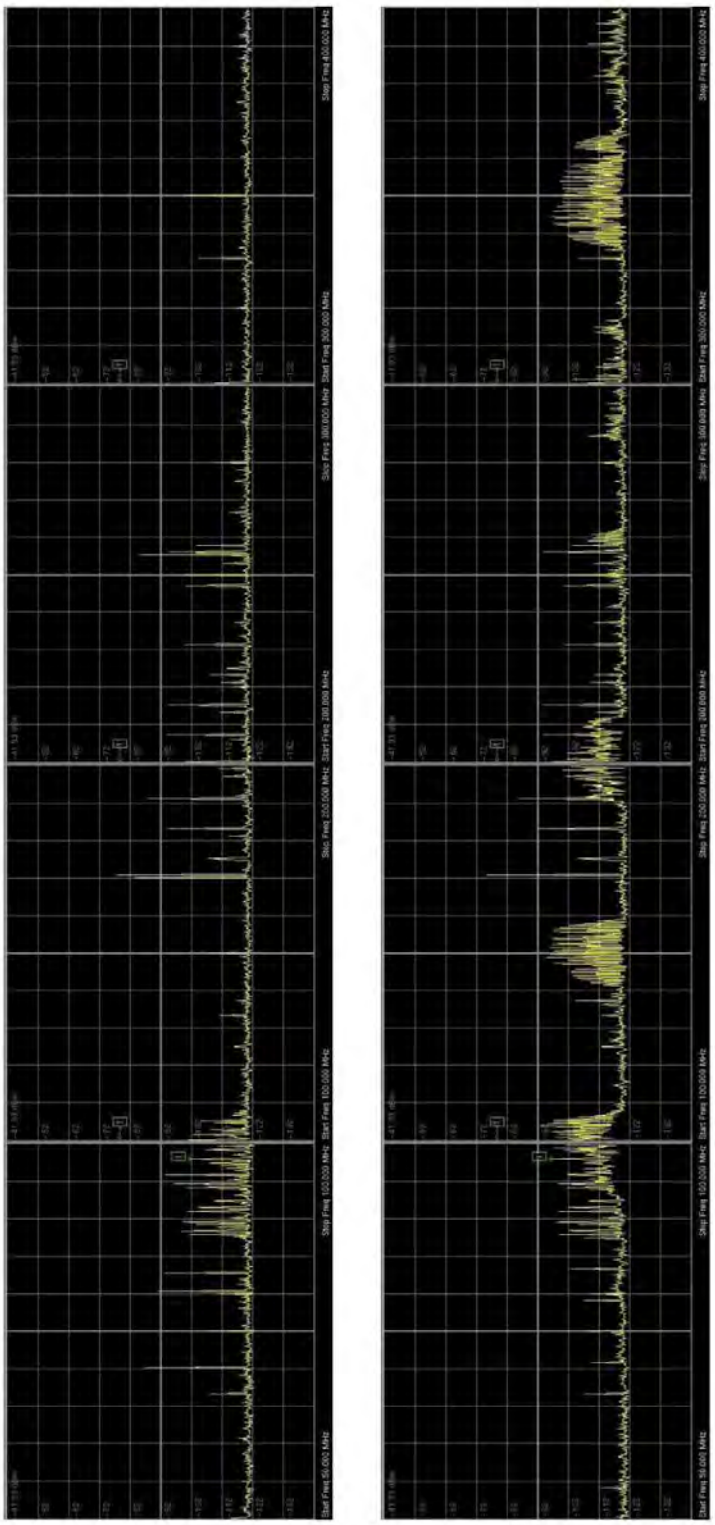

Figure 4.9: Screen-shots recorded with the Anritsu portable spectrum analyser in the Visitors Centre at HartRAO. Left: Measurement of the background environmental interference. Right: Measured interference with the flat screen LCD monitor powered on. Note that while the built-in pre-amplifier on the Anritsu spectrum analyser was used for these measurements, the noise floor of the RFI measurement systems was still about 20 dB lower than the Anritsu.

Higher levels of interference were generated when the instruments were connected together via their respective control cables. For example, when the Electronics Control Box and RF front-end were connected. The interference was a result of radiation associated with the common mode currents propagating along the connecting cables. The identification of this type of interference source formed the basis of the investigations done in the anechoic chamber at Houwteq. While a degree of insight was gained by doing these preliminary tests, proper investigations into the self-generated RFI could only be performed when the system was fully integrated in the trailer rack and was set up as it would be in the field.

4.5 Final Refinements

The final investigation of sources of self-generated RFI in the three measurement systems was done in an anechoic chamber facility in Houwteq, a facility operated under the auspices of the Department of Communication. Tests were performed on the more sensitive System 2 and these results were used to guide the final modifications applied to Systems 1 and 3. All three systems were tested in the anechoic chamber prior to being deployed in the field.

Initial investigations were done manually using a standard EMC antenna shown in Figure 4.10. From these tests it was realised that the interference measured by the EMC antenna was often not detected by the RFI measurement system and vice versa. Because of this, subsequent investigations were only performed for the interference that was measured by the RFI system.

Using the RFI measurement system, an overnight schedule of Mode 1 measurements was performed. The measurements included all antenna azimuth pointings and both polarisation orientations in the bands below 2 GHz, where interference had previously been detected. The following day, the data was analysed and further investigations were done for frequencies that showed spurious signals.

As was the case with the pre-validation of the shielding done at HartRAO, it was found that the self-generated RFI was caused by current loops flowing on various cables in the system. The busbar was effective at constraining stray currents in the rack and no interference was detected on the cables interconnecting these instruments. Instead, only currents on the long cables connecting to the Mast-Head Box and antenna rotators were detected (MESA Solutions (Pty) Ltd., 2005b). Undesirable loop currents were identified using ferrite chokes, an RF current clamp and an Anritsu portable spectrum analyser. The ferrite chokes were

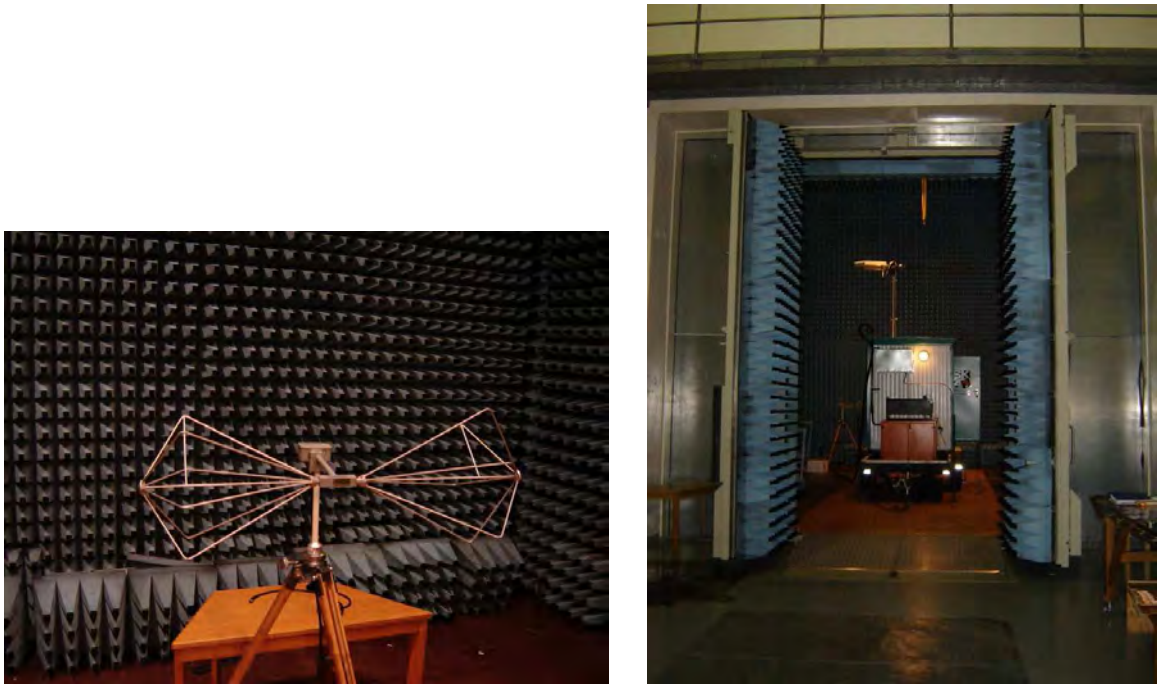

Figure 4.10: Left: EMC antenna used for initial investigations in the anechoic chamber. Right: RFI measurement System 2 in the Houwteq anechoic chamber.

used to increase the common mode impedance of the cables, which defeated the unwanted currents. These chokes provided both a tool for locating currents and a subsequent solution to the problem.

Once a current path had been identified, the chokes were used to re-route the currents via paths of lower impedance, producing lower interference. In some cases the eradication of RFI was also achieved by providing an alternative path (of lower impedance) for the current to flow along, e.g. to ground.

The control cables connected to the Mast-Head Box were found to radiate low levels of interference that was coupled to the HL033 antenna elements. The cables were screened by aluminium foil, which was wrapped tightly around them. To provide an alternative ground path, this foil was connected to the earthing system of the mast segments. As Systems 1 and 3 did not have the sensitivity of System 2 they did not require this modification. A figure of the aluminium foil screening is shown in Figure 4.11.

Common mode currents identified on the control cable connecting to the azimuth rotator also appeared to radiate interference. Despite the internal shielding in the cable it was found that the azimuth rotator unit, where the cables attached, was electrically isolated from the grounding system of the pneumatic mast segments. To defeat this, an appropriate current path was provided by a short copper cable that connected the azimuth rotator unit to the

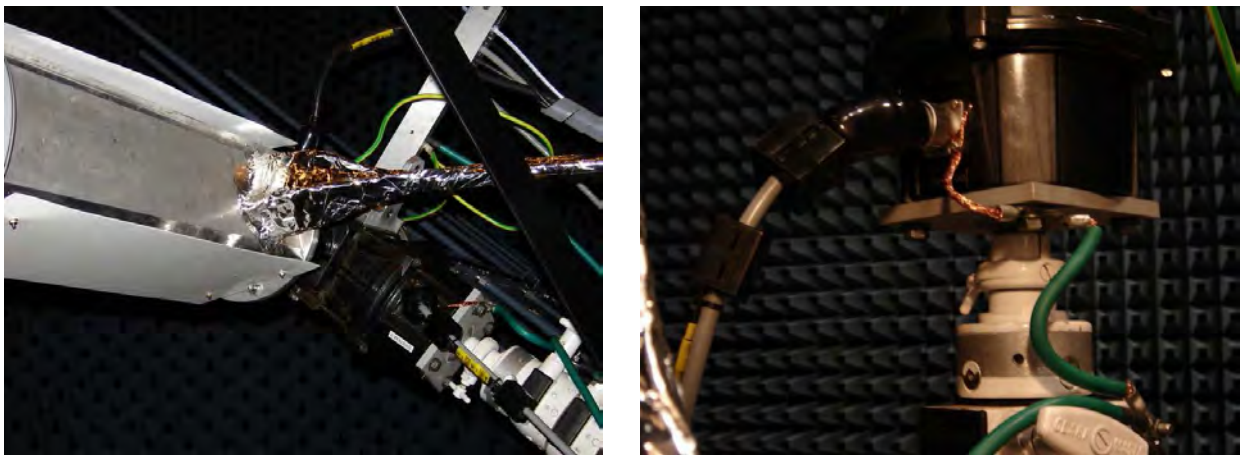

Figure 4.11: Left: Shielding the control cables connecting to the Mast-Head Box using aluminium foil on System 2. Right: Grounding of the azimuth rotator control cable to the earthing system of the mast segments. Note the guide-rope mast collar has been removed.

mast earthing system. This cable can be seen in Figure 4.11 and was shown to eradicate the problem.

An evaluation of the interference from the diesel generator and the air-conditioner was performed. The diesel generator produced interference in the region 80 MHz to 90 MHz and it was found that the air-conditioner produced substantial interference up to 320 MHz in its heater mode. In the cold mode, low levels of interference were detected below 108 MHz. The air-conditioner was therefore only used in this mode during field measurements. As the RFI from the diesel generator and air-conditioner only appeared in a specific combination of antenna pointing and polarisation, no further remedial measures were carried out.

Figure 4.12 shows a plot of the overnight measurements performed in the anechoic chamber with measurement System 2. The interference in the bands below 100 MHz was due to the air-conditioner running in cold mode and the radiation from the cables connected to the mast-head components (i.e. Mast-Head Box, azimuth rotator) prior to their screening. Despite the 100 dB isolation of the chamber, two signals at 166 MHz and 433 MHz were measured in two antenna directions. The RFI at 166 MHz is seen in this plot and both signals were shown to be unrelated to the measurement system.

The three production systems were deployed in the field as soon as the final checks had been performed in the anechoic chamber. The RFI measurement data produced by the systems was constantly monitored for self-generated RFI during the measurement campaign. The techniques to defeat the self-generated RFI appeared to be effective and robust. There was no degradation in efficiency over the measurement period, despite continuous use of the

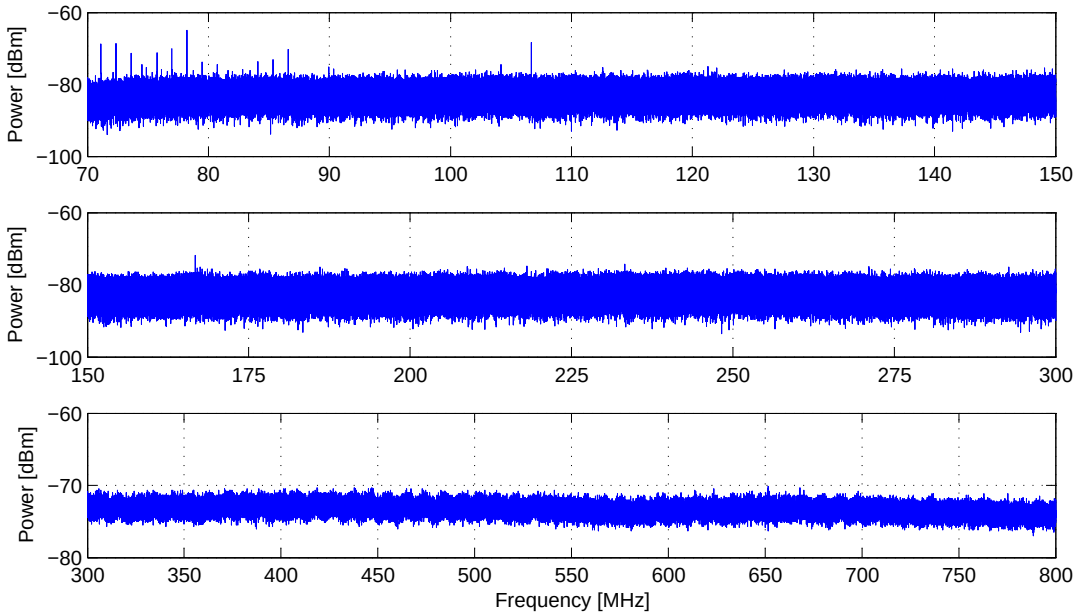

Figure 4.12: Interference measured by System 2 in the Anechoic chamber at Houwteq prior to the screening of the cables near the mast-head components mounted on the mast.

systems.

Chapter 5

Field Tests and Operations

This chapter deals with the operation of the RFI measurement system during the measurement campaign and describes the measurement parameters used for the Mode 1 and Mode 2 measurements. Procedures that were undertaken to monitor the stability of the measurement systems during operation are also discussed. This chapter details the field tests conducted during the cross-calibration procedure with the ASTRON/SSSM team at the Karoo 3 core site.

5.1 Background

As mentioned in Chapter 2, three RFI measurement sets were constructed for the RFI measurement campaign. Systems 1 and 3 were used to conduct remote site measurements and System 2 (more sensitive because of the extra gain) was used exclusively at the Karoo 3 core site. The measurement of remote sites was a requirement of SKA Memo 37 and it was at these sites where Mode 1 measurements were performed. To characterise the RFI environment for potential SKA array sites, remote sites at 75 km and 150 km from the core were measured. As more than 75% of the SKA will be within the first 75 km, it was important to characterise this area very well. In addition to measurements within the central Karoo area, measurements were also performed in other Southern African countries. These remote sites, including those in the Karoo, are indicated in Figure 5.1.

The field operation of the RFI measurement systems was carried out by ICASA representatives, who had been trained to operate the systems on behalf of the South African SKA Project. A standard operating procedure manual was compiled (see Appendix F.5) and was used by the operators to conduct the RFI measurements. The ICASA teams deployed the systems to the field and once a cycle of measurements had been completed, copied the

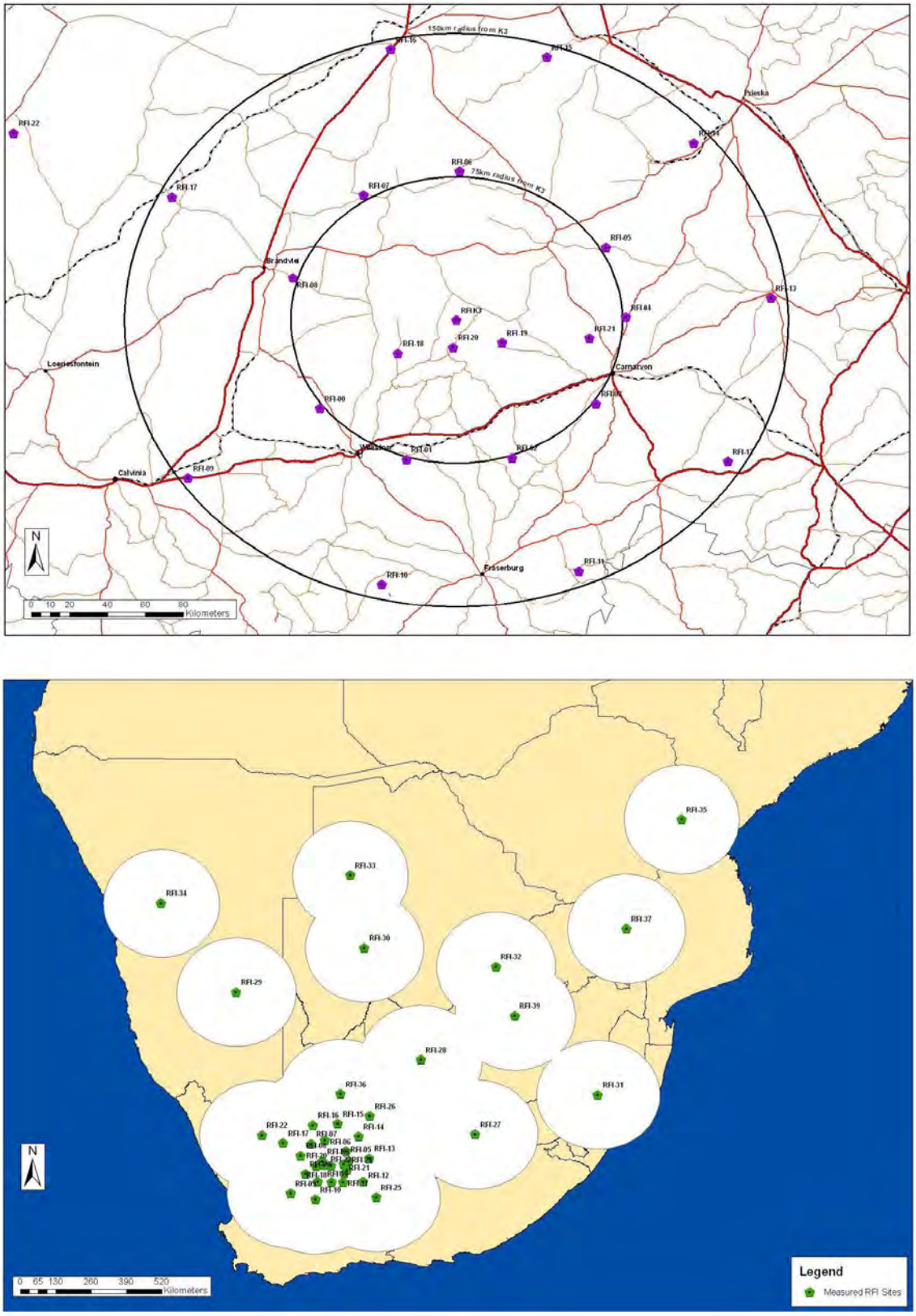

Figure 5.1: Top: Map of the remote site measurements done around the core area with concentric rings indicated at 75 km and 150 km from the core. Bottom: Map showing the remote sites measured in Southern Africa. The circles represent 200 km radius zones around each site.

measurement data to DVD media and couriered it to the data processing centre, at the SA SKA Project Office. Before commencing a cycle of measurements, operators ran a system integrity check application, to ensure the correct functioning of the system. While no data was recorded during this procedure, health check data (noise diode calibration sequences) were recorded during the RFI measurement schedule and allowed for any follow-up investigations at the data processing centre. These procedures are discussed further in Section 5.3.

To provide a calibration reference for the RFI measurements conducted by the SKA site proponents, the ASTRON/SSSM team visited each proposed core site. During their visit a cross-calibration procedure was performed between the South African RFI measurement systems and the SSSM system. As RFI measurement System 3 was still under construction at the time, only Systems 1 and 2 were used in this procedure. The mobile trailers that were used for the final production systems had also not been completed at this stage, and so these two measurement systems were set up in the core site container with the antenna masts placed at suitable positions outside the container. Details and results of the cross-calibration field tests are discussed in Section 5.4.

SKA Memo 37 required that antennas were pointed in different directions for both horizontal and vertical polarisations. The number of pointings required was specific to the beam patterns of the antennas used, and was necessary for providing adequate 360 degree coverage. The number of pointings were selected so that little or no overlap of the quarter power beam widths was achieved, for each antenna. Using this criterion and the beam patterns specified in Appendix D.1, three pointings for the HL033 antenna and five for the HL050 were selected.

5.2 Spectrum Analyser Operational Settings

As mentioned in Chapter 3, the Agilent spectrum analyser communicated with the Control PC via an USB-HPIB dongle. This allowed commands sent from the Control PC to set up and perform the spectrum sweeps on the analyser, and data to be read back to the PC. Two schedules of measurements based on Tables 1.1 and 1.2 from SKA Memo 37 were created, and tailored to the specific requirements of the South African RFI measurement systems.

The documentation supplied by Agilent does not provide details of the signal processing applied by the spectrum analyser video signal path. To reduce the uncertainty introduced by the unknown analogue and digital video signal averaging processes, a strategy was devised

that:

1. used the most basic "sample" detector mode;

2. recorded 10 spectrum samples per RBW so that deterministic data processing could be performed on the recorded samples;

This strategy was also implemented on the SSSM system that used a Rohde & Schwarz FSU26 spectrum analyser (Rohde & Schwarz, 2006b).

The spectrum analyser recorded 601 equally-spaced samples across each frequency scan. To achieve the requirement of 10 samples per RBW, the frequency span Δf_{sweep} for a sweep was calculated as:

$$\Delta f_{sweep} = \frac{\text{RBW} \times (601 - 1)}{10} \tag{5.1}$$

The sweep time (ΔT_{sweep}) across the frequency span (Δf_{sweep}) was configured so that the combined time spent in the RBW frequency interval (i.e. aggregated for all 10 samples) was equal to the dwell time (ΔT_{RBW}) specified by SKA Memo 37 for the appropriate band:

$$\Delta T_{sweep} = \frac{600 \times \Delta T_{\text{RBW}}}{10} \tag{5.2}$$

The sample period for each measurement across the span was therefore given by:

$$\Delta T_{sample} = \frac{\Delta T_{sweep}}{(601 - 1)} \tag{5.3}$$

Following the SKA Memo 37 protocol, some bands were swept a number of times for a given azimuth pointing and polarisation orientation. In the Mode 2 measurements these repeated scans were also used to make up the dwell times in the RBW frequency interval. This meant that for bands in which this was done, the total number of 'repeats' was equal to the number of scans needed to make up the dwell time multiplied by the number of repeats required by the protocol.

5.2.1 Mode 1 Bands and Measurement Schedule

The Mode 1 measurements were done for all RFI measurement sites, including the Karoo 3 core site. The measurement bands and associated spectrum analyser settings discussed in this section and Section 5.2 previously are detailed in Tables 5.1 and 5.2. Some of the bands specified by the protocol were split, to take into account the transitions between the signal paths of the RFI measurement system. These splits are indicated in the tables by horizontal

Band	$f_{low} - f_{high}$ MHz	Δf_{sweep} MHz	ΔT_{sweep} msec	RBW kHz	VBW Hz	ΔT_{RBW} msec	ΔT_{sample} msec
1	70 - 150	0.18	600	3	300	10	1
2	150 - 300	0.18	600	3	300	10	1
3	300 - 800	1.8	600	30	300	10	1
4	800 - 960	1.8	600	30	300	10	1
5	960 - 1400	440	50	1000	30000	0.114	0.083
6	1400 - 2000	1.8	600	30	300	10	1
7	2000 - 3000	1.8	600	30	300	10	1
8	3000 - 6000	60	600	1000	300	10	1
9	6000 - 9000	60	600	1000	300	10	1
10	9000 - 12500	60	600	1000	300	10	1
11	12500 - 18500	60	600	1000	300	10	1
12	18500 - 22000	60	600	1000	300	10	1
13	22000 - 26500	60	600	1000	300	10	1

Table 5.1: Mode 1 Measurement Bands and associated spectrum analyser settings as discussed in Section 5.2.

lines with the relevant spectrum analyser settings being maintained across the newly created bands.

The settings for band 5 did not strictly follow the protocol in SKA Memo 37 because of the limitation imposed by the 50 ms minimum sweep time of the Agilent spectrum analyser. Using Equations 5.1 and 5.3 a compromise was made such that a large number of fast band sweeps could be done in a reasonable amount of time as allowed by logistical time constraints. A dwell time ($\Delta T_{\rm sweep}$) of 83 μs with 18000 repeats was selected in place of the 10^6 repeats with 2 μs specified by the protocol.

Table 5.2 details the schedule of band measurements for the Mode 1 protocol used for the RFI measurement systems. N_{sweep}, calculated as:

$$N_{sweep} = \frac{(f_{high} - f_{low})}{\Delta f_{sweep}} \tag{5.4}$$

is the number of spectrum analyser sweeps required to cover a band ($f_{high} - f_{low}$). Due to the Δf_{sweep} not fitting an integer number of times into the frequency band specified in Table 5.1, the number of sweeps was rounded up to the nearest integer for some bands. The repetitions for each band (N_{rep}), represents the number of times the spectrum analyser sweep across a particular band in a single cycle of measurements.

For a given azimuth pointing and polarisation orientation the effective measurement time T_{band} spent in the band was calculated as:

$$T_{band} = \Delta T_{sweep} \times N_{sweep} \times N_{rep} \tag{5.5}$$

Band	$f_{low} - f_{high}$ MHz	N_{sweep}	N_{rep}	T_{band} sec	N_{hpol}	N_{vpol}	$T_{session}$ min
1	70 - 150	445	5	1335	3	3	133.5
2	150 - 300	834	1	500	3	3	50.0
3	300 - 800	278	1	167	3	3	16.7
4	800 - 960	89	20	1068	3	3	106.8
5	960 - 1400	1	18000	900	3	3	90.0
6	1400 - 2000	334	1	200	3	3	20.0
7	2000 - 3000	556	1	334	5	5	55.6
8	3000 - 6000	50	1	30	5	5	5.0
9	6000 - 9000	50	1	30	5	5	5.0
10	9000 - 12500	59	1	35	5	5	5.9
11	12500 - 18500	100	1	60	5	5	10.0
12	18500 - 22000	59	1	35	5	5	5.9
13	22000 - 26500	75	1	45	5	5	7.5
1–13	70 - 26500			1.31 hr			8.53 hr

Table 5.2: Mode 1 Measurement Schedule Parameters.

Measurements were taken for all required antenna azimuth pointings in both horizontal and vertical polarisation and the time spent per measurement cycle for each band ($T_{session}$) was calculated using:

$$T_{session} = T_{band} \times (N_{hpol} + N_{vpol}) \tag{5.6}$$

For frequency bands below 2 GHz, the Rohde & Schwarz HL033 antenna was used. This antenna required 3 azimuth pointings in both horizontal (N_{hpol}) and vertical (N_{vpol}) polarisation orientations, indicated in Table 5.2. Frequency bands above 2 GHz used the Rohde & Schwarz HL050 antenna and to satisfy the quarter power (i.e. -6 dB) beam width criterion specified in SKA Memo 37, required 5 pointings.

As can be seen from Table 5.2 the total integration time for a single cycle of Mode 1 measurements was 8.53 hours. This was the effective measurement time and did not include overheads such as setting up the spectrum analyser, setting up the RF signal path, rotating the polarisation and azimuth for the antennas, performing calibration measurements, storing the data to disk or readout latency of the spectrum analyser. In practice the Mode 1 measurements took approximately 27 hours for a single cycle of measurements and so for logistical reasons it was only practical to perform one cycle per remote site.

Two sets of noise diode calibration measurements were performed as part of the automated measurement schedule: one just prior to performing the RFI measurements and one immediately afterwards. The bands for these measurements were dictated by the signal paths of the RF system. The spectrum analyser settings (Δf_{sweep}, ΔT_{sweep}, RBW and VBW) used

are those detailed in Table 2.8 of Chapter 2 for the noise diode calibration method.

5.2.2 Mode 2 Bands and Measurement Schedule

Two Mode 2 measurement cycles were performed for the schedule that was run at the Karoo 3 core site using System 2. These measurement cycles consisted of 38 contiguous bands covering the 70 - 26500 MHz frequency range and were done for all permutations of azimuth pointing and polarisation orientation.

As mentioned in Chapter 1, the relatively narrow frequency bands listed in Table 5.3 correspond to the bands of interest to radio astronomy usage as specified in the CRAF Handbook for Radio Astronomy (CRAF, 1997) and shown in Table 1.2.

The calculations of schedule parameters for the Mode 2 measurement cycles were similar to those for the Mode 1 measurements. These parameters are shown in Tables 5.3 and 5.4.

The effective total measurement time to conduct 2 measurement cycles for the Mode 2 schedule was 51.6 hours, excluding overheads. However, in practice, it took approximately 11 days to complete the two cycles. Due to the long measurement time and the requirement of SKA Memo 37 to perform noise diode calibration exercises at least once every 24 hours, noise diode calibration measurements were done regularly during the RFI measurement schedule.

Bands covering a common RF signal path (e.g. RF path A, A*, B, C or D) were grouped together and measured sequentially for each azimuth pointing and polarisation orientation. Prior to the RFI measurements for each set of frequency bands, relevant noise diode calibrations (for paths ND A, ND B, ND C or ND D) were made at every antenna orientation.

The SKA RFP (International SKA Project Office, 2004) called for a set of Mode 2 measurements to be performed at least once a month. Following the final screening efforts at Houwteq, Mode 2 measurements were conducted on a monthly basis. However towards the end of the campaign continuous measurements were performed.

5.3 Performance Monitoring of the RFI Measurement System

To ensure the integrity of the RFI measurement data it was important to monitor system performance during operation in the field. Monitoring was done routinely during system operation and diagnostic plots were compared to the data obtained for system calibration pre-deployment.

Band	$f_{low} - f_{high}$ MHz	Δf_{sweep} MHz	ΔT_{sweep} msec	RBW kHz	VBW Hz	ΔT_{RBW} msec	ΔT_{sample} msec
1	70 - 150	0.18	600	3	300	10	1
2	150 - 153	0.06	600	1	300	10	1
3	153 - 322	0.18	600	3	300	10	1
4	322 - 329	0.14	600	3	300	12.9	1
5	329 - 406	1.8	600	30	300	10	1
6	406 - 410	0.4	600	30	100	45	1
7	410 - 608	1.8	600	30	300	10	1
8	608 - 614	0.6	600	30	100	30	1
9	614 - 1000	1.8	600	30	300	10	1
10	1000 - 1370	1.8	600	30	300	10	1
11	1370 - 1427	1.8	600	30	300	10	1
12	1427 - 1606	1.8	600	30	300	10	1
13	1606 - 1723	1.8	600	30	300	10	1
14	1723 - 2000	1.8	600	30	300	10	1
15	2000 - 2655	1.8	600	30	300	10	1
16	2655 - 2700	6	600	100	300	10	1
17	2700 - 3300	6	600	100	300	10	1
18	3300 - 3400	6	600	100	300	10	1
19	3400 - 4800	6	600	100	300	10	1
20	4800 - 5000	6	600	100	300	10	1
21	5000 - 6000	18	600	300	300	10	1
22	6000 - 6600	18	600	300	300	10	1
23	6600 - 6700	18	600	300	300	10	1
24	6700 - 8600	18	600	300	300	10	1
25	8600 - 8700	18	600	300	300	10	1
26	8700 - 12100	18	600	300	300	10	1
27	12100 - 12200	18	600	300	300	10	1
28	12200 - 12500	18	600	300	300	10	1
29	12500 - 14400	18	600	300	300	10	1
30	14400 - 14500	18	600	300	300	10	1
31	14500 - 18300	18	600	300	300	10	1
32	18300 - 18400	18	600	300	300	10	1
33	18400 - 18500	18	600	300	300	10	1
34	18500 - 22150	18	600	300	300	10	1
35	12150 - 22250	18	600	300	300	10	1
36	12250 - 23600	18	600	300	300	10	1
37	13600 - 24000	18	600	300	300	10	1
38	24000 - 26500	18	600	300	300	10	1

Table 5.3: Mode 2 Measurement Bands and associated spectrum analyser settings.

Band	$f_{low} - f_{high}$ MHz	N_{sweep}	N_{rep}	T_{band} sec	N_{hpol}	N_{vpol}	$T_{session}$ min
1	70 - 150	445	1	267	3	3	26.7
2	150 - 153	50	10	300	3	3	30.0
3	153 - 322	939	1	563	3	3	56.3
4	322 - 329	50	80	2400	3	3	240.0
5	329 - 406	43	1	26	3	3	2.6
6	406 - 410	10	222	1332	3	3	133.2
7	410 - 608	110	1	66	3	3	6.6
8	608 - 614	10	333	1998	3	3	199.8
9	614 - 1000	215	1	129	3	3	12.9
10	1000 - 1370	206	30	3708	3	3	370.8
11	1370 - 1427	32	100	1920	3	3	192.0
12	1427 - 1606	100	10	600	3	3	60.0
13	1606 - 1723	65	100	3900	3	3	390.0
14	1723 - 2000	154	1	92	3	3	9.2
15	2000 - 2655	364	1	218	5	5	36.4
16	2655 - 2700	8	100	480	5	5	80.0
17	2700 - 3300	100	1	60	5	5	10.0
18	3300 - 3400	17	100	1020	5	5	170.0
19	3400 - 4800	234	1	140	5	5	23.4
20	4800 - 5000	34	100	2040	5	5	340.0
21	5000 - 6000	56	1	34	5	5	5.6
22	6000 - 6600	34	1	20	5	5	3.4
23	6600 - 6700	6	100	360	5	5	60.0
24	6700 - 8600	106	1	64	5	5	10.6
25	8600 - 8700	6	100	360	5	5	60.0
26	8700 - 12100	189	1	113	5	5	18.9
27	12100 - 12200	6	100	360	5	5	60.0
28	12200 - 12500	17	1	10	5	5	1.7
29	12500 - 14400	106	1	64	5	5	10.6
30	14400 - 14500	6	100	360	5	5	60.0
31	14500 - 18300	212	1	127	5	5	21.
32	18300 - 18400	6	100	360	5	5	60.0
33	18400 - 18500	6	1	4	5	5	0.6
34	18500 - 22150	203	1	122	5	5	20.3
35	12150 - 22250	6	100	360	5	5	60.0
36	12250 - 23600	75	1	45	5	5	7.5
37	13600 - 24000	23	100	1380	5	5	230.0
38	24000 - 26500	139	1	83	5	5	13.9
1-38	70 - 26500			6.99 hr			51.6 hr

Table 5.4: Mode 2 Measurement Schedule Parameters.

During the course of the measurements, noise diode calibrations were done as part of the schedule discussed in Sections 5.2.1 and 5.2.2. This data was, however, only analysed after a schedule of measurements had been completed and was therefore subject to a delay of up to a week. To reduce the risk of losing data arising from system malfunction or deterioration of the RF sub-system, three procedures were therefore undertaken:

- System Integrity Checks in the field
- Monitoring of Calibration Data
- Post-deployment Calibration Procedures

As the measurement systems were required to operate in harsh environmental conditions, it was important that recovery measures were in place in the event of failure. One concern was for the computer hardware and especially the computer hard disks on which the measurement data and software was stored. To provide a quick turnaround time all measurement systems were equipped with two hard disks. These disks were duplicated using disk imaging software (Acronis True Image) and allowed a direct disk replacement when a failure occurred. During the measurement campaign only one hard disk failure was experienced. Fortunately, all data was recovered and measurements were continued shortly afterwards, with the backup hard disk.

5.3.1 System Integrity Checks

To validate correct functioning and health of the measurement systems, a system integrity check was done prior to commencement of the RFI measurements. These checks were performed manually by the ICASA field operators with a stand-alone application developed in LabVIEW running on the Control PC. The application functioned similarly to the RFI Measurement Scheduler VI with the exception that no data was recorded to disk. Controlling all aspects of the RF measurement system, sequential measurements were conducted for each noise diode signal path. The system integrity check application ran two measurements for each of the noise diode signal paths: one with the noise diode powered on and one with it power off. The data from both scans was displayed on the screen (see Figure D.2 in Appendix D.2) allowing the operator to determine if the system was working correctly. If the results from the integrity check were within specification, RFI measurements would be initiated and the operator would leave the site immediately.

Using this integrity check it was possible to determine if:

- the power and control cables were connected correctly. This ensured that there was power to the Electronics Control Box, RF Mast-Head Box electronics and the spectrum analyser;
- the RF cables were connected and the cable connections torqued correctly. This ensured the connection of the 10 MHz reference cable between the Electronics Control Box and the Mast-Head Box. The connection between the spectrum analyser and RF Mast-Head Box with the 10 m Sucoflex cable was also validated. An incorrectly torqued Sucoflex cable connection resulted in sharp notches in the spectrum which were easily identified, especially at high frequencies;
- the amplifiers were undamaged. Each amplifier could be identified by its characteristic passband which was typically more than about 10 dB above the noise floor of the spectrum analyser;
- the RF switching was working correctly. The RF switches were switched to specific states during the procedure which was necessary for determining the consistency of the switching;
- the correct functioning of the microcontroller. Correct communication and control of the microcontroller was asserted as a by-product of successful RF switching.

A screen-shot of the front panel for the System Integrity Check VI is shown in Appendix D.2 along with the associated block diagrams of the LabVIEW code.

5.3.2 Monitoring of Calibration Data

Identification of the deterioration of system performance and malfunction was vital to ensuring the reliability of the RFI measurement data. Due to the long measurement schedules and tight project time-lines, it was important that the recording of bad data was minimised.

An instance where the Sucoflex RF co-axial cable connector was not torqued correctly was picked up in the very first remote site measurement. The noise diode calibration data recorded during this measurement schedule is shown in Figure 5.2, illustrating the characteristic notch filter. The problem was a loose connection between the Sucoflex co-axial cable

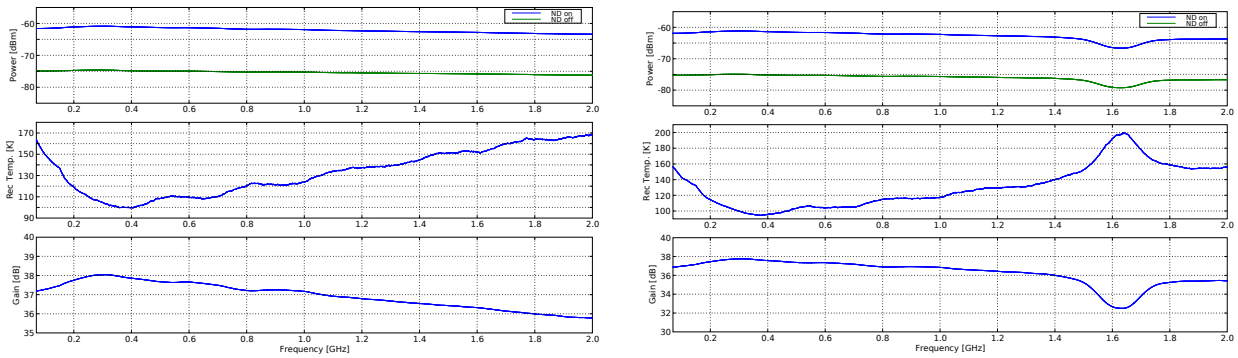

Figure 5.2: Noise diode data from signal path 'ND A' (0.07-2.0 GHz) for System 1 at remote site RFI-01. Left: Data from the calibration sequence done before the start of the measurement cycle. Right: Data from the calibration sequence done at the end of the measurement cycle showing the notch at 1.6 GHz. In both calibration sets, a raised noise floor below 400 MHz can be seen which is due to LNA 1's detuned passband.

and the spectrum analyser N-type bulk-head connector and was attributed to vibrations of the measurement trailer and equipment during transportation on dirt roads.

Intermittent problems with the RF switching were also detected with the system integrity check application. The switching fault was found to be caused by a software misconfiguration with the microcontroller on the Control PCB and an update was performed as soon as possible.

5.3.3 Post-Deployment Calibration

After more than half the remote sites had been measured the Mode 1 RFI measurement systems (Systems 1 and 3) were returned to the laboratory for post calibration. There was concern that the spectrum analysers and RF sub-systems may have suffered damage while being transported thousands of kilometres over rough dirt roads. Due to System 2 being permanently stationed at the Karoo 3 core site it was deemed unnecessary for this system to undergo this procedure.

To analyse the possible deterioration of the RF sub-system, noise diode calibration measurements were performed as done for the system temperature tests described in Section 2.3.3. Comparison with the initial results obtained pre-deployment to the field indicated little deterioration of the RF sub-system performance. The only variance detected was for the low band LNAs (LNA 1) in both System 1 and System 3. This change can be seen in Figure 5.2, which shows an increased system temperature for frequencies below 400 MHz. Despite the degraded performance, the system temperature requirement ($< 30000\,\mathrm{K}$) for the Mode 1 measurements was still met and no data was discarded. The amplifiers were returned

to the manufacturer for testing and it was found that their passbands had become slightly detuned.

To test that the spectrum analyser had not been damaged, noise calibration measurements were performed using a spare spectrum analyser (Agilent HP8563E) from the laboratory and were compared with data obtained pre-deployment. The spare analyser was calibrated and had not been in the field. Figure 5.3 shows the results of this comparison and no major variations between the two analysers were found. The raised noise floor in the lower frequency bands was a result of the detuned LNA passband mentioned above. The discrepancy in the noise diode off measurement at 18.5 GHz and 26.5 GHz was attributed to differences between the instruments and not specifically the deterioration of the spectrum analyser from the field.

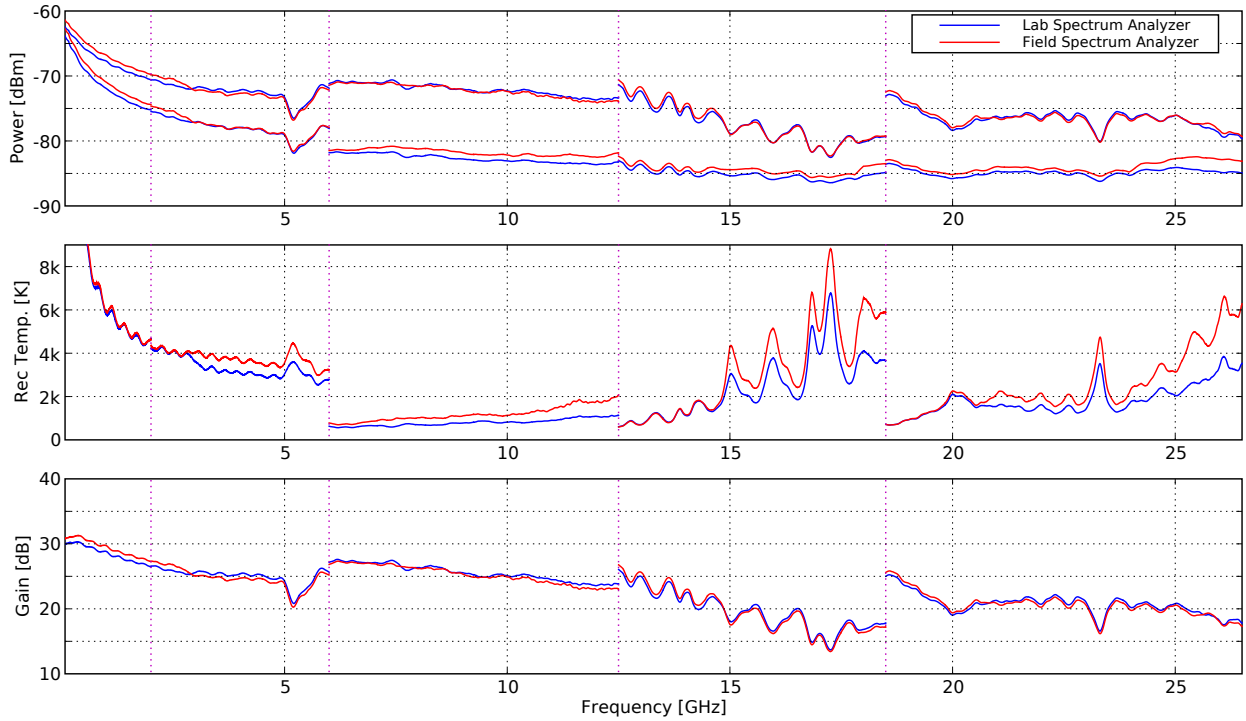

Figure 5.3: Performance comparison of an Agilent spectrum analyser which had been used for RFI measurements in the field and a calibrated Spectrum Analyser (same model) from the laboratory. The pink vertical lines indicate the RF signal path transitions.

5.4 Cross-Calibration of the Measurement Systems

During the course of the measurement campaign, a third party was contracted by the International SKA Project Office (ISPO) to conduct RFI measurements at each of the bidding countries proposed sites. The Dutch Astronomy Institution, Astron built an RFI mea-

surement system (Millenaar, 2005) and arrived to measure at the Karoo 3 core site in the Northern Cape for 6 weeks over April and May 2005. The system was called the SKA Site Spectrum Monitoring (SSSM) and it was built in accordance to the requirements of SKA Memo 37.

A necessary outcome of the visit was to cross-calibrate the instruments used at the host country with those of the Astron team (Hall, 2005). This was achieved using a pair of suitable transmitting antennas (R&S HL033 and HL050) and RF signal generator (HP8340B) installed on a vehicle. Using the appropriate antenna, a signal of known frequency and power was transmitted in the direction of the measurement site and measurements were recorded manually on the various receiver systems.

To ensure the systems were operating correctly, the predicted power levels of the received signals were calculated for each system and these were compared against their measured values. The received powers were also converted to units of spectral power flux density ($dB.W.m^{-2}.Hz^{-1}$), which allowed for a direct comparison between measurement systems, independent of their respective gains.

5.4.1 Cross-calibration Set-up

The South African team had two RFI measurement systems that were compared against the Astron system: the sensitive System 2 with the wide band post-amplifier and System 1 used for the RFI measurements at remote sites. Construction of System 3 was not completed at this time, however from the system performance plots shown in Appendix A.7 it was shown to exhibit similar performance to System 1. The level of RFI signals measured with System 3 at the Karoo 3 core site also confirmed this consistency between the systems.

The mobile transmitting system was set up at two measurement points located at roughly 40 metres and 185 metres from the receiver systems so that far-field conditions applied. Measurements below 2 GHz were done using the 40 m transmitter location and those above 2 GHz at 185 m. The transmitting antennas were pointed towards an azimuth position half-way between the receiver antenna sets to provide equal coverage of the main beam. The receiving antennas were directed towards the transmitting antenna to maximise the signal strength and measurements were only done in the vertical polarisation orientation to minimise the effect of ground reflections.

The set-up for the cross-calibration is shown in Figure 5.4 with a photograph taken during the procedure shown in Figure 5.5.

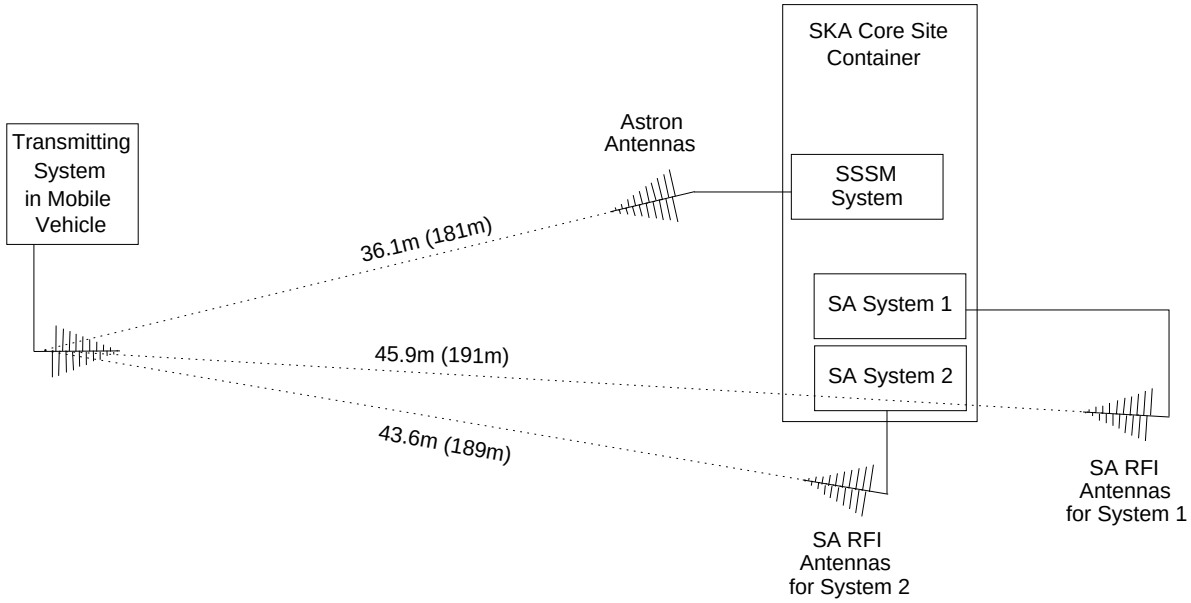

Figure 5.4: Set-up of the measurement systems for the cross-calibration procedure performed at Karoo 3 core site.

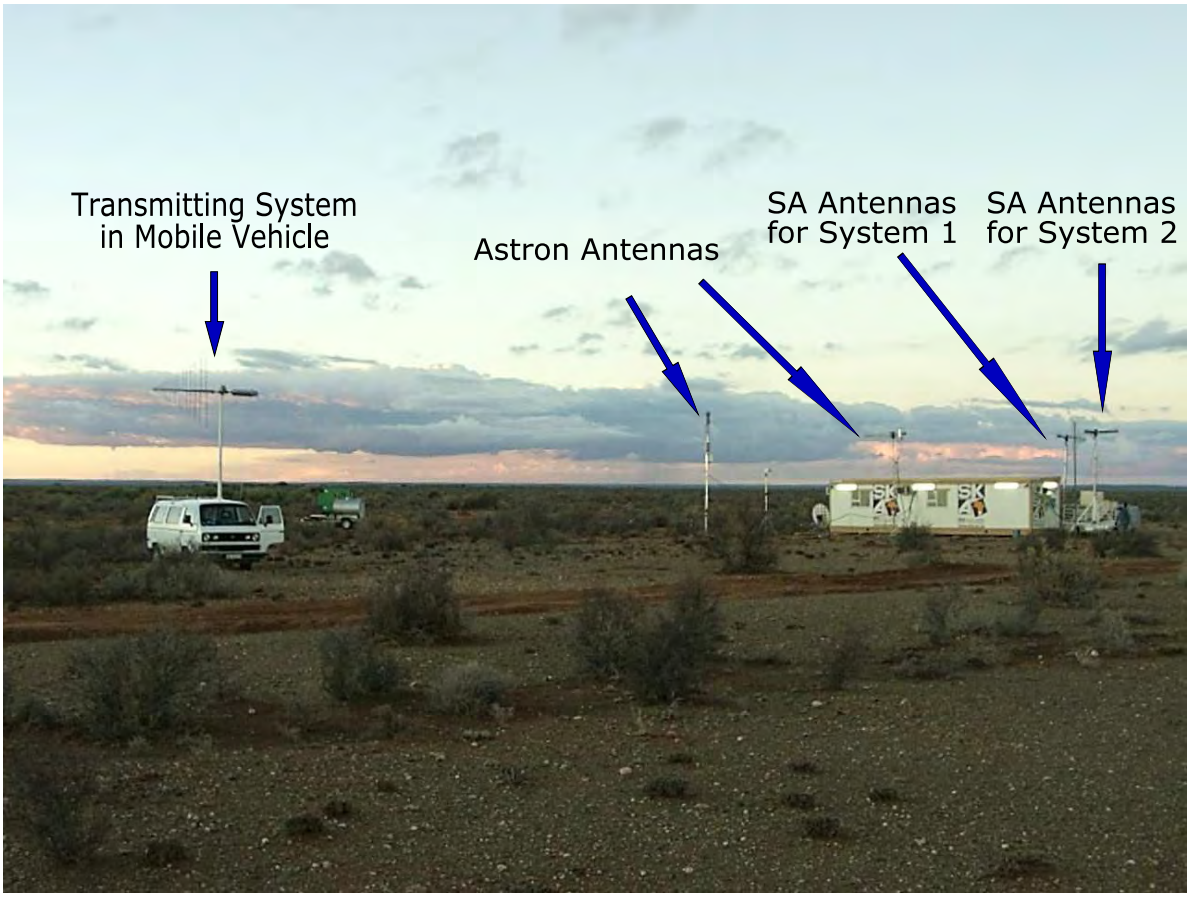

Figure 5.5: Photograph of the cross-calibration exercise that was conducted with the Astron SSSM team and the South African RFI measurement team in April 2005 at the Karoo 3 core site. The photograph shows the setup of the transmitting system in the mobile vehicle, the Astron SSSM RFI measurement System antennas and the South African antennas from RFI measurement systems 1 and 2.

5.4.2 Cross-calibration Comparison of Measurement Systems

Measurements were made in 10 MHz steps from 60 MHz to 0.1 GHz, 100 MHz steps from 0.1 GHz to 3 GHz, 200 MHz steps from 3 GHz to 6 GHz, and from 6 GHz to 26.5 GHz 500 MHz steps were used. In switching between different RF signal paths on the SSSM and South African RFI measurement systems, duplicate readings were taken in both RF signal paths at the frequency of the band transition.

The magnitude of the transmitted signal was set close to the level of the ambient RFI signals and was adjusted so that it could be clearly and unambiguously detected by all 3 measurement systems. The spectrum analyser settings for all systems were set up identically with 1 kHz resolution bandwidth (RBW) and video bandwidth (VBW). The detected power readings on the spectrum analysers were recorded manually by the measurement teams and were relayed back to operators in the mobile transmitting system over wired stage production headsets and communication terminals.

Friis' transmission formula (IEEE Standards, 1997) was rewritten in terms of gain (see Appendix D.4), resulting in the following equation that was used to predict power levels on the various measurement systems:

$$\mathrm{P}_{rec}(f)\,[\mathrm{W}] = \mathrm{P}_{trans}(f)\,[\mathrm{W}] \times \mathrm{G}_{trans}(f) \times \mathrm{G}_{rec}(f) \times \left(\frac{\lambda\,[\mathrm{m}]}{4\pi\,d\,[\mathrm{m}]}\right)^2 \tag{5.7}$$

In this equation, P_{rec} is the received power indicated on the spectrum analyser and P_{trans} the signal generator power, with G_{rec} and G_{trans} as the respective system gains. λ is the wavelength of the transmitted signal and d the distance between the two antennas.

The transmitting system did not have any amplifiers and therefore G_{trans} only included the cable losses and the antenna gains. Values for the cable losses were taken from differential measurements done in the laboratory using the Frequency Sweeper VI. For the R&S HL033 transmitting antenna gain the supplied manufacturer data was used. The R&S HL050 was not supplied with individual device gain data and so values obtained from the data sheet (Rohde & Schwarz, 2006a) were used as done for three RFI measurement systems.

For the receiving systems, the receiver gain G_{rec} consisted of the respective antenna and system gains for each system. The system and antenna gain data were as per the values discussed in Chapter 2 for each measurement system.

The plot in Figure 5.6 shows the predicted and detected power values for the various RFI measurement systems. In most cases the measured signals tracked the predicted values to within 4 dB. The measured signals were typically less than the predicted values, which

can be accounted for by destructive interference caused by reflections of the test signal off the ground and measurement container structures. Overall, this exercise indicated that the systems were functioning correctly.

To do a cross comparison of the flux scales of the systems, the dBm power values were converted to units of spectral power flux density using parameters for each respective system. The equation (Equation 6.1) for this calculation is specified in Chapter 6 where the calculation of the main RFI measurement results are discussed.

Figure 5.7 shows the resulting flux power values for the various RFI measurement systems. Here it is seen that the flux scales for SA RFI systems compared well to that of the Astron SSSM system.

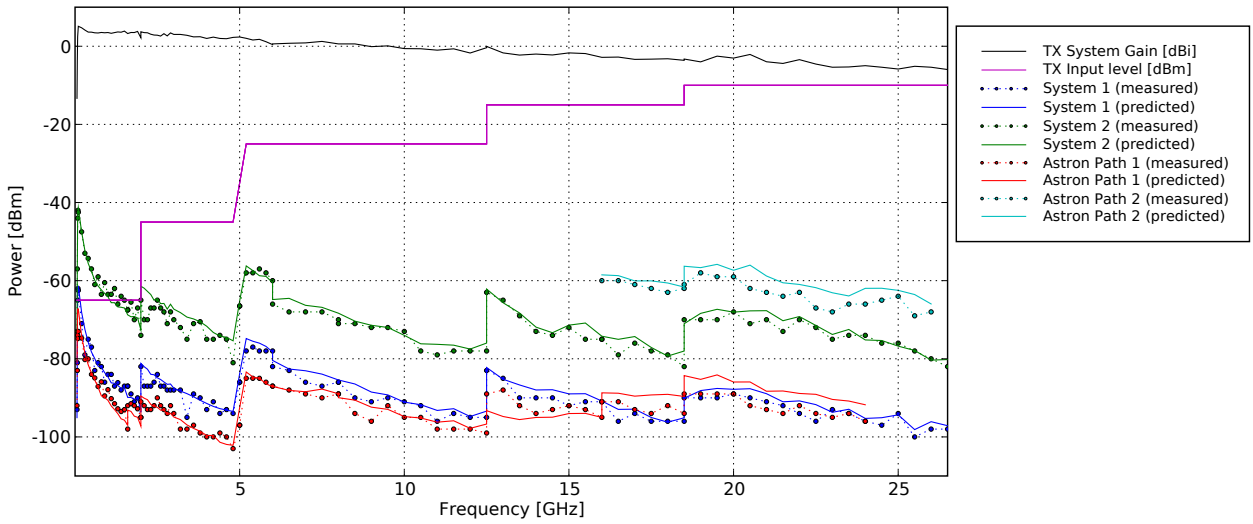

Figure 5.6: Measured and predicted signals of the measurement systems during the cross-calibration procedure. The levels of the transmitted signal (indicated as 'TX') are also shown.

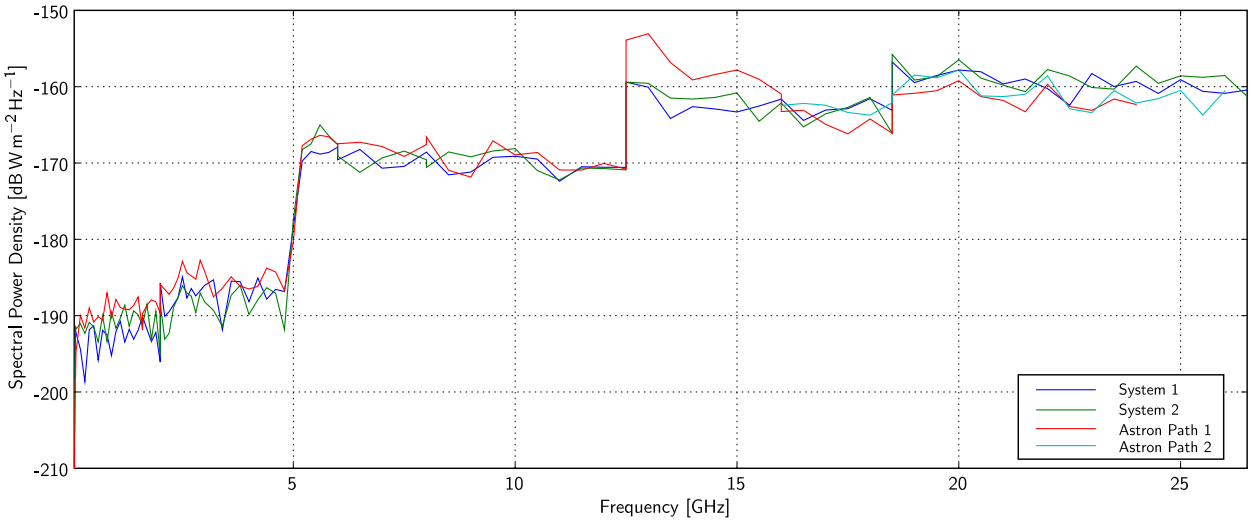

Figure 5.7: Spectral power flux density plot of the RFI measurement systems for the cross-calibration procedure.

Chapter 6

Data Processing

This chapter details the processing that was performed on the recorded RFI data to produce various data products. The processing included data archiving, data editing, calibration, merging and production of graphical output. The data products included "quick look" spectrum plots to monitor the measurement performance and the plots required by SKA Memo 37.

The tools that were developed to perform the necessary processing and produce the data products are described in some detail.

6.1 Background

Most of the development for the data processing software occurred towards the end of the RFI measurement campaign (see Figure 1.1). Prior to this, preliminary analysis was done using applications developed to produce un-calibrated spectrum plots of the data for quality assurance purposes. As soon as the relevant components for a new application became usable the old software was discarded and the new procedures were followed to re-process all the data. This parallel production and development mode was enforced by tight time constraints.

The calibration and analysis was reasonably straightforward. However, due to the large amounts of data, the sorting and processing was a substantial computing task and the implementation had to be carefully worked out. In total, approximately 100 GB of raw RFI data was recorded. This included more than 13000 files for 39 sites that were measured during the campaign. In order to facilitate the parallel production/development mode the processing was broken down into a serial sequence of operations and an appropriate chain of tools was developed to implement the processing pipeline. This approach avoided unnecessary re-

processing of data as the tools were developed. Figure 6.1 shows a flow chart diagram that outlines the steps for the data analysis pipeline. The processing steps performed will be referred to in this chapter and the table in Appendix E.1 outlines the programs used. The source code for all applications used may be found in electronic format on the accompanying CD (Appendix F).

The data analysis requirements laid out in SKA Memo 37, together with the Astron/SSSM Data Summary Report (Boonstra and Millenaar, 2006), were used as guidelines for the design of the data processing tools. The specification called for various spectrum plots for Mode 1 and Mode 2 measurements, as well as bar charts indicating spectral band occupancy.

Due to budget constraints the data analysis software was developed using open source software. The processing software was developed in the C and Python languages on a Linux platform. Most of the low-level processing tools were written in C. However, as further levels of complexity were added during the development of the software, Python was used more frequently. Python suits an environment where rapid application development (RAD) of complex file handling and database programs is required. The Python scripts allowed a number of low-level tasks (performed by the C programs) to be chained together and run on multiple data files. The author was already familiar with the PHP language and its capabilities, and so this was the language of choice for creating the interactive data-flagging application. A MySQL database running on the Linux platform stored the parameters for the measurement data and the information regarding the data-flagging.

6.2 Preliminary Data Analysis

The purpose of the preliminary data analysis was to ascertain whether or not the RFI systems were functioning correctly and that there were no spurious signals. Once all three measurement systems were deployed in the field and running simultaneously it was important that system malfunctions or bad RFI data were identified as soon as possible so that remedial action could be taken. In Chapter 5, it was mentioned that an incorrectly torqued connector of the RF feed cable was identified in the first remote site that was measured. This was realised during the system integrity check procedure, and was confirmed by the preliminary analysis once the data had been received from the field. This site was re-measured a few days later.

The preliminary data analysis was done on a low-end desktop PC. A collection of Bash

shell scripts extracted parameters from the RFI schedule file and passed these to a generic C program. The C program produced un-calibrated spectrum plots in spectrum analyser dBm power units and these were reviewed manually.

A similar C program and further set of Bash scripts generated noise diode plots. These plots displayed the spectral scans of the noise diode in its 'on' and 'off' states and were used for system health checks.

The software for the preliminary analysis became redundant once the full data processing suite was complete and the preliminary analysis code was not used for any subsequent processing.

6.3 Data Preparation

A Linux RAID server running an Apache web server and MySQL database facilitated the data archiving, data editing, calibration and merging functions for the analysis. To perform the calibration and data analysis it was necessary to do some pre-processing on the data. These data included:

- RFI Measurement Data
- Component Specification and Calibration Data

The RFI Measurement Data was measured by the spectrum analyser and recorded to file by the Control PC for each RFI measurement system. These data sets contained the RFI measurements used to characterise the RF environment and the noise diode calibration files, taken during the Mode 1 and Mode 2 measurement cycles.

The Component Specification and Calibration Data was required in order to calibrate the RFI Measurement Data. This consisted of the antenna gain data, the noise diode excess noise ratio (ENR) data and the system gain data measured by the direct gain method discussed in Section 2.3.2.

6.3.1 RFI Measurement Data

The raw RFI data collected from the RFI measurement systems was copied on to DVDs on site and then couriered to the processing office for analysis. A unique name based on the RFI measurement system number and date of the measurements was assigned to measurements conducted at each measurement site. The RFI measurement data along with the noise diode

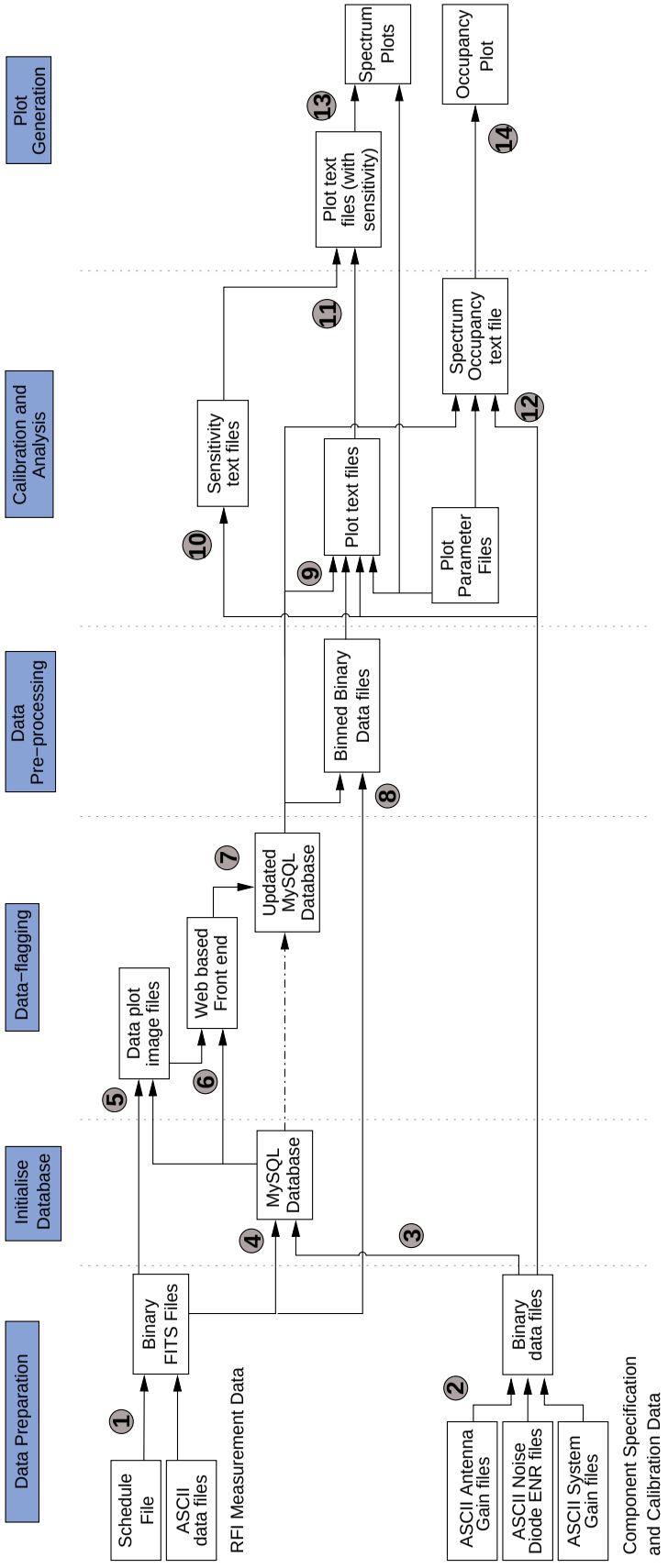

Figure 6.1: Overview of the data analysis pipeline. The various steps for the processing pipeline are indicated by the numbers 1 - 14.

calibration data files were transferred to directories named according to the batch names on the analysis machine.

The raw data as recorded by the RFI Measurement Scheduler VI was stored in "tab delimited" ASCII format and consisted of rows of frequency and power values read from the spectrum analyser. While this format was inefficient for storage, it allowed for easy data format translation by applications such as MS Excel and MathWorks MATLAB. These packages were used for data visualisation prior to the development of the analysis software. The large volume of RFI data meant that reading it into any general purpose commercial application was slow and sometimes impossible.

Each RFI measurement and noise diode calibration file contained timestamp information embedded in the filename. Other differentiating information included azimuth pointing number, polarisation orientation, noise diode state and the start and stop frequency. Spectrum analyser settings such as resolution bandwidth (RBW), video bandwidth (VBW), reference level and sweep time were not contained in the data files. This measurement specific information was located in the schedule files which were used by the RFI Measurement Scheduler VI to perform the automated Mode 1 and Mode 2 measurements.

To allow each measurement file to be self contained, and hence portable, the Flexible Image Transport System (FITS) (Wells and Greisen, 1979) format was chosen. All information relating to a measurement (e.g. RFI site, RFI measurement system, spectrum analyser settings, batch and timestamp) was inserted into the header section for each FITS file. As the header contained all the information for regenerating the corresponding frequency values, only the power values were stored. The ASCII format power values from the RFI measurement files were converted to the 16-bit unsigned binary format originally read back from the spectrum analyser and were stored in the FITS binary table format. The diagram in Figure 6.2 shows explicitly how the header information and power values were stored in these files and the conversion process is indicated as Step 1 in Figure 6.1.

During the process of converting to the FITS binary table format, incomplete and corrupt data files were manually discarded. Incomplete files resulted from power failures (caused by the diesel generator running out of fuel), computer failure or manual operator termination. The number of corrupt files that were discarded was small and the cause was attributed to deterioration of the DVD media. Computer failures occurred when the operating system 'locked up' and became unresponsive. This was a result of damage to the hardware during transportation and overheating issues, which caused the failure to one of the hard disks.

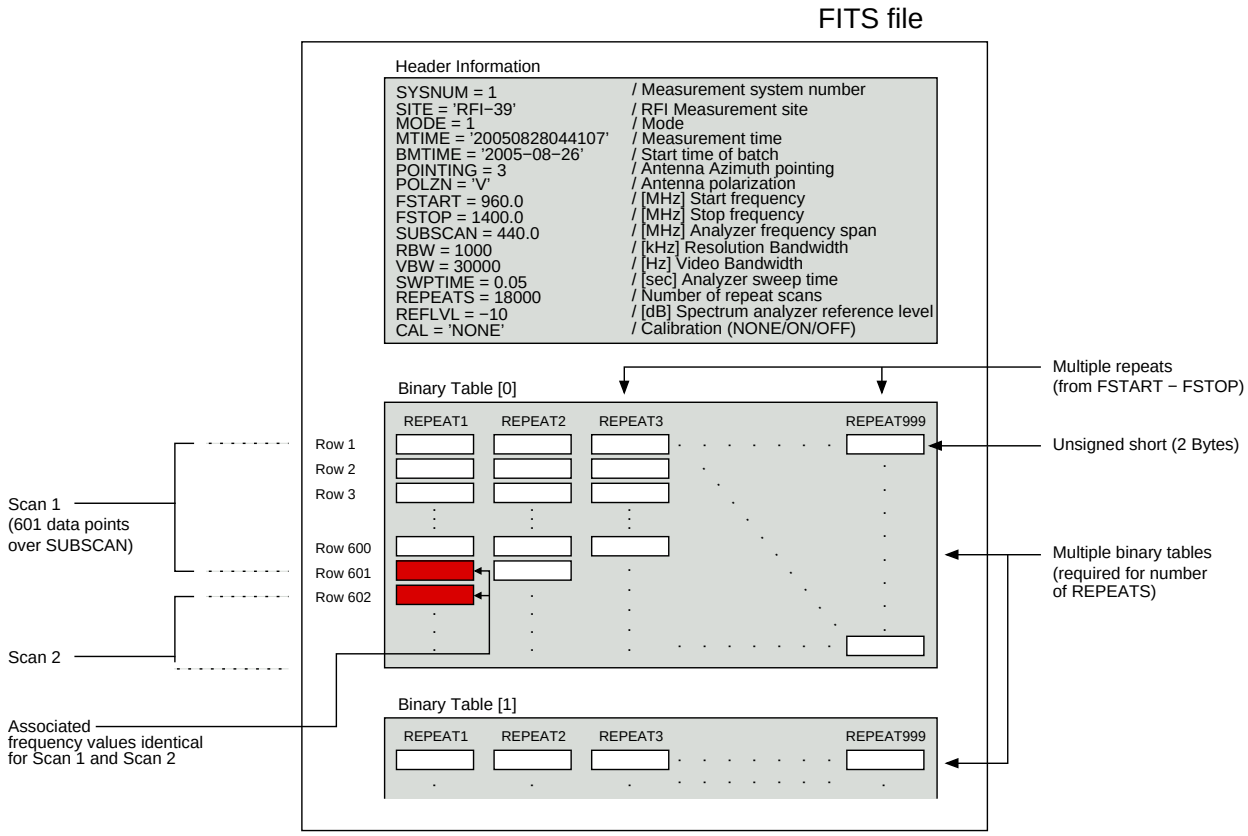

Figure 6.2: Example of the FITS binary table file format. The header section is used to store parameters associated with the measurement data and power values are stored in binary tables. Multiple scans (SUBSCANS) were performed by the spectrum analyser to cover the frequency band (FSTART - FSTOP) and this data is appended to the columns (as indicated for *Scan 1* and *Scan 2*). Each repeated frequency band measurement is assigned to a separate column and due to the limit of 999 columns for a table, multiple binary tables are used when there are more than 999 repeats (REPEATS). It is noted that despite the diagram indicating multiple sub-scans only one scan is needed (1400 MHz - 960 MHz = SUBSCAN (440 MHz)) for this specific data file.

Identification of incomplete measurements was aided by the use of the log file generated by the RFI Measurement Scheduler VI.

6.3.2 The Component Specification and Calibration Data

The sources for this data came from component data sheets, calibration data files (supplied on disk by the manufacturer) or as processing products from the system gain calibration procedure. The data comprised:

Noise diode excess noise ratio (ENR): obtained from the noise diode ENR calibration disk produced by the manufacturer.

Antenna gain: obtained from the calibration information provided by the manufacturer (HL033) and component data sheets (HL050).

System gain: obtained from measurements done using the direct gain calibration method (Section 2.3.2).

Separate files were used to store the noise diode data, antenna gain data and system gain for each system. A binary file format was chosen to improve retrieval time and the frequency and gain (or ENR) values were recorded. The process of preparing the Component Specification and Calibration Data files for use by the analysis program is indicated as Step 2 in Figure 6.1.

6.4 Data Management and Integrity

Archival functions were performed by a MySQL database that was set up to manage the RFI Measurement Data and Component Data files. The database was used extensively in the data analysis and its functions included:

- storing the name and location of all RFI Measurement and Component Data files on the filesystem;
- storing the system number, site and other measurement parameters contained in the headers of the FITS files;
- keeping track of data-flagging information;
- selecting groups of RFI measurements to be processed based on their measurement parameters;

- selecting relevant system calibration data (Component Data files) to be applied to RFI measurement data;

- retrieval of measurement parameters for performing calculations and data-flagging operations.

6.4.1 Database Initialisation

Before the database could be used it had to be initialised and populated with all the associated information for the RFI Measurement and Component Data files. This task was performed by executing standard Structured Query Language commands on the MySQL database with two Python scripts indicated as processing Steps 3 and 4 in Figure 6.1.

The scripts recorded the filename and filesystem path for each data file along with other information such as the measurement system number (i.e. 1, 2 or 3) and the operating frequency range. Step 3 was only performed once and loaded the Component Data (noise diode ENR, system gain and antenna gain) for all three systems into the database. As the calibration of the system gain was performed more than once for some of the RFI measurement systems, a timestamp indicating the date of re-calibration was recorded in the database. This provision allowed the relevant system gain data to be applied accordingly during the calibration of the RFI Measurement Data.

In Step 4, the Python script extracted all header information from the FITS files and recorded this in the database. By default, each entry was set to an 'unchecked' status, indicating that no data-flagging had been done on the measurement. The database initialisation for the RFI measurement data was done separately for each batch of measurements as and when they were received from the field.

6.4.2 Data-flagging

Because of system malfunctions, some data files contained bad data. The most common malfunction was that the RF co-axial switches in the Mast-Head Box did not switch to the correct state. These bad data files had to be identified and flagged for exclusion from further processing.

Apart from the switching malfunctions, measurements were also discarded in situations where it could be seen that:

- the system behaved non-linearly, due to the RF front-end being over-driven by nearby

broadcast transmitters;

- there was excessive locally generated RFI from the local environment;
- the RF cables had become loose, presumably from transport and vibration from the diesel generator during operation, and the system performance was degraded.

A dynamic web-based front-end was developed in PHP to perform data-flagging. This application interfaced with the MySQL database (Step 6) and allowed the flagging information to be updated, as indicated by Step 7 in Figure 6.1.

A program was developed using the PGPLOT (Pearson, 2007) libraries to generate raw data plots for each FITS file. Different colours were assigned for repeated scans in the measurement band and the plots were saved as PNG images, which were suitable for embedding in web pages. On user request, a web page was then generated dynamically for a selected measurement and served by the Apache web server. The page contained the plot image and the associated measurement parameters alongside. A screen-shot in Figure 6.3 shows an example of the generated web page.

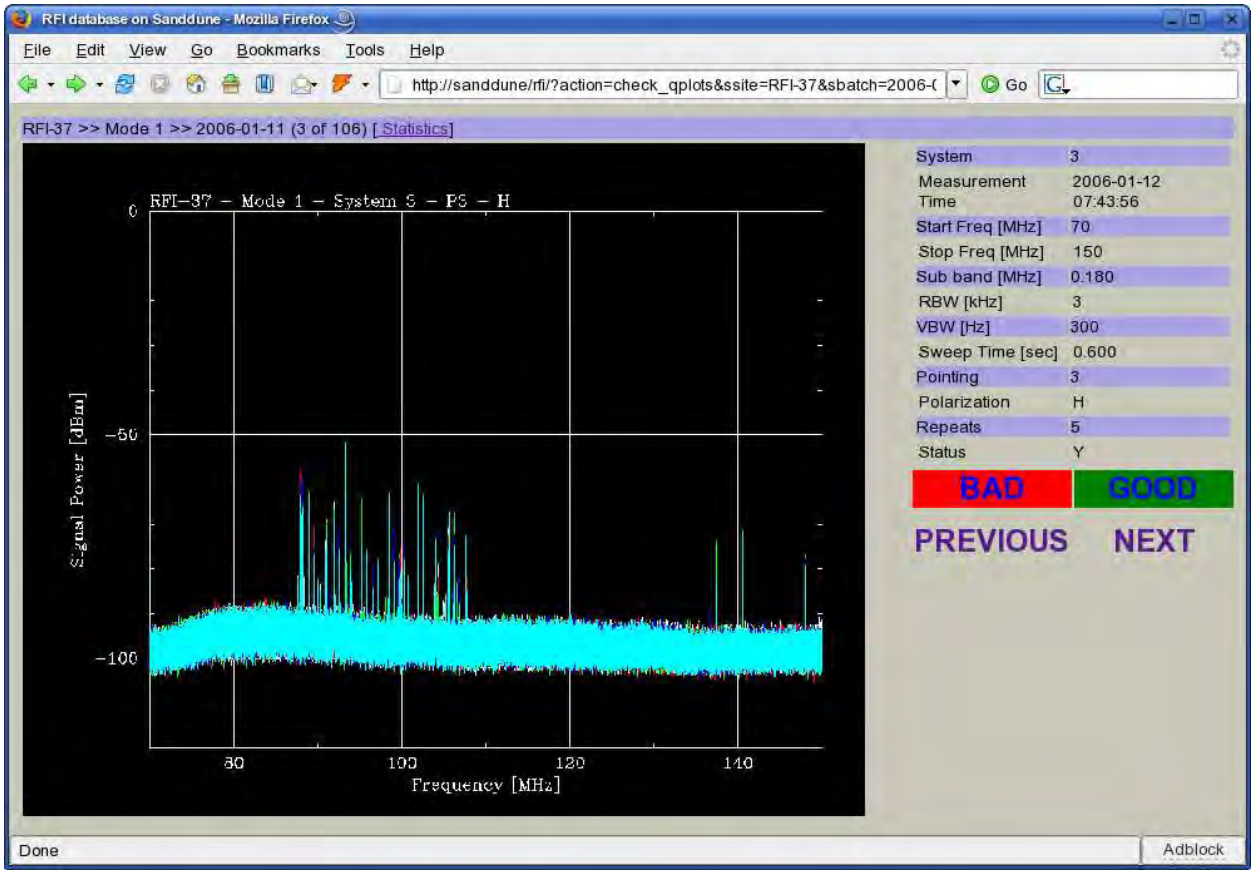

Figure 6.3: Screen-shot of the web-based interface used for data-flagging.

By following the hyperlinks ("GOOD", "BAD", "PREVIOUS", "NEXT") a user could interactively browse different batches of measurements and flag "GOOD" or "BAD" measurement data. Reviewing the raw data plot image, its parameters and sometimes by browsing other measurements in the same band, a decision could be made about the measurement's validity. Using the appropriate link, this change was permanently updated in the database.

As mentioned in Section 6.1, the total number of files in the system was considerable, with more than 11500 RFI measurement files and 2700 noise diode calibration files. The web-based data-flagging application facilitated concurrent data-flagging by multiple users and this allowed the flagging exercise to be completed in a few days. As the noise diode calibration files were not used for final calibration purposes, flagging was only performed on the RFI Measurement Data.

A statistical summary of the data-flagging done on all Mode 1 measurement batches is shown in Figure 6.4. Similar plots in Appendix E.2 show the corresponding success rates for the Mode 2 measurements at the Karoo 3 core site.

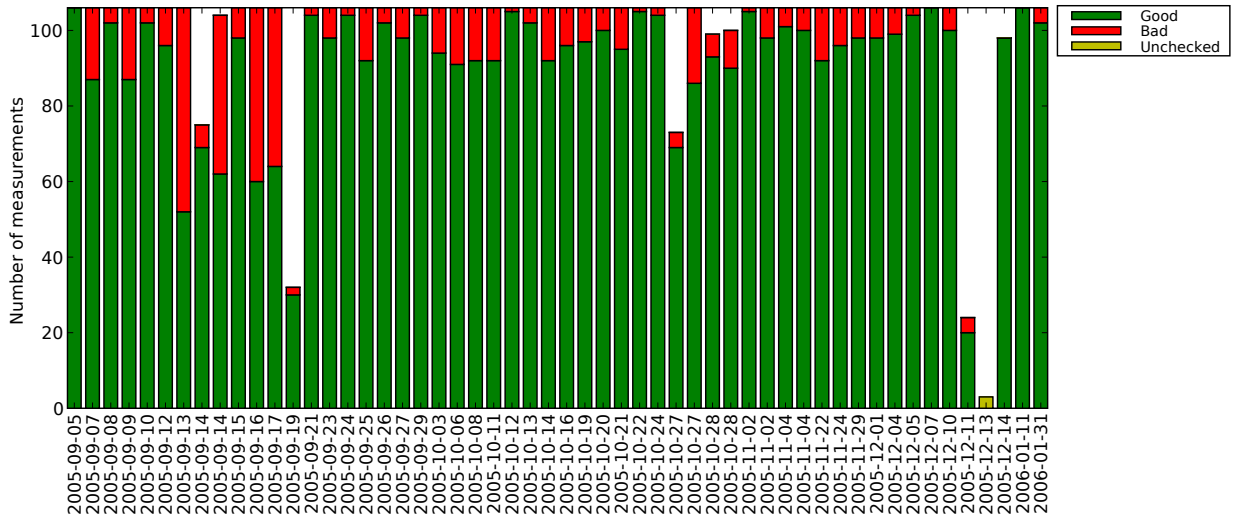

Figure 6.4: Statistics of the data-flagging done for all Mode 1 measurement batches. No distinction is made between the RFI measurement systems or the different remote sites.

6.5 Data Pre-processing

The spectrum analyser recorded 601 equi-spaced power samples across the sweep span Δf_{sweep}, i.e. frequency sample spacing of $\Delta f_{sweep}/601$. The choice of frequency span Δf_{sweep} (see Table 5.1 and 5.3 in Chapter 5) used on the spectrum analyser lead to an oversampling for the given RBW by a factor of 10 in most frequency bands, and for some bands there

were repeated scans (N_{rep}). These conditions led to multiple values being recorded for each frequency channel.

Prior to performing the calibration and analysis, the multiple values were aggregated into frequency bins defined by the RBW used for the measurements. For each FITS file a separate binary file was created containing the bin information. The values within each bin were sorted in amplitude to reduce processing effort in the analysis later on. The data pre-processing was performed in Step 8 (Figure 6.1) of the data analysis pipeline and was executed by a low-level C program and Python script.

6.6 Calibration and Analysis

For the calibration and analysis procedures the band specific measurement data in the binary files had to be combined in various ways:

Mode 1: measurements were combined for all antenna pointings and polarisations.

Mode 2: measurements were combined separately for each permutation of antenna pointing and polarisation.

A separate analysis was performed for each batch of Mode 1 measurements i.e. for each RFI remote site. Bands were combined for all pointing directions and polarisation orientations. This increased the number of data values to be processed, which had been low due to the single measurement cycle and low number of repeats (N_{rep}) for this mode. This suited the purpose of the Mode 1 protocol, which was to identify the levels of strong RFI sources.

For the Mode 2 analysis, 8 months of data measured at the Karoo 3 core site was used. Each independent pointing and polarisation was combined to identify the weaker transient signals. With multiple measurement batches and two measurement cycles per observing session, the number of data values for this mode was large.

6.6.1 Plot Parameter Files

To allow flexibility in performing the analysis, plot parameter files were used. These files served multiple purposes in the data analysis tool-chain:

- they provided a simple interface for specifying data selection criteria for the database;
- they allowed refinements to the plot generation without the need for re-running the data analysis;

- they were also used for the generation of spectrum occupancy statistics.

The files contained parameters for the frequency bands, RFI site, RFI measurement system number, azimuth pointing, polarisation orientation and measurement batches that were to be used. The format of the parameter files was ASCII text and the parameters were listed as variable declarations. This made it easier to create new or edit existing analyses and provided a consistent interface independent of the analysis software application or version.

An example of the usefulness of the parameter files was realised in the creation of an analysis chain for the batch of Mode 2 measurements recorded during the Astron/SSSM team visit. Different from the Mode 1 and Mode 2 requirements, the analysis was done by combining all pointings for each polarisation; so for the two plots, only two parameter files were needed. An example of one of these plot parameter files is shown in Appendix E.3.

6.6.2 Calibration

In order to calculate the signal levels received by the RFI measurement systems, the corresponding system and antenna gains needed to be applied to the spectrum analyser data stored in the binned binary data files. For cases in which there was no gain value for a specific frequency, linear interpolation was used to calculate a value. Interpolation was done using the existing antenna and system gain information stored in binary format from Step 2. Queries to the database were used to determine which system's antenna was required and for the system gain (G_{sys}) also which set of gain measurements to use – taking into account that some systems had been calibrated more than once for the system gain laboratory tests.

Equation 6.1 was used to calibrate the data in units of spectral power flux density and it is shown in decibel units as used in the analysis program.

$$\begin{aligned} S(f)\,[\mathrm{dB.W.m^{-2}.Hz^{-1}}] &= P_{\mathrm{SA}}(f)\,[\mathrm{dBm}] - G_{ant}(f)\,[\mathrm{dBi}] - G_{sys}(f)\,[\mathrm{dB}] - \\ &\quad 10\log(\mathrm{RBW}\,[\mathrm{kHz}]) + 20\log(f\ [\mathrm{MHz}]) - 95.54 \end{aligned} \tag{6.1}$$

The values G_{ant} and G_{sys} represent the antenna gain and system gain respectively. P_{SA} is the power value measured by the spectrum analyser and RBW is the resolution bandwidth. Appendix E.4 shows the expanded version of this equation and details the constants, which have been simplied to $95.54\,\mathrm{dB.W.m^{-2}.Hz^{-1}}$ here.

6.6.3 Statistical Analysis

The main part of processing required a statistical analysis of the spectral power flux density values, as required by SKA Memo 37 and this is indicated as Step 9 in Figure 6.1.

The data stored in each RBW frequency bin was combined for all measurements that were selected by the parameters in the plot parameter file. Flux densities within each bin were then sorted and the following statistics calculated: minimum, mean, maximum, 10^{th} percentile, 50^{th} percentile and 90^{th} percentile.

The significance of the percentiles in terms of characterising the RFI environment was to give an indication of the variation of signal levels over time. The maximum and 90^{th} percentile values were useful for detecting infrequent transient events. The mean provided a high sensitivity measurement for the "quiescent" RFI environment.

The Python script for the statistical analysis parsed the plot parameter file, generated the database queries and performed the appropriate calibration on the measurement data in the binned binary data files selected. After the statistics had been calculated the bin centre frequency and associated statistical values were stored in "tab-delimited" ASCII text files. These were used to generate the spectrum plots and this processing step is described in Section 6.7. It took approximately 12 hours to produce this data from the binary files for all the required Mode 1 and Mode 2 plots.

6.6.4 Spectrum Occupancy Analysis

The spectrum occupancy analysis required by SKA Memo 37 was performed by a slightly modified version of the Python script used for the calibration and statistical analysis. The process was controlled by a variable in the plot parameter file and was only performed for the Mode 2 measurements. All Mode 2 data for all pointings and polarisations were combined to calculate these statistics. A separate plot parameter file was created for this purpose.

After sorting the data in a given Mode 2 frequency band a median flux value was calculated. The number of flux values from all the bins in the band that were more than 6 dB above the band median was tallied. This count, together with the total number of measurements within the band and the 6 dB threshold flux relevant to the band were written to an ASCII text file, shown as Step 12 in Figure 6.1.

The purpose of the spectrum occupancy analysis was to identify how 'busy' each band was. By plotting the threshold levels onto the RFI spectrum power flux density plot, investi-

gation revealed that the occupancy values were biased to higher values for frequencies above 12 GHz. This was because at the higher frequencies the f^2 trend in the baseline and VSWR ripple added a significant fraction of the 6 dB headroom. An improvement to this analysis would have been to deal with narrower frequency bands or ultimately each frequency bin. This however was not pursued because of adherence to the SKA Memo 37 specification.

6.7 Plot Generation

An indication of measurement sensitivity on the data plots was a requirement of SKA Memo 37. Using the effective antenna area A_e (from Equation D.1 in Appendix D) the sensitivity for the Mode 1 and Mode 2 measurements was calculated using:

$$S_0\,[\mathrm{W.m^{-2}.Hz^{-1}}] = \frac{2 \times k\,[\mathrm{J.K^{-1}}] \times T_{\mathrm{rec}}\,[\mathrm{K}]}{A_e\,[\mathrm{m^2}]\sqrt{\mathrm{RBW}\,[\mathrm{Hz}] \times \Delta T_{\mathrm{RBW}}\,[\mathrm{s}] \times N_{rep}}} \tag{6.2}$$

The resolution bandwidth (RBW), T_{RBW} and number of repetitions (N_{rep}) were used as per the Mode 1 and Mode 2 schedule tables (Tables 5.2 and 5.4). A Python script calculated the sensitivities for the Mode 1 and Mode 2 measurements and wrote these values to ASCII text files (Step 10). The sensitivity data was merged with the plot text files accordingly in Step 11.

The plots for the flux spectral power were generated using the plot data text files and the plot parameter files used to generate this data. The parameter files also contained variables to turn the plotting of selected statistics 'on' or 'off'. Controls to change the scale or include the measurement sensitivity were also provided.

A Python script was written to plot the spectral occupancy graph from the occupancy data files in Step 14 and simple data scaling calculations were done for each band using this data.

Chapter 7

Results

This chapter presents a summary of the RFI measurement results for the Mode 1 and Mode 2 measurements. The results include flux spectra for the measurements conducted at the Karoo 3 core site as well as selected remote sites measured during the campaign. Spectra plots are presented for the measurements performed during the Astron/SSSM visit as well as a plot indicating spectrum occupancy for the combined Mode 2 measurements.

The spectra plots were calibrated using Equation 6.1 and produced according to the requirements in SKA Memo 37. Various percentile statistics are indicated in the plots and the presentation is based on the SKA Site Spectrum Monitoring (SSSM) Data Summary Report (Boonstra and Millenaar, 2006). The expected system sensitivity was calculated with Equation 6.2 and is indicated in these plots.

7.1 Summary Results for the Karoo 3 Core Site

The Mode 1 measurements at the core site were performed during November 2005 with RFI measurement System 2. Statistics for 100-percentile (maximum), 90-percentile and 50-percentile (median) were calculated and produced by combining the data for all antenna azimuth pointings and both polarisation orientations.

For the Mode 2 flux spectra, plots were generated using measurement data recorded between July 2005 and February 2006. The measurement data recorded prior to July 2005 was excluded. This was because screening efforts for System 2 had not yet been implemented (see Figure 1.1) and the data was therefore contaminated with self-generated RFI. Only the measurement data that was edited is included in these plots.

The Mode 2 measurement data was aggregated for each permutation of antenna azimuth pointing and polarisation orientation. The flux spectra contained statistics for 100-percentile

(maximum), 90-percentile, 50-percentile (median), 10-percentile and mean. However, for presentation purposes, the statistics were split across two plots. In addition, the transition between the two antennas at 2 GHz required that separate spectra were created above and below this frequency.

7.1.1 Summary Spectra of Mode 2 Measurements

The summary of Mode 2 measurement results is contained in Figures 7.1 to 7.4. These flux spectra are provided for pointing direction 1 and are produced independently for horizontal and vertical polarisation orientations. The remainder of the results for this mode are provided in Appendix F.24.

Two plots are shown for each combination of azimuth pointing and polarisation to facilitate the presentation statistics:

- the spectrum plots in the left-hand traces show the 90-percentile and median (50-percentile);
- the spectrum plots in the right-hand traces show the maximum, mean and 10-percentile.

The spectra shown here are representative of the RFI environment at the Karoo 3 core site. For frequencies above 2 GHz virtually no RFI was detected. Relatively significant RFI was however detected below 2 GHz and was contained in specific frequency bands allocated to terrestrial and space (satellite) borne services.

The predominant terrestrial services are FM radio broadcast signals (90 - 108 MHz), mobile GSM signals (900 - 960 MHz) and television broadcasts in the VHF (170 - 320 MHz) and UHF (480 - 830 MHz) bands. These relatively strong powered signals are measured at levels between -150 and -180 dB.W.m^{-2}.Hz^{-1} and occur in the 90-percentile and 50-percentile traces. Further broadcast signals are also detected in these bands. However, they only appear in the maximum traces and are typically between 10 and 20 dB above the noise floor of the system in the vertical polarisation. Additional RFI related to radar and avionic signals are detected in the L-band (around 960 MHz - 1.4 GHz) and appear in the 100-percentile traces. The traces for 100-percentile statistics show signals associated with mobile communications between 250 and 450 MHz.

Space born RFI from satellites operating in frequency bands 137 - 138 MHz and 240 - 270 MHz are seen in all traces. Signal levels for these broadcasts are between -165 (maximum) and -190 dB.W.m^{-2}.Hz^{-1} (10-percentile) for both polarisations.

Steps in the baseline levels are due to changes in RF signal path. Similar steps are also seen for the various measurement bands that were measured with different system settings (i.e. resolution bandwidth, video bandwidth). These changes resulted in varying system sensitivities and are indicated by the system sensitivity trace marked on the plots. The slope of the noise floor baseline gradually increases towards higher frequencies. This is due to the increased system temperature at high frequencies (see Figure 2.8) and is confirmed by the sensitivity trace indicated.

7.1.2 Summary Spectra of Mode 1 Measurements

The summary of Mode 1 measurement results is contained in Figures 7.5 to 7.7 for the frequency range 70 MHz - 3 GHz. The remaining flux spectra (3 - 26.5 GHz) indicating no RFI are provided in Appendix F.24.

The flux spectra show similar RFI to that detected during the Mode 2 measurements. The signal levels for the various trace statistics correspond with those of the Mode 2 measurements. It is noted that for some frequency bands (e.g. 150 - 300 MHz and 300 - 800 MHz) there is an overlap of the trace statistics (90-percentile and maximum). This is due to insufficient data points per resolution bandwidth frequency bin that allow the distinction of the 90-percentile and maximum traces.

The baseline steps also correspond to those of the Mode 2 measurements. This is expected due to the use of RFI measurement System 2 which was the same system used for the Mode 2 measurements.

7.1.3 Mode 2 Spectrum Occupancy

The spectrum occupancy statistics as required by SKA Memo 37 are presented in Figure 7.8 for the Mode 2 measurements conducted at the Karoo 3 core site between July 2005 and February 2006. These statistics were calculated using the "6 dB above the median" criterion as discussed in Section 6.6.4.

The occupancy statistics are biased for the upper frequency bands due to the overall f^2 trend in the spectra and VSWR ripples which have amplitudes that are a significant fraction of the 6 dB headroom, especially in the bands above 12 GHz.

7.2 Astron/SSSM Cross Comparison Results

This section presents the results for the Mode 2 measurements that were performed during April 2005 (see Figure 1.1) at the Karoo 3 core site with RFI measurement system 2. The measurements were conducted during the Astron/SSSM visit and are to be compared with the 'Data Summary Report' located in Appendix F.23. The results presented in Figure 7.9 depict flux spectra for each polarisation orientation with the data combined for all pointing directions.

The measurements shown here are not representative of the core site due to the radiation of self-generated RFI from the measurement system. The screening efforts had not been performed at this stage, and because of this significantly more interference is shown in bands below 400 MHz when compared to the Mode 2 measurements in Section 7.1.1. In order to provide a more realistic comparison the 50-percentile, mean and 10-percentile traces are shown.

A comparison of the flux spectra for the Mode 2 measurements by the Astron/SSSM and South African systems show:

- The noise floor levels and system sensitivity traces are consistent with the Astron/SSSM data and system performance. The flux spectra have differing spectral ripples and frequency steps relating to the specific signal paths of each system;
- GSM signal levels compare for frequencies around 960 MHz with a detected power of -175 dB.W.m^{-2}.Hz^{-1} in the horizontal and -160 dB.W.m^{-2}.Hz^{-1} for the vertical polarisations;
- Signals below 350 MHz compare quantitatively however the levels differ by more than 20 dB.W.m^{-2}.Hz^{-1} in some cases.

Due to the contamination by self-generated interference, a comparison of the Mode 1 spectra is not considered meaningful and therefore is not presented here.

7.3 Comparison of Mode 1 Measurement Sites

The spectrum plots in Figure 7.10 show a comparison between the Mode 1 measurements conducted at the Karoo 3 core site and remote sites RFI-19 and RFI-20. These plots depict

the frequency range from 150 MHz to 960 MHz and are chosen to illustrate the effect of terrain shielding on the level of RFI.

The remote sites RFI-19 and RFI-20 (see Figure 5.1 in Chapter 5) are located within 25 km of the Karoo 3 core site. The distance from these sites to local towns in the area (Williston and Carnarvon) is roughly the same. However, large variances (as much as 60 dB.W.m^{-2}.Hz^{-1}) are seen in signal power levels of their flux spectra.

For the Karoo 3 site a range of hills are situated within a few kilometres due south of the core area. Remote site RFI-20, which is south of the Karoo 3 site, is completely encircled by mountains while RFI-19 does not have any major topographical features nearby.

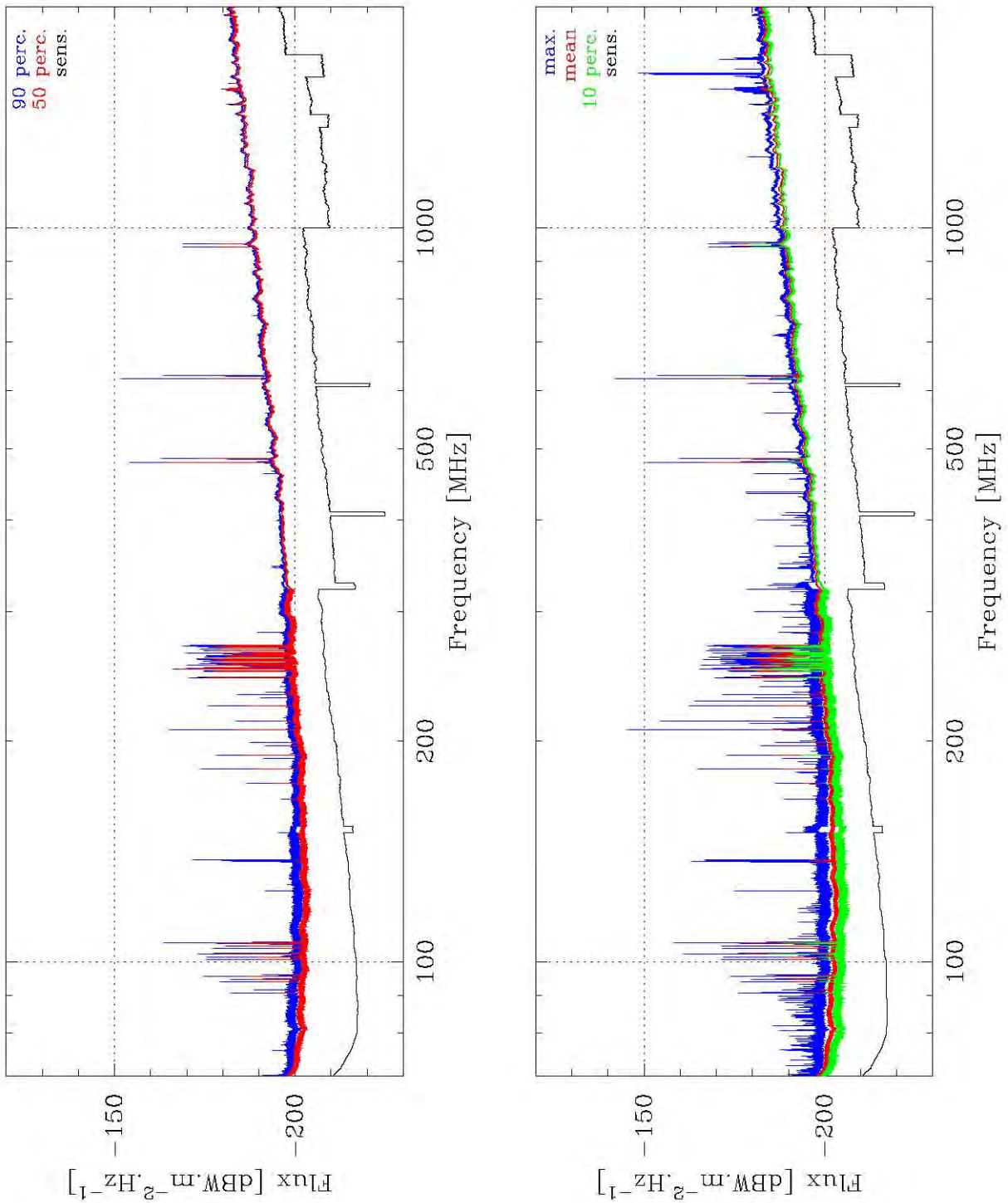

Figure 7.1: Summary Mode 2 spectra for Karoo 3 core site: 70 MHz - 2 GHz, horizontal polarisation, pointing direction 1. Left: 90^{th} percentile and median. Right: 10^{th} percentile, mean and maximum.

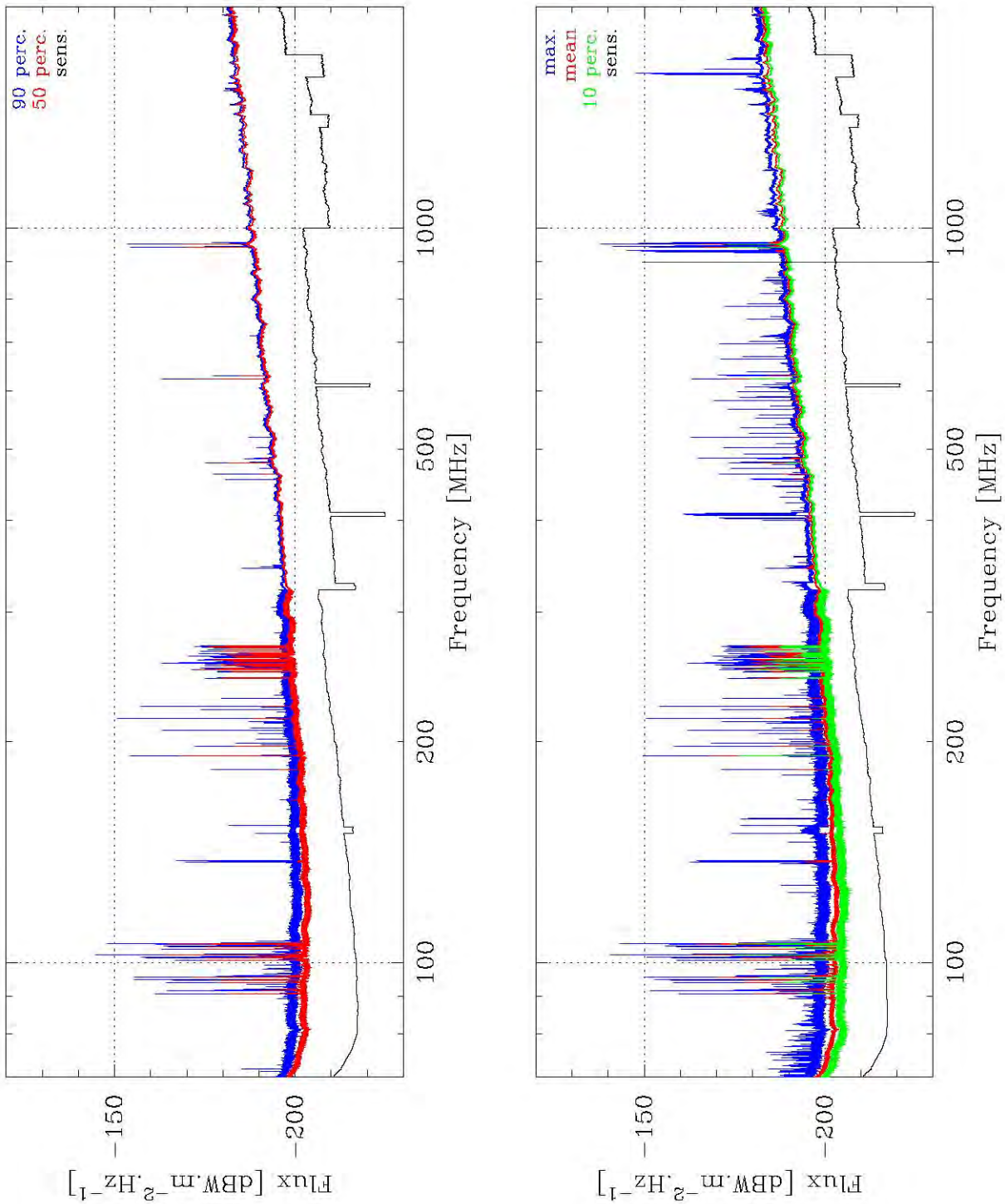

Figure 7.2: Summary Mode 2 spectra for Karoo 3 core site: 70 MHz - 2 GHz, vertical polarisation, pointing direction 1. Left: 90^{th} percentile and median. Right: 10^{th} percentile, mean and maximum.

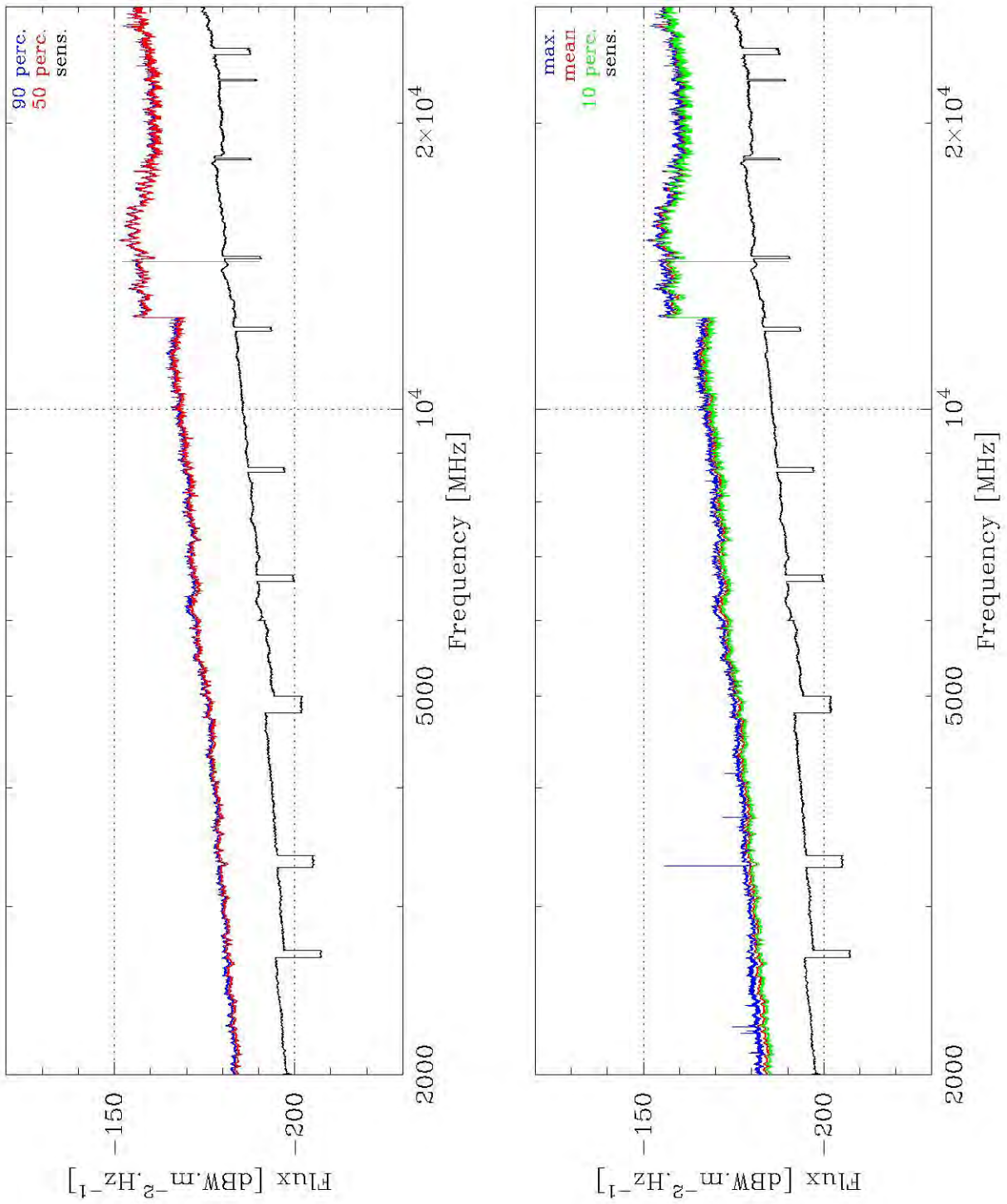

Figure 7.3: Summary Mode 2 spectra for Karoo 3 core site: 2 GHz - 26.5 GHz, horizontal polarisation, pointing direction 1. Left: 90^{th} percentile and median. Right: 10^{th} percentile, mean and maximum.

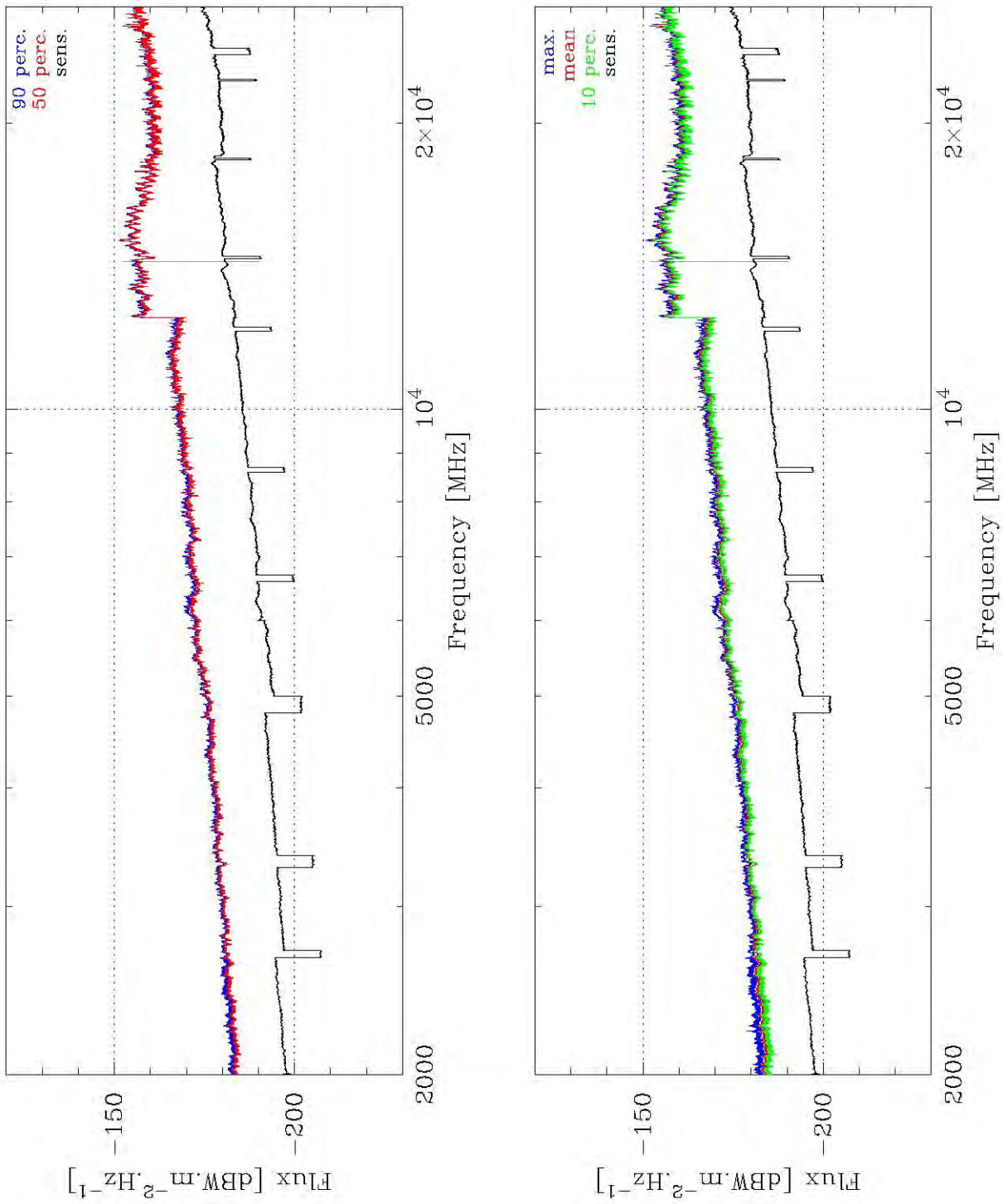

Figure 7.4: Summary Mode 2 spectra for Karoo 3 core site: 2 GHz - 26.5 GHz, vertical polarisation, pointing direction 1. Left: 90^{th} percentile and median. Right: 10^{th} percentile, mean and maximum.

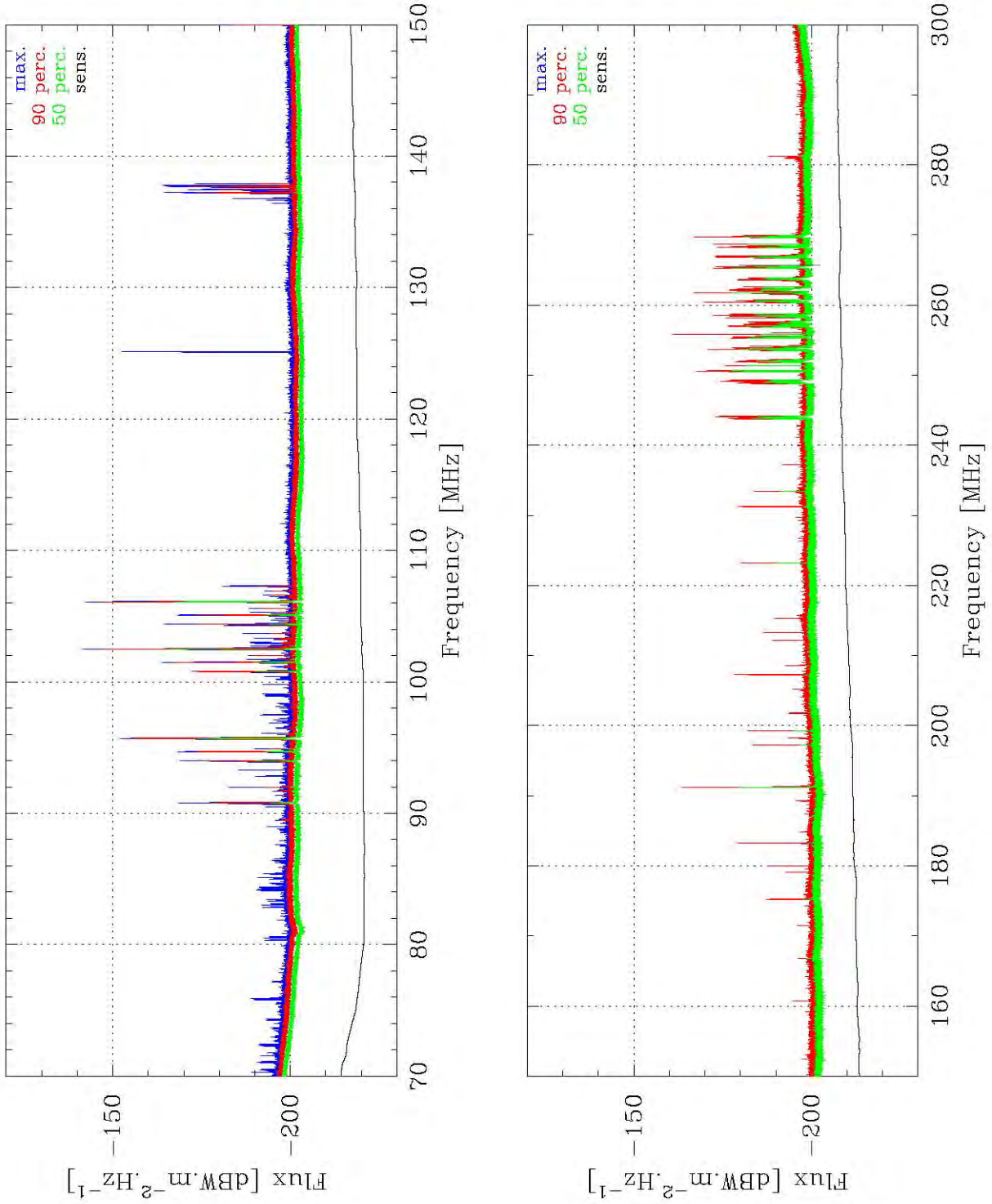

Figure 7.5: Mode 1 spectra for Karoo 3 core site. Data for all pointing directions and both polarisations have been combined for these plots. Left: 70 MHz - 150 MHz. Right: 150 MHz - 300 MHz.

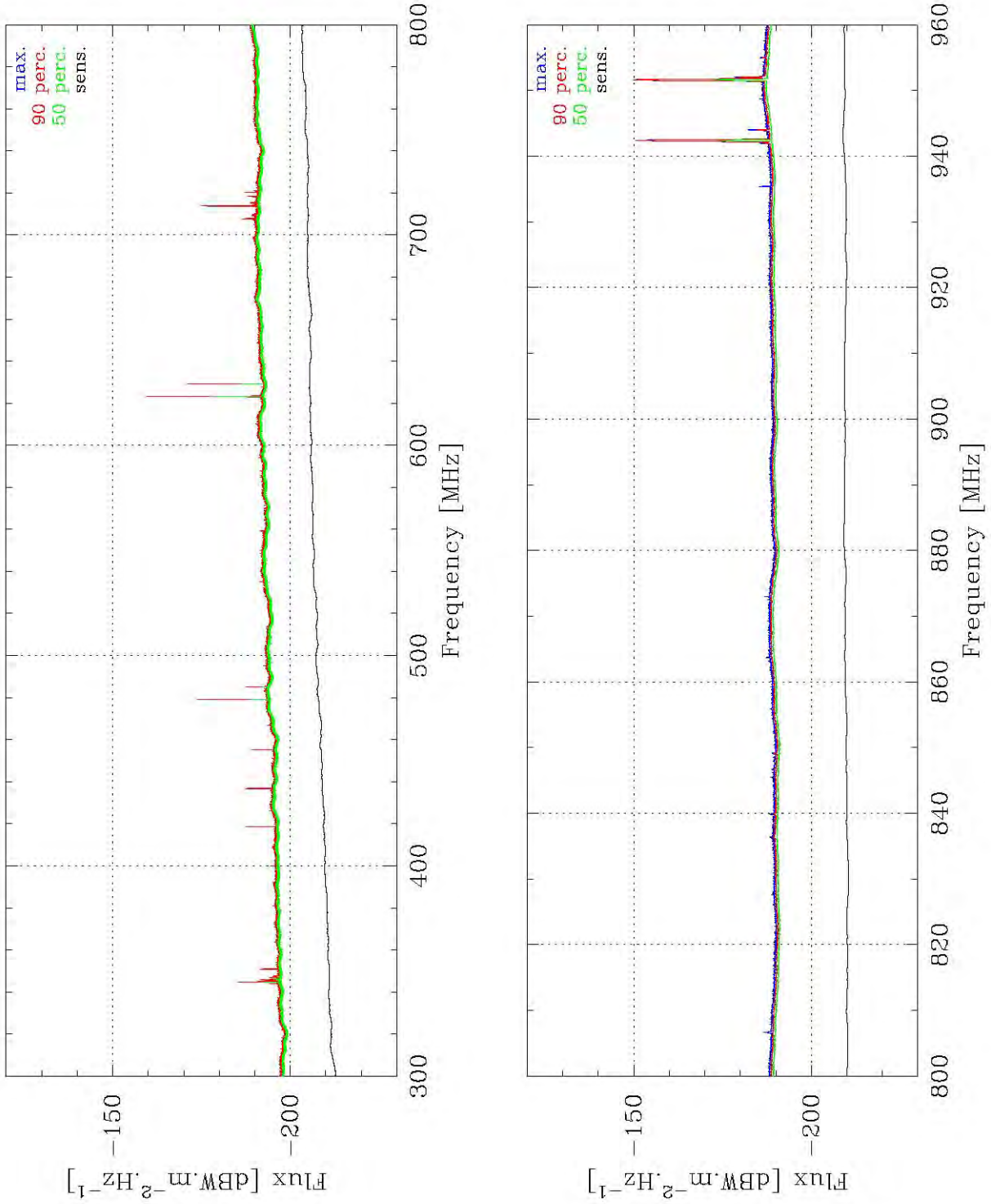

Figure 7.6: Mode 1 spectra for Karoo 3 core site. Data for all pointing directions and both polarisations have been combined for these plots. Left: 300 MHz - 800 MHz. Right: 800 MHz - 960 MHz.

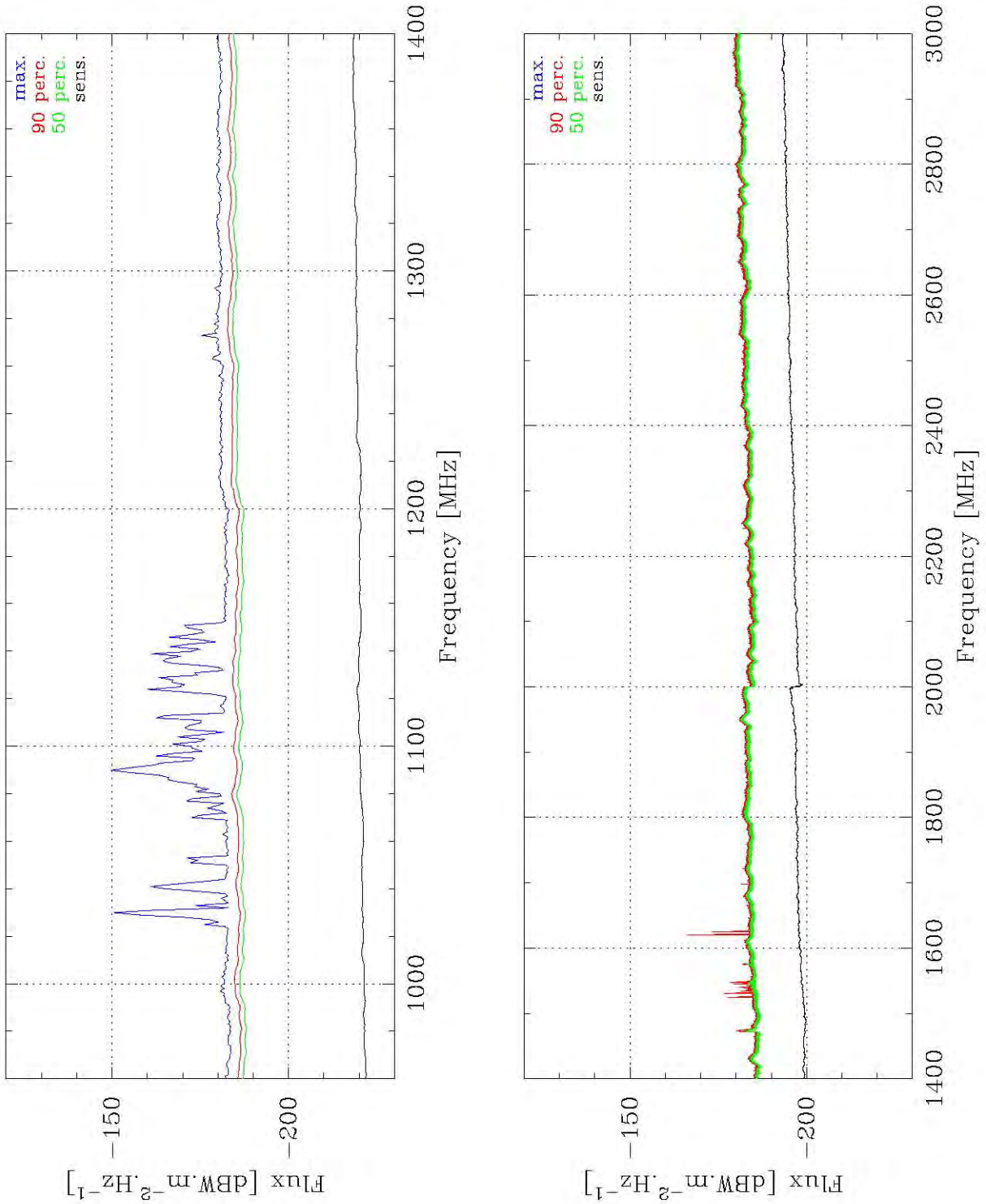

Figure 7.7: Mode 1 spectra for Karoo 3 core site. Data for all pointing directions and both polarisations have been combined for these plots. Left: 960 MHz - 1400 MHz. Right: 1400 MHz - 3000 MHz.

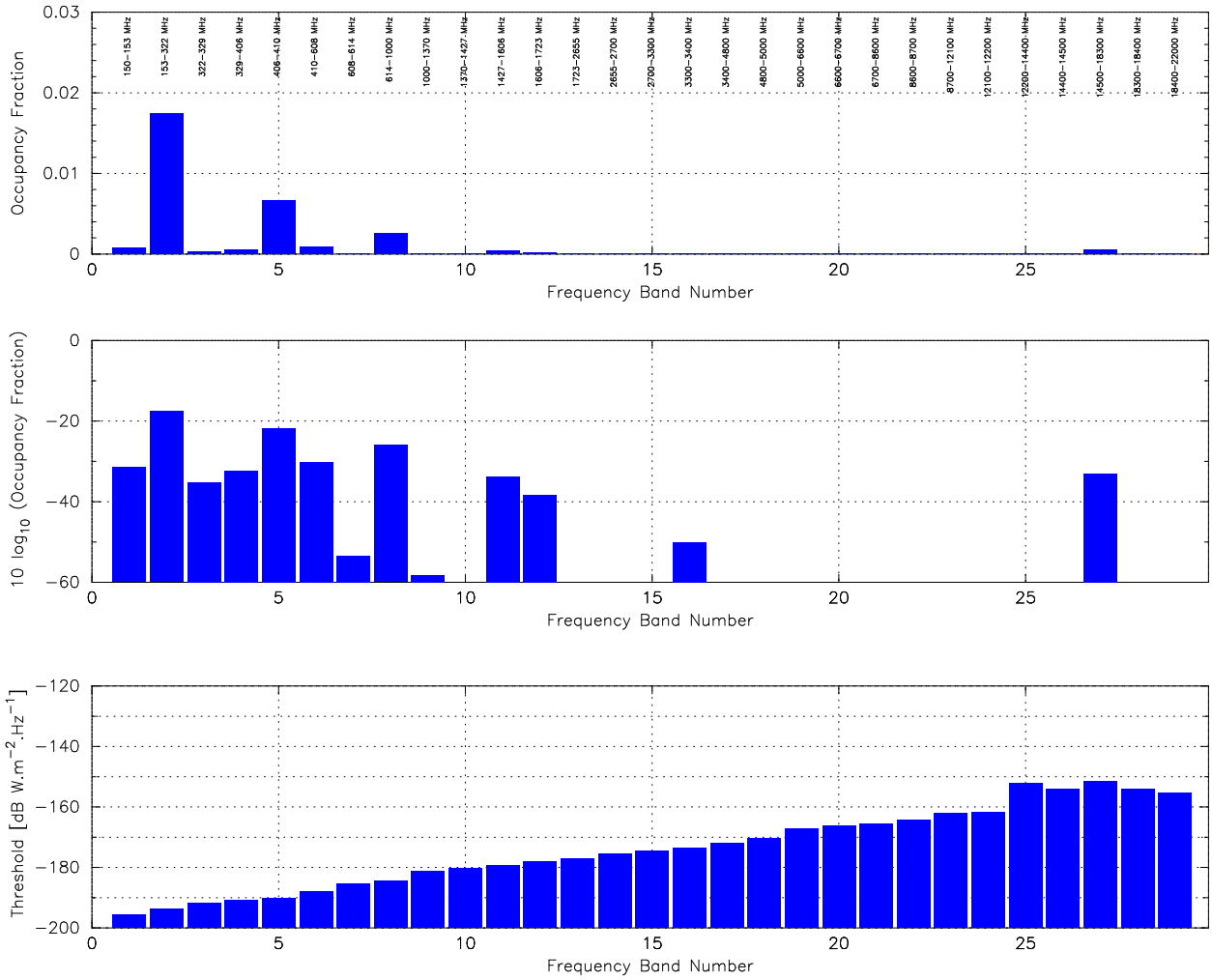

Figure 7.8: Spectrum occupancy for the Mode 2 measurements performed at the Karoo 3 core site during the period July 2005 - February 2006.

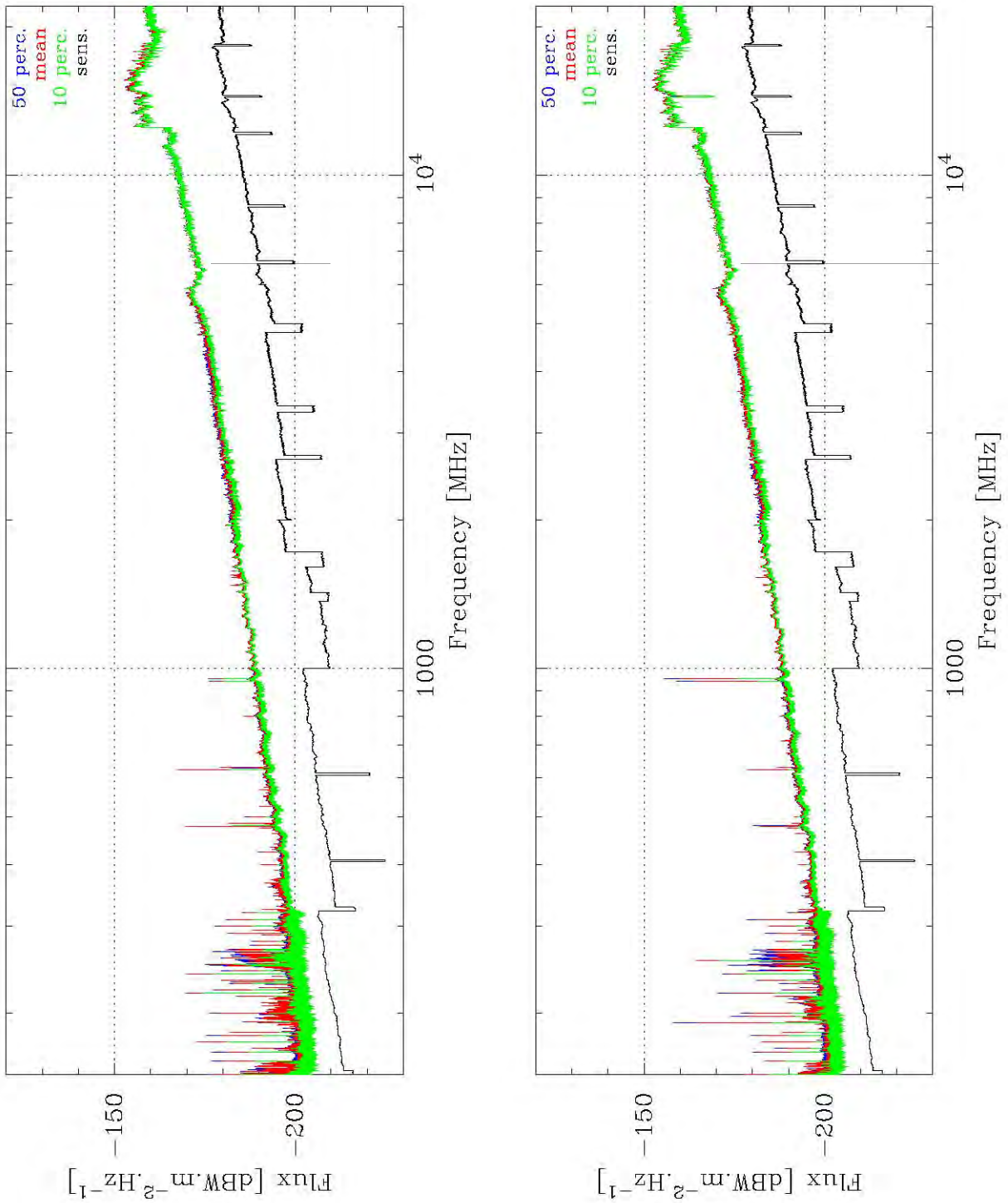

Figure 7.9: Mode 2 measurements recorded in April 2005 during the SSSM visit. The data for all pointings has been combined for the frequency range 150 MHz - 22 GHz. Left: Horizontal polarisation. Right: Vertical polarisation.

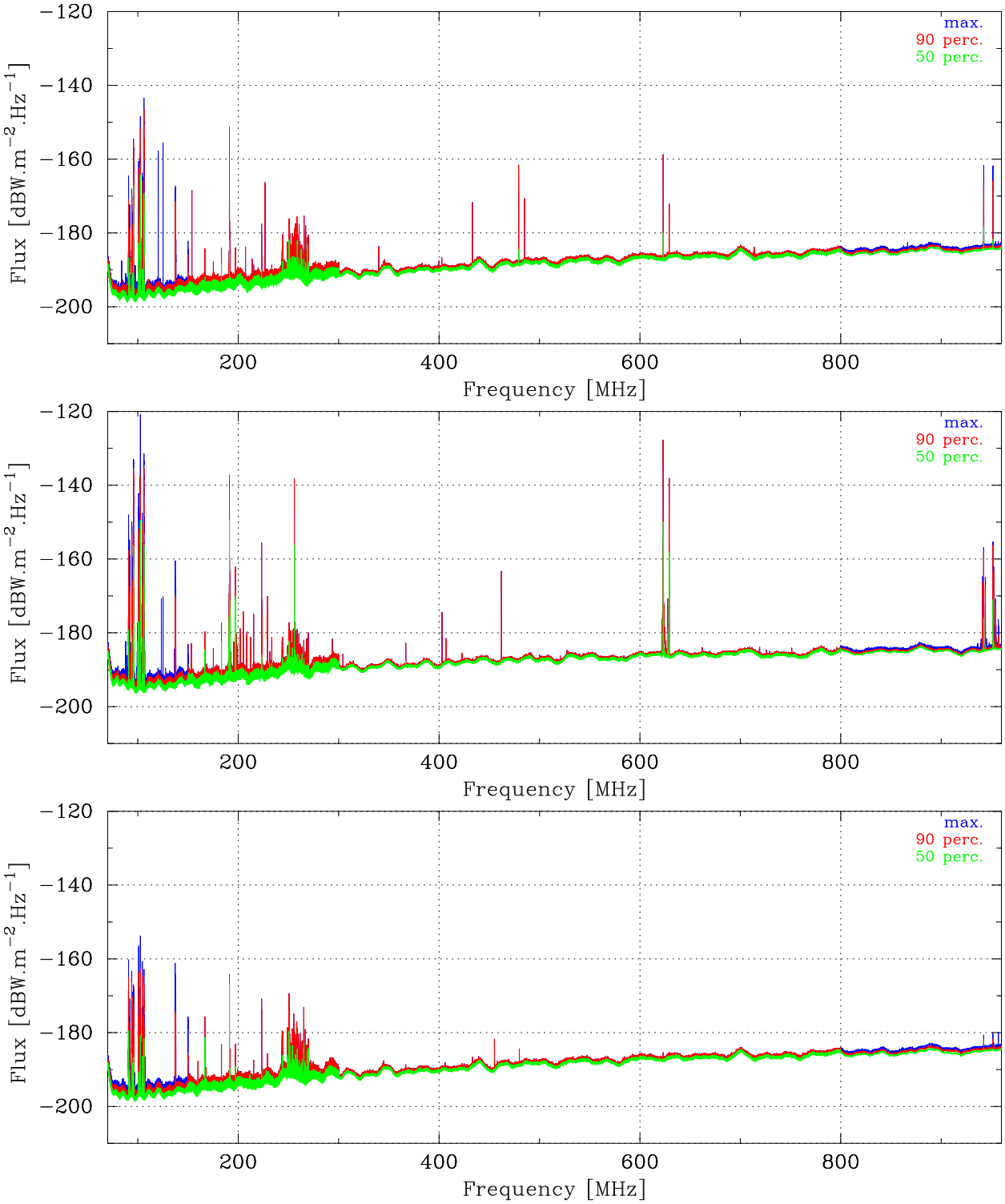

Figure 7.10: Comparison of flux spectra for the Mode 1 measurements performed at various remote sites. The effects of terrain shielding are illustrated by three remote sites which are located within 25 km of each other. The top plot represents the spectrum measured at the Karoo 3 site. The middle plot is the spectrum recorded at remote site RFI-19 which did not benefit from the shielding hills to the south of the Karoo 3 core site. The flux spectrum in the bottom plot was recorded at RFI-20 which is situated due south of the Karoo 3 site and completely surrounded by hills.

Chapter 8

Conclusion

The design and implementation of an RFI measurement system in accordance with the SKA Memo 37 specification was successfully accomplished. To overcome logistical constraints, this design was implemented for three RFI measurement system sets. All systems performed satisfactorily to the T_{sys} requirements for the Mode 1 and Mode 2 protocols. In addition measurements surpassing the operating frequency range specification (70 MHz - 22 GHz) were performed at all sites - up to 26.5 GHz.

The prototype system provided useful insight for the final design of the production systems, and gave early warning of self-generated and locally generated RFI problems. Subsequent screening efforts were shown to be effective at constraining self-generated RFI. Regular calibration and system checks performed during the operation of the systems ensured high quality of the measured data, which was void of self-generated RFI. These checks also showed the robustness and repeatability of the systems during their operation in the field.

The chain of tools developed to process the RFI data allowed flexibility in the generation of the various output products. It facilitated partial pre-processing of the data, reducing the time for the final analysis that was dictated by strict International SKA Project time-lines. The step-by-step process in which the analysis was performed suited the dual development/production cycle during the implementation of the processing software.

8.1 Analysis of Results

Results from the cross-calibration exercise performed with the Astron/SSSM team showed that the South African systems performed according to specification. The RFI measurements conducted during this period correspond to those measured by the Astron/SSSM system. These measurements are however not representative of the core site as they contained self-

generated RFI.

For the Mode 1 and Mode 2 measurements recorded at the Karoo 3 site, low levels of RFI were detected. This interference was mainly from broadcast services and typically occurs in the frequency bands below 2 GHz. The spectrum occupancy plots confirm this observation, despite being biased in the upper frequency bands.

The remote sites measured in the surrounding areas of the Karoo show similar low-level RFI to that of the core site. This establishes the area as a suitable location for SKA and other projects such as the Karoo Array Telescope and C-BASS in the future. Measurements at the remote sites show that the mountains are effective in shielding terrestrial sources of RFI and especially broadcast services. This means that the placement of antenna stations (for the SKA) should take into account the local topography to minimise terrestrial RFI.

8.2 Future Work

It is likely that follow-up measurements will be conducted in each of the potential host countries (South Africa and Australia) prior to the final decision, and awarding of the SKA. Because of this, regular maintenance and re-calibration of the three measurement systems should be undertaken. The nature of the SKA project is such that the technology that will be used is not entirely certain at this stage. In all likelihood, the initial phases of construction will place more emphasis on some regions of the spectrum than others. While it is possible to use the current RFI measurement systems for these operating frequencies, it is known that the set-up does not allow for quick measurements of the frequency bands because of the way in which spectrum analysers operate.

The efficiency and speed of the current measurement systems is limited by the spectrum analyser, which is an analogue swept-frequency device. The use of a wide-band digital spectrometer would improve the speed of measurements by some orders of magnitude and would also improve the detection probability of fast transient sources, such as radar and avionic signals. The faster system would also offer increased measurement sensitivity, approaching the ITU RA.796-2 levels (i.e. 50 dBW.m^{-2}.Hz^{-1} better than the existing system).

The survey conducted across Southern Africa is the first of its kind and this data recorded during the campaign should not be disregarded. Ekers and Bell (Ekers and Bell, 1999) suggest that techniques for RFI mitigation can only be employed in radio telescope receiver systems if sufficient detail about the sources is known. The RFI data should therefore

be correlated with transmitter databases and an analysis should be done to investigate tropospheric phenomena such as ducting. A possible future project would be to construct a phenomenological model that predicts RFI given input data, such as transmitter databases, weather and ionosphere conditions.

References

Agilent Technologies, 2004a, *Application Note 150 : Agilent Spectrum Analyzer Basics*

Agilent Technologies, 2004b, *Application Note 57-1: Fundamentals of RF and Microwave Noise Figure Measurements*

Ambrosini, R., Beresford, R., Boonstra, A.-J., Ellingson, S., Tapping, K., 2003, *RFI Measurement Protocol for Candidate SKA Sites*

Boonstra, A. J., Millenaar, R. P., 2006, *SKA Site Spectrum Monitoring Data Summary Report*

CRAF, 1997, *CRAF handbook for Radio Astronomy*, Chapt. 5, p. 81, European Science Foundation, second edition

Ekers, R. D., Bell, J. F., 1999, in *The Universe at Low Radio Frequencies*, IAU Symposium No. 199, IAU

Hall, P., 2005, *[Email] Guidelines for Use of International RFI Calibration Measurements*

IEEE Standards, 1997, *IEEE Std 211-1997: Standard Definitions of Terms for Radio Wave Propagation*

International SKA Project Office, 2004, *Request for Proposals for Siting the SKA*

International SKA Project Office, 2006, *[Online] Available:* `http://www.ska.ac.za (November,2006)`

International Telecommunication Union, 2003, *ITU Recommendation RA.769-2: Protection Criteria used for Radio Astronomical Measurements*

Kraus, J. D., 1966, *Radio Astronomy*, Chapt. 7, p. 258, McGraw-Hill

Leine & Linde, 2001, *BiLL RS-232/485 Bi-directional Serial Communication*

MESA Solutions (Pty) Ltd., 2005a, *Measurement Results for SKA RFI Investigation 29 - 30 June 2005*

MESA Solutions (Pty) Ltd., 2005b, *RFI Investigation of the SKA System 2 Mobile Unit at the ISSA Houwteq Facility*

Millenaar, R. P., 2005, *SKA Site Spectrum Monitoring System Design Considerations*

National Instruments, 2006, *Getting Started with LabVIEW*

Oxford University Physics, 2006, *[Online] Available:* `http://www-astro.physics.ox.ac.uk/research/expcosmology/groupcbass.html (November,2006)`

Pearson, T., 2007, *[Online] Available:* `http://www.astro.caltech.edu/~tjp/pgplot (January, 2007)`

Rohde & Schwarz, 2006a, *[Online] Available:* `http://www.rohde-schwarz.com/www/DownCent.nsf/file/hl050_brief_e.pdf/$file/hl050_brief_e.pdf (December,2006)`

Rohde & Schwarz, 2006b, *Operating Manual Rohde & Schwarz FSU26*

South African SKA Project, 2006a, *[Online] Available:* `http://www.ska.ac.za/kat (November,2006)`

South African SKA Project, 2006b, *Proposal to site the Square Kilometre Array: Analysis*

of the Radio Frequency Environment
Wangsness, R. K., 1979, *Electromagnetic Fields*, Chapt. 26, p. 487, John Wiley & Sons
Wells, D. C., Greisen, E. W., 1979, in G. Sedmak, M. Capaccioli, and R. J. Allen (eds.), *Image Processing in Astronomy*, p. 445
Williams, T., 2001, *EMC for Product Designers*, Chapt. 5–6, p. 153, Newnes

Appendix A

Radio Frequency Sub-System

A.1 Systems 1 and 3 Antenna Gains

For the R & S HL033 antennas the gain was provided in electronic format (on disk) for each antenna. As no specific antenna gain data was provided by the manufacturer for the R & S HL050 antennas, the antenna gains for all systems were assumed to be the same. Typical values were captured from the R & S HL050 data sheet (Rohde & Schwarz, 2006a) and are shown in Figures A.1 and A.2. These plots show the gain values for the antennas used in System 1 and System 3 respectively.

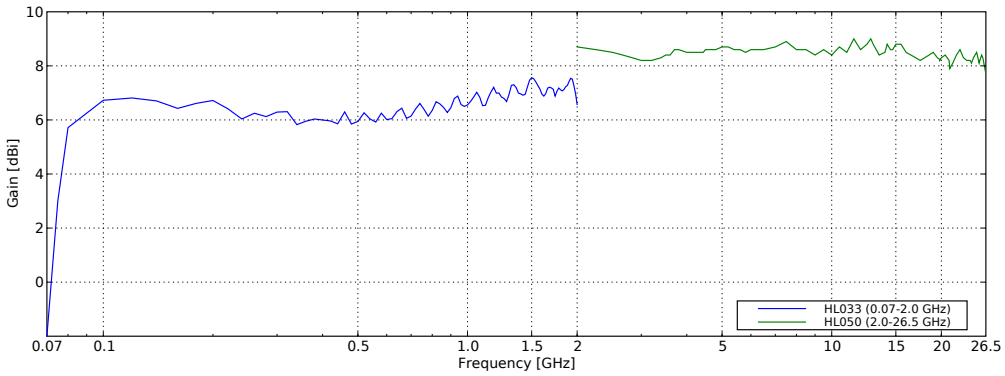

Figure A.1: Antenna gains for System 1.

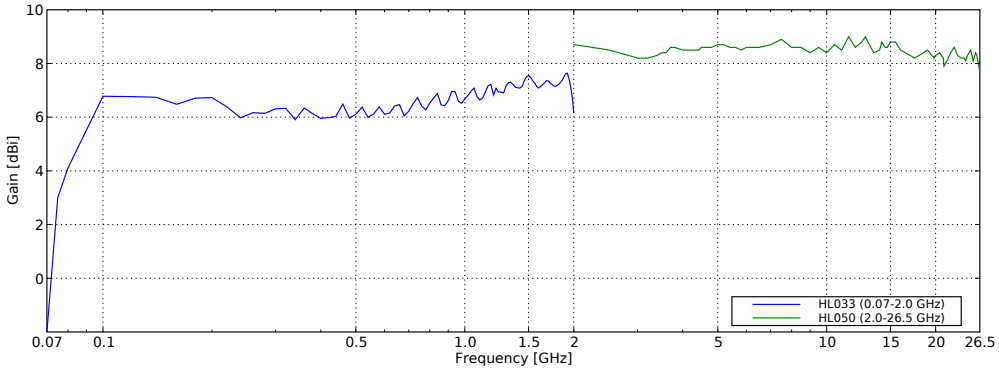

Figure A.2: Antenna gains for System 3.

A.2 Image Rejection High Pass Filters

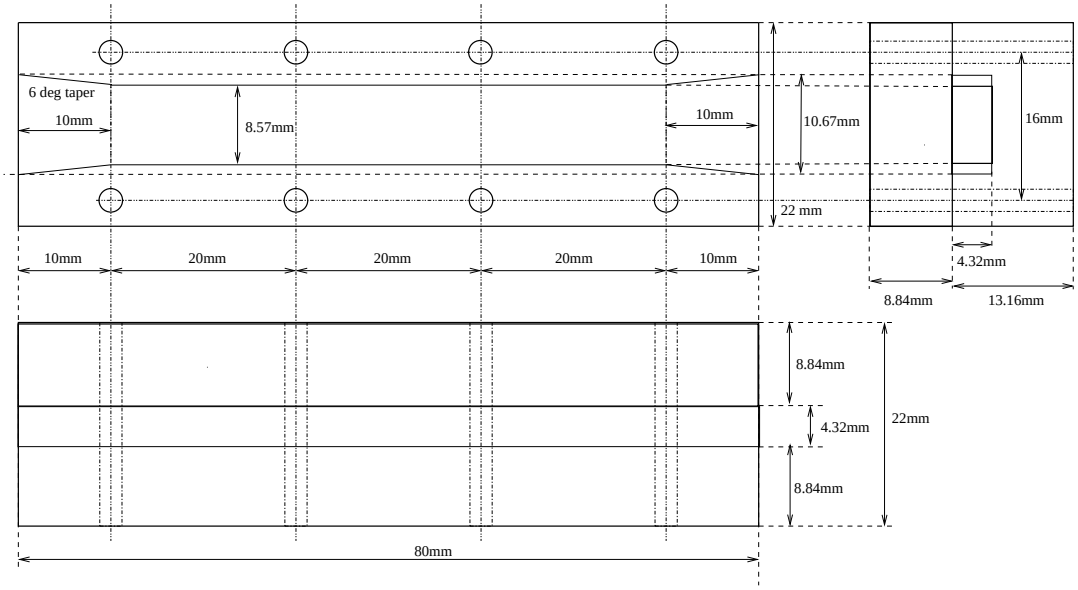

Figure A.3: Mechanical drawing of the 17.5 GHz high pass image rejection filter. Two pieces of aluminium are bolted together to form waveguides with ends drilled and tapped to match standard WR42 waveguide flanges. A similar design was used for the 11.5 GHz image rejection filter where the dimensions were scaled accordingly.

Figure A.4: The 11.5 GHz and 17.5 GHz image rejection high pass filters used in System 1.

A.3 Photographs of the RF Assembly

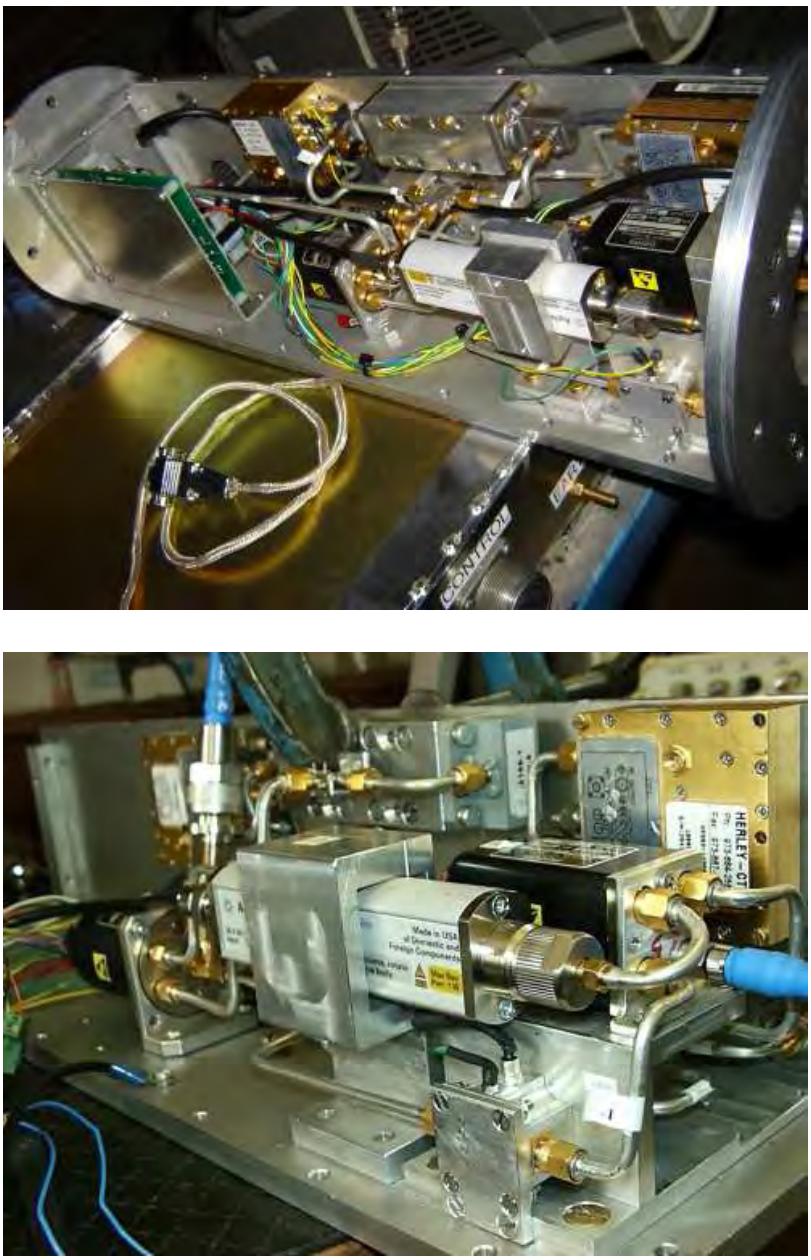

Figure A.5: Top: RF components in the Mast-Head Box waiting for aluminium cover plates to be fitted. Bottom: Front view of the RF Sub-system during the laboratory tests. Note the short, semi-rigid co-axial cables between the components, which reduce losses prior to amplification.

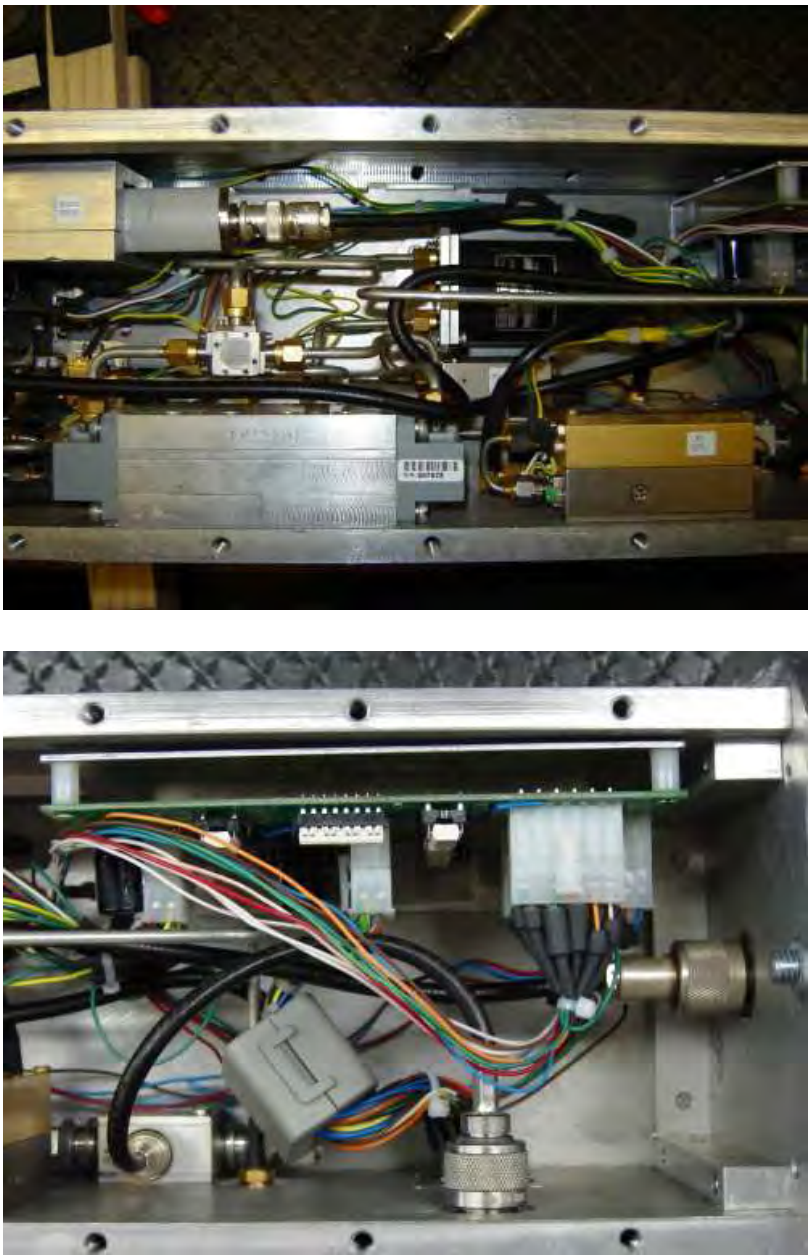

Figure A.6: Photographs taken from the top of the Mast-Head Box. Top: The noise diode, RF Switch 4, 11.5 GHz image rejection filter, 12 GHz LO and mixer are shown. Bottom: The RF Logic PCB, 10 MHz reference cable and power splitter are shown.

A.4 LabVIEW Frequency Sweeper VI Front Panel and Block Diagram

The LabVIEW Frequency Sweeper VI was developed in order to take measurements of the RF co-axial cables and the image rejection high pass filters used in the RF assembly. It was also used to perform direct gain measurements of the complete RF system, which were used for calibration purposes.

It supported various frequency synthesisers (Hewlett Packard HP8360L, Hewlett Packard HL8340B, Rohde & Schwarz SMR40) and for signal detection, measurements were performed with a spectrum analyser (Agilent HP8535EC/E). In the initial development stages it only supported the use of power meter (Agilent HP411) as a detection device. This was, however, superceded by the spectrum analyser which was more suitable for making sensitive measurements over a wide operating frequency range. The front panels for this application are shown in Figures A.7 and A.8 with the source code (block diagrams) in Figures A.9 and A.10.

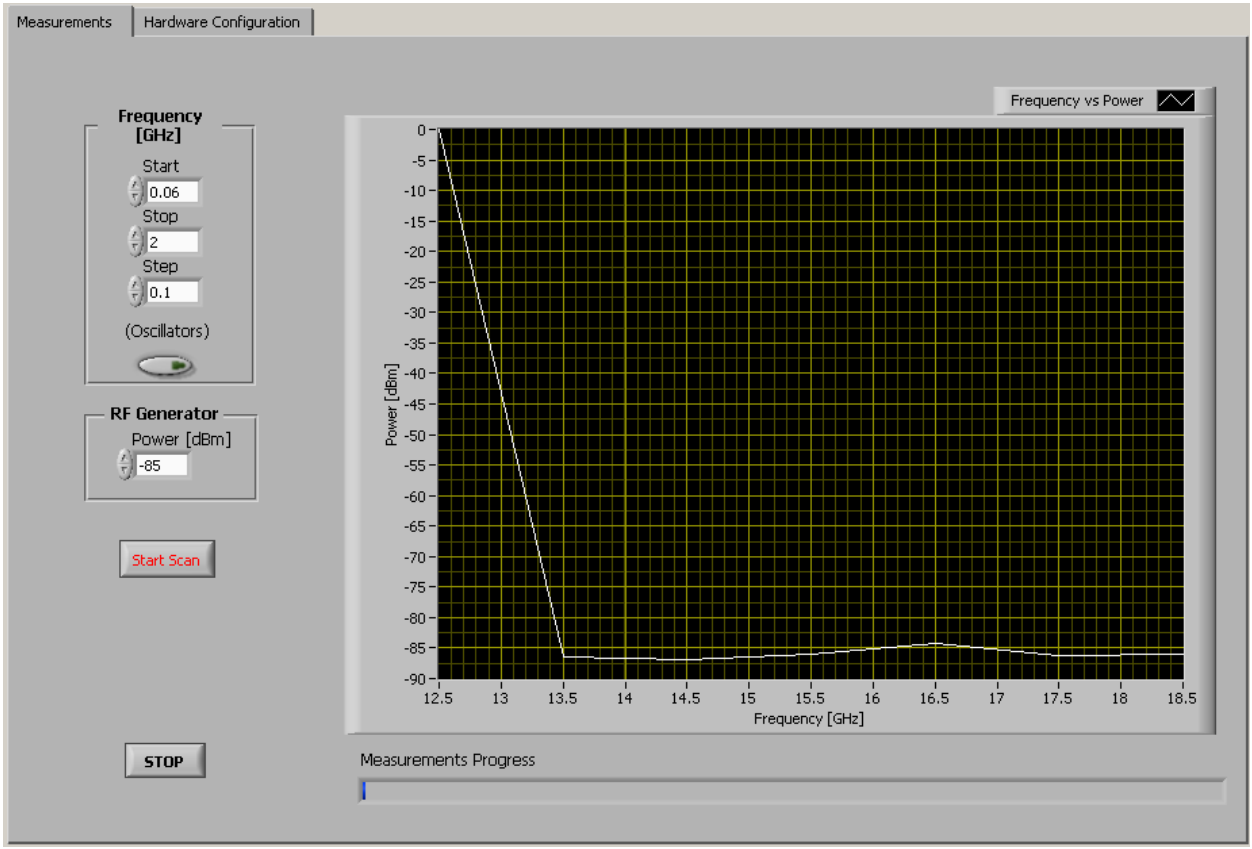

Figure A.7: User interface front panel for the LabVIEW Frequency Sweeper VI. Input parameters for the start, stop and step size frequencies are shown in the side panel. A facility to measure heterodyne devices (as in the RFI measurement system) was provided and this feature was activated by the 'Oscillators' button on the side panel. An option to adjust the output power level on the frequency synthesiser was also provided.

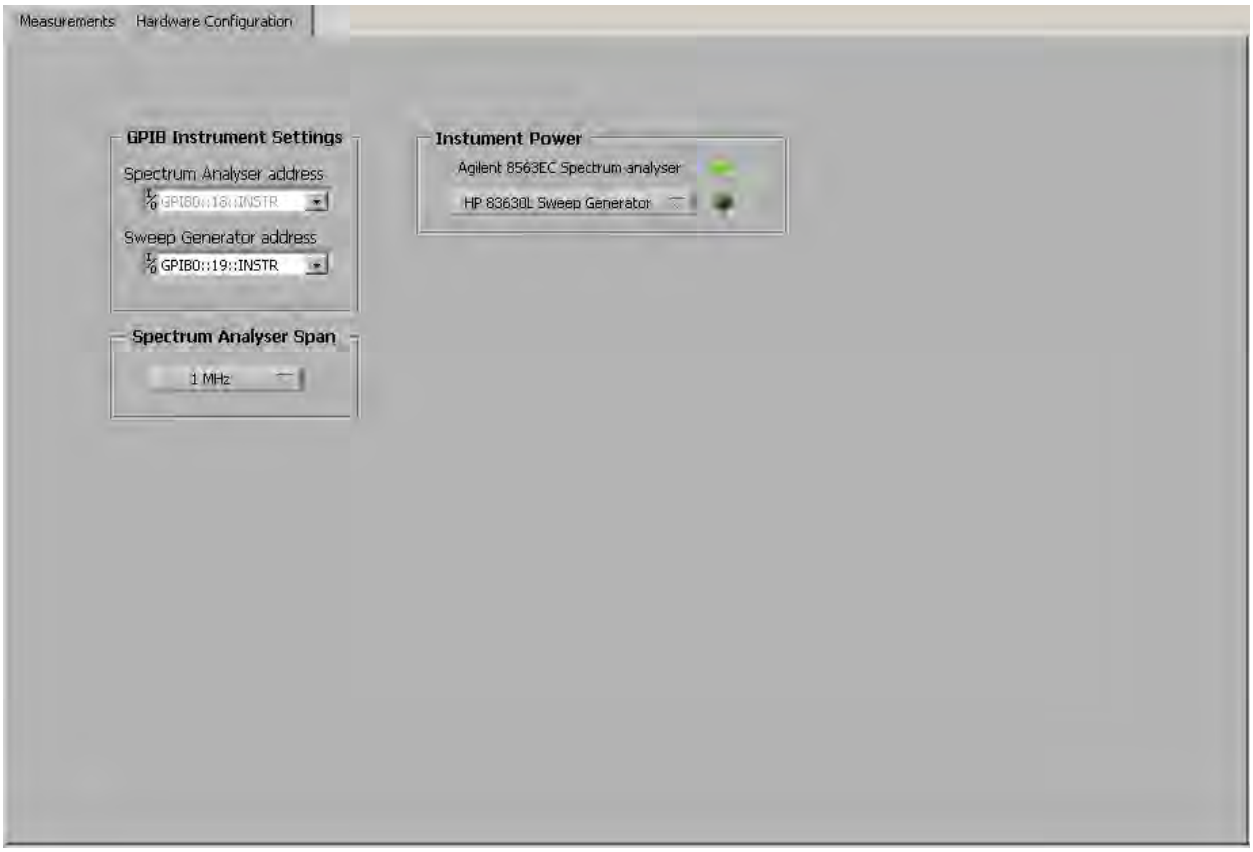

Figure A.8: The hardware and configuration panel of the LabVIEW Frequency Sweeper VI. The user controls allowed for the adjustment of the spectrum analyser frequency span and selection of frequency synthesiser (Hewlett Packard HP8360L/HP8340B or Rohde & Schwartz SMR 40). Green LEDs next to the selected instruments were used to indicated whether each of the instruments had power and whether communication via the HPIB bus was functioning correctly.

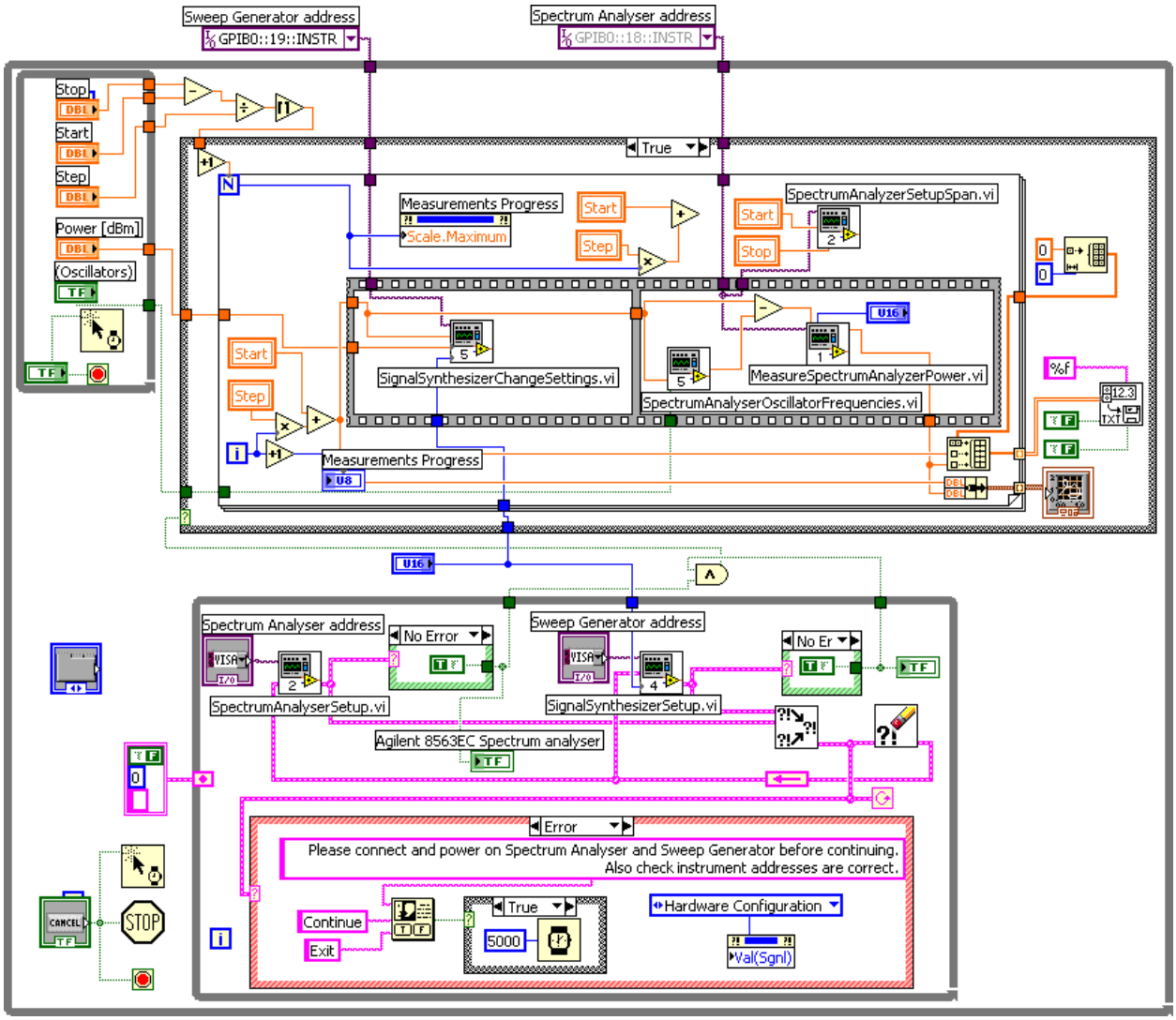

Figure A.9: LabVIEW Frequency Sweeper VI block diagram.

Figure A.10: The LabVIEW Frequency Sweeper VI block diagrams for the hidden cases not shown in Figure A.9.

A.5 Evaluation of the Image Rejection Filters

The noise floor for the System 1 image rejection filters is higher because it was measured using a power meter while those for Systems 2 and 3 were measured with the more sensitive spectrum analyser. The noise floor variance between Systems 2 and 3 is due to the different attenuation input settings used on the spectrum analyser. The filters for System 1 were already installed at this stage and were not re-measured for these plots.

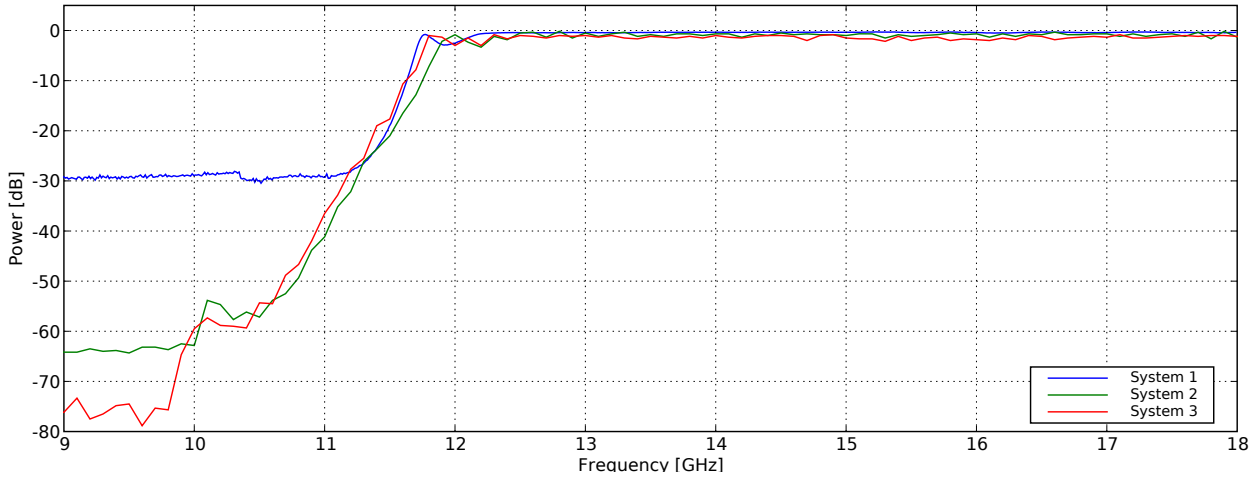

Figure A.11: Passband for the image rejection filters employed in each of the three RFI measurement systems. These filters were used in Paths C and ND C, which operated from 12.5 - 18.5 GHz.

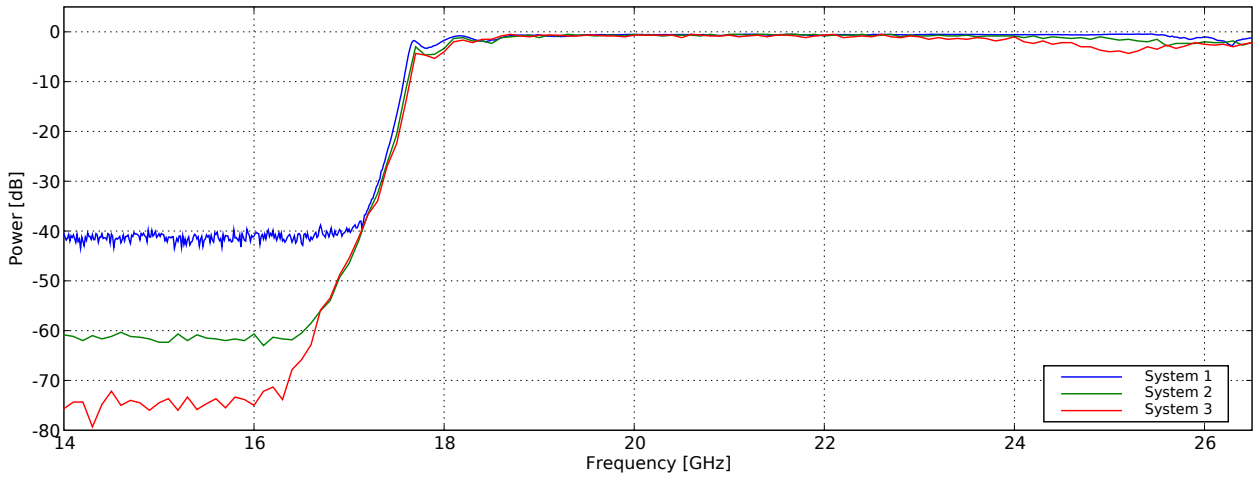

Figure A.12: Passband for the image rejection filters employed in each of the three RFI measurements systems. These filters were used in Paths D and ND D which operated from 18.5 - 26.5 GHz.

A.6 Noise Diode Excess Noise Ratio

Excess noise ratio (ENR) data was provided by the manufacturer for each noise diode and these values are shown in Figure A.13. These values and the interpolated data points between them were used to calculate the effective system temperature T_{sys} for each measurement system using Equation 2.3. The system gain was also calculated (Equation 2.5) using this data.

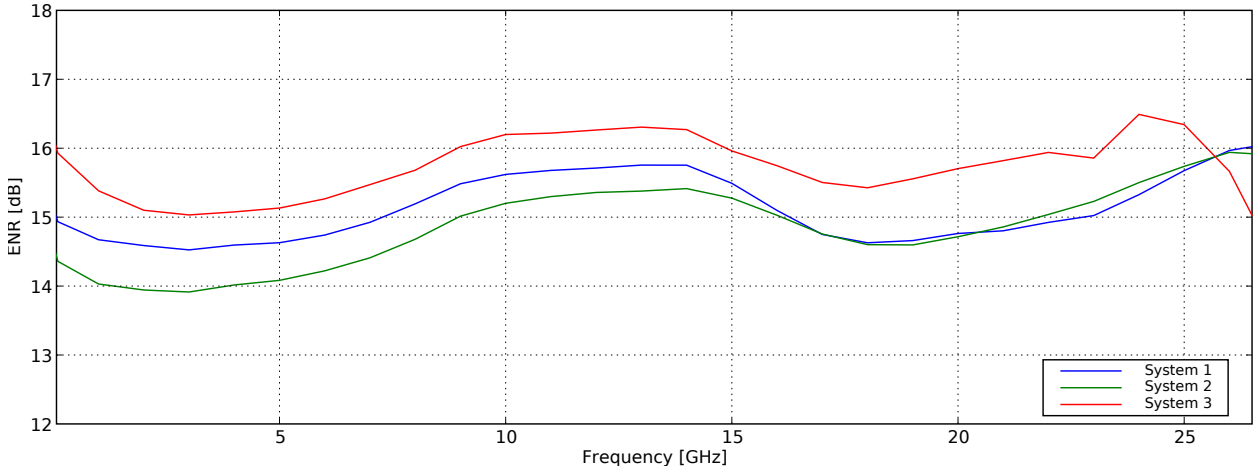

Figure A.13: ENR data for the Noise Diodes used in each RFI measurement system.

A.7 Performance of RFI Measurement Systems 1 and 3

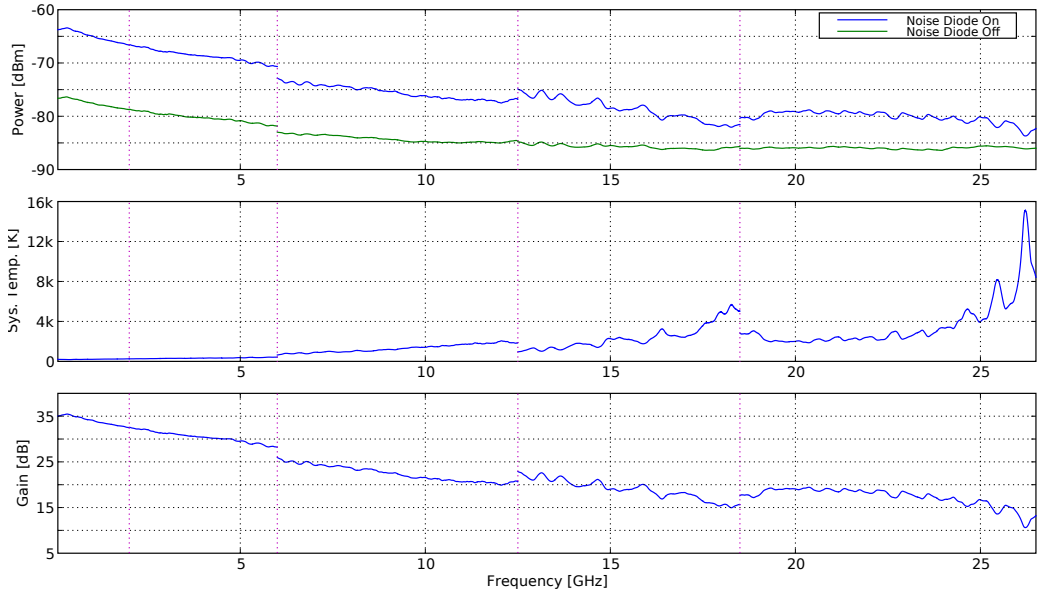

Figure A.14: Laboratory tests performed for RFI measurement System 1. Top: Noise Diode calibration measurements. Middle: System Temperature. Bottom: System Gain.

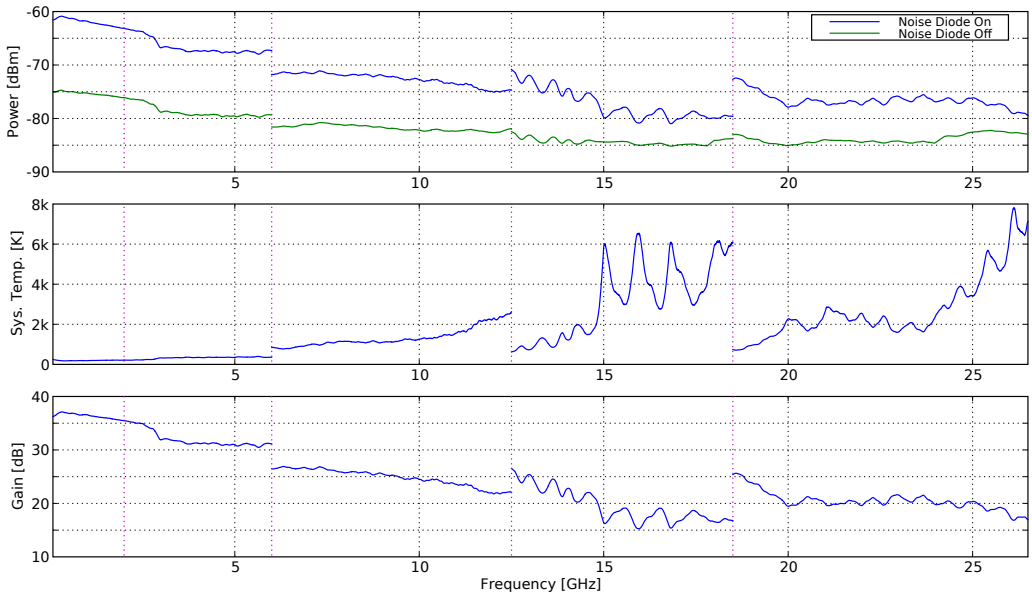

Figure A.15: Laboratory tests performed for RFI measurement System 3. Top: Noise Diode calibration measurements. Middle: System Temperature. Bottom: System Gain.

A.8 Matched Load Spectra

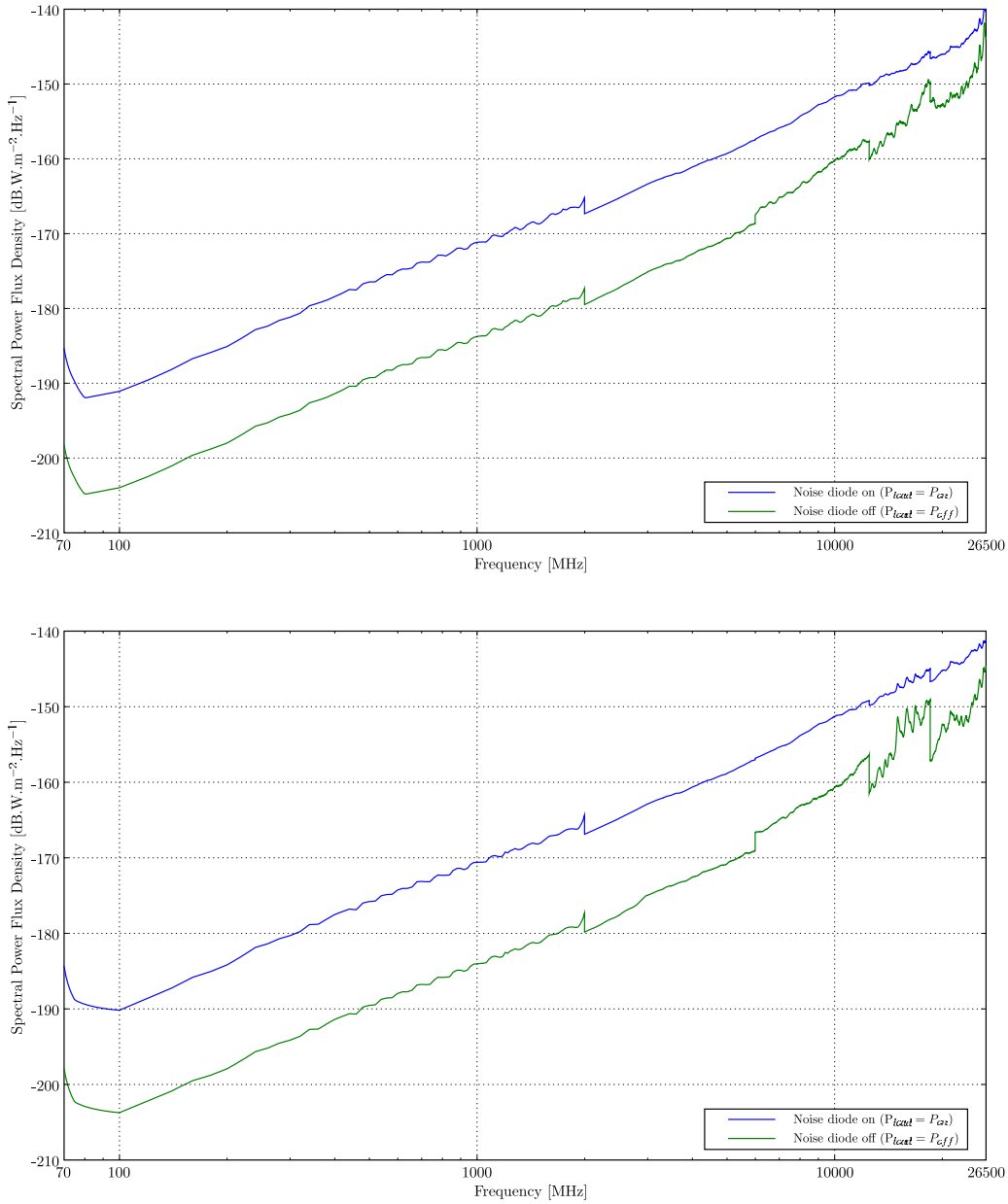

Figure A.16: Top: Matched Load Spectra for RFI Measurement System 1. Bottom: Matched Load Spectra for RFI Measurement System 3.

Appendix B

Control and Data Acquisition Sub-System

B.1 Prototype and Final System Photographs

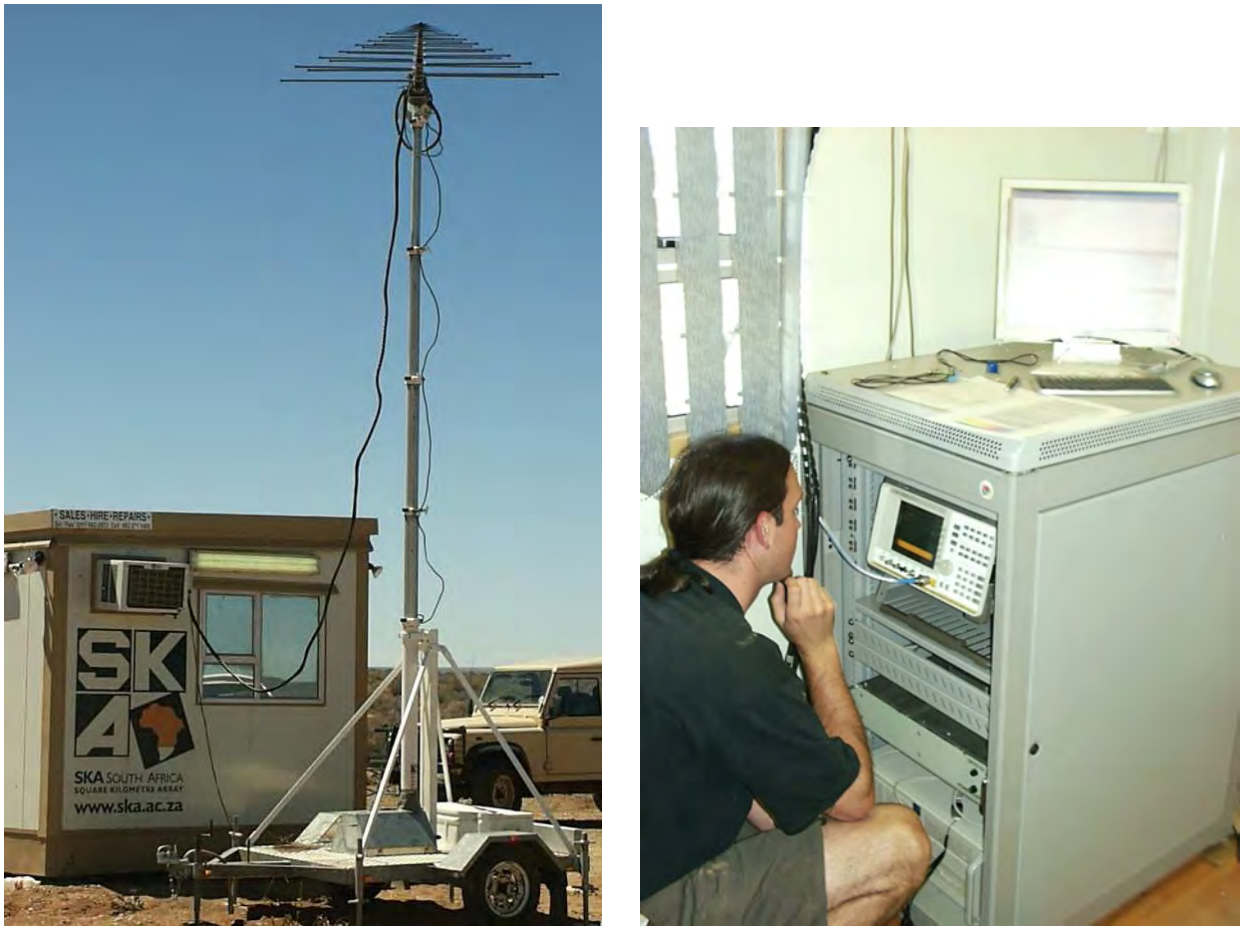

Figure B.1: Left: The prototype measurement system and trailer at the Karoo 3 core site during field test measurements in December 2004. Right: Equipment rack inside the container at the Karoo 3 core site. Electronics Control Box, spectrum analyser and Control PC with LCD monitor, keyboard and mouse are housed in the rack. Control and RF signal cables pass from the trailer outside and connect to the instruments in the rack.

Figure B.2: Top: One of the RFI measurement systems during field measurements at a remote site in the Karoo. Bottom: The measurement equipment installed in the rack of the measurement trailer. The front of the rack (left) is shown with the spectrum analyser, Control PC and Electronics Control Box installed. The Ethernet cable for providing control of the Control PC via the laptop is connected to the front of the Control PC. The back of the rack with copper busbar attached to the rack-mount instruments and the cabling are shown in the image on the right.

B.2 Power Supply PCB Schematics and Board Layout

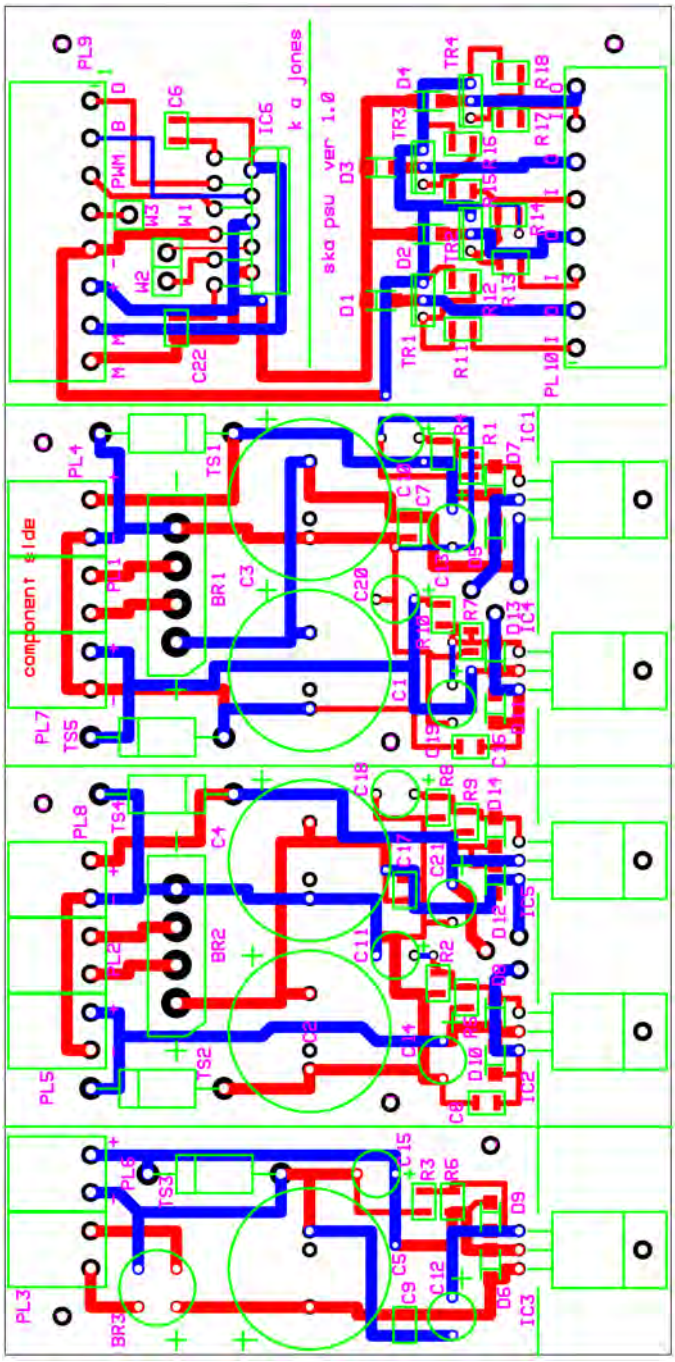

Figure B.3: Power Supply Unit Printed Circuit Board (PCB) layout. The Power Supply Unit PCB was housed in the Electronics Control Box.

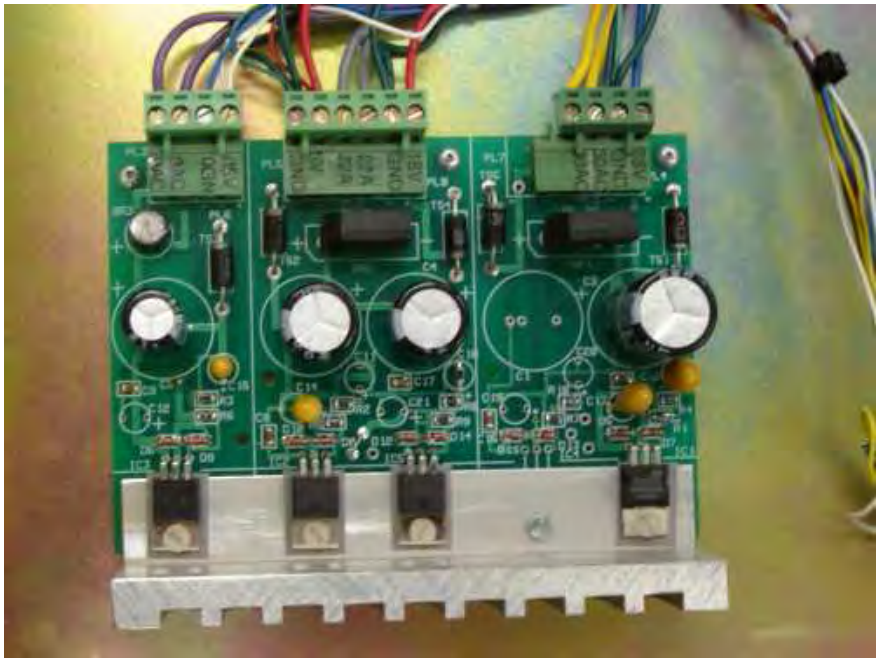

Figure B.4: Photograph of the Power Supply Unit PCB (in the Electronics Control Box). Note that the H-bridge section of the PCB used in the prototype system has been removed from the PCB in the final production system.

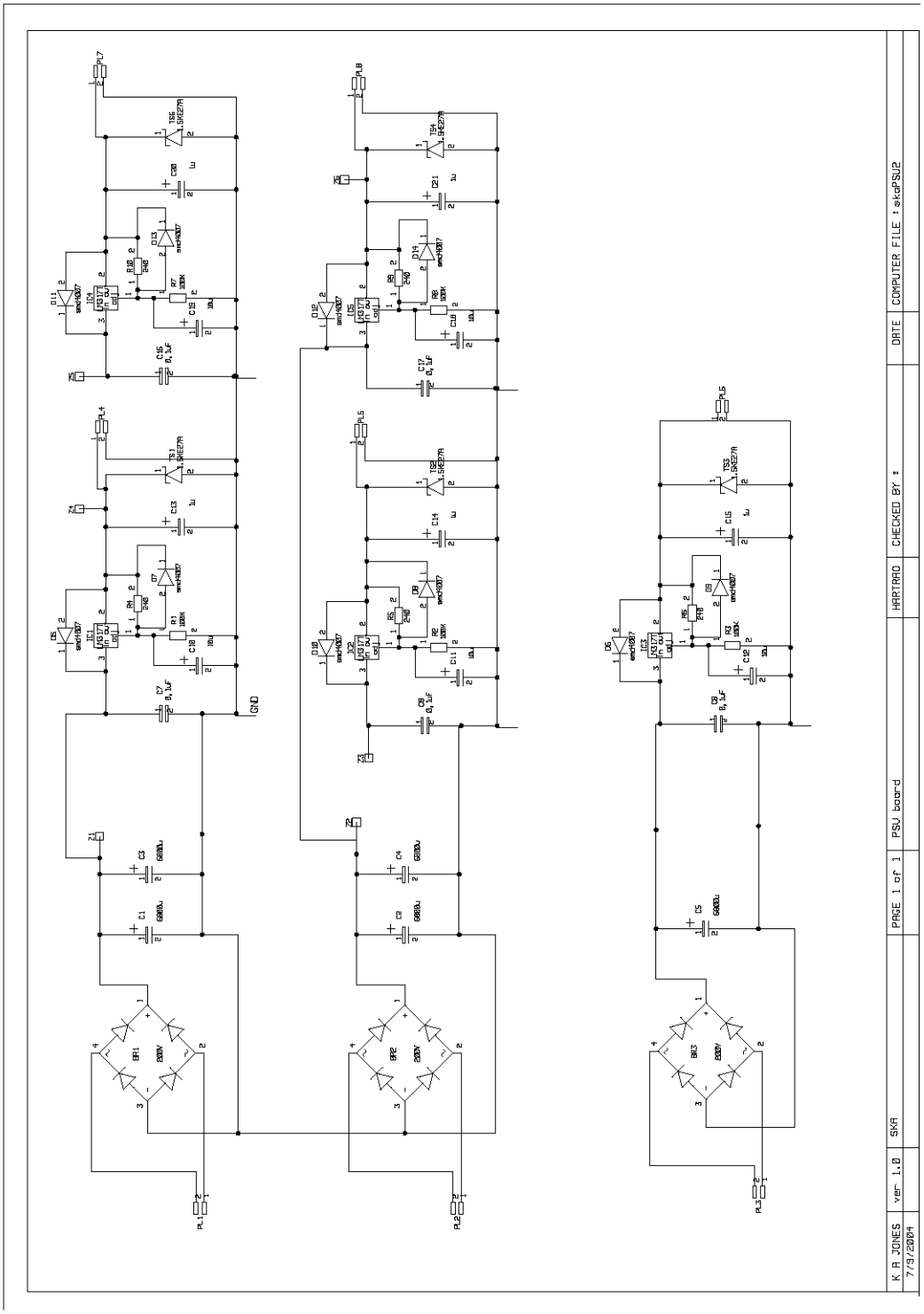

Figure B.5: Power Supply Unit PCB schematics (Page 1 of 2).

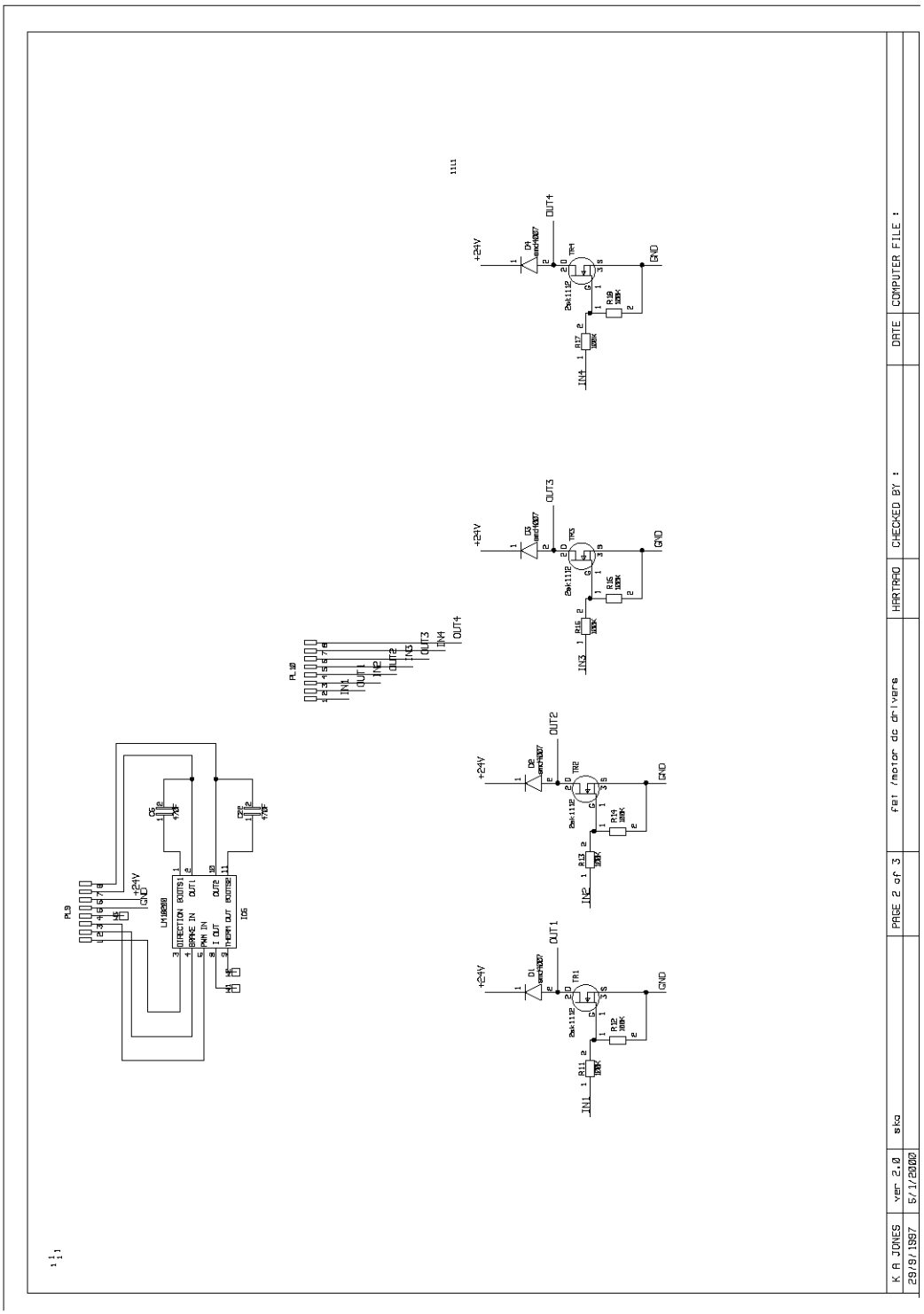

Figure B.6: Power Supply Unit PCB schematics (Page 2 of 2). These schematics show the H-bridge (LMD18200) chip which was used to drive a DC motor for the azimuth rotation in the prototype system.

B.3 Control PCB Schematics and Board Layout

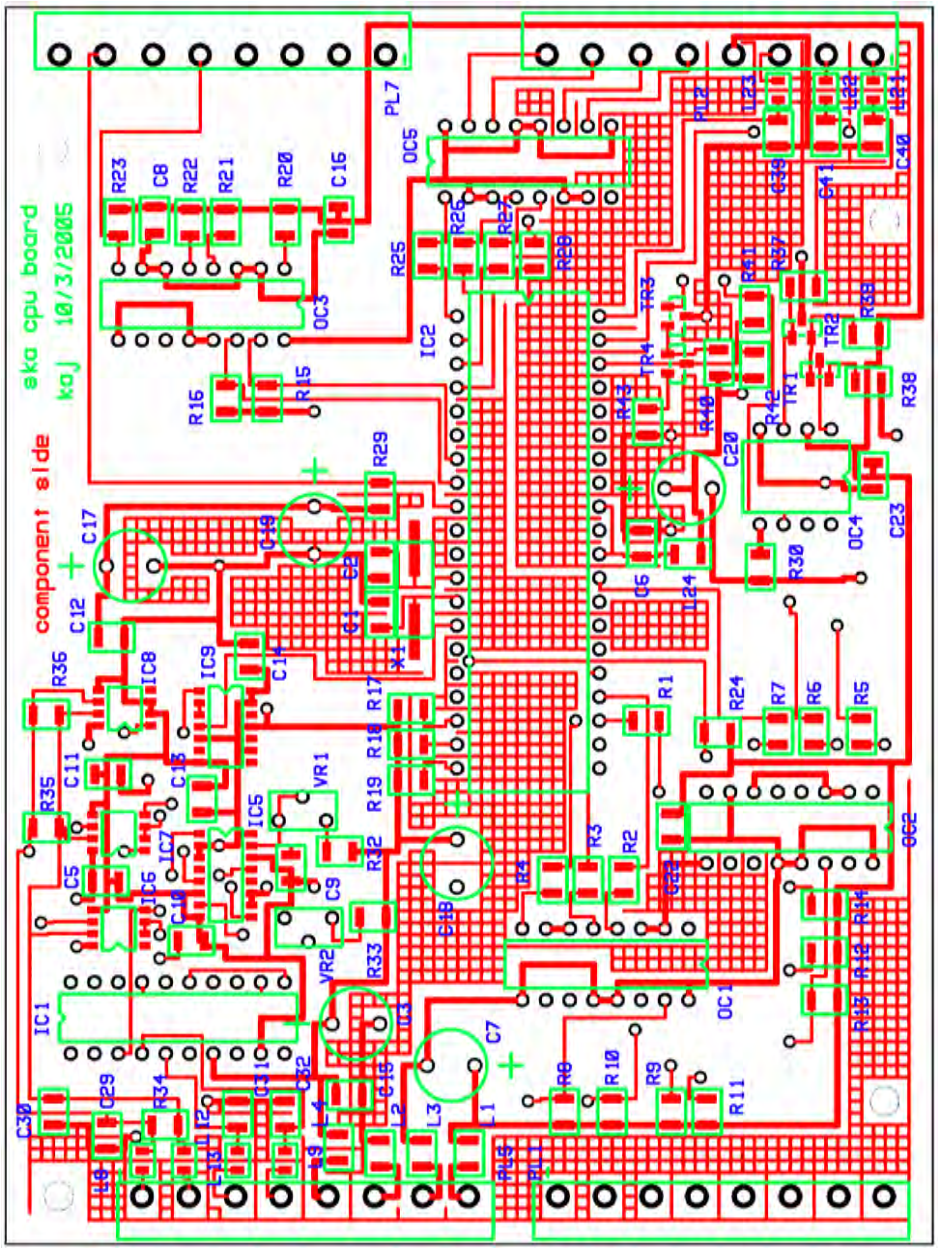

Figure B.7: Control Printed Circuit Board (PCB) layout.

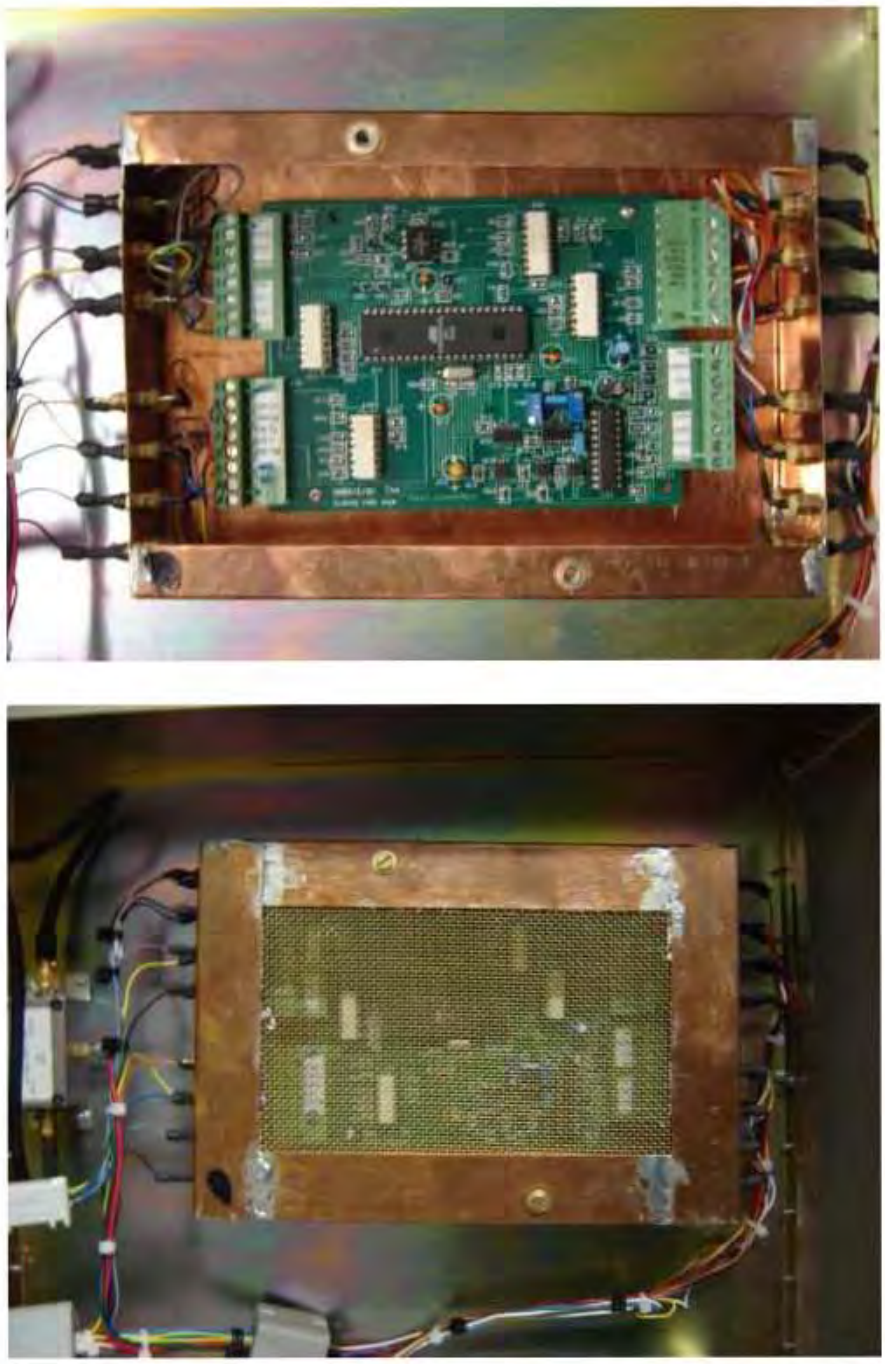

Figure B.8: Top: Control PCB installed in its copper Faraday cage (with the lid removed). Bottom: Control PCB with the lid to the Faraday cage installed.

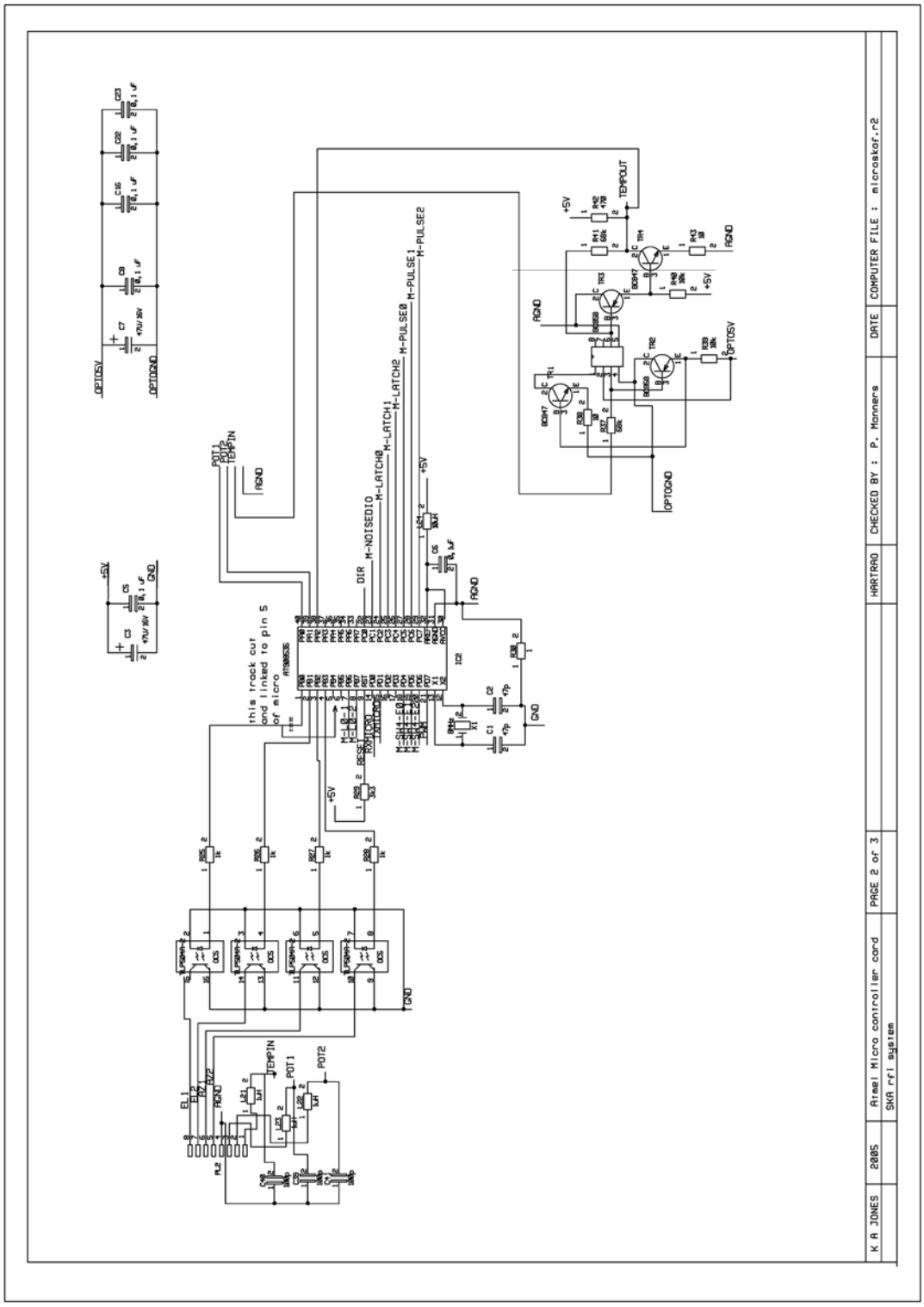

Figure B.9: Control PCB Schematics (Page 1 of 3).

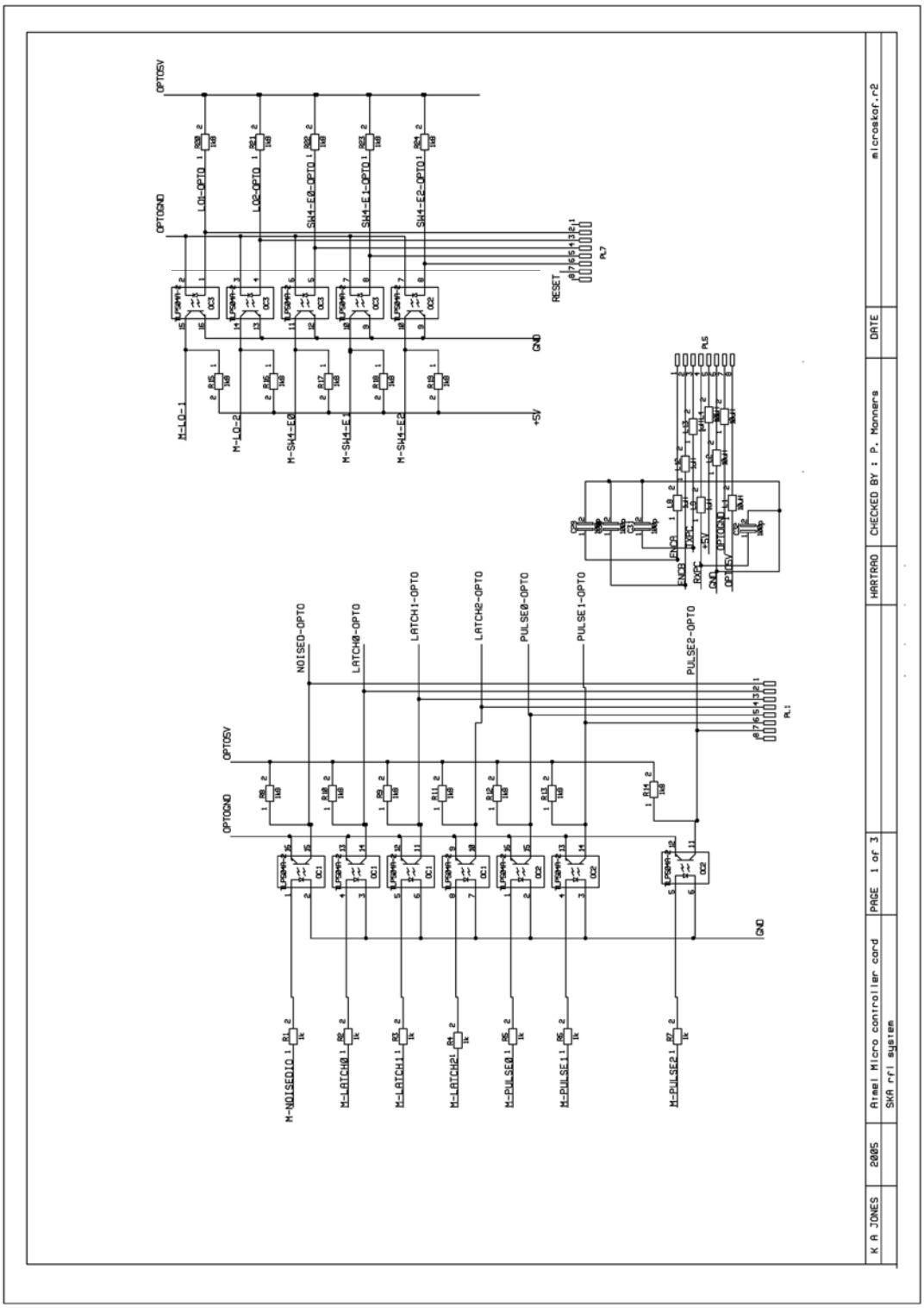

Figure B.10: Control PCB Schematics (Page 2 of 3).

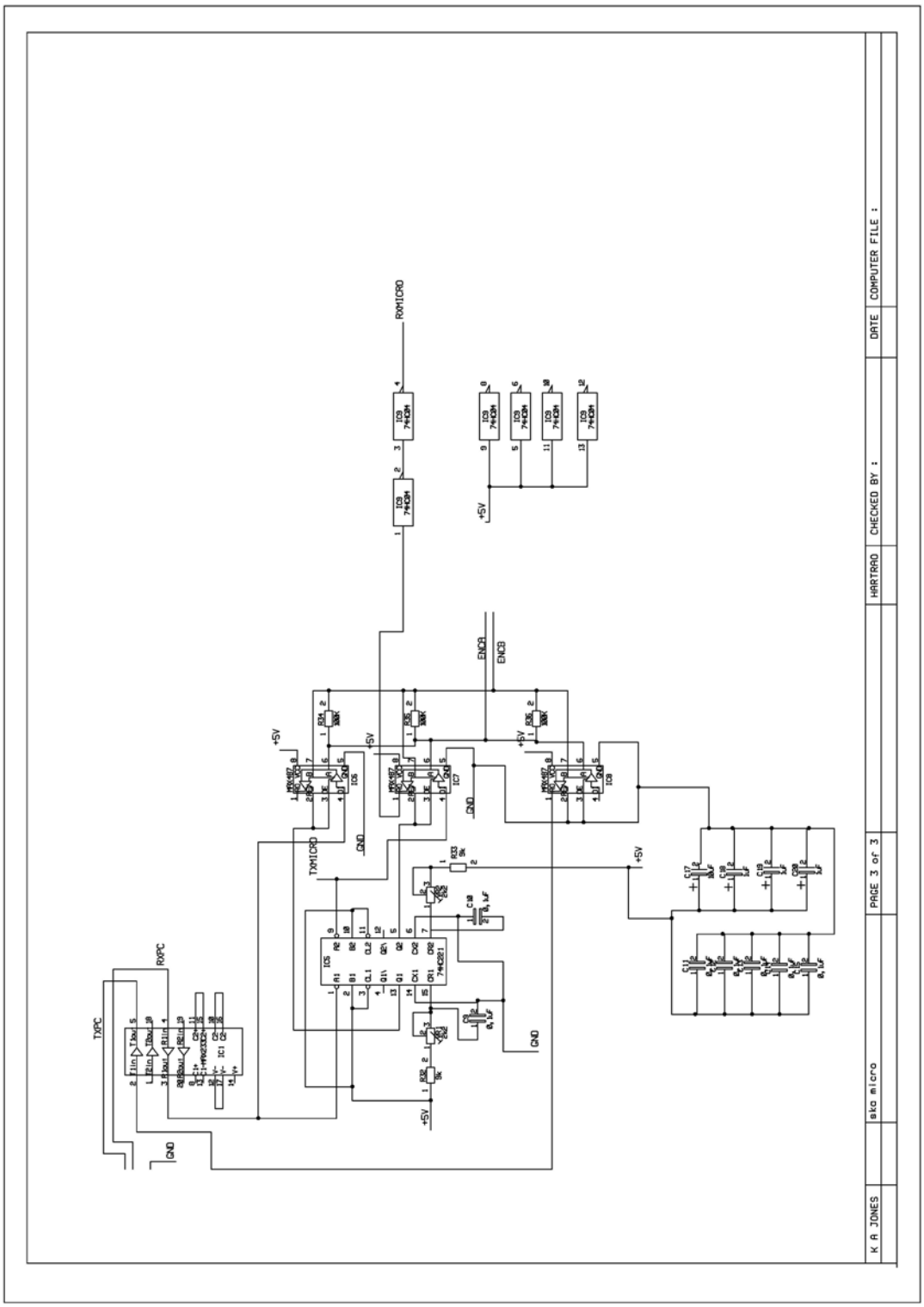

Figure B.11: Control PCB Schematics (Page 3 of 3).

B.4 RF Logic PCB Schematics and Board Layout

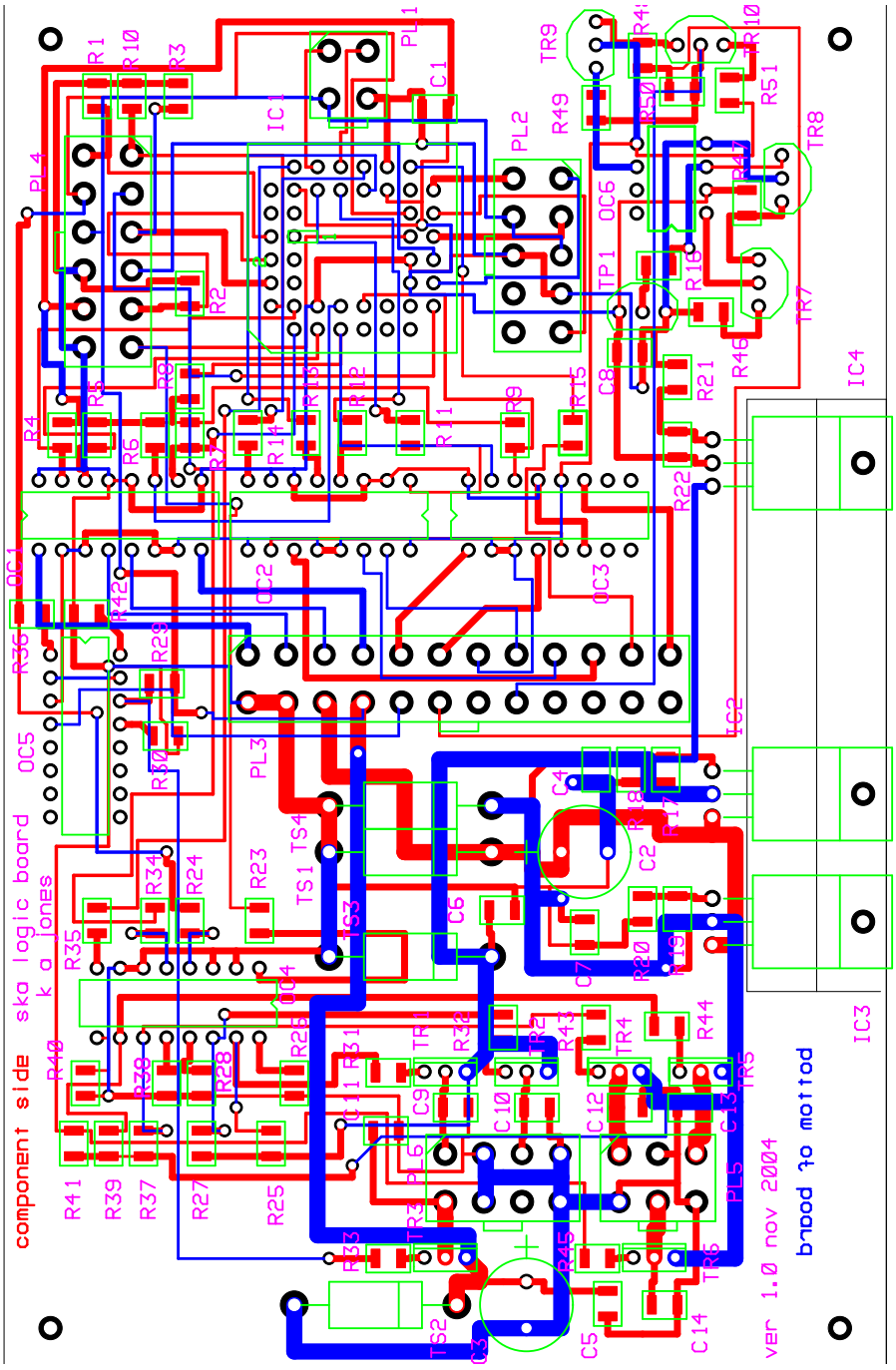

Figure B.12: RF Logic Printed Circuit Board (PCB) layout.

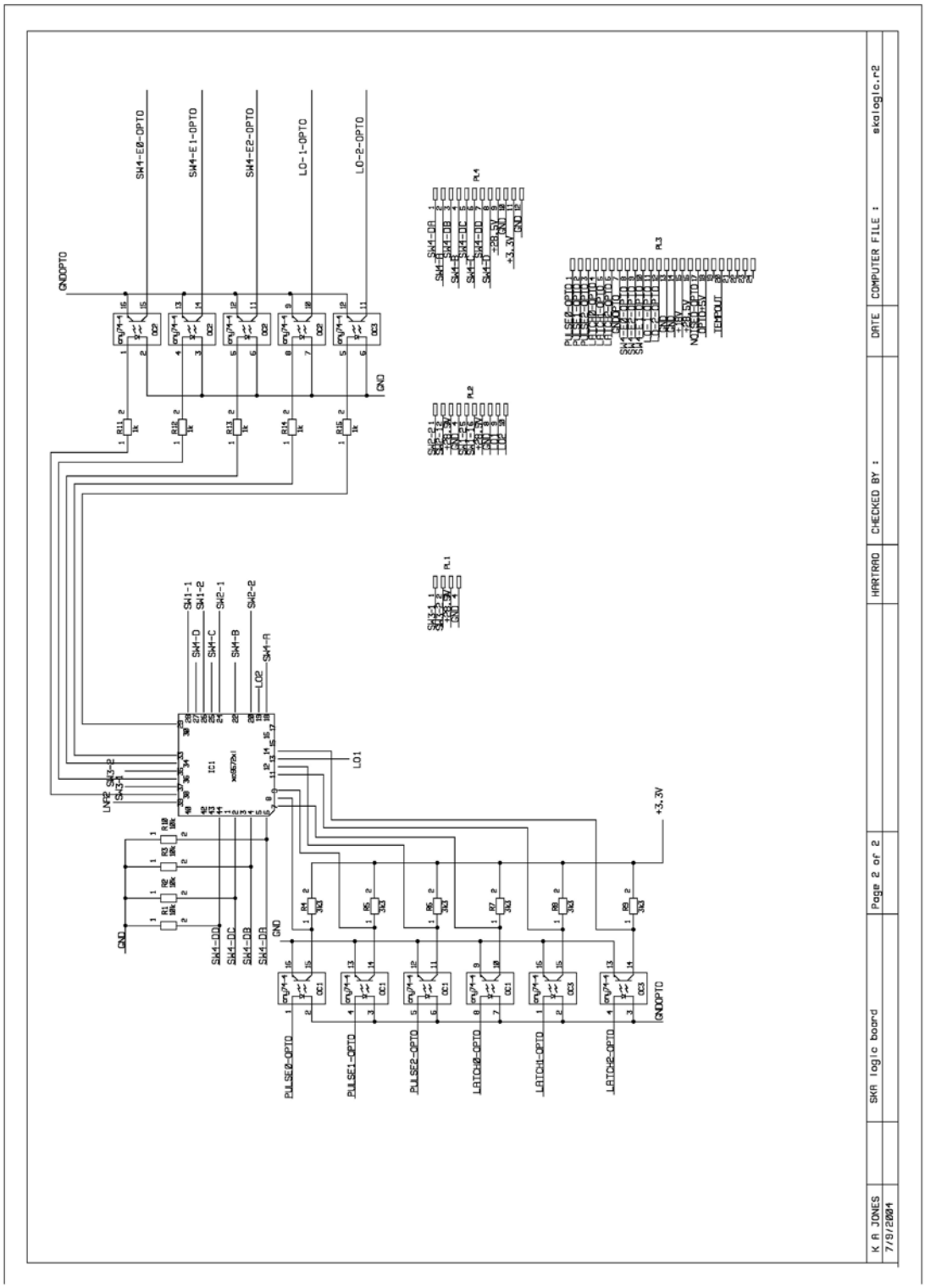

Figure B.13: RF Logic PCB schematics (Page 1 of 2).

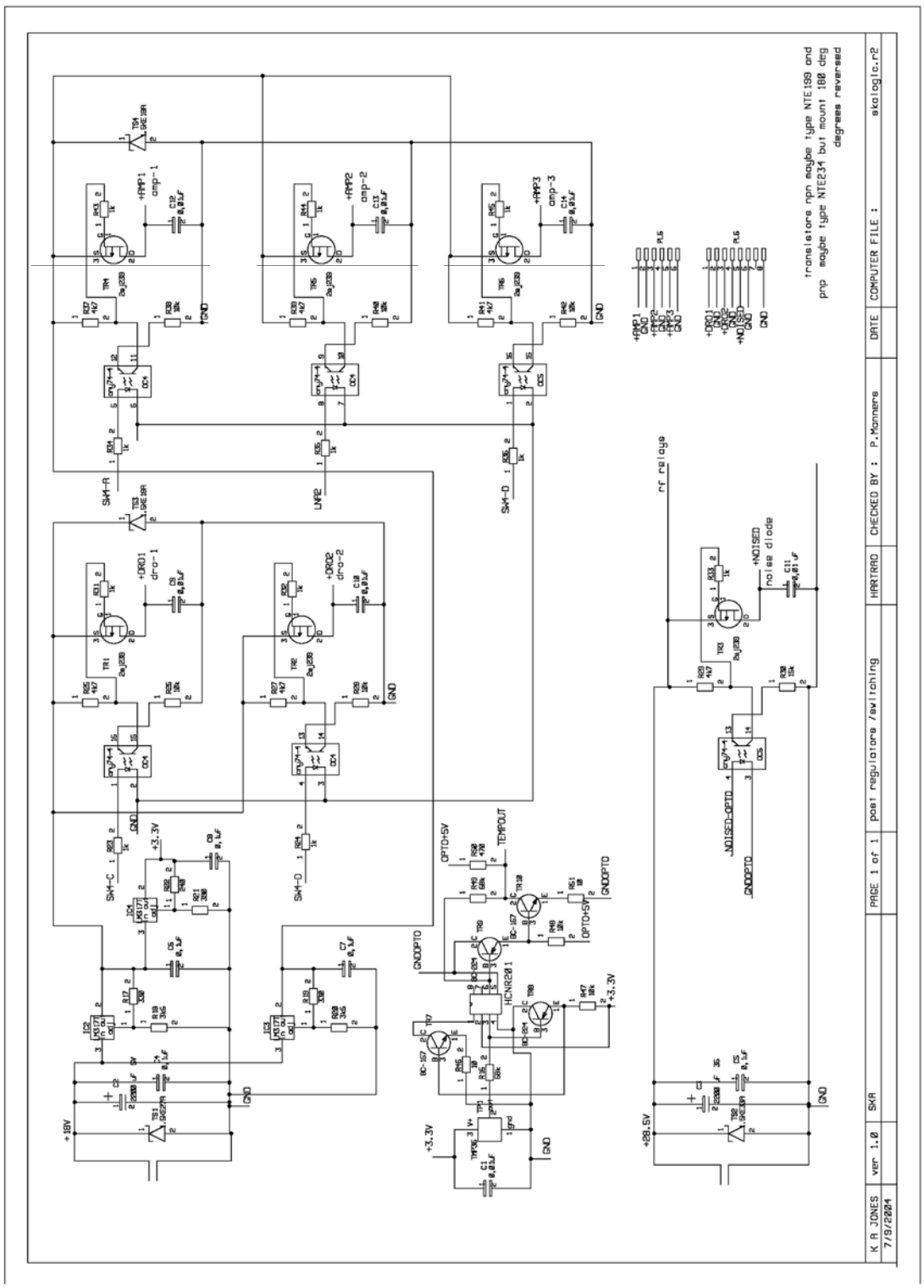

Figure B.14: RF Logic PCB schematics (Page 2 of 2).

B.5 CPLD Logic

RF Path	Input	RF Switch 4				LNA 1	LNA 2	LNA 3	12 GHz LO	18 GHz LO
		SW4-A	SW4-B	SW4-C	SW4-D					
A, A*, ND A	000	1	0	0	0	1	0	0	0	0
B, ND B	001	0	1	0	0	0	1	0	0	0
C, ND C	010	0	0	1	0	0	1	0	1	0
D, ND D	011	0	0	0	1	0	0	1	0	1
Unused	100	0	0	0	0	0	0	0	0	0
Unused	101	0	0	0	0	0	0	0	0	0
Unused	110	0	0	0	0	0	0	0	0	0
default	111	0	0	0	0	0	0	0	0	0

Table B.1: CPLD logic (truth table) for the latched RF switching lines from the microcontroller. The input lines in the Input column of the table were labelled LATCH2, LATCH1 and LATCH0 where LATCH0 was the least significant bit and LATCH2 the most significant bit. When first powered up, the microcontroller was set to the *default* state.

RF Path	Input	RF Switch 1		RF Switch 2		RF Switch 3	
		SW2-1	SW2-2	SW1-1	SW1-2	SW3-1	SW3-2
A*, ND D	000	0	1	0	1	1	0
default	001	0	0	0	0	0	0
B	010	0	1	1	0	1	0
A, C	011	0	1	1	0	0	1
D, ND A	100	1	0	0	1	1	0
Unused	101	0	0	0	0	0	0
ND B	110	1	0	1	0	1	0
ND C	111	1	0	1	0	0	1

Table B.2: CPLD logic (truth table) for the pulsed switching lines from the microcontroller. The input lines in the Input column of the table were labelled PULSE2, PULSE1 and PULSE0 where PULSE0 was the least significant bit and PULSE2 the most significant bit. When first powered on the microcontroller was set to the *default* state.

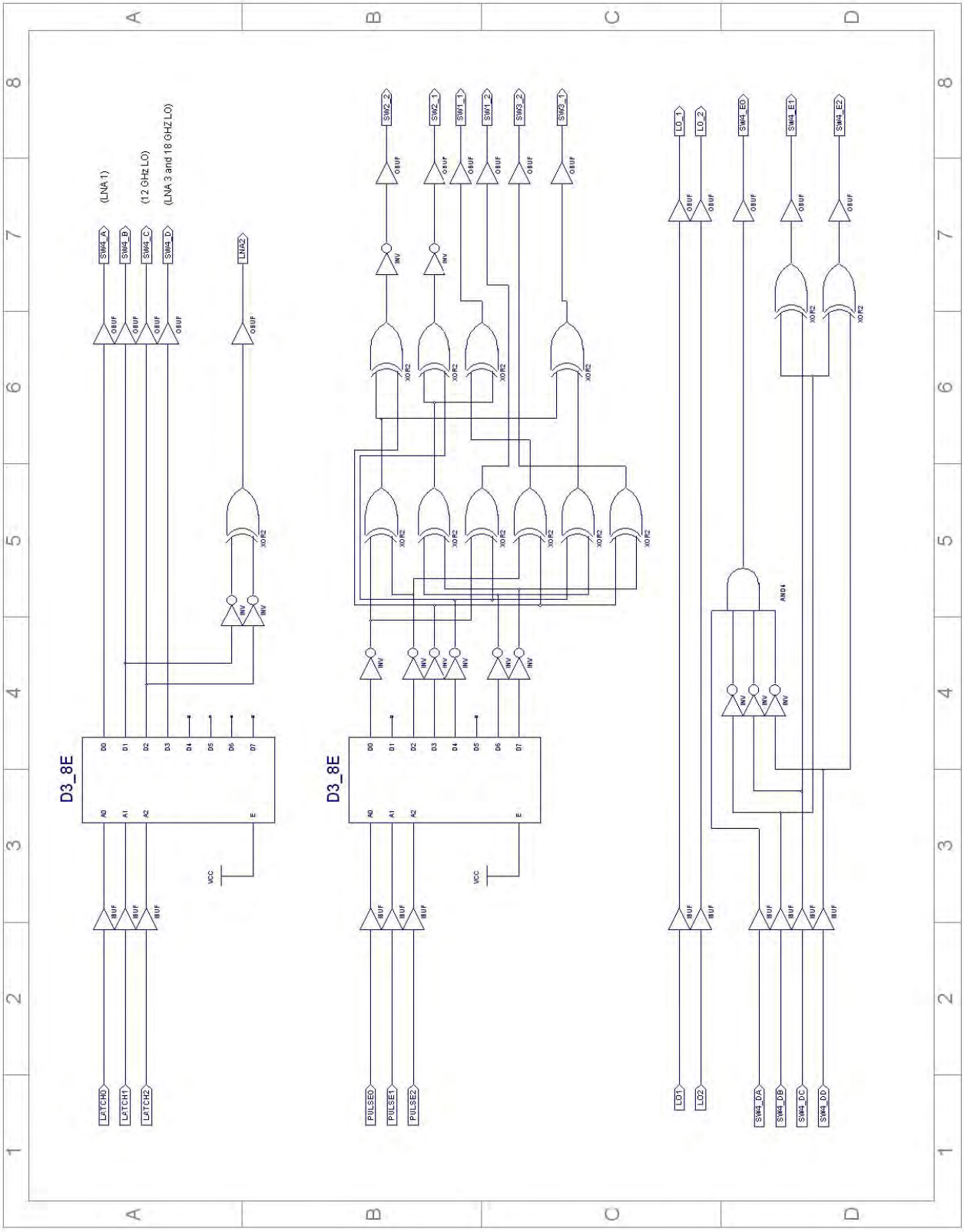

Figure B.15: Diagram of the control logic which was implemented on the Xilinx XC9572XL CPLD for performing the switching and feedback functions of the RF components.

Position Detector lines from Switch 4				Encoded lines		
SW4-DA	SW4-DB	SW4-DC	SW4-DD	SW4-E2	SW4-E1	SW4-E0
1	0	0	0	0	0	1
0	1	0	0	0	1	0
0	0	1	0	1	1	0
0	0	0	1	1	0	0
0	0	0	0	0	0	0

Table B.3: Possible states for positions of Switch 4. The CPLD encoded the detected signal lines from the switch and connected these to the microcontroller on the Control PCB. The Data Byte returned as part of the control message from the microcontroller was constructed using the state of the two LOs' frequency lock lines (i.e. LO-1, LO-2) and the three encoded lines (i.e. SW4-E2, SW4-E1, SW4-E2) indicating the position of Switch 4.

B.6 RFI Measurement Scheduler VI Block Diagram

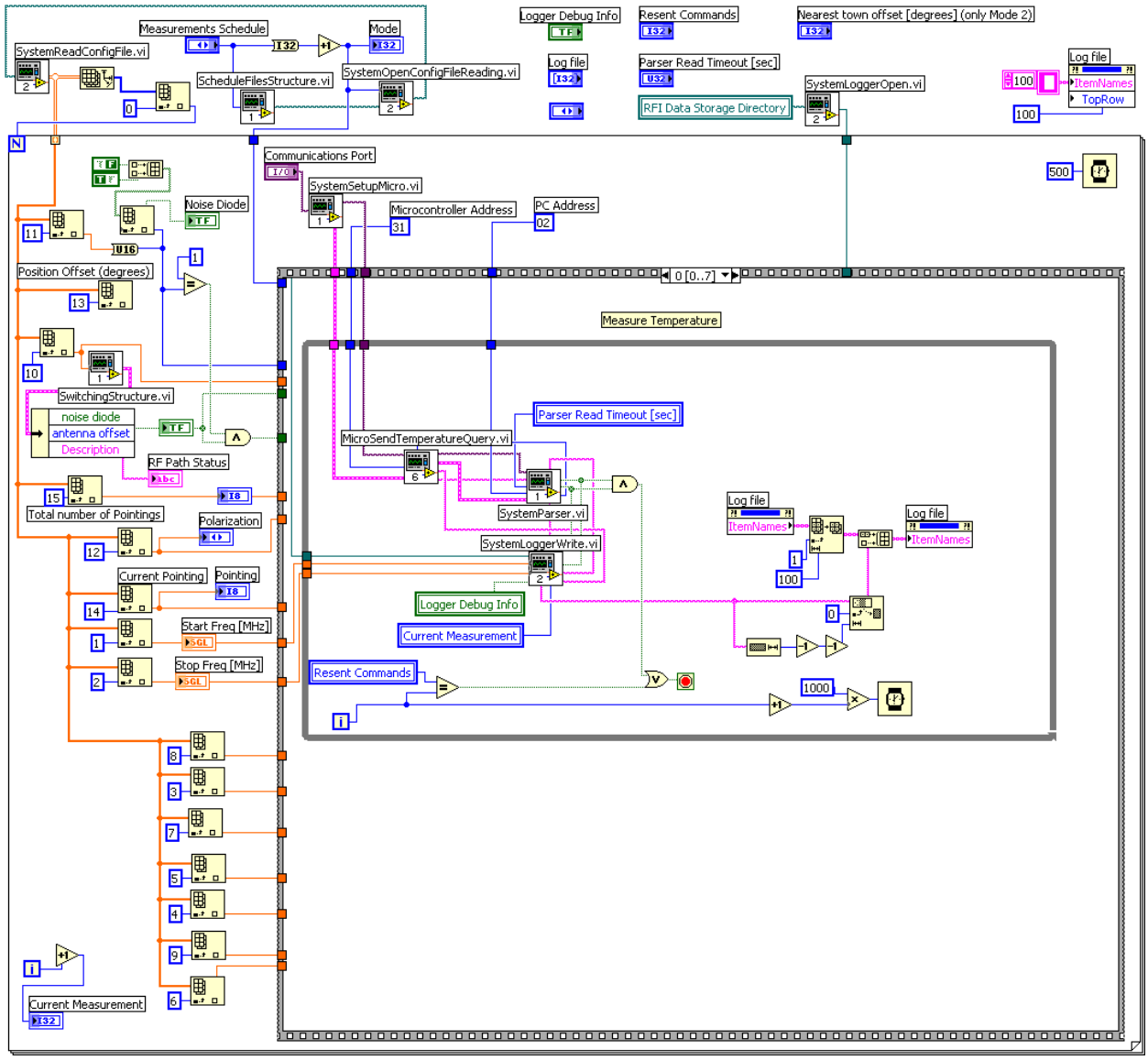

Figure B.16: LabVIEW block diagram for the RFI Measurement Scheduler VI. The first part (Measure Temperature) in the measurement sequence according to Figure 3.8 in Chapter 3 is shown.

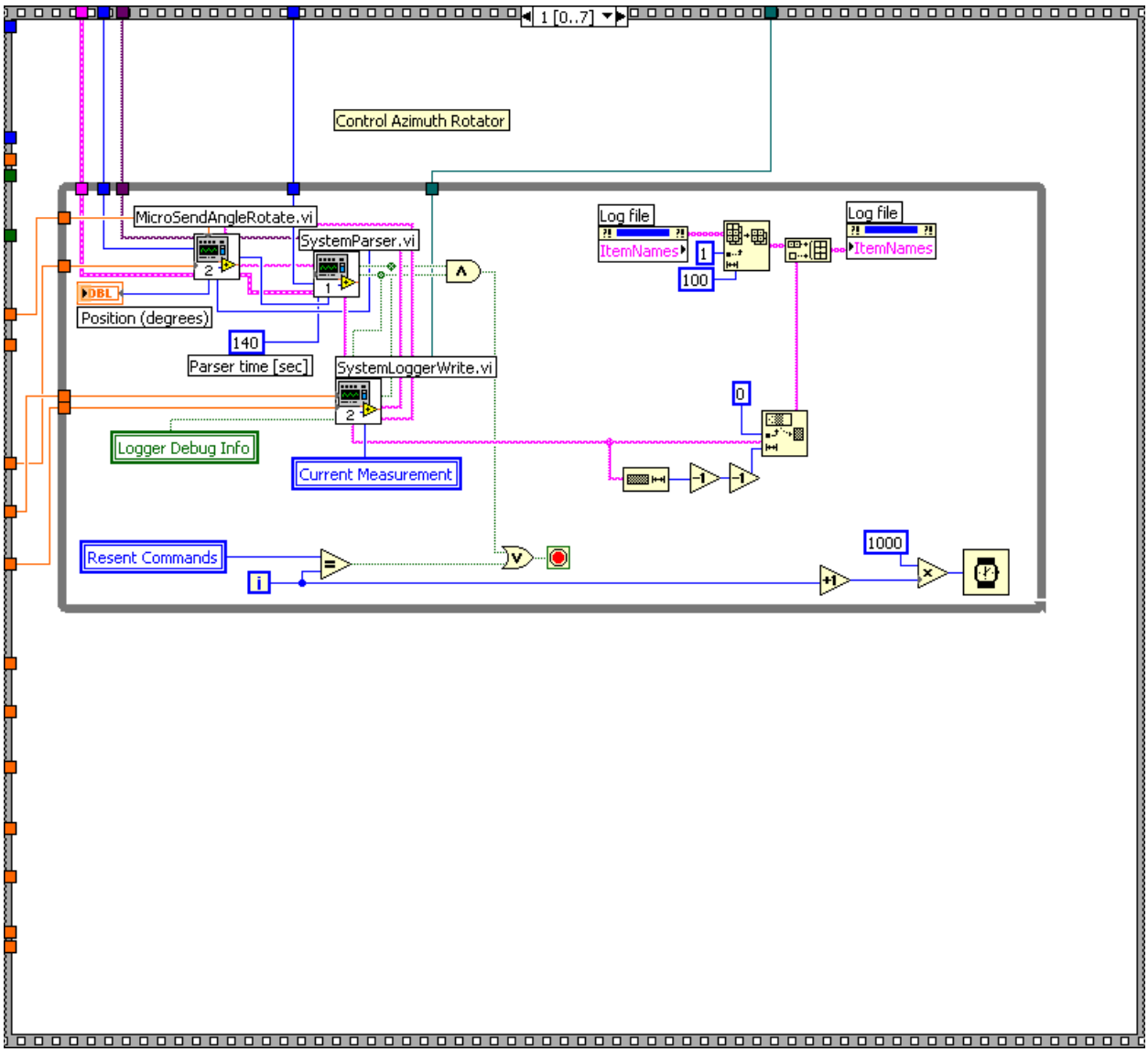

Figure B.17: LabVIEW block diagram of the *Control Azimuth* control sequence in the RFI Measurement Scheduler VI.

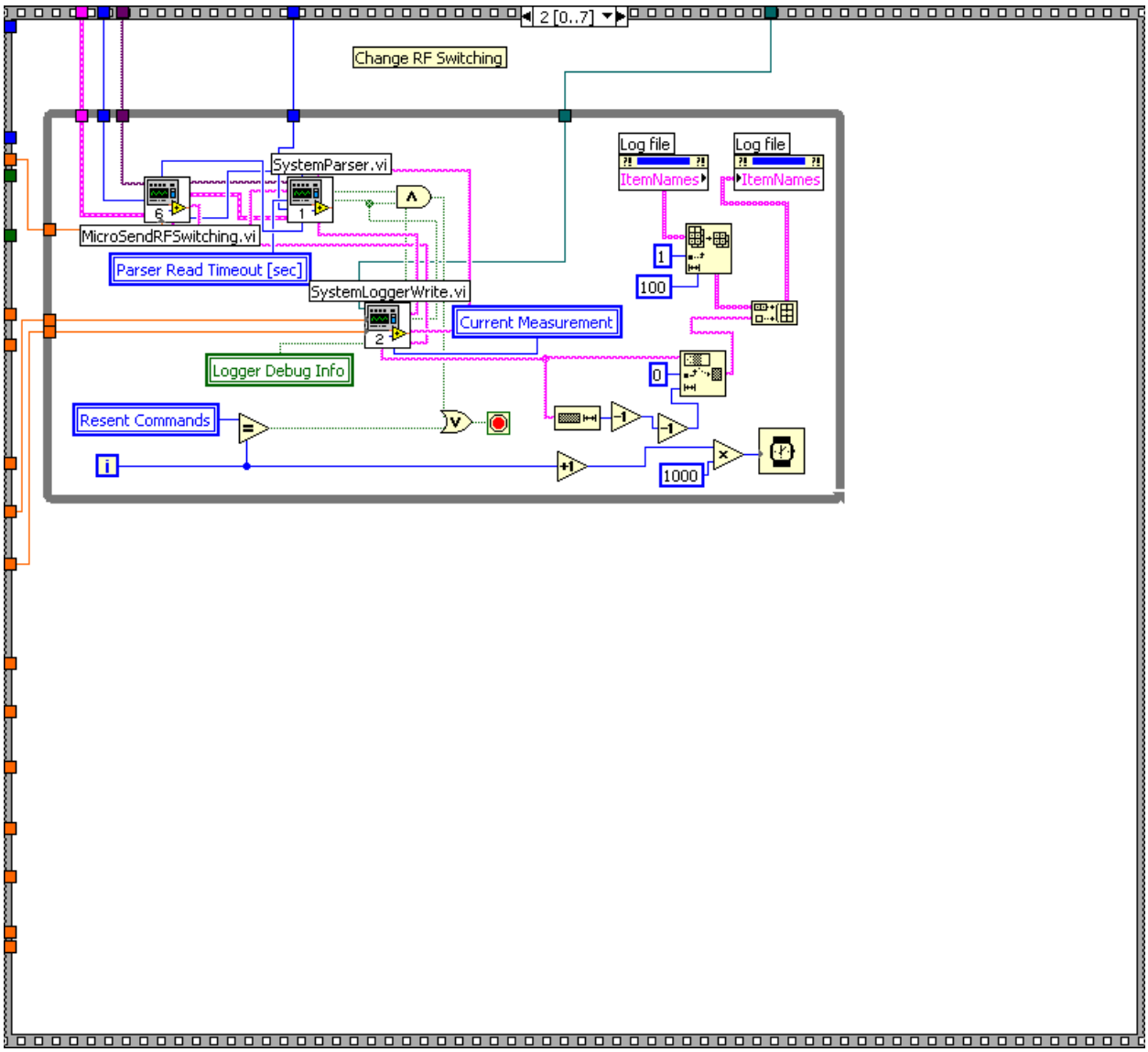

Figure B.18: LabVIEW block diagram of the *RF Switching* control sequence in the RFI Measurement Scheduler VI.

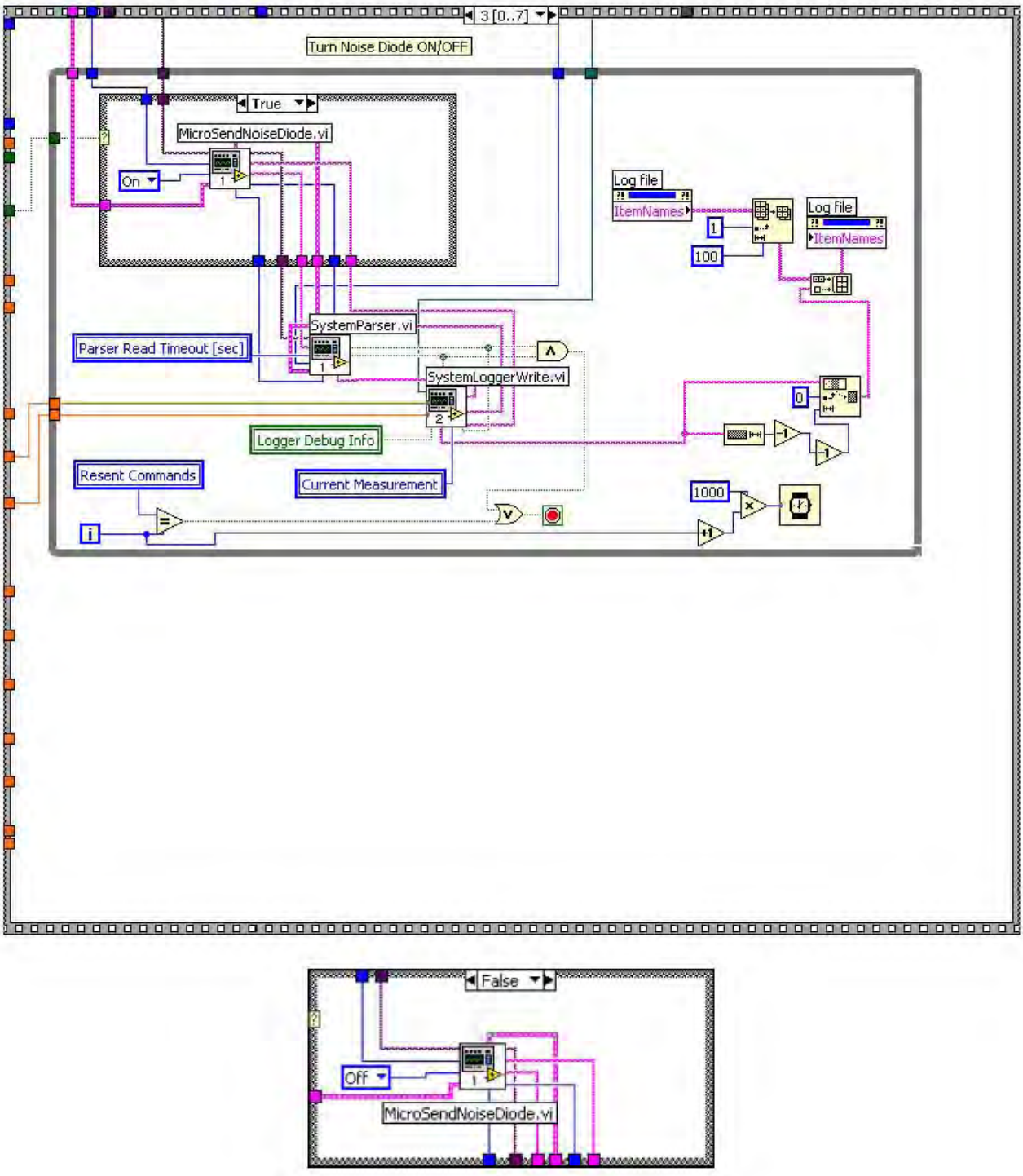

Figure B.19: Top: LabVIEW block diagram of the *Noise Diode ON* control sequence in the RFI Measurement Scheduler VI. Bottom: Block diagram for the optional *Noise Diode OFF* control sequence.

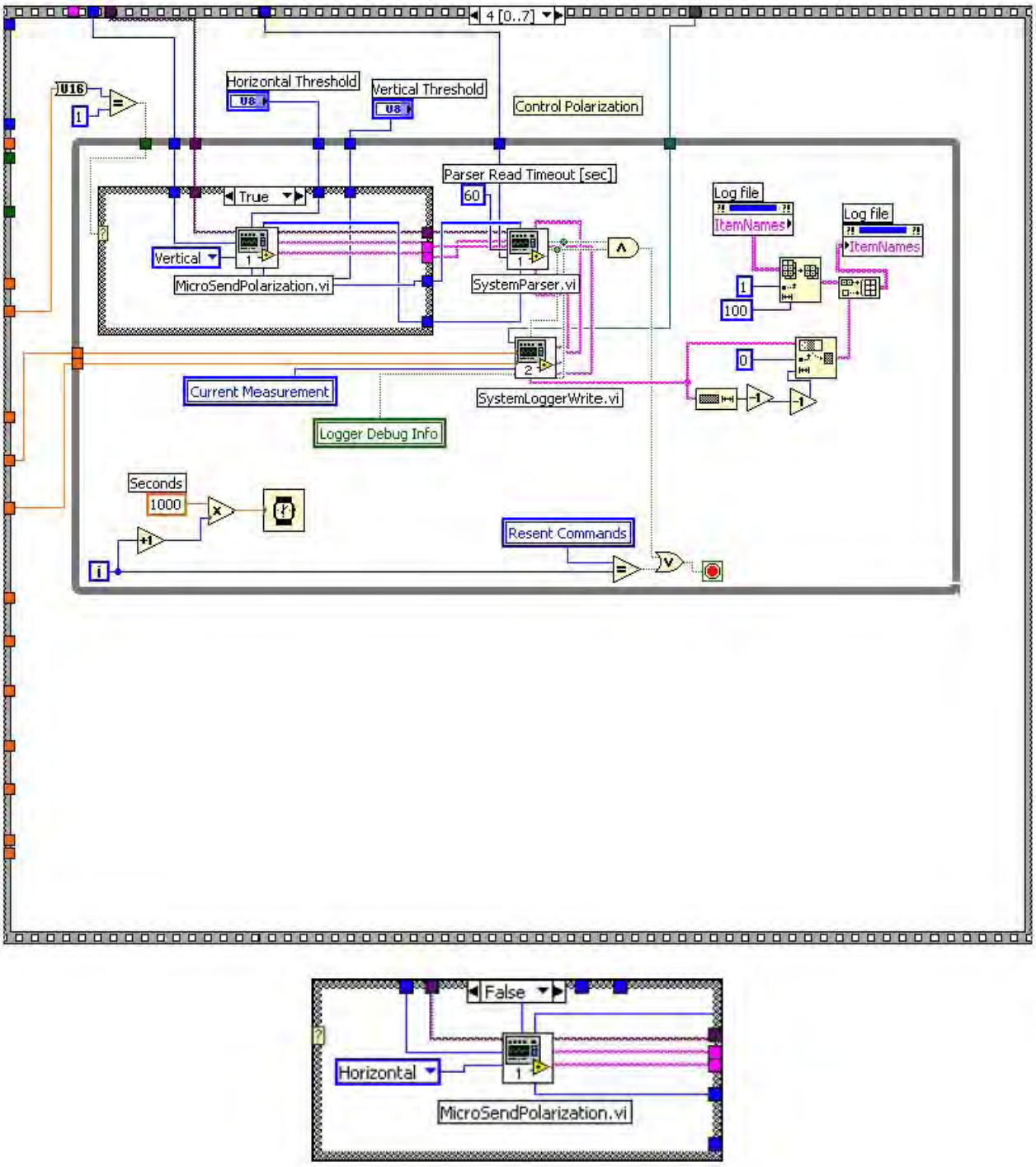

Figure B.20: Top: LabVIEW block diagram of the *Control Polarisation* (vertical) control sequence in the RFI Measurement Scheduler VI. Bottom: Block diagram of the *Control Polarisation* (horizontal) control sequence.

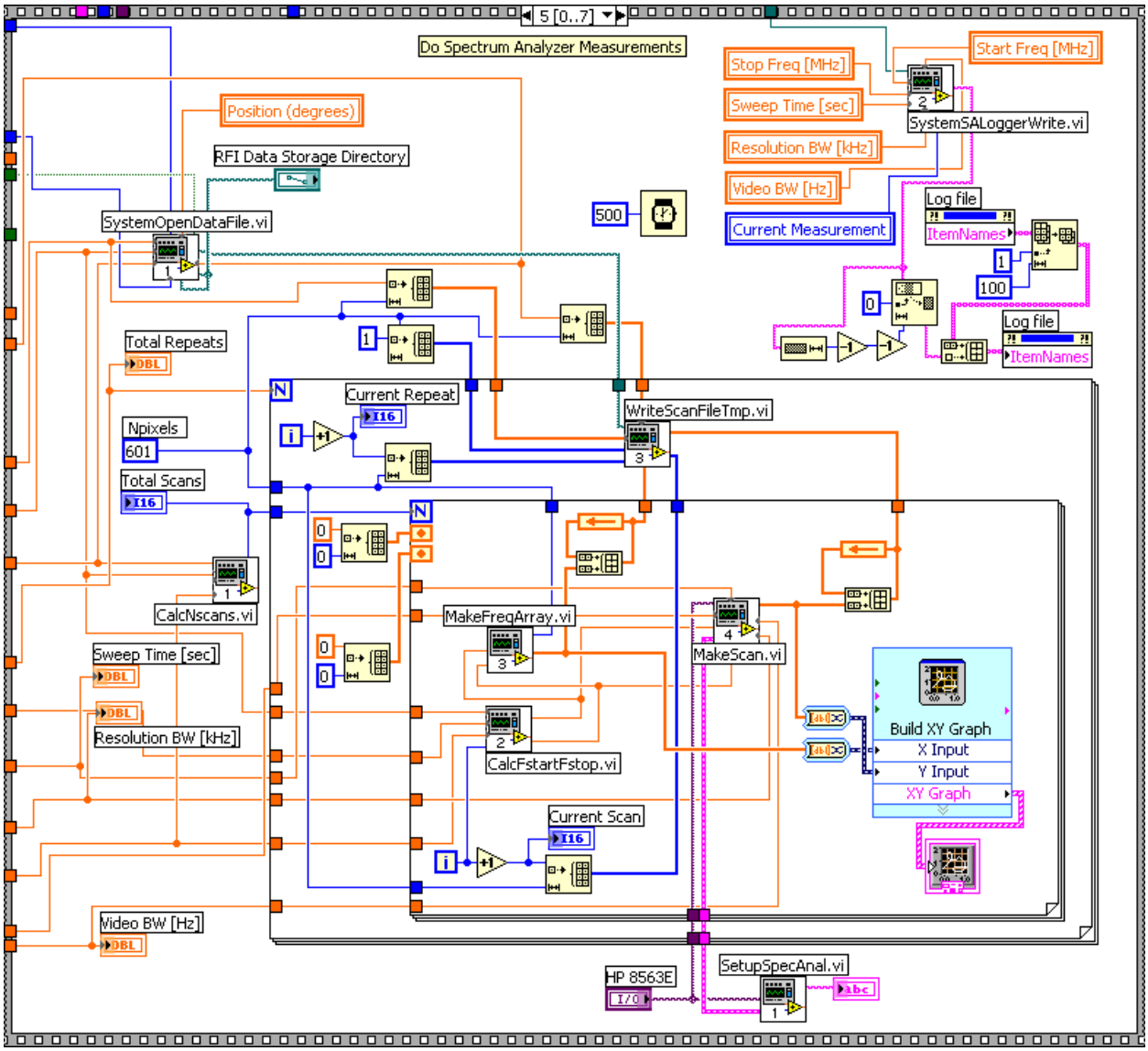

Figure B.21: LabVIEW block diagram of the Spectrum Analyser Measurements control sequence in the RFI Measurement Scheduler VI.

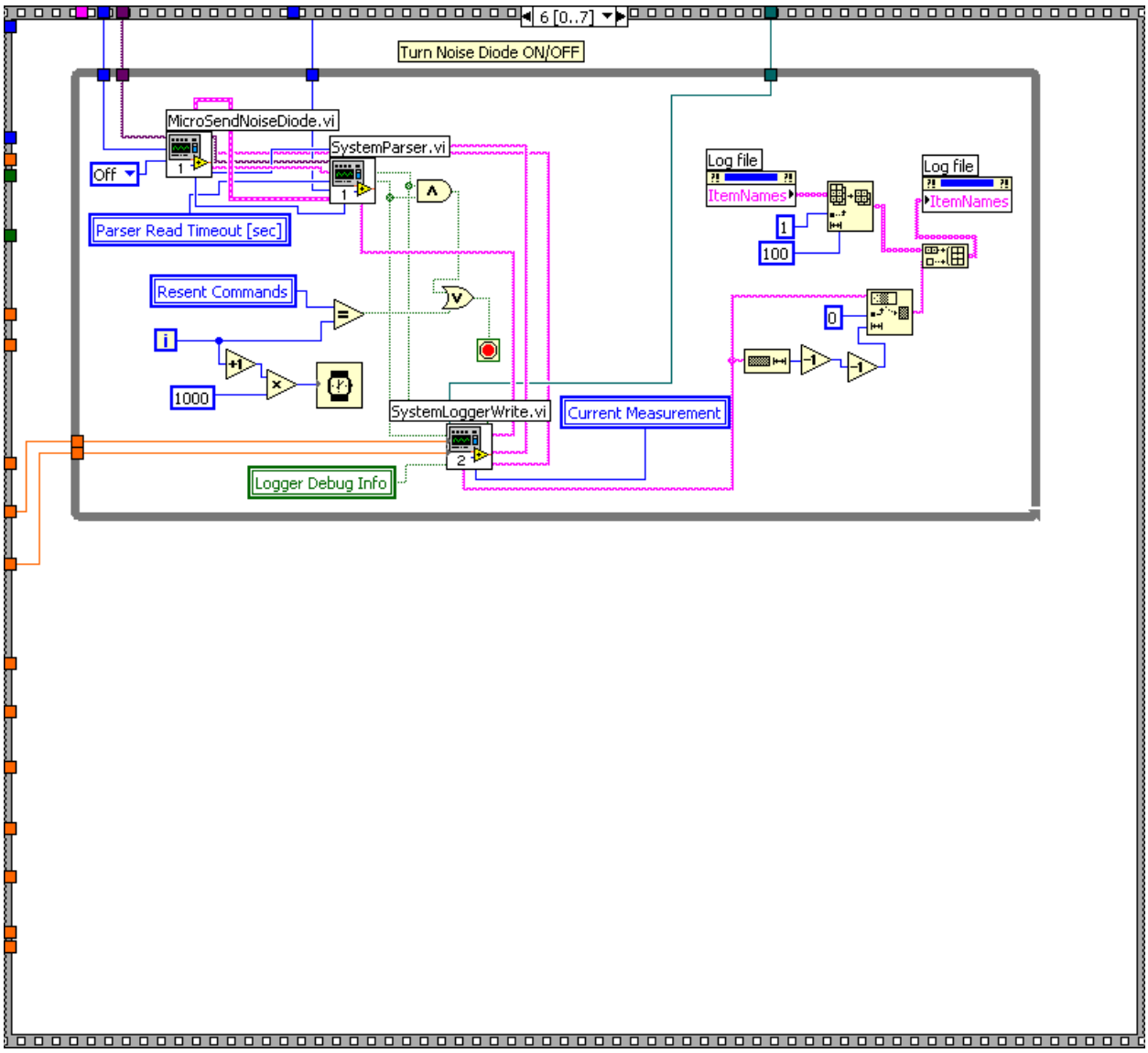

Figure B.22: LabVIEW block diagram of the *Noise Diode OFF* control sequence in the RFI Measurement Scheduler VI.

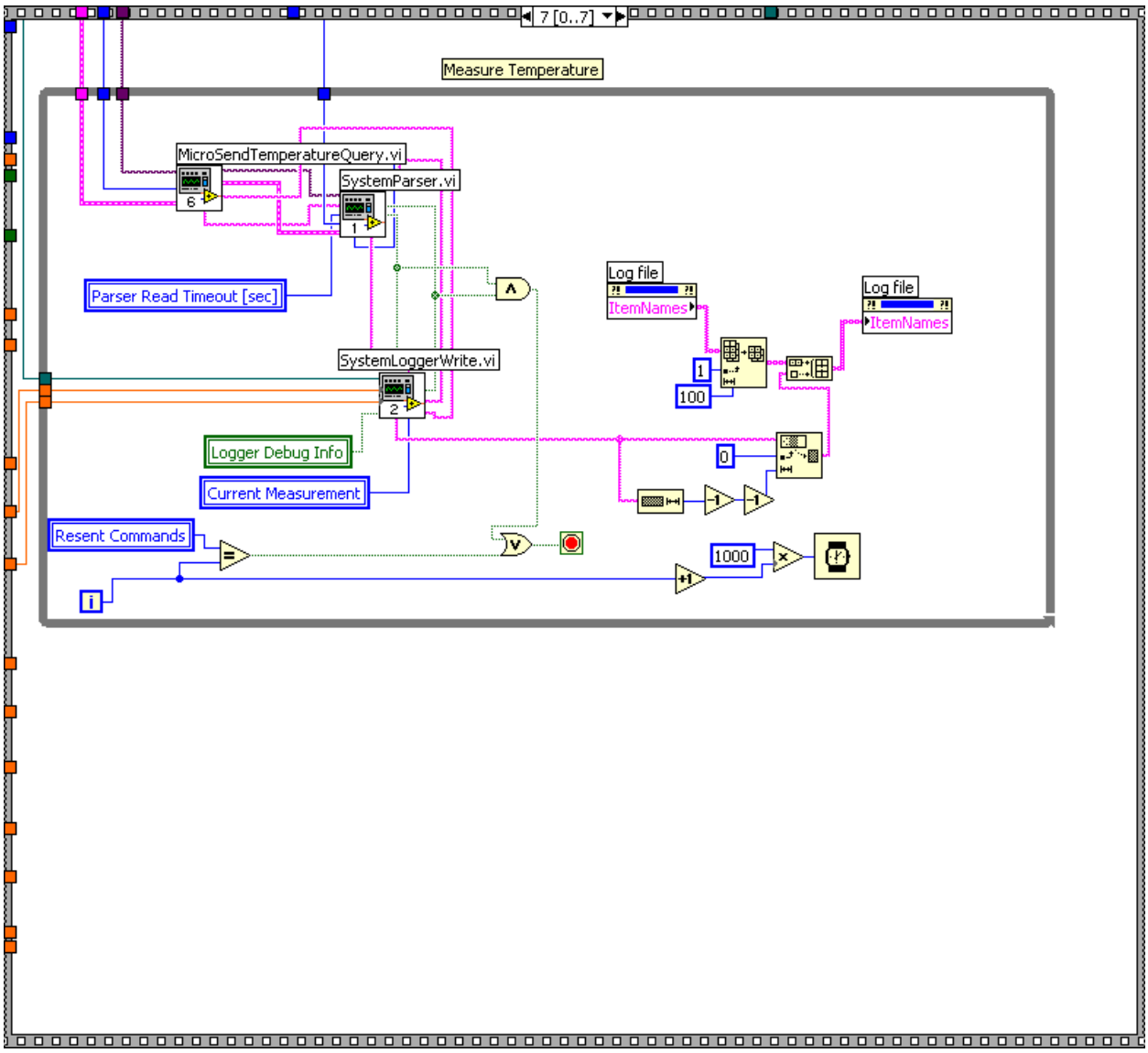

Figure B.23: LabVIEW block diagram of the *Measure Temperature* control sequence in the RFI Measurement Scheduler VI.

B.7 Microcontroller Control Flow Diagram

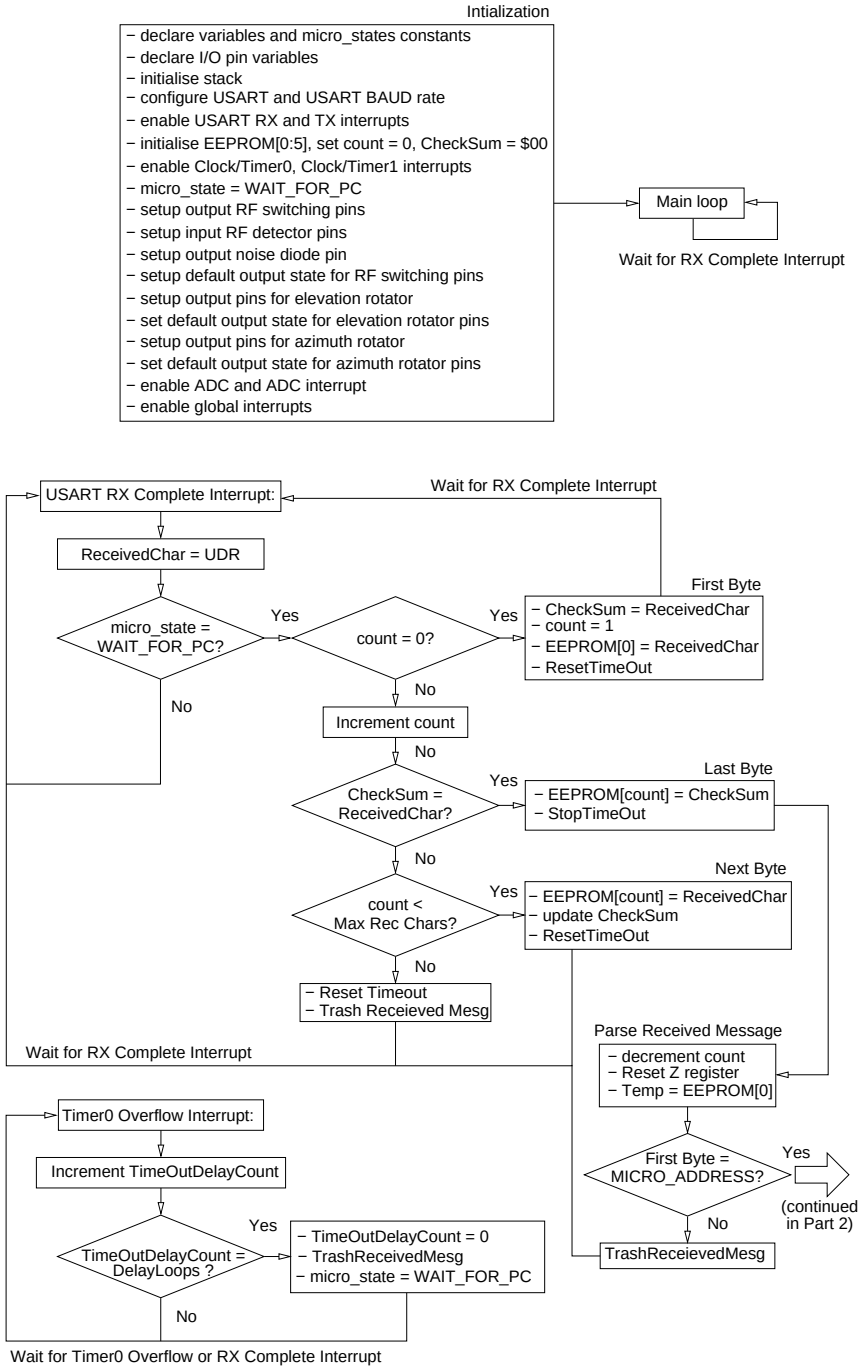

Figure B.24: Microcontroller Control Flow Chart (Part 1 of 5).

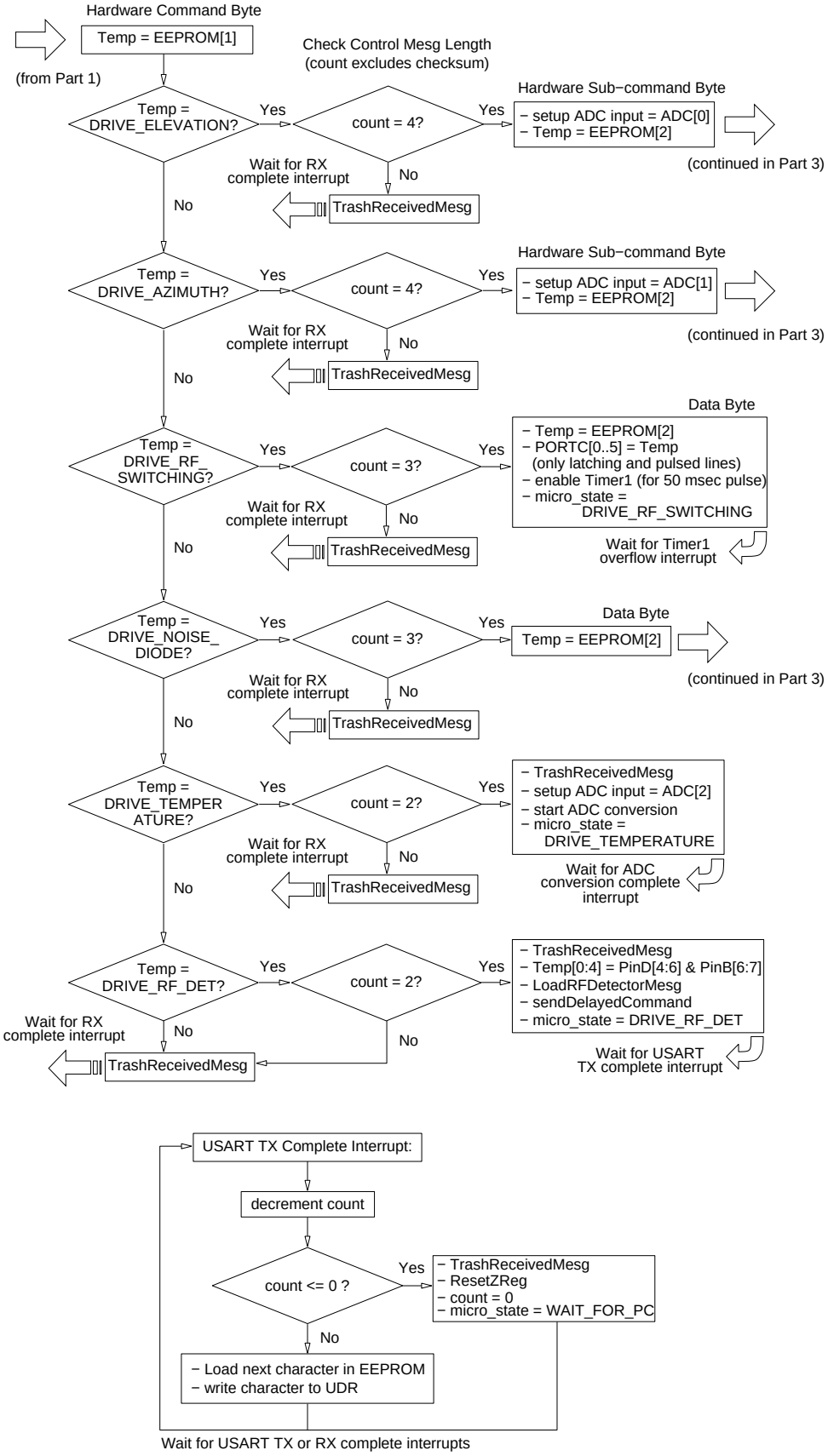

Figure B.25: Microcontroller Control Flow Chart (Part 2 of 5).

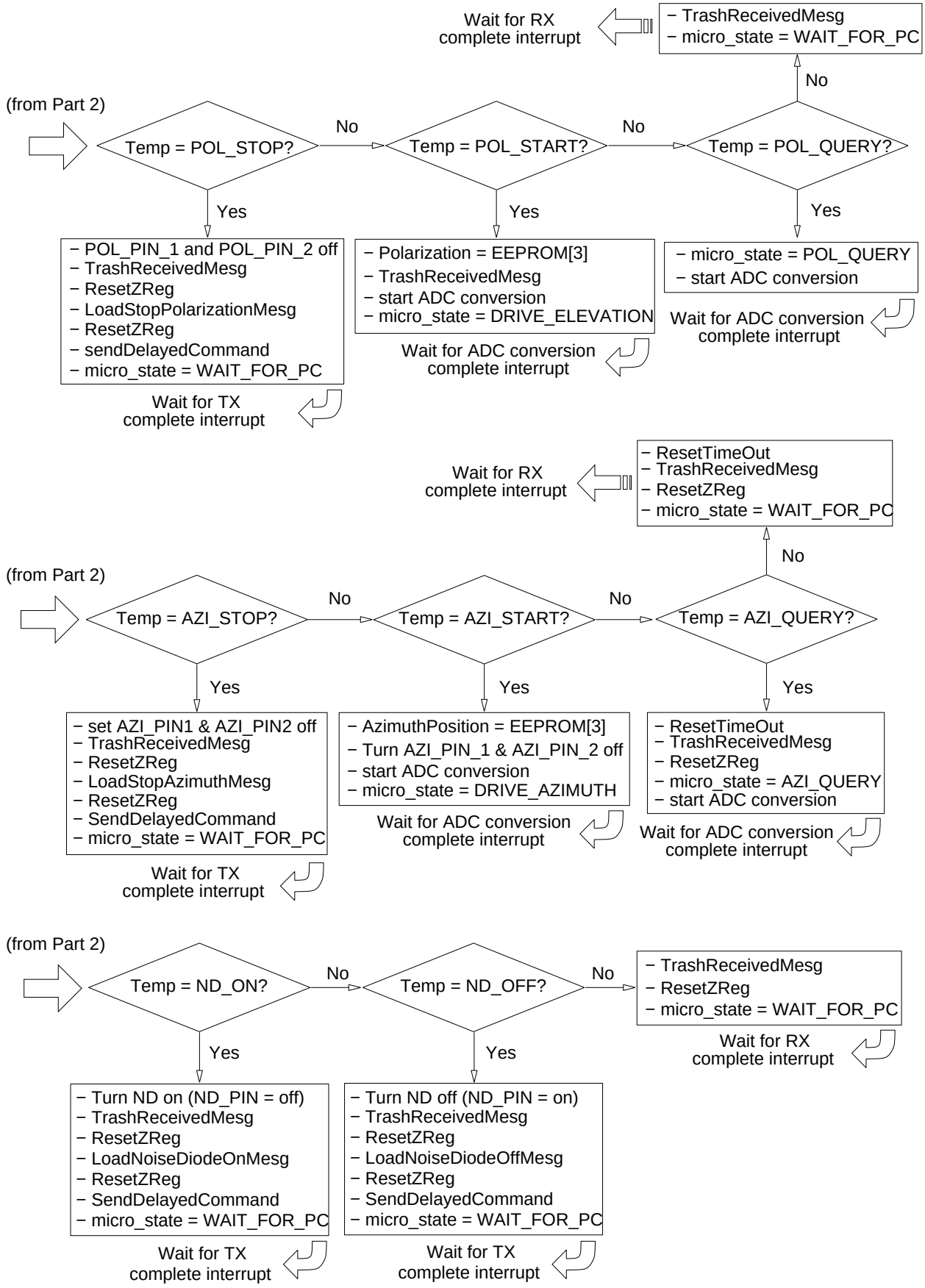

Figure B.26: Microcontroller Control Flow Chart (Part 3 of 5).

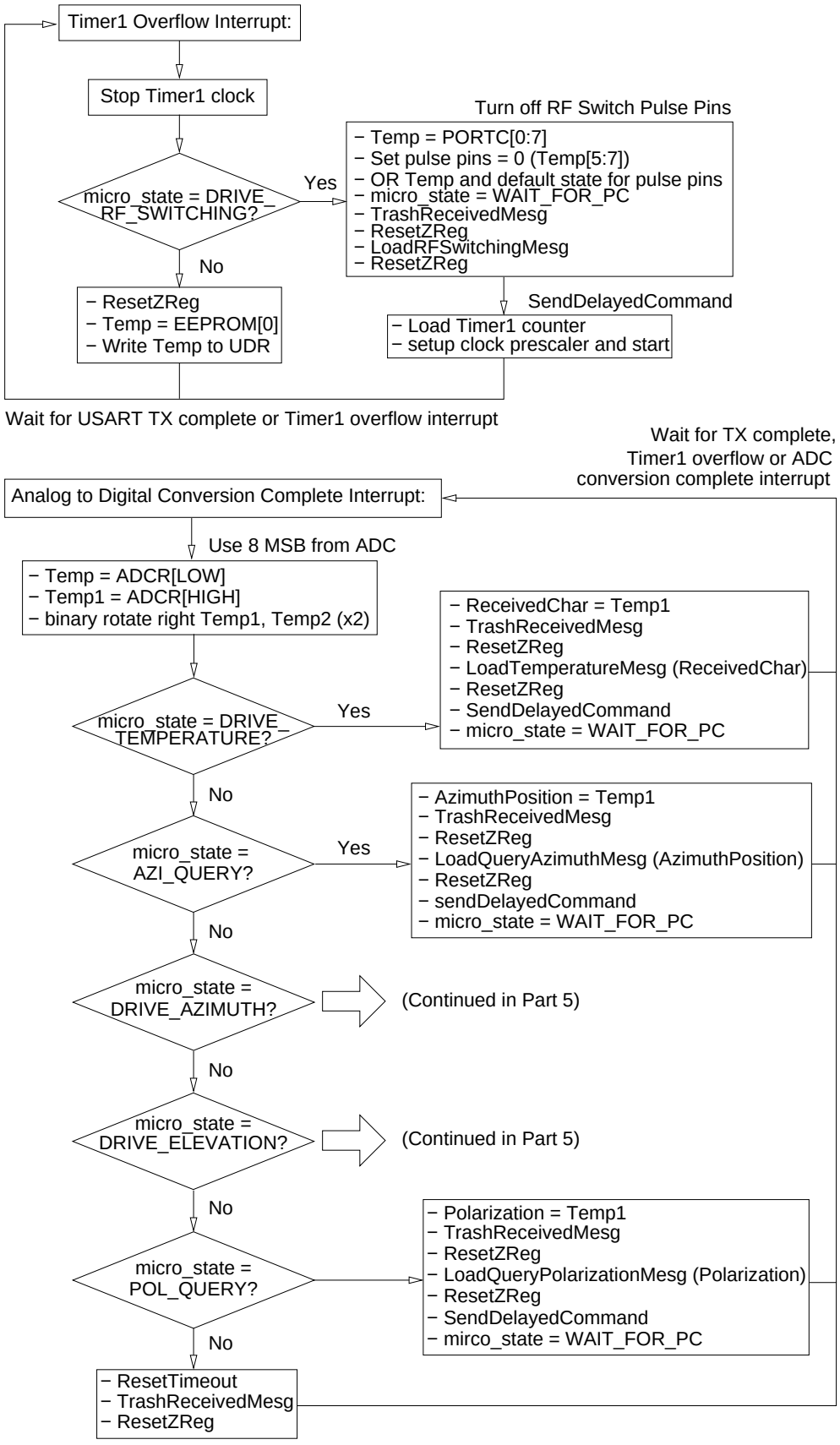

Figure B.27: Microcontroller Control Flow Chart (Part 4 of 5).

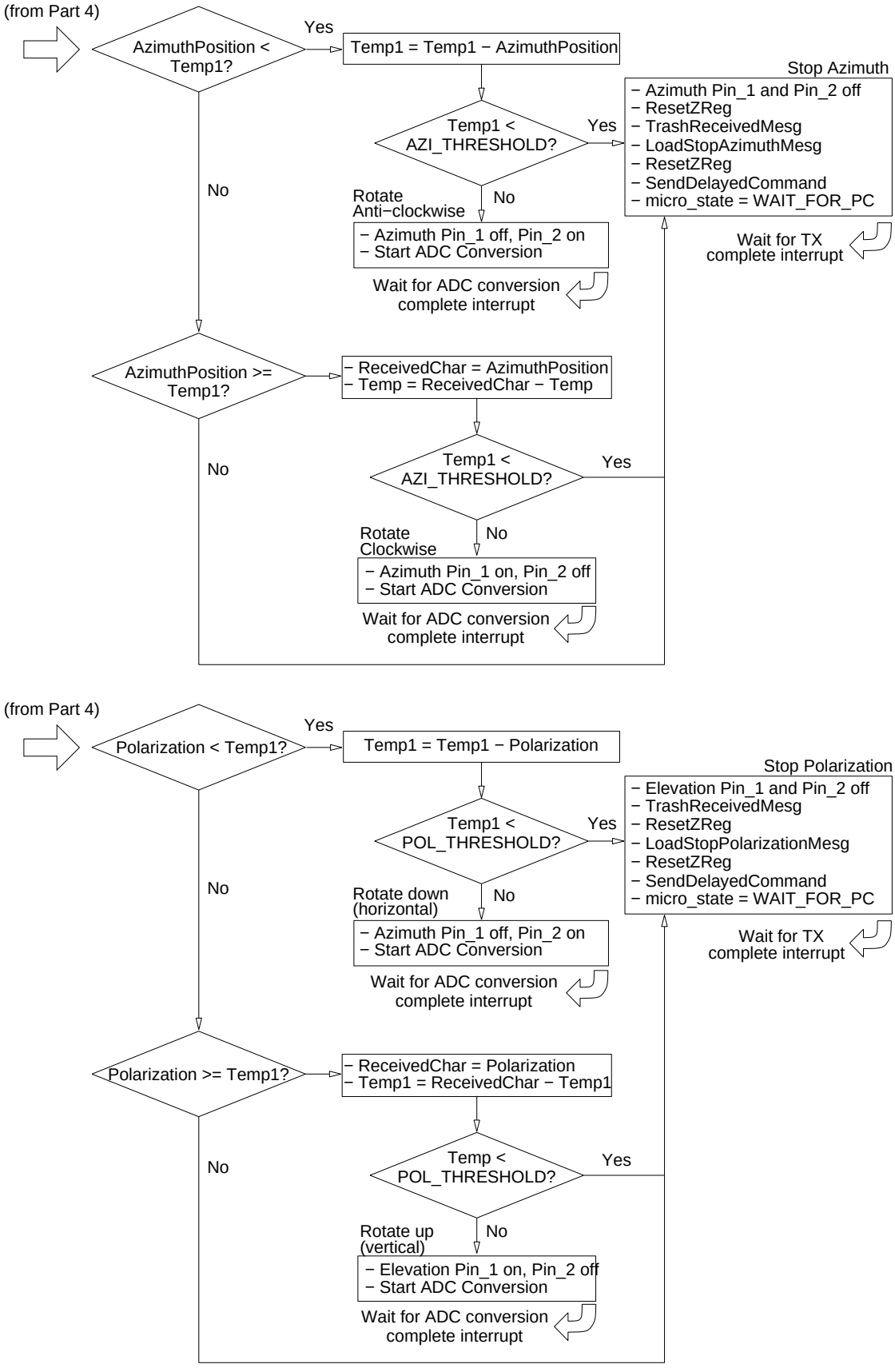

Figure B.28: Microcontroller Control Flow Chart (Part 5 of 5).

Appendix C

Locally Generated RFI

C.1 Interference Sources at the Karoo 3 Core Site

Frequency MHz	Suspected Source / Direction	Comment
70.0026	Mast	Suspect Electronics Control Box or electronics in Mast-Head Box.
71.6218	Mast	Suspect Electronics Control Box or electronics in Mast-Head Box.
71.8809	Container UPS area	
71.9959	Electronics Control Box	Suspect 8 MHz harmonic of crystal.
72.4134	Electronics Control Box	
75.0018	Mast	Suspect Electronics Control Box or electronics in Mast-Head Box.
75.0726	General area of container	
75.3426	General area of container	
75.3511	General area of container	
75.4309	General area of container	
79.9950	General area of mast and Electronics Control Box	
80.0000	General area of mast and Electronics Control Box	
84.6800	General area of mast and Electronics Control Box	
87.4980	General area of container	
87.9930	General area of mast and Electronics Control Box	Suspect 8 MHz harmonic of crystal.
90.5130	Mast	Suspect Electronics Control Box or electronics in Mast-Head Box.

Table C.1: List of interference sources (70 - 90 MHz) found at the Karoo 3 core site during field test measurements with the prototype system in December 2004.

Frequency MHz	Suspected Source / Direction	Comment
90.8030	General area of mast and Electronics Control Box	
91.7 to 110	Broad band noise	IC replaced on veroboard version of Control PCB. Noise disappeared.
111.9920	Mast	Suspect 8 MHz harmonic of crystal.
116 to 118	Broad band noise	IC replaced on veroboard version of Control PCB. Noise disappeared.
95.7000	SABC Carnarvon	Commercial broadcast.
95.9000	SABC	Commercial broadcast.
100.8000	SABC	Commercial broadcast.
119.9903	General area of mast and Electronics Control Box	Suspect 8 MHz harmonic of crystal.
120.0000	General area of mast and Electronics Control Box	
127.9870	General area of mast and Electronics Control Box	Suspect 8 MHz harmonic of crystal.
127.9900	Electronics Control Box	
128.0000	General area of mast and Electronics Control Box	
135.9887	Mast	Suspect 8 MHz harmonic of crystal.
137.1953	Satellite	
137.6603	Satellite	
143.6820	General area of container	
143.7838	General area of container	
143.7916	Diesel generator	
143.8790	Laptop	HP laptop computer
143.9880	General area of mast and Electronics Control Box	Suspect 8 MHz harmonic of crystal.
147.2460	Mast	
151.9885	General area of container	Suspect 8 MHz harmonic of crystal.
152.7240	General area of mast and Electronics Control Box	
152.3693	ICASA DF Vehicle	Suspect engine management or vehicle alarm system.
152.7220	General area of container	
162.2000	ICASA DF Vehicle	Suspect engine management or vehicle alarm system.
166.3660	General area of mast and Electronics Control Box	

Table C.2: List of interference sources (90 - 166 MHz) found at the Karoo 3 core site during field test measurements with the prototype system in December 2004.

Frequency MHz	Suspected Source / Direction	Comment
175.9866	Electronics Control Box	Suspect 8 MHz harmonic of crystal.
200.0806	Mast	Suspect 8 MHz harmonic of crystal.
231.9800	Mast	Suspect 8 MHz harmonic of crystal.
207.2500	SABC	
223.2620	SABC	
233.4280	General area of mast and Control Box Electronics	
233.4530	North direction, away from SKA site	
247.9790	Mast	
250.0018	South direction, away from SKA site	
250.3501	North west direction, from SKA site	
250.4526	North west direction, from SKA site	
250.7018	East direction, away from SKA site	
250.6500	East direction, away from SKA site	
270.0000	General area of container	
270.3130	General area of container	
271.9780	Electronics Control Box	
287.9950	Electronics Control Box	Suspect 8 MHz harmonic of crystal.
349.9000	General area of container	
366.8153	General area of container	
375.9675	Electronics Control Box	
393.2547	UPS	UPS inside site container.
414.2130	ICASA DF Vehicle	Suspect engine management or vehicle alarm system.
433.3780	SKA Toyota Vehicle	Suspect engine management or vehicle alarm system.
623.2500	SABC TV Carnarvon	
629.2500	SABC Carnarvon	TV sound carrier
940.4430	GSM South	
942.4330	GSM West	
1124.0000	RADAR	Confirmed ATNS, either from De Aar or Sutherland
1125.0000	RADAR	Confirmed ATNS, either from De Aar or Sutherland

Table C.3: List of interference sources (175 - 1125 MHz) found at the Karoo 3 core site during field test measurements with the prototype system in December 2004.

C.2 Identification of RFI Sources at the Karoo 3 Core Site

Figure C.1: Photographs of the procedures undertaken to identify RFI sources at the Karoo 3 core site. Top: The handheld directional antenna (Rohde & Schwartz HE200) is used to locate interference in the equipment rack (left) inside the site container and the vehicles on site (right). Bottom: Equipment in the ICASA DF vehicle is used for coarse direction finding of the RFI sources.

C.3 Spectrum Analyser Screening

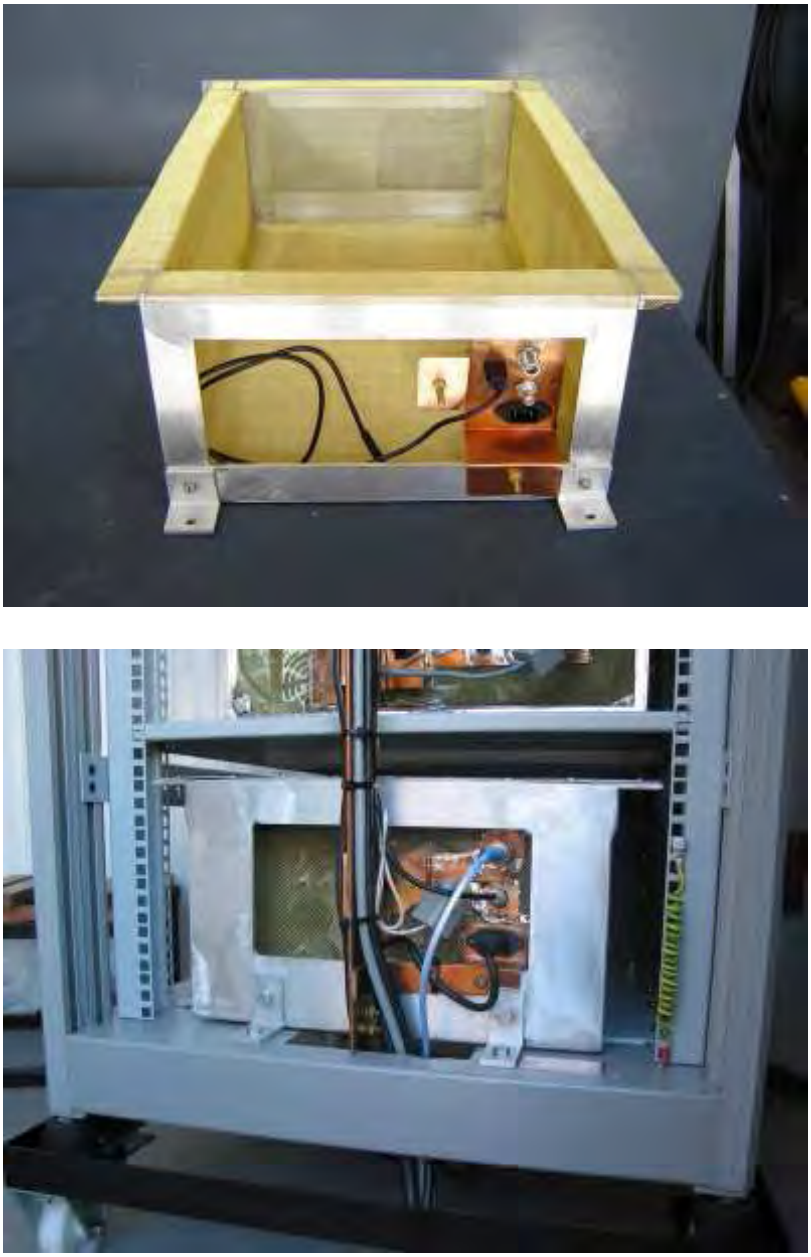

Figure C.2: Top: Spectrum analyser Faraday cage with bulk-head connectors, mains filter and copper flange for attachment to the copper busbar. Bottom: Spectrum analyser installed in the trailer rack with power and control cables strapped to the busbar.

C.4 Evaluation of Preliminary Screening at HartRAO

Figure C.3: Photograph taken in the HartRAO Visitors Centre during preliminary validation of the screening on RFI measurement System 2. The Anritsu portable spectrum analyser (on chair in the foreground) is connected to the R & S HL033 antenna which is directed at the RFI measurement system components on the bench.

Appendix D

Field Tests and Operations

D.1 Antenna Beam Patterns

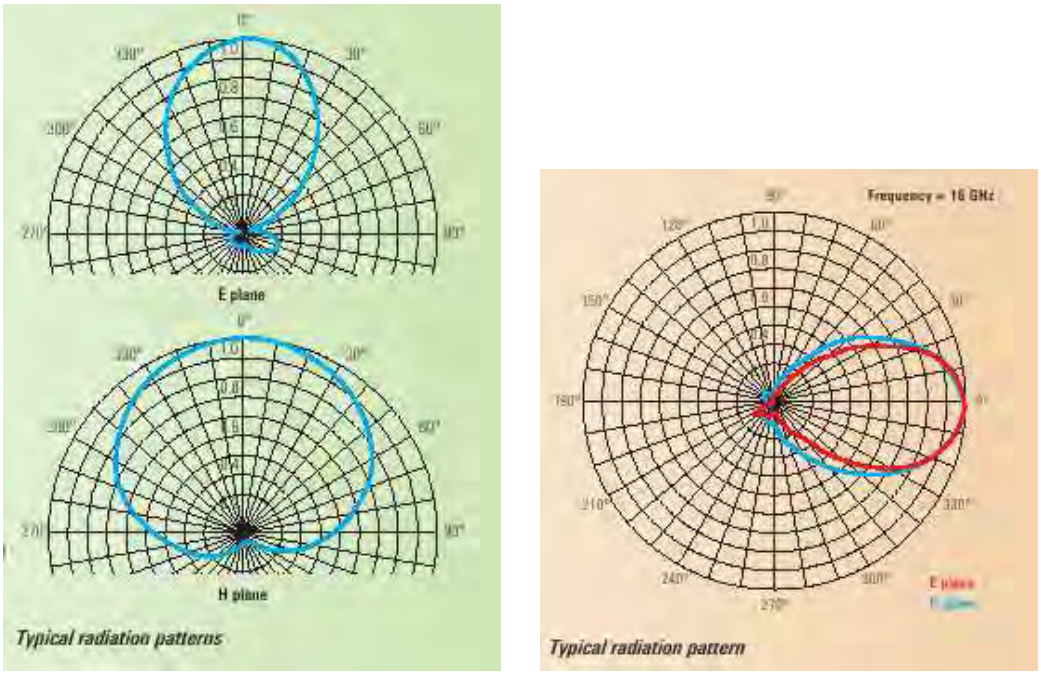

Figure D.1: Beam pattern data provided in the manufacturer data sheets for the Rohde & Schwarz HL033 (left) and HL050 (right) antennas.

D.2 LabVIEW System Integrity Check VI Front Panel and Block Diagram

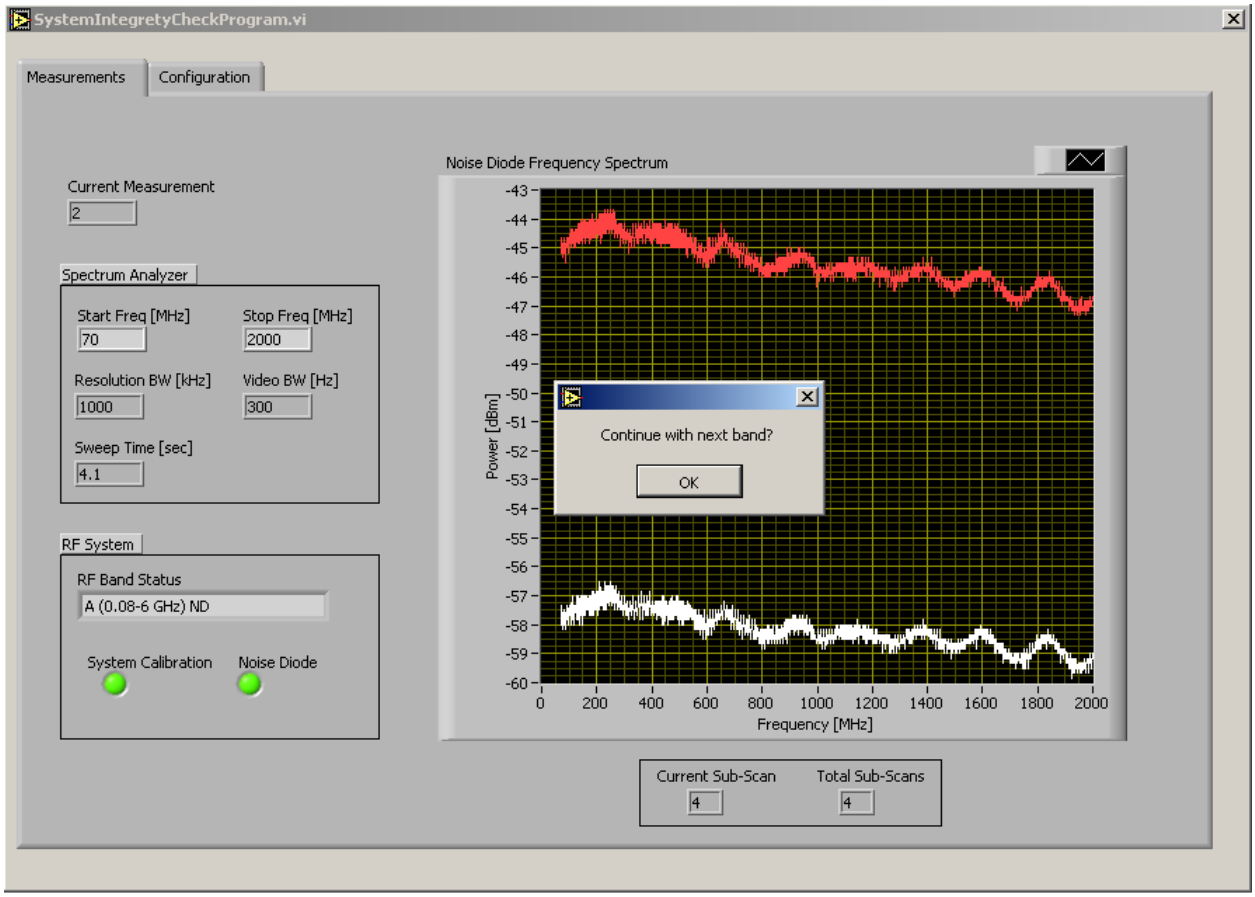

Figure D.2: Front panel of the LabVIEW System Integrity Check VI showing the noise diode measurements for the 0.07-2.0 GHz band.

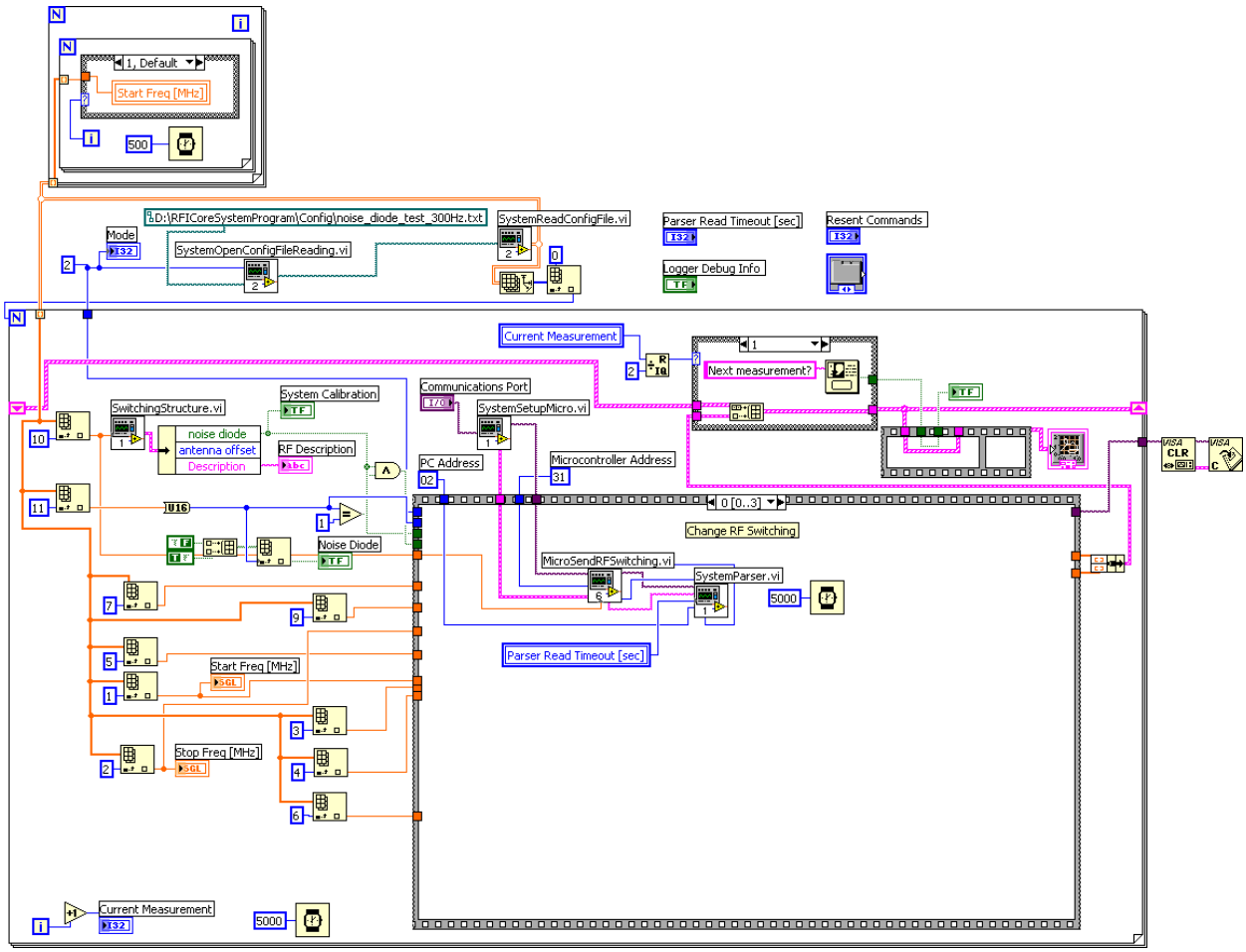

Figure D.3: LabVIEW block diagram of the system integrity check application. The first part of the sequence is shown, namely to change the RF switches.

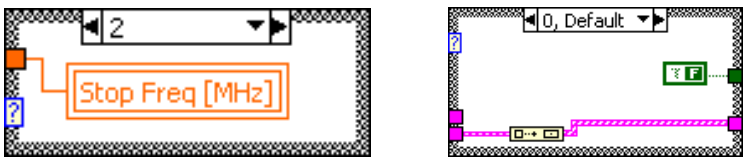

Figure D.4: Case select statement hidden in Figure D.3.

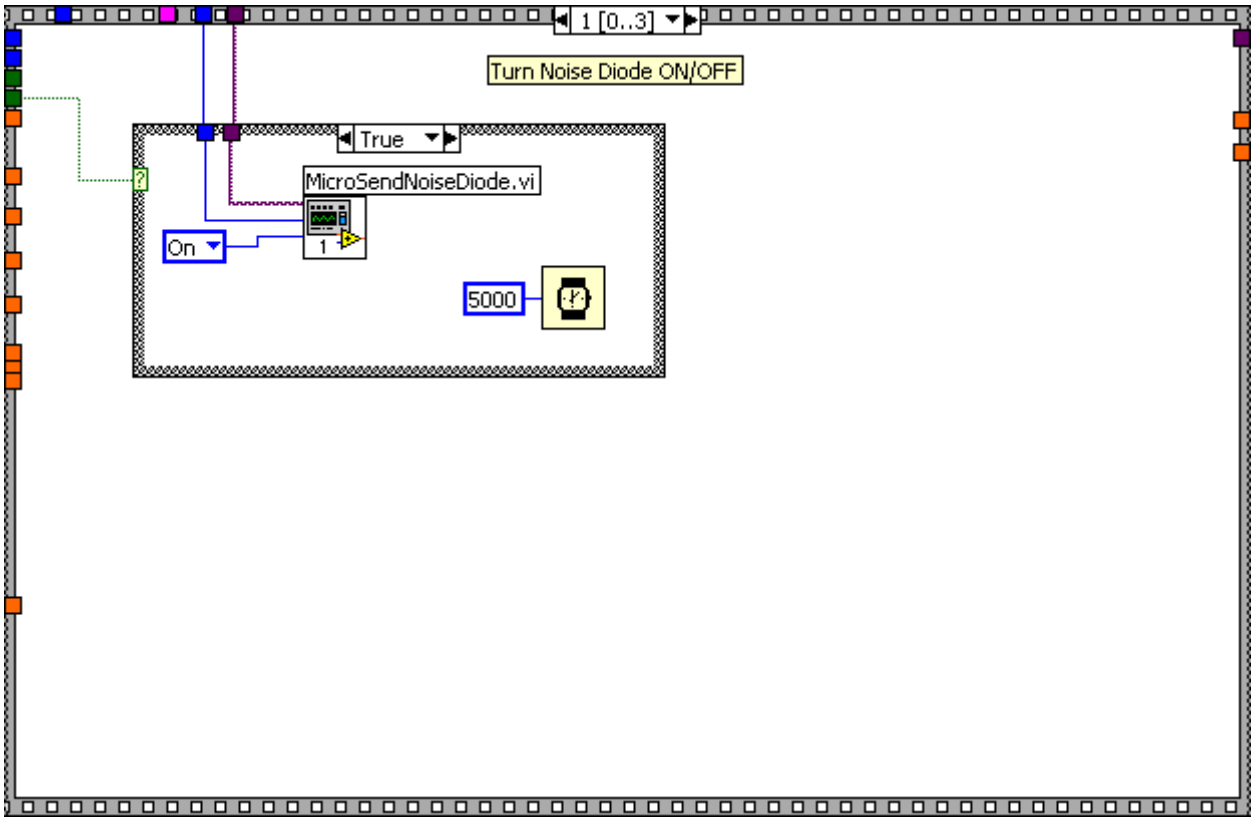

Figure D.5: Block diagram of the sequence for turning the noise diode on.

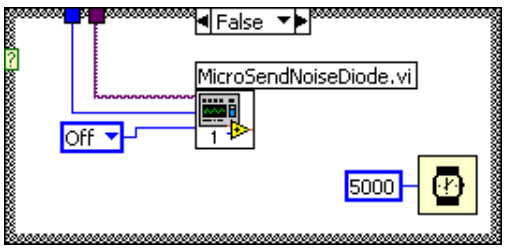

Figure D.6: Case select part of block diagram (Figure D.5) for turning the noise diode off.

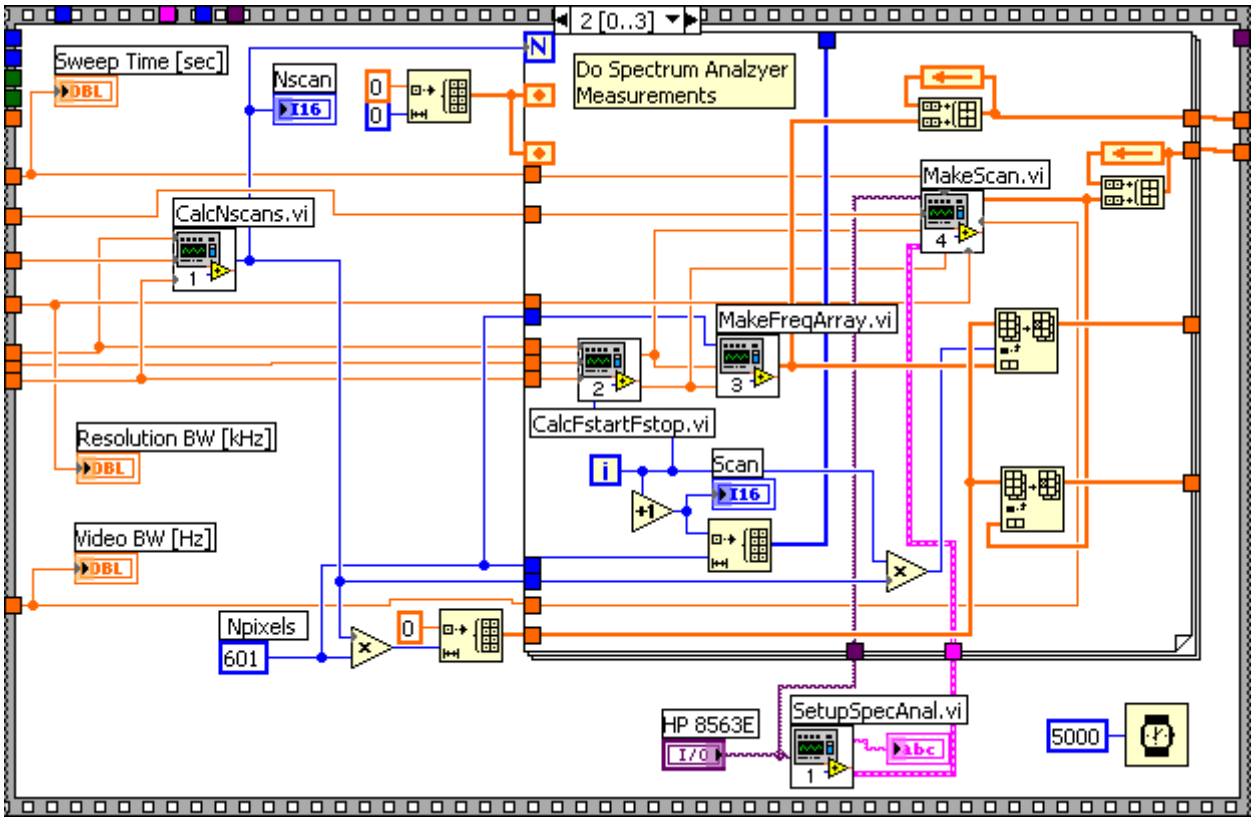

Figure D.7: Block diagram of the sequence for performing the measurements with the spectrum analyser.

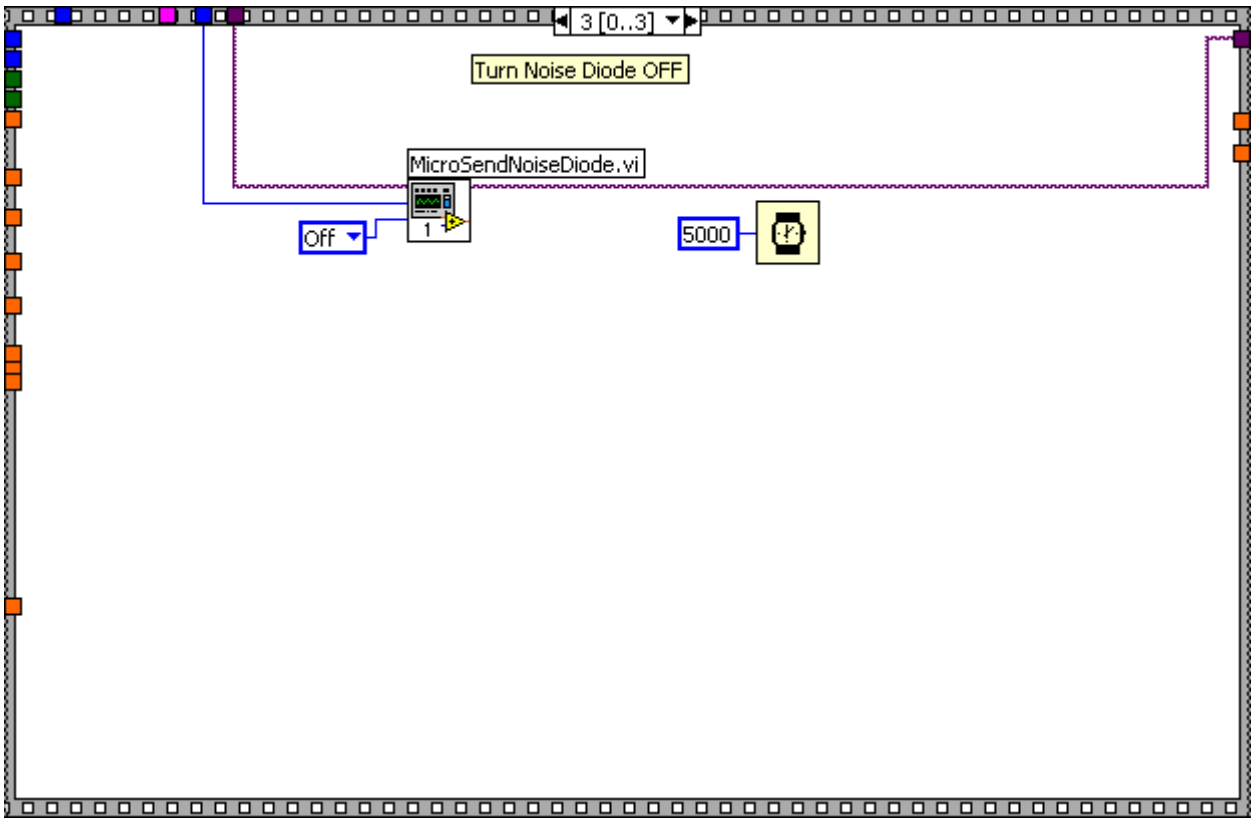

Figure D.8: Block diagram of the sequence for turning the noise diode off.

D.3 Astron and SA SKA Cross-calibration Photographs

Figure D.9: Photographs of the cross-calibration exercise done at the Karoo 3 core site during April 2005.

D.4 Equations for Cross-calibration Procedures

The Friis Transmission formula (Equation D.3), defines the ratio of power transfer between two antennas, taking into account losses due to free space propagation over a distance d. The effective antenna aperture A_e defined in Equation D.1 was substituted into Equation D.3 and then rewritten in terms of gain (Equation D.2) for each measurement system.

$$A_e(f)\,[\mathrm{m}^2] = \frac{\lambda^2\,[\mathrm{m}^2]}{\Omega_a\,[\mathrm{sr}]} \tag{D.1}$$

$$G_{ant}(f) = \frac{4\pi}{\Omega_a(f)\,[\mathrm{sr}]} \tag{D.2}$$

$$\frac{\mathrm{P}_{rec}\,[\mathrm{W}]}{\mathrm{P}_{trans}\,[\mathrm{W}]} = A_{rec}\,[\mathrm{m}^2] \times A_{trans}\,[\mathrm{m}^2] \times \frac{1}{(\lambda\,[\mathrm{m}]\,d\,[\mathrm{m}])^2} \tag{D.3}$$

Appendix E

Data Processing

E.1 Summary of Data Processing Tools

Step	Program	Comments	Appendix
1	`convascii2fits.py` `ascii2fits.c`	Generation of multiple FITS files, using `ascii2fits C program`.	F.6 F.7
2	`txt2bin.py`	Convert text files (antenna gain, system gain, noise diode ENR) to binary.	F.8
3	`sys2mysql.py`	Load system gain, noise diode ENR and antenna gain files into database.	F.9
4	`updatefits2mysql.py` `readfits.c`	Insert/update FITS file details in database using `readfits C program` to extract FITS header information.	F.10 F.11
5	`mysql2qplots.py` `showrfi.c`	Generate data plots (PNG) using the C program `showrfi`.	F.12 F.13
6, 7	`check_qplots.php`	Data-flagging application.	F.14
8	`convfits2dat.py` `fits2dat.c`	Generate binary DAT files from FITS files using `fits2dat C program`.	F.15 F.16
9	`multidat2txt.py`	Perform calibration and statistical analysis by combining binary data files.	F.17
10	`sens.py`	Generate sensitivity text file.	F.18
11	`merge2txtsens.py`	Append sensitivity to plot file.	F.19
12	`multidat2occ.py`	Generate occupancy statistics from binary files.	F.20
13	`txtsens2plot.py`	Generate plot using plot text file (with sensitivity) and plot parameter file.	F.21
14	`occ2plot.py`	Generate occupancy plot from occupancy text file.	F.22

Table E.1: Summary of data processing tools used in each processing step in the data analysis pipeline. Steps correspond to Figure 6.1.

E.2 Summary of Data-flagging Statistics

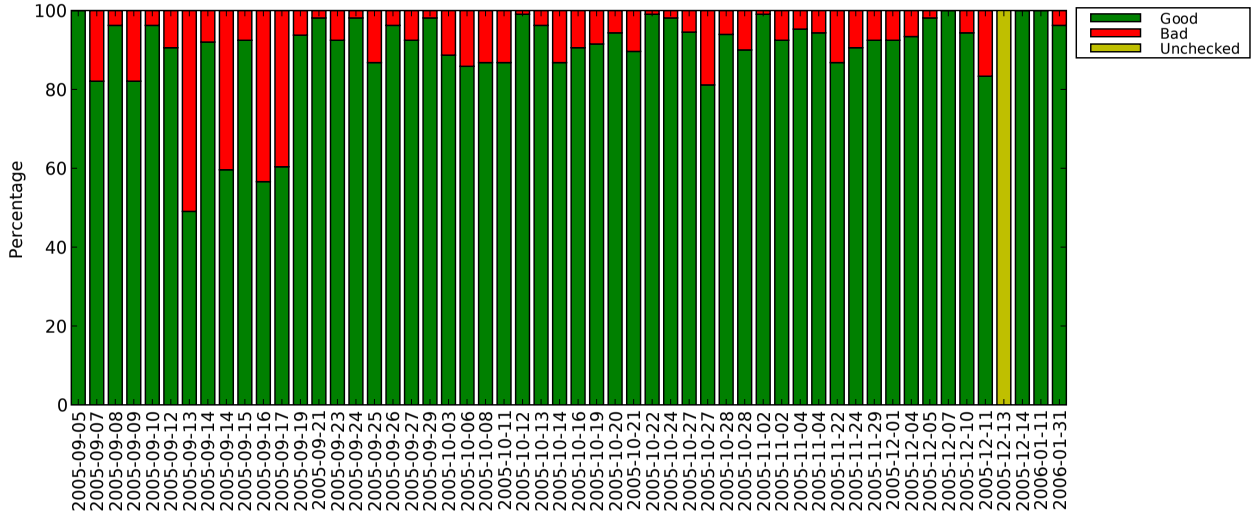

Figure E.1: Summary of Mode 1 data-flagging statistics as a percentage of the total number of measurements in each batch.

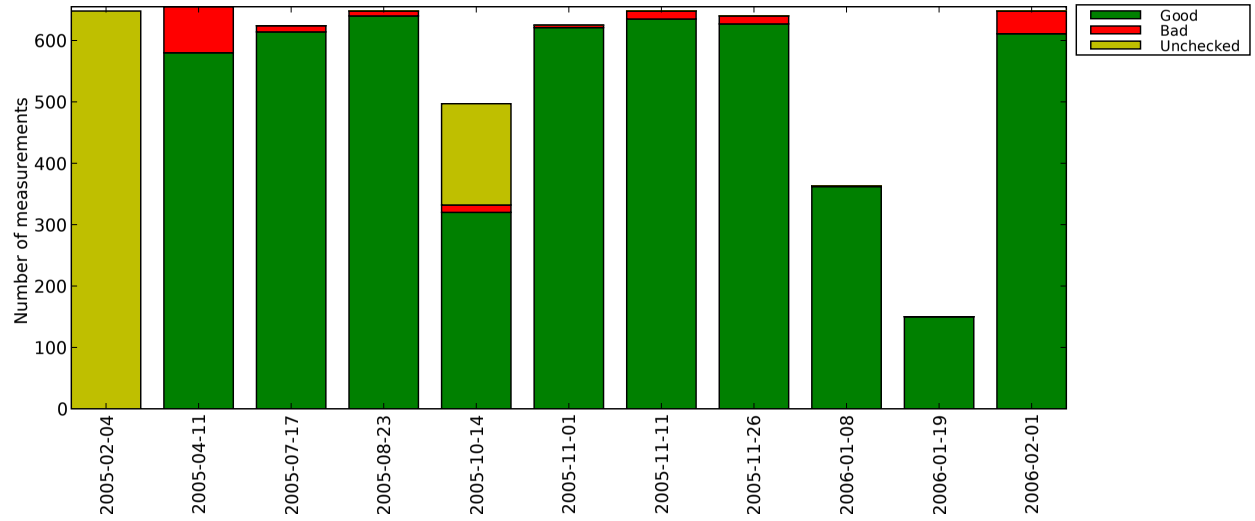

Figure E.2: Summary of Mode 2 data-flagging statistics.

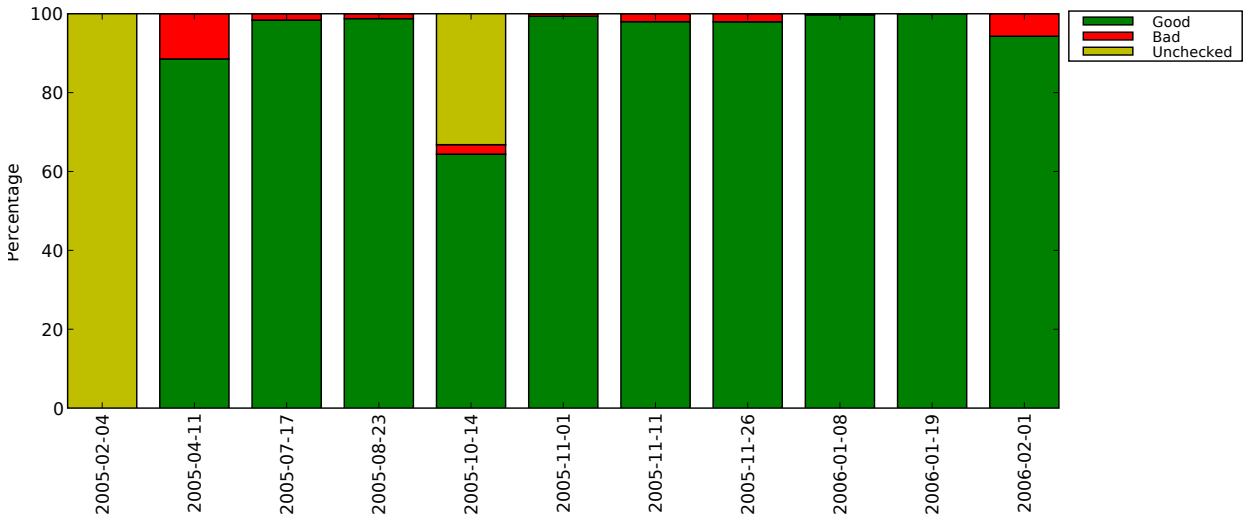

Figure E.3: Summary of Mode 2 data-flagging statistics as a percentage of the total number of measurements in each batch.

E.3 Example Plot Parameter File

```
##########################################################################
# Plot Parameter File for the April 2005 Mode 2 Measurements at the      #
#    Karoo 3 core site.  Pointings are combined for horizontal           #
#    polarisation.                                                       #
#                                                                        #
#  1. Selection criteria:                                                #
#       which pointings / polarisations / batches to combine for analysis #
#  2. Plot settings:                                                     #
#       what statistics to display on the plot                           #
#                                                                        #
# Syntax:                                                                #
#     Parameter=option1:option2:option3                                  #
##########################################################################

####################
# Selection criteria
####################
# Sites
sites=RFI-K3

# System and Mode
system=2
mode=2

# Batch start date
start_date=2005-04-11

# Pointings
pointings_2ghz=1:2:3
pointings_26ghz=1:2:3:4:5

# Polarization
polarizations=H

####################
# Plot settings
####################

# Frequency start and stop [MHz]
start_freq_mhz=70.0
stop_freq_mhz=26500.0

# Statistics
maximum=n
percent90=n
median=y
mean=y
```

```
percent10=y
sensitivity=y
timestamp=n

# Y-Axis limits in dB W m^(-2) Hz^(-1)
y_axis_min=-210.0
y_axis_max=-120.0

# X-Axis limits as per start_freq_mhz and stop_freq_mhz
# X-Axis [M]hz or [G]hz
freq_axis=M
log_scale=Y
mark_sys_meas_bands=N
```

E.4 Data Calibration Equation

Equation E.1 shows the details of the equation used to calibrate the data in units of spectral power flux density.

$$S(f)\,[\mathrm{W.m^{-2}.Hz^{-1}}] = 8\pi \times \frac{P_{\mathrm{SA}}(f)\,[\mathrm{W}]}{G_{ant}(f) \times G_{sys}(f)} \times \frac{f^2\,[\mathrm{Hz^2}]}{c^2\,[\mathrm{m^2.s^{-2}}]} \times \frac{1}{\mathrm{RBW}\,[\mathrm{Hz}]} \tag{E.1}$$

The values G_{ant} and G_{sys} represent the antenna gain and system gain respectively. P_{SA} is the power value measured by the spectrum analyser, RBW is the resolution bandwidth and c is the speed of light.

Appendix F

Electronic Media on CD

The text for this Appendix is provided on CD in electronic format. The contents of the CD are as follows:

Appendix F.1 Mode 1 Schedule file.

Appendix F.2 Mode 2 Schedule file.

Appendix F.3 ATmega8535 Microcontroller Assembler code.

Appendix F.4 Video clip of mast induced interference at the Karoo 3 core site.

Appendix F.5 Standard Operating Proceedure for the RFI Measurement System.

Appendix F.6 Source code for `convascii2fits.py`.

Appendix F.7 Source code for `ascii2fits.c`.

Appendix F.8 Source code for `txt2bin.py`.

Appendix F.9 Source code for `sys2mysql.py`.

Appendix F.10 Source code for `updatefits2mysql.py`.

Appendix F.11 Source code for `readfits.c`.

Appendix F.12 Source code for `mysql2qplots.py`.

Appendix F.13 Source code for `showrfi.c`.

Appendix F.14 Source code for `check_qplots.php`.

Appendix F.15 Source code for `convfits2dat.py`.

Appendix F.16 Source code for `fits2dat.c`.

Appendix F.17 Source code for `multidat2txt.py`.

Appendix F.18 Source code for `sens.py`.

Appendix F.19 Source code for `merge2txtsens.py`.

Appendix F.20 Source code for `multidat2occ.py`.

Appendix F.21 Source code for `txtsens2plot.py`.

Appendix F.22 Source code for `occ2plot.py`.

Appendix F.23 ASTRON/SSSM Data Summary Report

Appendix F.24 Mode 1 and Mode 2 Measurement Results